



DISSERTATION

Biohydrogen Production Based on the Catalyzed Water Gas Shift Reaction in Wood Gas

ausgeführt zum Zwecke der Erlangung des akademischen Grades eines Doktors der
technischen Wissenschaften

unter der Leitung von Univ. Prof. Dr. Hermann Hofbauer
und der Betreuung von Dr. Reinhard Rauch
und Univ. Prof. Dr. Wolfgang Linert

Institut für Verfahrenstechnik, Umwelttechnik und Technische Biowissenschaften

eingereicht an der Technischen Universität Wien
Fakultät für Maschinenwesen und Betriebswissenschaften

von

DI (FH) DI Silvester Fail

Matrikelnummer 0852801

Schottenfeldgasse 55/10

1070 Wien

Wien, 16. Oktober 2014

Danksagung

An dieser Stelle möchte ich mich zunächst bei meinem unmittelbaren Betreuer Reinhard Rauch dafür bedanken, dass er mir sein Vertrauen geschenkt hat und es mir ermöglicht hat meine Dissertation am Institut für Verfahrenstechnik der TU Wien durchzuführen. Die Betreuung war einwandfrei. Hermann Hofbauer möchte ich für die motivierenden Gespräche und seine konstruktiven Ratschläge danken. Die Institutsleitung war bei ihm in sehr guten Händen.

Großer Dank gilt allen Bürokollegen im "Crowded Office", welche mich während der Dissertation begleitet haben. Langjährig haben mich Harald Zeman und vor allem Nicolas Diaz unterstützt. Es ehrt mich sehr, dass ich mit dem "besten Chilenen" zusammenarbeiten durfte. Außerdem möchte ich der nächsten Generation an Verfahrenstechnikern danken. Es hat Spaß gemacht die Diplomarbeiten meiner Freunde Florian Benedikt, Julian Hinteregger, und Michael Kraussler zu begleiten. Vielen Dank für die vielen heiteren Momente und Eure Unterstützung. Besonders hervorheben möchte ich die tolle Arbeit von Matthias Binder, Fabian Pollesböck, Antonio Plaza und Alberto Cortez. Euer Beitrag zu dieser Dissertation war enorm und ich kann Euch nicht genug dafür danken. Bei Ellen Schanz möchte ich mich für die Motivation und die Aufmunterung während der anstrengenden Schreibphase bedanken. In diesem Zeitraum war das Leichtathletik Training mit Michael Stollhof genau der richtige Ausgleich für die vielen Stunden vor dem Computer und hat mir sehr viel bedeutet. Ich danke Euch allen für die gleichermaßen lehrreiche wie auch unterhaltsame Zeit. Die Zusammenarbeit und die Stimmung waren immer gut. Es gab keinen Tag an dem ich nicht gern ins Büro ging.

Weiters, möchte ich mich bei den Projektpartnern von Air Liquide, Energie Burgenland, cts und Industrieanlagenbau Binder bedanken. Besonders möchte ich die fachliche Unterstützung von Marius Hackel hervorheben. Sebastian Niederhauser möchte ich für die einwandfreie Programmierung der Automatisierung der Versuchsanlage und sein Engagement danken. Stellvertretend für das Biomassekraftwerk Oberwart möchte ich mich bei Rene Javorits für die uneingeschränkte Unterstützung der Belegschaft bedanken. Das Arbeitsumfeld in Oberwart war perfekt!

Schlussendlich danke ich meiner Freundin Stephanie und meiner ganzen Familie für Ihre Unterstützung. Ich bin sehr stolz auf meinen Großvater Herbert Mackinger der mein Interesse an der Verfahrenstechnik geweckt hat. Danke.

Abstract

Catalysis of the water gas shift reaction (WGSR) is an interesting process for the biomass-based production of hydrogen. In this predominately experimental work, the catalytic refinement of wood gas derived from biomass steam gasification was investigated. Two different commercial water gas shift catalysts were tested: a Co/Mo-based catalyst which was developed for "sour shift" applications in gas mixtures containing hydrogen sulfide; and a Fe/Cr-based catalyst which was developed for "sweet shift" processes downstream sulfur removal. Both catalysts were investigated at two different experimental setups. At the "Test rig for chemical kinetics" at the Vienna University of Technology, experiments were carried out on a laboratory scale using synthetic gas mixtures simulating the wood gas composition. Based on these results, empirical power law rate models were established in order to describe the reaction kinetics for both catalysts (Equation 1 and 2). Both models were valid for a hydrogen sulfide content of 100 vol.ppm_{db}, which was considered as a typical value for wood gas.

$$r_{wt.(Co/Mo)} = 0.034 \exp\left(\frac{-66.3}{R T}\right) p_{CO}^{1.28} p_{H_2O}^{0.05} p_{CO_2}^{-0.11} p_{H_2}^{-0.36} \left(1 - \frac{1}{K_p} \frac{p_{CO_2} p_{H_2}}{p_{CO} p_{H_2O}}\right) \quad (1)$$

$$r_{wt.(Fe/Cr)} = 117.8 \exp\left(\frac{-101.9}{R T}\right) p_{CO}^{1.77} p_{H_2O}^{0.23} p_{CO_2}^{-0.17} p_{H_2}^{-0.12} \left(1 - \frac{1}{K_p} \frac{p_{CO_2} p_{H_2}}{p_{CO} p_{H_2O}}\right) \quad (2)$$

Also, a pilot plant was designed, assembled, commissioned, and optimized within this thesis in order to investigate the catalysis of the WGSR on a bigger scale using real wood gas. This facility ("Pilot plant for catalytic wood gas processing") was processing wood gas generated by means of dual fluidized bed steam gasification of wood chips at the commercial heat and power plant in Oberwart, Austria. About 2 $\frac{m^3}{h}$ of dry wood gas were processed over three fixed bed reactors connected in series. At this facility, the influence of various reaction parameters, the long-term stability, and the catalytic side effects were investigated.

The activity of the Co/Mo-based catalyst was enhanced with increasing sulfur loads in the feed, whereas the activity of the Fe/Cr-based catalyst was decreased with higher sulfur loads. In combination with the rather low sulfur loads of the present wood gas, the performance of the Fe/Cr-based catalyst was considerably better than the performance of the Co/Mo-based catalyst. Strongly depending on the reaction parameters (temperature, gas hourly space velocity, and steam to dry gas ratio) up to 95 % of the present carbon monoxide was converted to hydrogen and carbon dioxide according to the WGSR. In cooperation with other research projects, this shifted gas mixture was further processed to produce pure hydrogen based on wood gasification. Also, the usage of the generated hydrogen in a PEM fuel cell was demonstrated.

Zusammenfassung

Die Katalyse der Wassergasshift-Reaktion (WGSR) stellt eine interessante Technologie bei der Wasserstoffherstellung auf Basis von holzartiger Biomasse dar. In dieser experimentellen Arbeit, wurde die katalytische Aufbereitung von Holzgas aus einer Wirbelschichtdampfvergasung untersucht. Zwei verschiedene kommerzielle Katalysatoren wurden getestet. Katalysator 1 (Co/Mo-basiert) wurde für Gasgemische entwickelt, welche beträchtliche Anteile an Schwefel enthalten. Katalysator 2 (Fe/Cr-basiert) wurde für schwefelfreie Gasgemische entwickelt. Beide Katalysatoren wurden an zwei unterschiedlichen Apparaturen getestet. An der Kinetikapparatur der Technischen Universität Wien wurden die Katalysatoren im Labormaßstab mit künstlichen Gasmischungen beaufschlagt und empirische Kinetikmodelle aufgestellt (Power law rate Modelle). Die verwendeten Gasmischungen wurden dabei an die Zusammensetzung von Holzgas angepasst und ein Schwefelwasserstoffgehalt von 100 vol.ppm_{db} eingestellt. Die erhaltenen Modelle für beide Katalysatoren sind unter Gleichung (3) und (4) angeführt.

$$r_{wt.(Co/Mo)} = 0.034 \exp\left(\frac{-66.3}{R T}\right) p_{CO}^{1.28} p_{H_2O}^{0.05} p_{CO_2}^{-0.11} p_{H_2}^{-0.36} \left(1 - \frac{1}{K} \frac{p_{CO_2} p_{H_2}}{p_{CO} p_{H_2O}}\right) \quad (3)$$

$$r_{wt.(Fe/Cr)} = 117.8 \exp\left(\frac{-101.9}{R T}\right) p_{CO}^{1.77} p_{H_2O}^{0.23} p_{CO_2}^{-0.17} p_{H_2}^{-0.12} \left(1 - \frac{1}{K} \frac{p_{CO_2} p_{H_2}}{p_{CO} p_{H_2O}}\right) \quad (4)$$

Außerdem wurde im Zuge dieser Dissertation eine Versuchsanlage realisiert, um diese Katalysatoren im größeren Maßstab mit realem Holzgas zu beaufschlagen. Diese Anlage wurde am Standort des Biomassevergasungskraftwerks Oberwart aufgebaut, an dem Holzgas durch die Zweibettwirbelschichtdampfvergasung von Holzhackschnitzel hergestellt wird. Ein Teilstrom des dort produzierten Holzgasgemisches wurde entnommen und über die Versuchsanlage geleitet, welche mit drei seriell geschalteten Festbettreaktoren ausgestattet war. Die Pilotanlage wurde auf einen trockenen Holzgasvolumenstrom von $2 \frac{m^3}{h}$ ausgelegt. Vor Ort wurde der Einfluss verschiedener Betriebsparameter, die Langzeitstabilität der Katalysatoren und die Auswirkung der Katalysatoren auf Schwefel- und Teerverbindungen untersucht.

Die Aktivität des Co/Mo-basierten Katalysators wurde durch höhere Schwefelgehalte gesteigert. Im Gegensatz dazu, wurde die Aktivität des Fe/Cr-basierten Katalysators durch die Zugabe von Schwefelwasserstoff reduziert. In Kombination mit den relativ geringen Schwefelkonzentrationen im Holzgas des Kraftwerks Oberwart erzielte der Fe/Cr-basierte Katalysator wesentlich bessere Kohlenmonoxid Konversionsraten. In starker Abhängigkeit von den Betriebsbedingungen (Temperatur, Raumgeschwindigkeit, Wassergehalt) konnten Konversionsraten von bis zu 95 % erzielt werden. In Kooperation mit anderen Forschungsprojekten, konnte das Gasgemisch im Ausgang der Versuchsanlage zu hochreinem Wasserstoff aufbereitet werden. Die Anwendung dieses Wasserstoffs in einer PEM Brennstoffzelle wurde demonstriert.

Contents

1	Introduction	4
1.1	The importance of hydrogen	5
1.2	Renewable hydrogen production	5
1.2.1	Electrochemical methods	5
1.2.2	Biological methods	6
1.2.3	Thermochemical methods	7
1.3	Aim of this work	8
2	State of the art	10
2.1	Industrial processes for hydrogen production	10
2.1.1	Steam reforming	10
2.1.2	Partial oxidation and catalytic partial oxidation	12
2.1.3	Autothermal reforming	13
2.2	Industrial catalysis of the water gas shift reaction (WGSR)	14
2.3	Biomass gasification	15
2.3.1	Fixed bed gasification	16
2.3.2	Fluidized bed gasification	17
2.3.3	Entrained flow gasification	17
3	Theoretical background	18
3.1	Biomass gasification	18
3.2	Tar	21
3.2.1	Composition, classification, and conversion	22
3.2.2	Tar removal techniques	25
3.2.3	Sampling and analysis	26
3.3	Catalysis	28
3.3.1	Hydrodesulfurization (HDS)	30
3.3.2	Water gas shift reaction (WGSR)	32
3.3.3	Catalytic tar removal	38
3.4	Catalyst deactivation	39
3.4.1	Fouling via coking and carbon deposition	41
3.4.2	Poisoning	43

3.4.3	Thermal degradation	43
3.5	Reaction mechanisms and kinetics of the WGSR	44
3.5.1	Reaction mechanisms	44
3.5.2	Kinetic models and the power law rate model	46
3.6	Catalyst testing	47
4	The DFB steam gasification technology with particular focus on the CHP plant Oberwart	51
4.1	DFB and SER	51
4.2	CHP plant Oberwart	54
4.3	Research site Oberwart	57
5	Experimental	60
5.1	Applied catalysts	60
5.2	Test rig for chemical kinetics	62
5.2.1	Design	63
5.2.2	Experimentation	65
5.2.3	Chemical analysis	67
5.2.4	Data treatment	67
5.3	Pilot plant for catalytic wood gas processing	69
5.3.1	Design of pilot plant	69
5.3.2	Automation and visualization	77
5.3.3	Temperature control	79
5.3.4	Experimentation	83
5.3.5	Chemical analysis	86
5.3.6	Data treatment	89
5.4	Process chains for the production of pure hydrogen	90
6	Results and discussion	92
6.1	Wood gas composition CHP plant Oberwart	92
6.2	Co/Mo-based catalyst	99
6.2.1	Test rig for chemical kinetics	99
6.2.2	Pilot plant for catalytic wood gas processing	105
6.3	Fe/Cr-based catalyst	115
6.3.1	Test rig for chemical kinetics	115
6.3.2	Pilot plant for catalytic wood gas processing	120
6.4	Optimum temperature for the catalysis of the WGSR	137
7	Process chains for biohydrogen production	140
7.1	Process chain 1: WGSR - Gas scrubbing - Membrane separation - Pressure swing adsorption	141
7.2	Process chain 2: WGSR - Gas scrubbing - Pressure swing adsorption	161

8	Conclusions and outlook	199
9	Annex	204
	List of Figures	206
	List of Tables	211
	Nomenclature	214
	Bibliography	219

Chapter 1

Introduction

Since the beginning of the industrial revolution, the predominantly used energy carriers have changed with respect to their molar hydrogen to carbon ratio. In the second half of the twentieth century, liquid hydrocarbons (ratio 2/1) surpassed coal (ratio 1/2) as the most important energy carrier. Nowadays, also because of the hydraulic fracturing technology, natural gas mainly consisting of methane gains in importance. Methane with a ratio of 4/1 stands out due to low carbon dioxide emissions per energy content. This trend from solids to liquids and gases is sometimes used to predict an age of energy gases. Big complex macromolecules are replaced by smaller and simpler compounds with a more pronounced hydrogen content. Some authors consider a global hydrogen economy as the logical consequence of this historical decarbonization [31, 44].

A hydrogen based economy can meet the requirements of a modern society as far as the demand for electricity, heat and mobility are concerned. Hydrogen can also be applied as a versatile feedstock for the chemical industry. Literature provides a series of roadmaps for the establishment of a sustainable hydrogen economy in various countries [74]. According to its chief executive officer, also OMV - the biggest Austrian oil producer - sees its future in providing hydrogen [57]. Anyway, the attractive potential of hydrogen is accompanied by uncertainties related to the corresponding key technologies and costs. The development of renewable energy sources, fuel cells, storage technologies and the transportation infrastructure are important question marks over the viability of that movement. Substantial research and development breakthroughs still have to be achieved on these issues [24].

Today hydrogen production is strongly based on fossil fuels. This raises a couple of questions. How much hydrogen is required worldwide and what kind of feedstock is employed. How can hydrogen be generated based on renewables? Does lignocellulosic biomass provide a suitable feedstock? What kind of technology can be applied to produce hydrogen from wood? The introduction tries to give answers.

1.1 The importance of hydrogen

In 2010 a worldwide production capacity of approximately 110 million $\frac{m^3}{h}$ of hydrogen was installed. 50 % of this production was used for the synthesis of ammonia according to the Haber-Bosch process. 14 % was required for the synthesis of methanol. 22 % of the overall production was used for various applications in refineries such as hydrodesulfurization and hydrocracking. Furthermore hydrogen was needed in numerous reduction processes in industry [30].

The worldwide demand for hydrogen is growing because of the need to process heavier and dirtier feedstocks in refineries. More hydrogen for hydrodesulfurization processes is also required because of more stringent environmental regulations which claim the production of almost sulfur free products. In addition the evolving interest in using hydrogen as an energy carrier will result in a large hydrogen demand in the future [78].

In 2007 nearly 96 % of the overall hydrogen generation was derived directly from fossil fuels. The most frequently used feedstock was natural gas with an estimated share of 49 % among this volume. 29 % of liquid hydrocarbons were used and 18 % of the global hydrogen production was based on coal. The remaining 4 % of the total volume was generated by means of water electrolysis. LindeTM was the largest hydrogen producer worldwide, followed by Air LiquideTM, Air ProductsTM and PraxairTM[15].

About 1.4 % of the worldwide consumption of fossil energy is only required for the Haber-Bosch process, which underlines the global importance of hydrogen generation aiming at the production of inorganic fertilizer [8].

An overview of renewable production methods for hydrogen is given in Chapter 1.2.

1.2 Renewable hydrogen production

Generally, hydrogen production can be classified in three categories: electrochemical, biological and thermochemical methods. All of these methods can be realized on a renewable base. In the case of electrochemical methods, electricity must be derived from sustainable sources of energy. In the case of thermochemical methods, processing of biomass has to be carried out. At this place the term biohydrogen (BioH₂) should be defined as hydrogen either generated by biomass (see Chapter 1.2.2) or out of biomass (see Chapter 1.2.3).

1.2.1 Electrochemical methods

The most important electrochemical method is the already mentioned electrolysis of water. Driven by electricity, water molecules are broken into hydrogen and oxygen. Industrial electrolyzers operate at efficiencies of 52–85 % (calculated according to $\frac{V_{H_2} \cdot HHV_{H_2}}{P_{el}}$) strongly depending on the size and type of the apparatus [38].

Water electrolysis is the key element of power-to-gas concepts which currently enjoy great popularity. The fluctuating output of renewable electricity generated by wind power and photovoltaics creates a growing need for energy storage. As the capacity of pumped storage hydro

power stations is limited, the conversion of electricity into chemical energy by means of electrolysis represents a promising complementing technology. This explains why an increasing number of power-to-gas facilities are currently being installed. These facilities usually employ the commercially available alkaline electrolyzers. Some sites also use PEM electrolyzers for the electrolysis of water. The generated hydrogen can be stored and reconverted into electricity in times of an undersupply. The PEM fuel cell technology can be used for the reverse electricity generation. Few plants have also demonstrated the application of the generated hydrogen within a methanation process enabling the feeding of methane into the natural gas grid [38].

Photoelectrochemical methods are also subsumed under the electrochemical methods for hydrogen production. Photons are employed in photoelectrochemical cells fabricated out of semiconductors to produce hydrogen from water. The corrosion-resistant cells generally provide energy efficiencies smaller than 0.6 % [11].

1.2.2 Biological methods

Hydrogen can be produced biologically or photo-biologically by different microorganisms over a series of metabolisms. The advantages of these methods are an operation at ambient pressure and temperature as well as the usage of renewable feedstock and/or solar energy [20]. However, related work is usually carried out on a laboratory scale and the practical applications still need to be demonstrated [87]. A series of hydrogen producing metabolisms can be distinguished: Biophotolysis of water using green algae or cyanobacteria, biological water gas shift reaction, photo-fermentation, dark fermentation and hybrid systems. The biological hydrogen production is catalyzed enzymatically using hydrogen-producing enzymes, such as hydrogenase and nitrogenase. These enzymes employ active centres including complexes of iron, molybdenum or nickel. Cofactors usually contain sulfur. Dark fermentation and photo-fermentation are considered to be the most promising approaches for BioH₂ production by means of microorganisms [20, 87].

Dark fermentation is carried out in the absence of light by anaerobic bacteria but also some micro-algae. One mole of glucose can be converted fermentatively to produce two moles of acetic acid, two moles of carbon dioxide and four moles of hydrogen. The organic acids which are formed as a by product can be used in an anaerobic biogas plant for methane production [117].

Photo-fermentative hydrogen production is carried out by some photosynthetically active bacteria in an oxygen deficient atmosphere. Catalyzed by the enzyme nitrogenase, one mole of glucose can be converted into 12 moles of hydrogen and six moles of carbon dioxide [20].

It is interesting to notice that the active metals of the employed enzymes are also integral part of the industrial catalysts applied for large scale hydrogen production. Within this thesis an iron-based and a molybdenum-based catalyst were investigated.

1.2.3 Thermochemical methods

Thermochemical methods can be applied to produce hydrogen from a feedstock containing carbon and hydrogen (for example: coal, liquid or gaseous hydrocarbons). The well established industrial hydrogen production technologies (discussed later in Chapter 2.1) are based on the thermochemical processing of fossil hydrocarbons [20]. Aiming at thermochemical production of BioH_2 , thermal processing of biomass has to be carried out. This processing can be carried out non-oxidative (pyrolysis) or oxidative (gasification).

The non-oxidative processing of biomass occurs in the absence of an oxidant. It can be carried out with different sources of energy to directly break the C-H bonds. Most frequently heat is used leading to a thermal decomposition (pyrolysis) of the biomass. Plasma and radiation are investigated as alternative driving forces for the non-oxidative processing of biomass [87]. Pyrolysis of biomass is usually carried out at a temperature range of 220–700 °C. At these temperatures, biomass is decomposed irreversibly forming an incondensable and a condensable gaseous fraction as well as the pyrolysis coke (see Chapter 3.1). The incondensable fraction contains hydrogen, especially when a high heating rate of the biomass, a long residence time of the gas phase and a high decomposition temperature are applied [61]. A series of catalytically active materials have been tested on their ability for increasing the hydrogen yields of a pyrolysis process [21, 27]. Besides hydrogen, the released gaseous fraction contains methane and higher hydrocarbons. Also, carbon monoxide is formed via decarbonylation reactions in the pyrolyzed biomass. Methane and higher hydrocarbons can be steam reformed to produce additional hydrogen and carbon monoxide. Carbon monoxide can be converted according to the water gas shift reaction (WGSR) in order to produce additional hydrogen. Due to high biomass heating rates, the fluidized bed technology is considered as the most promising reactor type for hydrogen generation based on biomass pyrolysis [87].

The oxidative processing of biomass (gasification) is driven by thermal energy input and occurs in the presence of an oxidant like oxygen, steam or carbon dioxide. The most abundant feedstock for biomass gasification is solid lignocellulosic biomass including wood. A promising method for the production of hydrogen based on rather dry woody biomass is the steam gasification technology leading to the production of hydrogen-rich wood gas (see Chapter 2.3 and Chapter 4). In literature, this gaseous product is also called synthesis gas, syngas, product gas or producer gas.

If the gasification of aqueous biomass suspensions (e.g. microalgae) is desired, a promising technology seems to be the gasification in supercritical water because high drying costs of the feedstock can be avoided. Thereby at least the critical point of water at 374 °C and about 220 *bar* has to be reached. The usually applied supercritical gasification temperature ranges from 500–700 °C. Operating pressures up to 350 *bar* are reported in literature. Generally, a molar hydrogen fraction in the order of 40 vol.%_{db} and carbon monoxide contents lower than 1 vol.%_{db} can be achieved. A moisture content of the biomass of at least 35 wt.% is required for the gasification in supercritical water [79, 87].

It can be considered that the feedstock represents the major operating cost of a hydrogen facility based on thermochemical processing of biomass. In their "Survey of the Economics of Hydrogen Technologies" Padró and Putsche found that the costs of the biomass feedstock come up to about 40 % of the overall costs of hydrogen production. For the smallest facility with a capacity of 22000 $\frac{m^3}{d}$ production costs of 17.1 $\frac{\$}{GJ_{H_2}}$ were calculated (in comparison to 5–11 $\frac{\$}{GJ_{H_2}}$ based on steam methane reforming) [90]. Similar results were presented by Huisman et al. who calculated production costs in the range of 10–15 $\frac{\$}{GJ_{H_2}}$. Also in this publication, the price of the biomass was considered as the most important influence on the costs of production [59]. Current prices of wood chips are in the range of 80–90 $\frac{\$}{t_{db}}$ [32].

This PhD thesis addresses the hydrogen generation via steam gasification of solid wood. More precisely, this work is focusing on the oxidative downstream processing of wood gas by means of the catalyzed water gas shift reaction (WGSR). The WGSR is desired for two reasons. Firstly, additional hydrogen is formed increasing the product yield of the entire process. Secondly, the produced carbon dioxide can be separated more easily from the a gas stream than carbon monoxide. In a pressure swing adsorption unit, CO₂ can be removed more efficiently because the adsorption of carbon monoxide on activated charcoal is inferior to the adsorption of carbon dioxide [105]. CO₂ can also be removed efficiently in gas scrubbers operated with water, aqueous solutions of ethanolamines [60], methanol (RectisolTM scrubber), or dimethyl ethers of polyethylene glycol (SelexolTM scrubber) [78].

1.3 Aim of this work

The dual fluidized bed (DFB) steam gasification technology was developed at Vienna University of Technology. Based on a carbon containing feedstock, a gas mixture rich in hydrogen and carbon monoxide and low in nitrogen is generated. This technology (described in Chapter 4) is commercially available for the gasification of wood chips and pellets. The generated wood gas can be used to carry out a series of chemical syntheses based on the contained hydrogen and carbon monoxide (synthesis gas or syngas). It also provides an interesting feedstock for the production of pure hydrogen.

The aim of this work was to investigate the sulfur resistant catalysis of the water gas shift reaction (WGSR) in wood gas. This technology is interesting for the adjustment of the appropriate H₂/CO ratio for the chemical synthesis of methane, Fischer-Tropsch diesel, dimethyl ether, methanol or mixed alcohols. Above all it represents an important unit operation toward hydrogen production based on lignocellulosic biomass.

More precisely, two commercially available catalysts with different formulations (Catalyst 1: Co/Mo-based, Catalyst 2: Fe/Cr-based) should be investigated. The catalysis of the WGSR should be carried out on two different scales. Two different experimental setups should be applied.

On the one hand, both catalysts should be exposed to synthetic gas mixtures simulating the wood gas composition. Therefore, a laboratory device ("Test rig for chemical kinetics") was used to carry out experiments on a 50 $\frac{L_n}{h}$ scale. The aim was to describe the chemical

kinetics of the catalyzed reaction by means of establishing empirical power law rate models for both catalysts. Also, the influence of sulfur on the catalyst activity should be investigated. Based on the experimentation at this test rig, the basic operation parameters (Gas hourly space velocity, temperature, steam to dry gas ratio) should be defined in order to enable a proper design of a pilot plant which can be used for the processing of real wood gas.

On the other hand, the catalysts should be exposed to real wood gas derived from the commercial DFB steam gasification power plant in Oberwart, Austria. Therefore, a pilot plant with a capacity of about $2000 \frac{L_n}{h}$ should be designed, assembled, commissioned and optimized for its long-term operation. At this "Pilot plant for catalytic wood gas processing" a parameter study with both catalysts should be carried out. Also, their long term stability should be demonstrated. Besides the catalysis of the WGSR, catalytic side effects on sulfur components and tar components should be studied. A mathematical model should be implemented in order to optimize the applied temperature of reaction in the pilot plant.

Furthermore, it was desired to demonstrate the integration of this catalysis unit into process chains aiming at the production of pure hydrogen based on wood gasification. In cooperation with other research projects, different configurations should be realized involving also a gas scrubbing unit, a membrane separation unit and a pressure swing adsorption unit. In order to demonstrate the high purity of the product, a polymer electrolyte membrane (PEM) fuel cell should be operated with the generated BioH₂.

Chapter 2

State of the art

This chapter provides the state of the art technology of the industrial processes related to this work. First of all, the basic principles of large scale hydrogen production based on steam reforming, partial oxidation, and autothermal reforming are described. Also, the mature process for hydrogen production based on natural gas is described and the production of hydrogen based on coal is discussed. Both technologies involve the catalysis of the WGSR which is described subsequently. Finally, this chapter gives an overview of the state of the art of the biomass gasification technology which provides the basis for hydrogen production within this work.

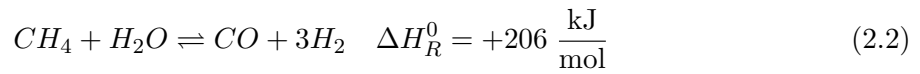
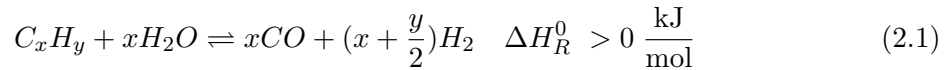
2.1 Industrial processes for hydrogen production

Large scale hydrogen production is predominately based on reforming of gaseous, liquid, or solid hydrocarbons (C_xH_y). In a first step, synthesis gas is generated in a process which usually involves the presence of a catalyst, high temperatures, and the addition of a reforming agent. Depending on whether H_2O or O_2 or a mixture of both is used as an agent, it can be distinguished between steam reforming (Chapter 2.1.1), partial oxidation (Chapter 2.1.2) and autothermal reforming (Chapter 2.1.3). Another process which did not reach a commercial status yet is the dry reforming technology using CO_2 as a reforming agent. This technology should not be discussed here. Depending on the feedstock and the reforming agent, the molar ratio of $\frac{H_2}{CO}$ in the synthesis gas varies from 1–5. In order to generate pure H_2 , this gas mixture has to be subjected to several downstream processes [78].

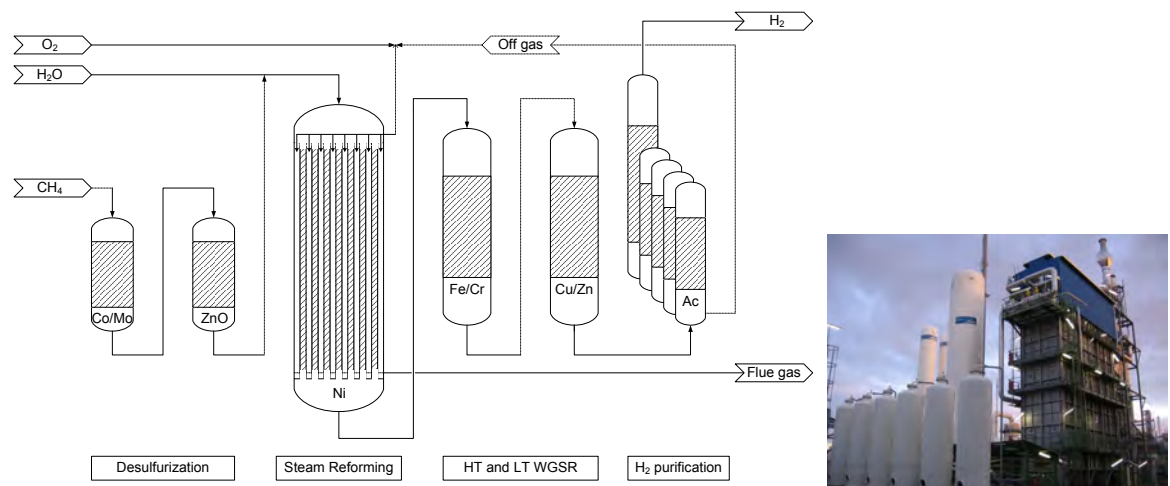
2.1.1 Steam reforming

The general steam reforming reaction of hydrocarbons (C_xH_y) is given in Equation 2.1. Among these reactions, the most important reaction is steam reforming of methane (also steam methane reforming (SMR), see Equation 2.2). Natural gas mainly consisting of

methane is the most important feedstock for the large scale production of hydrogen.



Additional hydrogen molecules are extracted from water which leads to the generation of a synthesis gas with a high molar ratio of $\frac{H_2}{CO}$. The steam reforming reaction is strongly endothermic and usually catalyzed with supported nickel catalysts. Noble metal catalysts (Pt, Pd, Ir, Rh, Ru) are sometimes used because of a high degree of coking resistance and very high activities. However, high costs are limiting the application of these catalysts. Heat from combustion is required in order to provide the desired reaction temperature of 800–1000 °C. In a steam reformer, the catalyst is usually placed in reactor tubes which themselves are located in a combustion chamber. Additional fuel is burned outside the reactor tubes which can be seen as an allothermal heat supply for the endothermic reaction. The reaction leads to a volume expansion hence it is thermodynamically favoured at low pressures. Nevertheless the usual operating pressure is 20–40 bar which enables a more compact reactor design and the direct downstream operation of a pressure swing adsorption unit for hydrogen purification. Excess steam is added (steam to carbon ratios of 2.5–3) in order to provide favorable equilibrium conditions and to reduce the risk of carbon deposition on the catalyst surface. Besides the actual reforming reaction, a series of chemical reactions are occurring in a steam reformer. These reactions are also encountered in biomass gasification and are therefore presented in Chapter 3.1. Steam methane reforming is a well developed technology. Besides methane also gaseous hydrocarbons, liquid hydrocarbons and alcohols can be used as a feed [78].



(a) Basic flowchart of the industrial hydrogen production based on steam methane reforming (SMR) of natural gas ; high temperature (HT), low temperature (LT), activated carbon (Ac); based on [78]. (b) Picture of an industrial PSA system (left), [30]

Figure 2.1: Hydrogen production based on steam methane reforming (SMR).

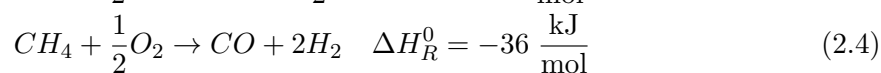
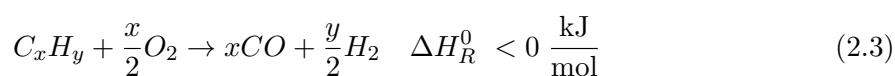
Figure 2.1 (a) shows a typical flowchart of an industrial hydrogen production facility based on SMR. In Figure 2.1 (b) a picture shows the core elements of a corresponding plant. It can be seen that the generation of hydrogen via SMR is usually a four step process involving the desulfurization of the feed, the reforming step, the catalysis of the WGSR (see Chapter 2.2 and Chapter 3.3.2) and the purification of hydrogen.

Desulfurization is mainly applied in order to avoid catalyst deactivation during downstream processing. It includes the conversion of organic sulfur components to H₂S in a hydrodesulfurization (HDS, see Chapter 3.3.1) stage and the subsequent removal of H₂S. Downstream the steam reformer, the gas mixture is cooled down and the generated CO is converted according to the WGSR forming additional H₂ as well as CO₂. As described later, the catalysis of the WGSR is usually a two step process. CO is a strong poison for the catalysts applied for the synthesis of ammonia. Small amounts of residual CO downstream the shift converters are sometimes removed by means of the catalysis of the methanation reaction (reverse reaction of Equation 2.2) which consumes hydrogen. If a high quality of the product is required, hydrogen purification is usually carried out by means of the pressure swing adsorption (PSA) technology. Alternatively, also CO₂ scrubbing in different solvents can be applied. The off gas of the hydrogen purification step is usually burned in the steam reformer to provide the required reaction temperature [78].

Steam gasification of coal or biomass can be regarded as steam reforming of solid hydrocarbons. At Vienna University of Technology, both process were demonstrated [64]. However, large scale coal gasification aiming at the production of hydrogen is rather carried out with pure oxygen as a gasification agent (see Chapter 2.1.2).

2.1.2 Partial oxidation and catalytic partial oxidation

The production of synthesis gas based on partial oxidation or catalytic partial oxidation of hydrocarbons share the same fundamental reaction in Equation 2.3. In contrast to steam reforming of hydrocarbons, the partial oxidation reactions are exothermic. Equation 2.4 shows the partial oxidation reaction of methane.



The exothermic partial oxidation (POX) reaction can be carried out in the absence of a catalyst at high temperatures and high pressures (homogeneous POX). Generally, pure O₂ is used to avoid a dilution of the synthesis gas with N₂ and thereby facilitate the downstream processing. Large scale homogeneous POX reactors are usually operated at 1150–1500 °C and pressures between 25 and 80 *bar*. The reactors are more compact than allothermal steam reformers and can be operated with a broad variety of feedstock. Anyway, lower efficiencies are reported because of the high operating temperatures that require burning of additional fuel. Steam might be added to the feed to reduce the risk of soot formation.

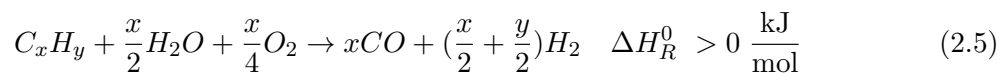
In order to enhance feed conversion rates, the catalytic partial oxidation technology was developed. Compared to the uncatalyzed POX it allows higher gas hourly space velocities and lower reaction temperatures in the range of 750–1150 °C. Catalysis is usually carried out in a fixed bed over first row transition metals (Ni, Co, and Fe) or noble metals (Ru, Rh, Pd, Pt, and Ir) which again show a reduced risk of carbon formation.

Coal gasification with pure oxygen can be regarded as the partial oxidation of a solid hydrocarbon. Basically, coal gasification can be carried out with O₂, H₂O, or CO₂ as a gasification agent. Large scale industrial hydrogen plants based on coal gasification usually employ pure oxygen as gasification agent. The theory behind coal gasification is basically similar to the theoretical background of the gasification of biomass and will be discussed in Chapter 3.1. The generated gas mixture is mainly composed of CO, H₂, and CO₂. At rather low operating temperatures also considerable contents of CH₄ can be present. A series of different coal gasification systems were installed including fixed bed, fluidized bed and entrained flow reactors operating at temperatures ranging from 870–2000 °C. The large scale coal gasification plants usually employ entrained flow reactors fed with dry pulverized coal (Shell gasification technology) or a coal-water slurry (GE gasification technology). Pure O₂ used as a gasification agent results in high temperatures allowing to discharge ash in the liquid state. Downstream the gasifier the synthesis gas with the liquid slag is quenched in water. Slag is solidified and separated from the gasifier. Quenching also leads to the water saturation of the synthesis gas what provides an ideal precondition for the catalysis of the WGSR. Strongly depending on the sulfur content of the feedstock, either sulfur is removed upstream to the catalysis of the WGSR ("sweet shift") or sulfur is removed downstream the catalysis of the WGSR ("sour shift"). Processing aiming at the production of pure hydrogen is basically similar to hydrogen production based on SMR [78].

Besides the production of hydrogen for the synthesis of ammonia, the coal gas mixture can be further processed and used for the synthesis of methanol or Fischer-Tropsch products. This coal to liquid approach is mainly followed in South Africa (by the company SasolTM) with its limited access to crude oil during the Apartheid regime. Also, coal gasification aiming at electricity generation was realized on a demonstration scale. The so called integrated gasification combined cycle (IGCC) technology employs a combined cycle consisting of a gas turbine and a steam process. In contrast to the reforming of gaseous hydrocarbons, sulfur removal from the feed can only be achieved in the gaseous phase downstream the coal gasifier. Currently, the biggest coal gasifier installed within an IGCC plant has a capacity of 2400 tons of coal per day [78].

2.1.3 Autothermal reforming

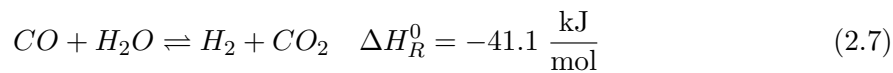
Applying the autothermal reforming technology (ATR) steam reforming can also be carried out in a single reaction chamber .



Thereby oxygen is directly added to the reformer burning a partial fraction of the feed which leads to an in situ generation of the required process heat. No external heat source and no heat exchangers are required which lowers the capital costs. ATR is carried out at temperatures in the range of 900–1150 °C and pressures up to 80 *bar*. This technology allows a more compact reactor design than the conventional allothermal steam reforming. It is especially desired for chemical syntheses requiring a $\frac{H_2}{CO}$ ratio of 2. This ratio is desired for the Fischer Tropsch synthesis as well as the methanol synthesis. The ATR technology requires the catalysis of the combustion reaction as well as the steam reforming reaction. This can be achieved within one catalyst bed or within a two staged system [78].

2.2 Industrial catalysis of the water gas shift reaction (WGSR)

The industrial hydrogen production processes based on steam reforming, catalytic partial oxidation or coal gasification usually involve catalysis of the WGSR in Equation 3.5.



Catalysis of the WGSR is mostly carried out in a two stage system with a desulfurized feed ("sweet shift"). Initially, a high temperature (HT) stage with a Fe/Cr-based catalyst is employed. The inlet temperature of this adiabatic fixed bed reactor is usually set to 350–400 °C. The exothermic WGSR leads to a temperature increase toward the exit of the fixed bed reactor. It is operated at pressures ranging from atmospheric pressure up to 80 *bar* and feed gases containing 3–75 vol.% of CO. The HT WGSR can be carried out in a wide range of steam to dry gas ratios. Usually CO concentrations of 2–4 vol.%_{db} can be achieved at outlet. Downstream the HT stage, the gas mixture is cooled down and introduced into a low temperature (LT) stage employing a Cu/Zn-based catalyst. This more active catalyst enables inlet temperatures as low as 200 °C representing favourable equilibrium conditions for high CO conversion rates. CO concentrations of 0.1–0.3 vol.% can be achieved at the outlet of the LT stage [111]. Both stages are usually designed as downflow reactors. An effective gas distribution and gas collection system should be installed at the converter inlet and outlet to ensure a good gas distribution and a low pressure drop over the catalyst bed. Therefore, aluminium oxide in the form of fused alumina or aluminium balls is usually employed. Both reactors should be provided with thermocouple sheaths to monitor the temperature gradients during activation and operation. H₂S is usually produced during the activation period of the HT catalysts.

The LT shift reactor is equipped with a bypass which is used during this activation

procedure in order to avoid sulfur poisoning of the LT catalyst. Nitrogen supply is required for the start up, shut down and emergency vent of the system. A positive nitrogen pressure is required during maintenance when the vessels are opened to the ambient in order to avoid an oxidation of the reduced catalyst. A typical arrangement of a WGS converter is illustrated in Figure 2.2[111].

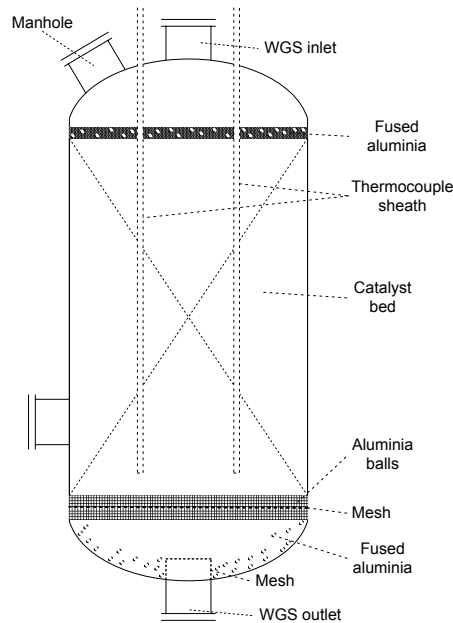


Figure 2.2: Typical arrangement of an industrial WGS converter; based on [111].

2.3 Biomass gasification

Nowadays biomass gasification is mostly used within decentral cogeneration systems aiming at the simultaneous production of electricity and heat. These plants are also called combined heat and power (CHP) plants. However, considerable research activities are carried out worldwide in order to go one step further toward polygeneration concepts. Within this work polygeneration is defined as the simultaneous production of biofuels or chemicals, heat, and electricity. Synthesis gas produced by biomass gasification can be used to synthesize a broad range of valuable components such as synthetic natural gas (SNG), methanol, mixed alcohols, dimethyl ether, and Fischer Tropsch diesel and kerosine. A review of the state of the art of these approaches is provided in [97].

Various gasification technologies for solid biomass are available. Basically, the established systems differ in the type of heat supply and the employed gasification agent. An autothermal heat supply is achieved by a partial in situ combustion of biomass using air or oxygen. An allothermal heat supply is achieved with an external heat transfer medium. O_2 , H_2O , or CO_2 can be used as gasification agents. If air is used as a gasification agent the generated gas is diluted with N_2 decreasing its heating value and its suitability for downstream applications

[61]. Different construction types of biomass gasifiers have been developed during the last

Advanced Review

These reactor types are schematically illustrated in Figure 2.3.

wires.wiley.com/wene

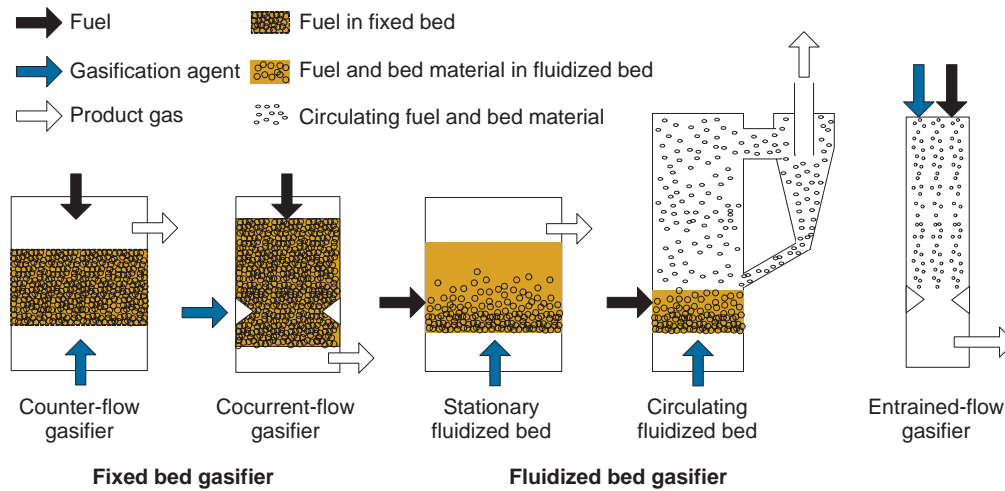


FIGURE 1. Different types of gasifiers.

Figure 2.3: Different reactor types of biomass gasifiers; reprint with permission from [97].

- Type of reactor: fixed bed-fluidized bed-entrained flow
- Type of gasification agent: oxygen-steam and entrained flow reactors

Allothermal-Autothermal

Autothermal gasification is the direct heating of the reaction by means of partial oxidation within the gasification reactor. If air is used as oxidizing agent during the process, the product gas contains a high amount of nitrogen. Biomass provides for homogeneous conditions on the field of thermal biomass gasification facilities are plotted and classified with respect to the applied technology (CHP syn-

of the advantages over autothermal gasification processes. Another important advantage is the distinguished between fixed bed fluidized beds no problematic waste produced. All carbon containing streams from the product gas cleaning (e.g., dust, tars) can be recycled to the combustion zone and there enables the production of a gas which is very low in tar components, which is used for the gasification reactions.⁵ Selection criteria for the type of gasifier are the scale, the type of biomass and the application of the generated gas.

Fixed Bed-Fluidized Bed-Entrained Flow

The International Energy Agency (IEA Bioenergy, Task 33, Thermal Gasification of Biomass) provides for homogeneous conditions on the field of thermal biomass gasification facilities are plotted and classified with respect to the applied technology (CHP syn-). The composition of the gas and the level of undesirable components (tar, dust, ash content) produced during biomass gasification process are dependent on many factors such as feedstock composition, reactor type, and operating parameters (temperature, pressure, oxygen fuel ratio).

thesis, green), the type (pilot, demo, commercial) construction, operational etc.). Additional information usually includes the type of gasifier, the type of biomass, the thermal energy input, and the output to operate it under pressurized conditions.

Allothermal (or indirect) gasification is characterized by the separation of the processes of heat production and heat consumption.⁴ The allothermal gasification facility almost always consists of two reactors, one heated by direct energy of the biomass gasified

2.3.1 Fixed bed gasification
In fixed bed reactors, the gas velocities are not high enough to move the particles. Depending on the flow direction of the solid biomass and the gasification agent it can be distinguished between counter-flow reactors and cocurrent-flow reactors. Small scale fixed bed gasifiers usually operate with air as a gasification agent and an autothermal heat supply by means of spin-off the heat from the biomass by the generated gas. Dinitrogen contains large amount of nitrogen products (CO₂, H₂O) are in the product gas and take part in the chemical reactions, mainly in water-gas shift reaction.

Oxygen Blown-Steam Blown

Typical composition of a dry gas produced during the biomass gasification process is shown in Table 1. As can be seen, the concentration of the gas compounds during oxygen and steam gasification is completely different. On the other hand, higher amount of hydrogen in the product gas can be found during the steam gasification. The hydrogen found in the product gas

which is inappropriate for synthesis applications [61]. Allothermal gasifiers generally produce two gas streams: a medium calorific product gas (gasification reactor) with little or no nitrogen and a flue gas (combustion reactor). The production of an N₂-free gas without the need of pure oxygen is one

2.3.2 Fluidized bed gasification

If gas velocities are increased, a stationary fluidized bed is formed which requires the addition of a stabilizing bed material (for example sand). A further increase leads to the release of solids out of the reactor. The particles can be recirculated by means of a cyclone forming a circulating fluidized bed. High turbulence in the fluidized bed leads to homogeneous reaction conditions and temperatures in the bed. No reaction zones are formed enabling an accurate process control as well as good upscale conditions. Instead of quartz sand, also a catalytically active bed material can be used in order to enhance the gasification reactions as well as the tar conversion reactions in the gas. Compared to the stationary fluidized bed, the circulating fluidized bed enables a higher fuel load per cross-sectional area and therefore a more compact design [61].

In Värnamo, Sweden a plant with a total fuel input of 18 MW_{th} was built which demonstrated for the first the IGCC technology based on biomass gasification. The facility delivered 6 MW of electricity and 9 MW of district heat. Biomass gasification was achieved in a circulating fluidized bed gasifier operated with a mixture of oxygen and steam as a gasification agent. In 2000 the operation of the demonstration plant was stopped because of economic reasons [108].

The dual fluidized bed (DFB) steam gasification is a special form of the fluidized bed technology with an allothermal heat supply. It is currently employed commercially in Güssing (AT), Oberwart (AT), Senden (DE), and Gothenburg (SE). The process is described in detail in Chapter 4. Aiming at the production of BioH_2 , this type of gasifier seems to be an appropriate technology as it is generating a gas mixture rich in hydrogen (40%) and low in nitrogen (1–2%). The hydrogen content of generated wood gas can be further increased by means of the operation of the sorption enhanced reforming (SER) concept in a DFB gasifier. This technology is also discussed in Chapter 4.

2.3.3 Entrained flow gasification

Entrained flow reactors are mostly used for the gasification of coal. For the gasification of biomass this technology did not reach a commercial status yet. Entrained flow gasification of biomass is described well in [46].

On a demonstration scale, entrained flow gasification of biomass is carried out within the *bioliq*[®] project. This project was launched in 2005 by the Karlsruhe Institute of Technology (KIT) and several industrial partners. It involves the pyrolysis of biomass (2 MW scale), the pressurized entrained flow gasification of this pyrolysis oil (5 MW scale), gas cleaning of the synthesis gas, synthesis of dimethyl ether (DME), and synthesis of Fischer Tropsch products based on DME. The gasifier is realized according to the Lurgi Multi-Purpose-Gasification concept. O_2 is used as a gasification agent and ash is removed in the liquid state as slag. High temperatures in the gasifier result in the generation of a synthesis gas free from tar components and low in methane. The gasifier is designed for pressures up to 80 bar , which avoids an energy intensive compression upstream the pressurized synthesis reactors [67].

Chapter 3

Theoretical background

The aim of this chapter is to cover the theoretical background with respect to this work. First of all, the mechanisms of biomass gasification and the generation of wood gas should be explained. To a high degree the application of wood gas is limited by the presence of tar components. Section 3.2 therefore aims to define this term and to explain the mechanisms of tar formation, tar conversion as well as the applied tar removal techniques. Finally, the theoretical aspects with respect to catalysis, catalyst deactivation, and catalyst testing are discussed.

3.1 Biomass gasification

Generally, thermochemical conversion of wood via gasification or combustion is very similar. Combustion of biomass can be regarded as a complete oxidation of the contained carbon and hydrogen. It usually proceeds in the presence of a stoichiometric surplus of oxygen. Flue gas mainly containing of CO_2 and H_2O is formed and large amounts of heat are released. As opposed to combustion, gasification of biomass can be seen as an incomplete oxidation of combustibles in the presence of an oxygen containing gasification agent (O_2 , H_2O , or CO_2). The process leads to the formation of a combustible gas mixture. This gas can be referred to as product gas, producer gas, syngas, or synthesis gas. The rather old term “wood gas” was chosen within this work. It was regarded as the most representative term as gasified wood was the applied feedstock for experimentation. The thermochemical conversion of a wet wood particle as a function of time and temperature is illustrated in Figure 3.1. In that case, a hypostoichiometric oxygen addition (air-fuel equivalence ratio <1) does not allow a complete oxidation of the gas phase what results in the generation of wood gas. Under these conditions, three stages of thermochemical conversion can be distinguished: Drying, devolatilization, and gasification. The stages take place one after the other at distinct temperature ranges. If no gasification agent is added, the thermochemical conversion only involves the drying process and the devolatilization step. The technical process of heating organic material in the absence of a gasification agent is termed pyrolysis [61].

Figure 3.1 shows that if a wood specimen is exposed to elevating temperatures the first

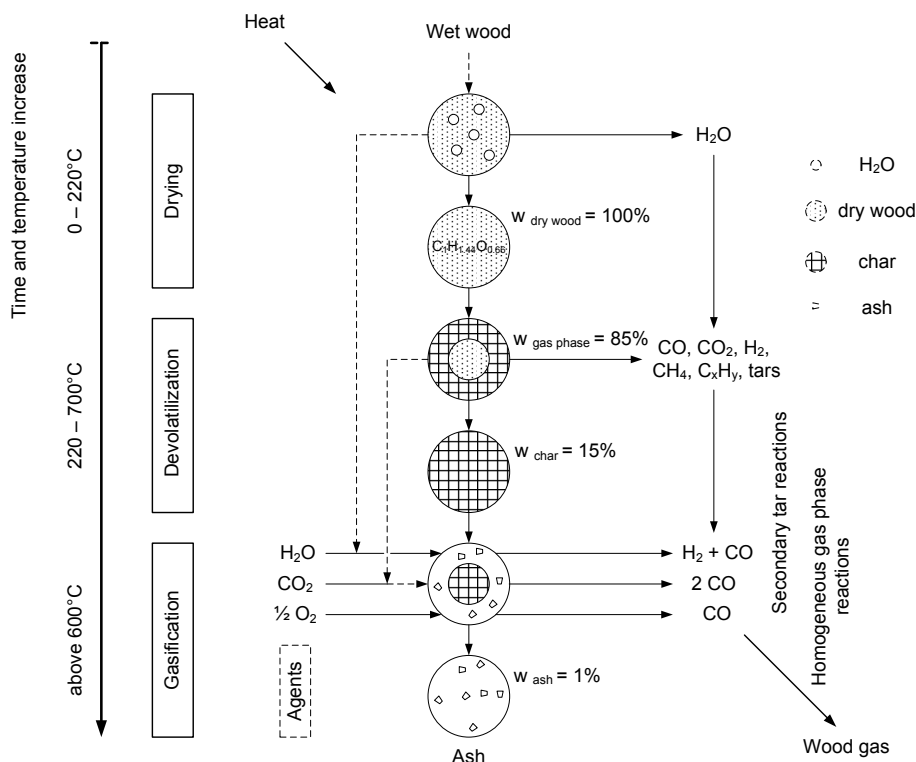


Figure 3.1: Thermal conversion of a wood particle; based on [61].

thing to occur is a drying process. Wood drying starts with the evaporation of free water and continues with the removal of adsorbed water leading to the mechanical deformation of the particle. At approximately 220 °C the water evaporation is completed [61].

The absence of water allows a further increase in temperature, which is accompanied by the release of volatile components (devolatilization). Volatiles are generated which can be classified into a condensable (pyrolysis oil, bio oil, tar) and an incondensable gaseous phase (pyrolysis gas). The devolatilization is called pyrolysis if it occurs in the absence of a gasification agent. The condensable fraction is composed of H₂O and a chemically very heterogeneous group of organic compounds (tar, see Chapter 3.2). The incondensable fraction consists mainly of CO, H₂, CO₂, CH₄, C₂H₄ and C₂H₆. Solid charcoal mainly composed of elementary carbon is formed as a residue of this process. Devolatilization occurs almost independently from the surrounding atmosphere as the released volatiles are avoiding a contact with charcoal. In the first stage of the pyrolytic decomposition between 220–280 °C mainly CO₂, formic acid and acetic acid are formed in endothermic processes. Between 280–500 °C exothermic reactions occur and flammable gases including CO, H₂, CH₄, methanol and formaldehyde are released. At higher temperatures mainly CO and H₂ are formed in endothermic reactions. Regarding the effect of temperature on the different wood components, the unstable hemicelluloses are predominately decomposed at temperatures ranging from 250–320 °C. The more stable celluloses are decomposed at a temperature range from 320–400 °C. The solid residue of the devolatilization process is mainly composed of carbon derived from the decomposition of lignin as the most stable wood component. Still 50 %

of the initial mass of lignin remains at a temperature of 500 °C. At approximately 700 °C the thermal decomposition of wood in the absence of a gasification agent is terminated. The main operating parameters of this process are the heating rate, the residence time and the temperature. These factors strongly affect the yield of each pyrolysis fraction (pyrolysis gas, pyrolysis oil, and charcoal) as well as its composition [61].

Thermogravimetric analysis (TGA) provides a good technique for the investigation of the devolatilization of a biomass sample. Figure 3.2 illustrates a typical graph obtained by TGA of dry wood.

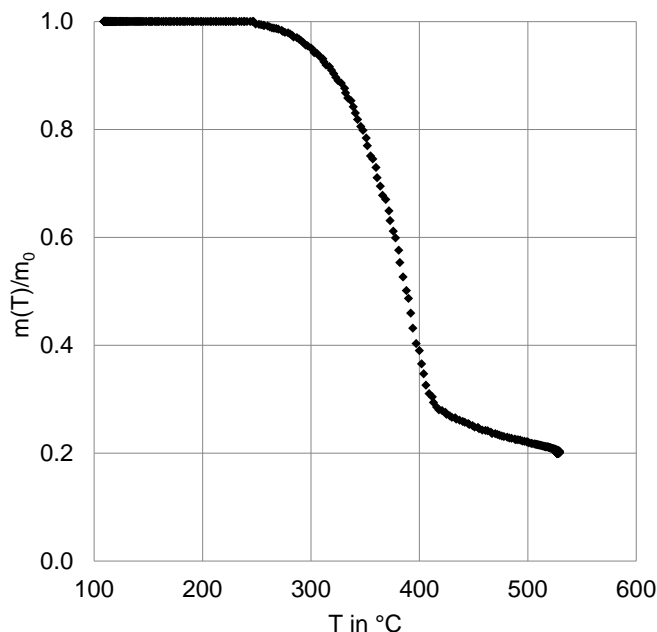


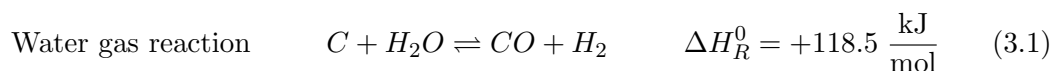
Figure 3.2: Thermogravimetric analysis (TGA) of maritime pine *Pinus Pinaster* in N₂ atmosphere; heating rate 0.4 $\frac{^{\circ}\text{C}}{\text{s}}$; m(T) mass as a function of temperature; m₀ initial mass of dry specimen; printed with permission from [81].

In Figure 3.2 devolatilization starts at about 250 °C with the decomposition of hemicelluloses. The main mass reduction occurs in a temperature range from 300–400 °C which basically represents the range of decomposition of celluloses as the most important wood component (40–50 wt.% in the dry wood). At higher temperatures mainly the more stable lignin is decomposed and charcoal is formed. At the same time mass reduction decreases significantly [61].

If an oxidizing agent is present, residual charcoal derived from devolatilization is subsequently affected by the process of gasification. Gasification can only occur if the release of volatile matter is terminated allowing the contact of charcoal with the oxygen containing gasification agent. Depending on the present agent (O₂, H₂O, or CO₂), the gasification reactions can be exothermic or endothermic. The net heat balance of the steam gasification technology is endothermic requiring an autothermal or an allothermal heat supply. If no gasification agents are added, a partial gasification with reactants derived from drying or pyrolysis is possible (see Figure 3.1). Generally, at least 600 °C are required for the gasification of solid

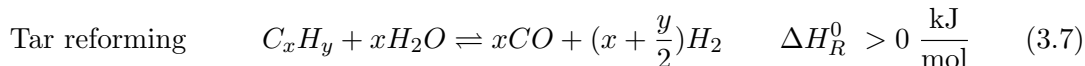
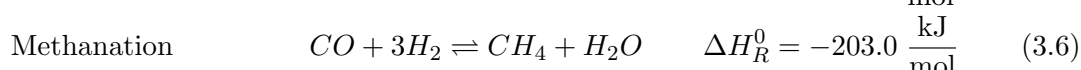
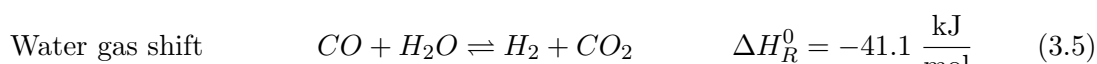
carbon. The most important gasification reactions are listed below (Equations 3.1–3.4).

Heterogenous gasification reactions



The gaseous products of pyrolysis and gasification subsequently undergo several homogeneous gas phase reactions which can be catalyzed by charcoal or the presence of a catalytically active bed material. The most important gas-gas reactions are listed in Equations 3.5–3.7.

Homogenous gas phase reactions



The equilibrium of the reactions 3.5–3.7 is strongly affected by the operating temperature. The equilibrium of the Equations 3.6 and 3.7 is also influenced by the operating pressure.

3.2 Tar

”Tar“ is primarily produced as a consequence of the thermal biomass decomposition during the devolatilization stage (see Figure 3.1). Many different definitions of ”tar“ can be found in literature. In [61] tar is defined as all organics boiling at temperatures above that of benzene. In [40] tar is referred to as the condensable fraction of the volatiles released during pyrolysis. Maybe the most deliberate definition with respect to thermal biomass gasification is the one presented by T.A. Milne in 1998 [82].

“The organics, produced under thermal or partial-oxidation regimes (gasification) of any organic material, are called “tar” and are generally assumed to be largely aromatic.”

Each work covering ”tar“ should define exactly what substances are considered as tar components. Additionally, the author is requested to document thoroughly the methods of tar sampling and analysis [82].

In principle the quoted definition includes benzene, toluene and xylene (BTX) . Within this work, the BTX components were analyzed by means of a different analytical method than the higher tar components. The term ”tar“ is therefore defined as:

“The mixture of cyclic and polycyclic mostly aromatic compounds with a molar mass higher than benzene, toluene and xylene (BTX).”

Depending of the usage of the wood gas (combustion in a boiler, combustion in gas engines, gas turbines, hydrogen fuel production, fuel cells, and chemical synthesis) it is very important to achieve the desired gas composition as far as the tar content and composition is concerned. A series of contaminant constraints are stated in literature. However, very few well defined and long term data related to tar tolerance of the different energy conversion techniques can be found [82].

Biomass tar is also defined in the European Prestandard CEN/TS 15439:2006 (D) [3]. The document provides technical specification for the analysis of gravimetric tar, the applied solvents, the equipment, sampling and sample preparation, and the determination of single tar components and particles.

3.2.1 Composition, classification, and conversion

A very broad range of tar components can be encountered in wood gas derived from biomass gasification. This enormous chemical diversity can be explained by the heterogeneity of wood (composed of cellulose, hemicellulose, and lignin) as well as its low thermal conductivity, which inhibits isothermal pyrolysis of one particle. Additionally, tar is very reactive and undergoes secondary reactions in the gaseous phase [61].

The following list states the most frequently encountered organic components produced during biomass gasification. The components are structured according to their substance class [3]. Not all of these substances can be considered as tar according to the already stated tar definition within this work.

- **Acids**
formic acid, propionic acid, butyric acid, acetic acid.
- **Sugars**
levoglucosan, alpha-D-glucose, beta-D-fructose, cellobiosan.
- **Alcohols**
methanol, ethanol.
- **Phenols**
phenol, cresols (o,m or p), xylenols.
- **Aldehydes and ketones**
formaldehyde, acetaldehyde, acetone, 2-cyclopenten-1-one, methyl-2-cyclopentene-1-one.
- **Guaiacoles**
guaiacol, cresol, ethylguajacol, eugenol, isoeugenol.

- **Furans**

benzofuran, methylbenzofurane, dimethylbenzofurane, dibenzofuran, dimethylfuran, furfural, methylfurfural, furfuryl alcohol, (methyl-or dimethyl-) benzofurans and dibenzofurans.

- **Mixed oxygen-rich (saturated) compounds**

hydroxyacetaldehyde, hydroxyacetone, vanillin, glyoxal, (di-,tri-) methoxybenzene, timethoxyphenole.

- **Aromatic compounds**

benzene, toluene, xylene (o,m and p), ethylbenzene, styrene, indene (1H-indene), methyl indene.

- **Polycyclic aromatic hydrocarbons (PAH)**

naphthalene, (1- or 2-) methylnaphthalene, diphenyl, acenaphthylene, acenaphthene, fluorene, phenanthrene, anthracene, fluoranthene, pyrene, benzo(a,b,c)fluorene, benzo(a)anthracene, chrysene, benzo(b,j,k)fluoranthene, benzo(a,e)pyrene, dibenzo(a,h)anthracene, perylene indeno(1,2,3-cd)pyrene, benzo(g,h,i)perylene, dibenzopyrenes, anthanthren, coronene.

- **Nitrogen-containing aromatic hydrocarbons**

pyridine, methylpyridines, pikoline, (iso-)chinonolin.

Evans and Milne [34] suggested a classification of these components into four major fractions: primary, secondary, tertiary, and condensed tertiary tar. A detailed list of typical tar components with respect to these fractions is presented in [82].

- **Primary products**

cellulose- and hemicellulose-derived decomposition products such as levoglucosan, glycolaldehyde, and furfurals; and lignin-derived methoxyphenols (mequinol, guaiacol, eugenol)

- **Secondary products**

phenolics and olefins

- **Tertiary products**

methyl/alkyl derivatives of aromatics (methyl acenaphthylene, methylnaphthalene, toluene, and indene).

- **Condensed tertiary products**

benzene and polycyclic aromatic hydrocarbons (PAH) without substituents (naphthalene, acenaphthylene, anthracene/phenanthrene, pyrene)

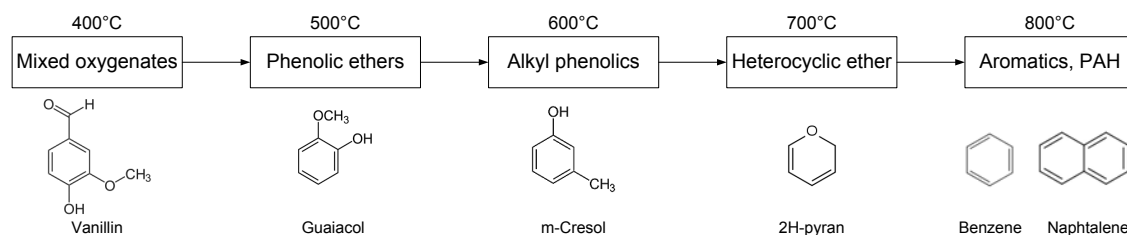


Figure 3.3: Tar conversion as a function of temperature, based on [33].

Tar components are generated and transformed as a function of the pyrolysis temperature. This procedure is illustrated in Figure 3.3, also providing corresponding sample substances of tar.

Tar transformation of the primary tar components occurs as a result of dehydration, decarbonylation, and decarboxylation reactions. Besides, free radical processes in the gas phase can lead to the formation of aromatics [82, 61]. At higher temperatures primary tar thermally cracks to produce CO, H₂ and other light gases. However, this reduction is not true for the aromatic tertiary tar products which tend to grow in molecular weight with increasing temperatures. This resulting fraction of condensed aromatics is highly refractory and more resistant to catalytic downstream processing of the gas. The tertiary tar components are also less susceptible to oxidation by O₂ or H₂O. This results in a trade-off regarding the optimum gasification temperature [82]. Basically, the same trend of tar conversion was also observed by Wolfesberger [116] reviewing numerous DFB steam gasification experiments at the Vienna University of Technology with respect to the tar content in the generated producer gas. It was demonstrated that the relative content of tertiary tar (mainly naphthalene) is significantly rising with the gasification temperature and pressure. At the same time, the primary and secondary tar components (phenols, furans) were mostly declining [116].

With respect to the construction type of the gasifier, it can be considered that cocurrent (downdraft) fixed bed gasifiers provide the cleanest gas and counter-flow (updraft) fixed bed reactors provide wood gas rich in tar. Fluidized bed reactors typically show an intermediate tar level. The corresponding tar contents differ in one order of magnitude. As a very gross simplification, counter-flow reactors are generating wood gas with a tar content of $100 \frac{g}{m_n^3}$, fluidized bed systems provide a tar content of about $10 \frac{g}{m_n^3}$, and cocurrent wood gasifiers a tar content of about $1 \frac{g}{m_n^3}$ [82].

Milne and Evans [82] provide a literature review of common tar contents in oxygen or steam-blown gasifiers which are generally given in $\frac{g}{m_n^3}$ or wt.% of the feed. The tar content in fluidized bed reactors varies between 0.5 and 50 $\frac{g}{m_n^3}$ (0.5–15 wt.% of the feed) strongly depending on the reaction parameters. Besides the type of gasifier and the gasification agent, relevant reaction parameters determining the amount of tar in the generated wood gas are:

- Type of biomass (including composition and feed preparation like torrefaction)
- Particle size range and distribution

- Water content
- Residence time at a specific temperature
- Reactor geometry
- Degree of fluidization in a fluidized bed
- Point of introduction of the feed into a fluidized bed reactor
- Gas distribution in fixed beds (channelling)
- Presence of a catalyst

Typical tar components contained in wood gas derived from steam gasification are: naphthalene, acenaphthylene, fluorene, phenanthrene, benzaldehyde, phenols, benz[a]anthracene, fluoranthene, pyrene, and benzopyrene [33]. Finally, the measured "tar content" depends strongly on the applied method of tar sampling and analysis which necessitates an accurate definition of the applied experimental method [82].

3.2.2 Tar removal techniques

On the one hand, tar generation can be influenced during the gasification process (primary methods, in-situ methods). Therefore, generally high gasification temperatures, steam as a gasification agent, long residence times, and a catalytically active bed material should be applied. On the other hand, downstream processing can be carried out to further decrease the tar content in the generated wood gas prior to gas application. Downstream tar removal can be achieved via physical methods (absorption or adsorption) or chemical methods (non catalytic cracking/thermal cracking or catalytic conversion) [91].

A typical technology for the physical removal of tar via absorption is wet gas scrubbing. This can be carried out by using water as well as organic solvents as a scrubbing medium. Water is effective as a quenching medium leading to tar condensation and subsequent coalescence of these organics. Additionally, some tar components with a hydrophilic character are absorbed well in water. A series of scrubbing devices including spray towers, impingement scrubbers, packed bed scrubbers, and venturi scrubbers have been implemented for this purpose. Water scrubbing generally requires an undesired and expensive waste-water treatment. A more effective approach toward tar removal is scrubbing with organic liquids. Most tar components dissolve chemically (absorption) in a hydrophobic scrubbing solvent. For disposal, the loaded solvent can be burned or gasified in the gasifier. Possible organic scrubbing solvents are diesel, fatty acid methyl ester (FAME–Biodiesel), vegetable oil, waste cooking oil, or engine oil [91]. Both operational DFB biomass steam gasification plants in Austria (Güssing and Oberwart) employ gas scrubbing with rapeseed methyl ester (RME) over a structured packed column. A sophisticated approach for tar removal is the OLGA approach from the ECN (Energy research Centre of the Netherlands). A heavier and a lighter tar fraction are separated from the gas in a multiple stage system involving a collector and

an absorber. The loaded scrubbing medium of the collector is recycled into the gasifier. The organic solvent from the absorber operating at lower temperatures is regenerated in a stripper operated with air or steam [17].

Wet electrostatic precipitators are a special construction type aiming at physical tar removal. The gas loaded with tar and particles is quenched in water and subsequently introduced into an electric field with two electrodes. A high voltage discharge electrode charges the particles and tar droplets. They drift toward the earthed electrode where they are neutralized and collected. Depending on the operating parameters an almost complete removal of tar and dust particles can be achieved with wet electrostatic precipitators. They were successfully implemented into an updraft gasifier at Harboore, a downdraft gasifier at Wiener Neustadt and a circulating fluidized bed gasifier at ECN [7, 112, 113].

Adsorption methods can be applied for a physical tar removal in the vapour phase. So far mostly biomass-based pyrolysis char was investigated on a laboratory scale. Analogous to organic scrubbing solvents, the loaded adsorbent can be recycled into the gasifier [91]. Also sand bed filters have been tested for tar adsorption [7].

Tar components can be cracked thermally in absence of a catalyst. Even if no agent is added, high temperatures easily crack primary and secondary tar components. However, this can lead to the formation of unsubstituted aromatics like benzene (see Figure 3.3) which require at least 1000 °C at sufficient residence times. Soot can be formed during the thermal cracking of tar components which might pose a problem itself. The addition of steam is reported to produce fewer refractory tar components like phenols. The generated tar fraction is easier to be reformed catalytically. Oxygen addition (partial oxidation) is reported to produce more refractory tar at lower levels [82]. The catalytic tar removal via tar reforming is described in Chapter 3.3.3.

3.2.3 Sampling and analysis

A series of different tar analysis techniques are described in literature: elemental analysis, solvent fractionation and chromatography, gas chromatography coupled with mass spectrometry (GC/MS), size exclusion chromatography, ion chromatography. The different techniques are embedded in even more numerous sampling methods [82]. Also, many different solvents like acetone, toluene, anisole, dichloromethane, and even water were used for tar sampling [80].

This diversity of methods makes it very difficult to compare the analytical results of different sources. It represents a significant barrier to the further development of the biomass gasification technology [80]. To address this problem, the members of the IEA (International Energy Agency) Biomass Gasification Task published two sampling and analysis protocols which can be seen as reference methods. These methods describe the simultaneous sampling of tar and particles. Particle analysis was no subject to this thesis, as wood gas for experimentation was always extracted downstream a gas filter and was considered to be free from particles. One of the published tar protocols is suitable for small scale, fixed bed, engine

based systems ($<1 MW_{el}$). The other protocol was developed for larger plants ($>1 MW_{el}$).

The main elements of the tar protocol for small scale systems are isokinetic sampling, a heated filter for particulate collection, a water condenser and a series of impingers, containing cooled solvent for tar absorption. The method should enable gravimetric and chromatographic tar determination. Tar absorption at $-79\text{ }^{\circ}\text{C}$ in dichloromethane (no solubility in water) is recommended. However, this solvent is not undisputed as it is a toxic compound providing a health hazard [4, 80].

In [104] another provisional protocol for tar sampling and analysis of large-scale biomass gasifiers is presented. Sampling lines for rather clean and particle-free gases as well as isokinetic sampling of streams containing solids are described. Dichloromethane is also recommended as a solvent and the tar absorption occurs over 6 impinger bottles (1–4 cooled in a water/ice bath, 5 and 6 cooled to $-79\text{ }^{\circ}\text{C}$ in an acetone/ CO_2 bath).

The recommended concept of tar sampling according to the European Prestandard CEN/TS 15439:2006 (D) [3] is illustrated in Figure 3.4. Generally, the obtained results of tar contents should be given in $\frac{mg}{m_n^3}$

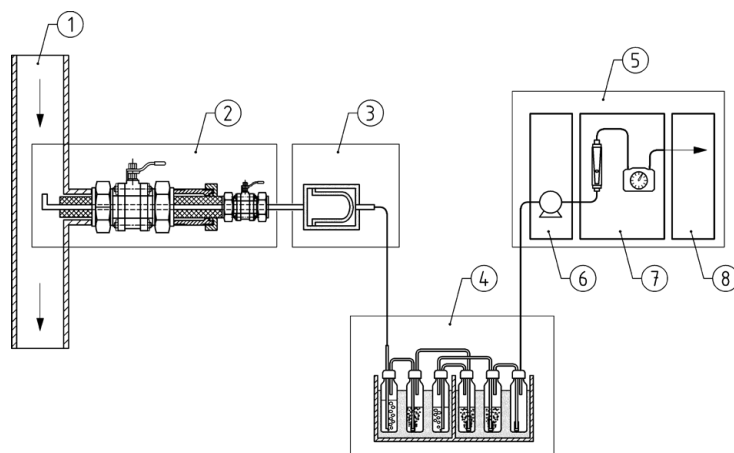


Figure 3.4: Recommended sampling line for tar sampling in [3]; 1. gas stream, 2. isokinetic sampling, 3. trace heated filter, 4. cooled impingers with solvent, 6. gas pump, 7. variable area flow meter, needle valve, and gas meter, 8. vent.

A sampling stream between $0.1\text{--}0.6 \frac{m_n^3}{h}$ should be withdrawn. Depending on the tar content in the sampling stream, an overall volume of at least $0.1 m_n^3$ should be taken. The gas scrubbing bottles (impingers) should be partly equipped with porous plates. Isopropyl alcohol (miscible in water) is suggested as a solvent. Tar absorption should be carried out at two temperature levels ($35\text{--}40\text{ }^{\circ}\text{C}$ and $-15\text{--}-20\text{ }^{\circ}\text{C}$). A small amount of the sample should be analyzed by means of GC/MS in order to quantify single tar components. The remaining sample should be introduced into a vacuum evaporator in order to remove the solvent. The solid residue is weighed, which gives the gravimetric tar content of the gas [3].

Full characterization of the tar content is a difficult, expensive, and time-consuming task. Operators of biomass gasification power plants usually do not have access to the appropriate analytical equipment [82].

3.3 Catalysis

About 85–90 % of all chemical transformations in industry involve the presence of catalysts. They reduce the activation energy of a chemical reaction and therefore increase its reaction rate. The catalyst does not affect the equilibrium constant of a reaction, it only affects its kinetics. To the same extent, the reaction rate of the forward and the reverse reaction are increased. A catalyst can only be effective if there is a moderate bonding between reactants and catalyst. If the bonding is too weak no intermediate products can be formed which are required for the energetically more favorable pathway of the catalyzed reaction. If a reactant, an intermediate, or the product is adsorbed too strongly, the catalyst is poisoned because of the occupation of its active sites [23].

Catalysts are defined as materials which accelerate chemical reactions without themselves undergoing change. However, this definition is too optimistic because the properties of real catalysts change in the course of time [111].

It can be distinguished between homogeneous catalysis, biocatalysis and heterogeneous catalysis. In homogeneous catalysis, both the catalyst as well as the reactants are in the same phase. Biocatalysis is achieved with special proteins (enzymes) which are extremely active and selective. In heterogeneous catalysis, solid surfaces catalyze gas-phase reactions [23].

Essential catalyst properties are the activity (ability of a catalyst to convert feedstock to products), the selectivity (ability of a catalyst to generate the desired product out of all possible products), and the stability (time for which the catalyst keeps a sufficient level of activity and/or selectivity) [111].

This thesis deals with heterogeneous catalysis. Heterogeneous catalysts are usually composed of nanometer-sized particles supported on an inert carrier. The aim of the support material is mainly to avoid the sintering of these active particles and to provide a large surface by means of a porous structure [23]. This carrier needs to be refractory, compatible with the active catalytic species, and physically stable offering a maximum possible surface area. Commercially, a wide range of differently shaped catalyst pellets are available. The optimum size and shape of these fabricated pellets is influenced by heat and mass transfer as well as the pressure drop over the fixed bed reactor [111]. Mainly alumina (Al_2O_3 in the different crystal structures: α, η, γ) and silica (SiO_2) are used as support materials. Special catalysts are also based on titania (TiO_2) or carbon. Catalysts used for hydrodesulfurization and catalysis of the WGSR are usually supported on γ -alumina. Industrial catalysts are usually made by precipitation (support and active phase made together) or impregnation of the support material. The main principles of the production of industrial catalysts are reviewed in Chapter 1 of the "Catalyst Handbook" [111]. The support material is often reported to affect the activity of the active phase. For example, catalysis of the WGSR is more effective over Pt particles supported on Al_2O_3 than over Pt particles supported on SiO_2 [41]. Commercial catalysts frequently contain promoters which change the catalyst structure in order to improve the activity, the selectivity, or the stability.

Generally, heterogeneous catalysis occurs in 7 different steps [111]:

1. Transport of reactants through the gas phase to the exterior of the catalyst pellet
2. Transport of reactants through the pore system of the catalyst pellet to a catalytically-active site
3. Adsorption of reactants at the catalytically-active site
4. Chemical reactions between reactants at the catalytically-active site (frequently several reaction and transport steps itself, transport of intermediate products can be either through the gas phase or across the catalyst surface)
5. Desorption of products from the catalytically-active site
6. Transport of products through the catalyst pore system from the catalytically-active site to the exterior of the catalyst pellet
7. Transport of products into the gas phase from the exterior of the catalyst pellet

It can be seen, that heterogeneous catalysis includes gas phase diffusion of the reactants, adsorption processes, surface reactions, desorption processes, and gas phase diffusion of the products. Surface diffusion may also take place. Any one of these steps can be rate limiting [26]. Adsorption and desorption are important stages of the overall catalytic process. It can be distinguished between physical adsorption (only physical interaction with the surface), associative chemisorption (chemical bonding of the gas molecule with the surface), and dissociative chemisorption (dissociation of the gas on the surface, adsorption of its atoms) [111].

Basically, heterogeneous catalysis can be carried out in fixed bed reactors or fluidized bed reactors. A special reactor type for 3 phase heterogeneous catalysis is the Slurry technology [47].

Fixed bed reactors for industrial applications are realized in many different construction types. The most simple type of reactor is the single adiabatic bed reactor. This converter type is used when the temperature rise due to the catalyzed reaction is rather small (no exceeding of the maximum temperature of the catalyst) and when the conversion is equilibrium limited. There are however a series of catalyzed reactions which require heating or cooling of the catalyst bed. An allothermal steam reformer is a perfect example of a heated fixed bed reactor. Cooled reactors are required for the methanol synthesis, ammonia synthesis, HT-WGS for coal based plants, and the methanation reaction aiming at the production of SNG. Cooled converters can be divided in 4 reactor types which are listed in Table 3.1.

Fluidized bed reactors for heterogeneous catalysis stand out due to a very good temperature control (isothermal conditions, high heat transfer), a compact reactor design (smaller catalyst particles, good mass transfer, less influence of pore diffusion), and the possibility of a permanent addition of fresh catalyst [47]. However, they are not state of the art technology for hydrodesulfurization (HDS) and catalysis of the WGSR and should therefore not be discussed within this thesis.

Table 3.1: Catalyst cooling in industrial fixed bed reactors.

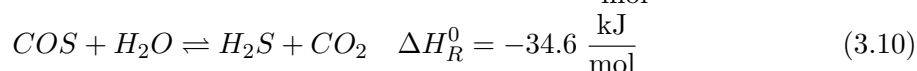
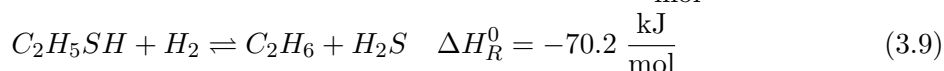
Type of cooling	Principle
Multibed reactor with quench	Addition of cold feed to hot reacted gas upstream the next catalyst section
Multibed with interbed cooling	Heat exchangers in between multiple beds; cooling with feed or steam
Tube-cooled reactors	Catalyst cooling by passing feed through tubes inside the bed (approaching the optimum operating temperature line possible - see Figure 6.28)
Steam-raising	Steam production in inner bed tubes for temperature regulation

The design and the operation of an industrial reactor is always a trade-off between different factors. For example, if the inlet temperature of a LT-WGS catalyst is set low, a low CO slip is possible because of a favorable equilibrium conditions of the WGSR (see Figure 3.8). However, at lower temperatures the reaction rate is lowered what necessitates an increased reactor volume and therefore higher costs of investment [111].

3.3.1 Hydrodesulfurization (HDS)

Most industrial syntheses require the removal of sulfur from the feed in order to prevent catalyst poisoning (also see Chapter 3.4.2). This is usually achieved by means of a two-stage process. First, a hydrodesulfurization (HDS) stage is operated where the organic sulfur components are catalytically converted to H₂S. Second, chemisorption on ZnO is applied to remove H₂S from the feed. For high sulfur loads in the feed, a washing step for H₂S followed by a Claus process are additionally operated upstream the ZnO unit [111].

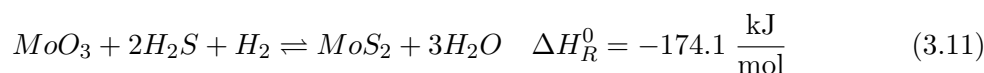
Under excess H₂, HDS catalysts accelerate the hydrogenolysis of organic sulfur compounds to form saturated hydrocarbons and H₂S. Two example reactions are given in Equation 3.8 (Thiophene hydrogenolysis) and Equation 3.9 (Ethanethiol hydrogenolysis). Usually cobalt molybdate or nickel molybdate catalyst are applied. Nickel formulations are used for applications where the risk of methanation is higher. Once sulfided the Ni/Mo-based catalysts are less active for the catalysis of the methanation reaction. Generally, the catalyzed HDS-reactions are exothermic [111]. Besides sulfur, also nitrogen and oxygen can be removed from heterocyclic hydrocarbons (Denitrification and oxygen removal) [56]. Under an excess of steam also the hydrolysis of COS according to Equation 3.10 is catalyzed.



Co/Mo-based catalysts are produced by impregnation of alumina with an aqueous solution

of $(\text{NH}_4)_6\text{Mo}_7\text{O}_{24}$ and $\text{Co}(\text{NO}_3)_2$ and the subsequent drying and calcination. They usually have an internal surface of 200–400 $\frac{\text{m}^2}{\text{g}}$. The calcinated catalysts contain Al_2O_3 , MoO_3 , CoO , and also CoAl_2O_4 , and CoMoO_4 . The amount of MoO_3 is usually three to four times the amount of CoO . To achieve full activity, the catalyst needs to be sulfided in a reducing (H_2 -containing) atmosphere at up to 300 °C. Various sulfur compounds can be applied for this activation procedure but mostly H_2S is used. The procedure leads to the formation of the corresponding metal sulfides and the liberation of water. The thereby formed MoS_2 particles are said to be the active species and the different species of Co are assumed to promote its activity. The sulfiding reaction is reversible, with lower partial pressures of sulfur leading to a sulfur release. Depending on the sulfur content in the feed, operational HDS catalysts contain between 0.5–3.0 wt.% of sulfur [18, 111]. To maintain activity, the catalysts require sulfur to be present in the feed [23].

The sulfidation reaction of MoO_3 is shown in Equation 3.11.



In Figure 3.5 the different chemical species present on an operational HDS catalyst are illustrated.

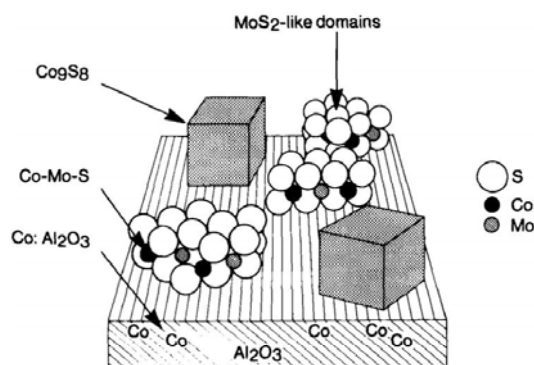


Figure 3.5: Schematic illustration of a sulfided Co/Mo-based hydrodesulfurization catalyst with MoS_2 as an active species; from [110].

The MoS_2 particles are either attached to the catalyst support by basal bonding or edge bonding. Co is present as crystallites of Co_9S_8 , Co-ions on the edge of the MoS_2 phase (“Co-Mo-S“ phase), and as Co-ions in the crystal structure of the Al_2O_3 support [18].

The reaction mechanism of the hydrogenolysis of thiophene on a Co/Mo-based catalyst is shown in Figure 3.6.

The hydrodesulfurization is usually carried out at 280–400 °C, 30–50 bar (set by the inlet pressure of the reformer), and space velocities of less than 3000 h^{-1} [18, 111]. The most important side reaction accelerated by Co/Mo-based catalysts is the WGS in Equation 3.5. Also the methanation reaction can be catalyzed and olefins can be hydrogenated to saturated hydrocarbons. In the presence of H_2S , olefins can also be converted to organic sulfides. Acetylenes tend to polymerize which leads to the formation of high molecular weight

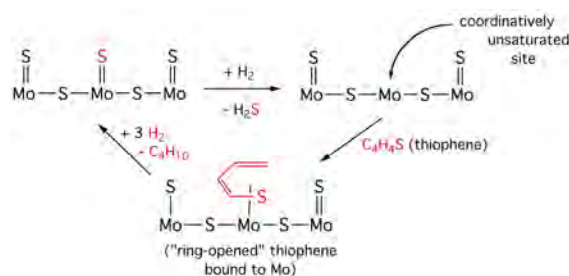


Figure 3.6: Reaction mechanism of the hydrogenolysis of thiophene on MoS₂; from [114].

compounds on the catalyst surface (coking - also see Chapter 3.4.1). The HDS catalysts can be deactivated by the adsorption of hydrocarbons with a high molecular weight (asphaltenes) nitrogen compounds and Ni [13, 111].

3.3.2 Water gas shift reaction (WGSR)

Water gas is an equimolar mixture of H₂ and CO. It is produced at high temperatures by the endothermic water gas reaction (see Equation 3.1) when steam is passed over incandescent coke. Under excess steam and lower temperatures, CO is converted to CO₂ according to the WGSR given in Equation 3.5. The WGSR was discovered in 1888 and it gained technical importance with the development of the Haber-Bosch process. The reaction is especially important for the synthesis of ammonia because the yield of H₂ per carbon input can be increased drastically. Besides, CO presents a strong catalyst poison for the ammonia synthesis catalysts. The first commercial WGSR catalyst based on oxides of Fe and Cr was already developed in 1912 [111].

The WGSR is moderately exothermic ($\Delta H_R^0 = -41.1 \frac{\text{kJ}}{\text{mol}}$). At high temperatures, the equilibrium of the reaction is shifted toward the reactants. As illustrated in Figure 3.7 the equilibrium constant (K_p at constant pressure) decreases with temperature. At 800 °C the equilibrium constant is approximately 1 [78]. A series of equations for the calculation of its temperature dependence are presented in literature. Within this work, K_p was calculated by means of the Equation given in Figure 3.7 (T in K) provided by [83]. This simple model is reported to be sufficiently accurate for design computations [106]. Low temperatures provide favorable equilibrium conditions for high CO conversion rates. However, at low temperatures the reaction rates diminish and the reaction becomes kinetically controlled [78]. In other words, the reaction is thermodynamically favored at low temperatures and kinetically favored at high temperatures [106]. Higher quantities of steam are enhancing the CO conversion according to the WGSR [111]. The equilibrium of the equimolar WGSR is hardly affected by pressure. However, WGS catalysis is usually operated at pressures around 20–30 bar (depending on the outlet pressure of the steam reformer). Higher pressures enable a compact reactor design because of enhanced reaction kinetics. Enhanced kinetics can be explained by higher partial pressures of reactants and intermediates on the catalyst surface [23].

Different key figures of the WGSR can be stated in order to characterize the reaction.

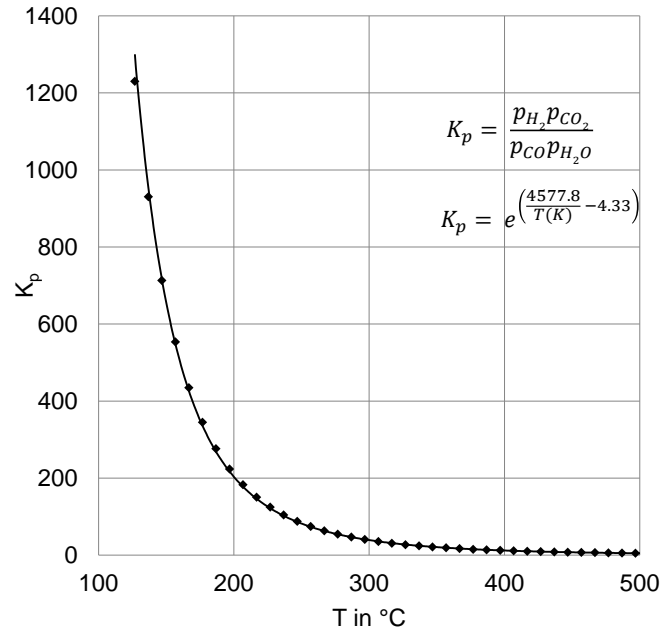


Figure 3.7: Variation of the equilibrium constant K_p of the WGSR at constant pressure with the temperature, based on [83].

Besides the temperature and the operating pressure, the gas hourly space velocity (GHSV, see Equation 3.12) affects strongly the catalysis. Low GHSV represent long residence times and therefore a long time span for the convergence to equilibrium conditions. The GHSV can also be regarded as the reciprocal value of the residence time at standard conditions (here: atmospheric pressure and 0 °C). The GHSV can be calculated on a wet base (molar flow of H₂O considered as an ideal gas at standard conditions) and on a dry base. The molar fraction of steam in the gas mixture can be calculated according to Equation 3.13. The steam to carbon ratio (defined in Equation 3.14) and the steam to dry gas ratio (defined in 3.15) are typical values given frequently to characterize the reaction conditions during heterogeneous catalysis (WGS, steam reforming, methanation,...). The steam to carbon ratio is an important figure to describe the risk of carbon formation within the present gas composition (see Chapter 3.4.1). The steam to CO ratio in the feed is especially suitable to describe the catalysis of the WGSR as it denotes the excess of steam with respect to the present CO. The CO conversion rate in Equation 3.17 is the key figure to evaluate the performance of the WGSR. The equilibration of the WGSR with respect to the present operating temperature (T_{op}) can be calculated by means of Equation 3.18.

$$\text{Gas hourly space velocity} \quad GHSV = \frac{\dot{V}_{reactants}}{V_{catalyst}} \quad \left[\frac{m^3}{m^3 h} = h^{-1} \right] \quad (3.12)$$

$$\text{Water content} \quad Y_{H_2O} = \frac{\dot{n}_{H_2O,in}}{\dot{n}_{gas_{dry},in} + \dot{n}_{H_2O,in}} \quad [-] \quad (3.13)$$

$$\text{Steam to carbon ratio} \quad H_2O/C = \frac{\dot{n}_{H_2O,in}}{\dot{n}_{C,in}} \quad [-] \quad (3.14)$$

$$\text{Steam to dry gas ratio} \quad H_2O/gas_{dry} = \frac{\dot{n}_{H_2O,in}}{\dot{n}_{gas_{dry},in}} \quad [-] \quad (3.15)$$

$$\text{Steam to carbon monoxide ratio} \quad H_2O/CO = \frac{\dot{n}_{H_2O,in}}{\dot{n}_{CO,in}} \quad [-] \quad (3.16)$$

$$\text{CO conversion rate} \quad X_{CO} = \frac{\dot{n}_{CO,in} - \dot{n}_{CO,out}}{\dot{n}_{CO,in}} \quad [-] \quad (3.17)$$

$$\text{Degree of WGS equilibration} \quad WGS_{eq.} = \frac{\dot{n}_{CO,in} - \dot{n}_{CO,out}}{\dot{n}_{CO,in} - \dot{n}_{CO,eq.(T_{op.})}} \quad [-] \quad (3.18)$$

$$\text{H}_2 \text{ recovery} \quad H_2 \text{ rec} = \frac{\dot{n}_{H_2,out}}{\dot{n}_{H_2,in}} \quad [-] \quad (3.19)$$

Many metals and metal oxides are catalyzing the WGSR. The turnover frequency (defined as reacting molecules per active site and time) at 300 °C of various alumina supported metals decrease in the order Cu, Re, Co, Ru, Ni, Pt, Os, Au, Fe, Pd, Rh and Ir [41]. However, noble metal catalysts are frequently presented in literature for the catalysis of the water-gas shift reaction because of their good stability with respect to coking and carbon deposition. A review article of these activities is presented in [89]. Despite the promising properties of noble metal catalysts, they did not reach the commercial stage yet [106].

As already discussed roughly in Chapter 2.2, it can be distinguished between industrial "sweet shift" applications and "sour shift" applications. "Sweet shift" is applied for a desulfurized feed. The established two stage systems involve a HT step with a Fe/Cr-based catalyst and a LT step employing a Cu/Zn-based catalyst. "Sour shift" applications employ catalysts based on Co/Mo formulations (similar to HDS catalysts) and can be used in coal gasification plants which usually provide a sulfur-rich feed. Table 3.2 summarizes the properties of these catalysts in combination with the applied operation conditions that can be found in literature.

A "sweet shift" process is usually provided with an inter-bed cooling in order to reduce the inlet temperature of the LT stage to the desired reaction temperature. In the ideal case, both reactors reach the equilibrium composition with respect to the outlet temperatures. Figure 3.8 illustrates the trends of temperature and CO content over the two adiabatic beds. The LT WGS catalysts are significantly more active than the HT catalysts what allows an equilibration of the WGSR even at temperatures as low as 200 °C. The minimum reaction temperature of the LT stage is limited by the dew point of the feed at the present operating pressure. LT WGS catalysts cannot be used at higher temperatures because they are susceptible to sintering [111].

Table 3.2: Overview of the main reaction conditions during industrial catalysis of the WGSR over a LT and a HT stage, collected from [78, 111].

	HT WGS	LT WGS	HDS / "Sour shift"	Unit
Catalyst formulation	Fe ₂ O ₃ : 90–95 Cr ₂ O ₃ : 5–10 -	CuO: 30 ZnO: 30–50 Al ₂ O ₃ : 15–30	MoO ₃ : 75 CoO: 25 -	wt.% wt.% wt.%
Catalyst support	γ-Al ₂ O ₃	-	γ-Al ₂ O ₃	
Active species	Fe ₃ O ₄ crystallites	Cu crystallites	MoS ₂	
Promotor	Cr ₂ O ₃	ZnO	Co ₉ S ₈	
T _{in}	340–360	150–200	250–400	°C
T increase	50–100	20	up to 150	°C
Pressure	20–30 (up to 80)	10–30	5–27	bar
GHSV	400–1200	3600	4800–24000	h ⁻¹
Sulfur influence	activity reduction	deactivation	activity increase	-
Stability	up to 15	2–3	2–10	years
Pellet dimensions	3.6–4.9 x 5.4–9.5	3.6 x 5.4		mm x mm
Bulk density	1.08–1.25			$\frac{kg}{L}$
BET surface	60–120	75–90	200–400	$\frac{m^2}{g}$
CO at the exit	2–3	0.1–0.3	1–4	vol.% _{db}

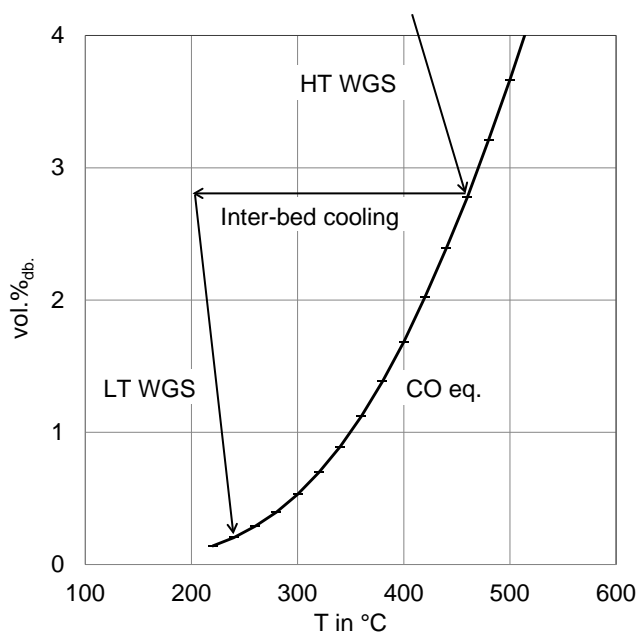
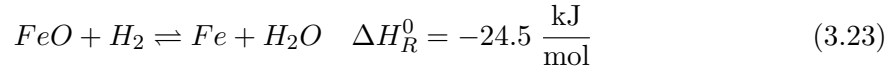
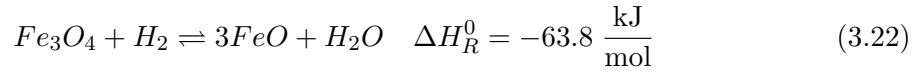


Figure 3.8: Schematic illustration of the industrial catalysis of the WGSR over a two stage adiabatic bed system "sweet shift", equilibrium CO content (CO eq.) calculated based on the gas composition in Table 6.1, 50 mol.% H₂O in the wet gas mixture; based on [111].

HT WGS catalysts (Fe/Cr-based)

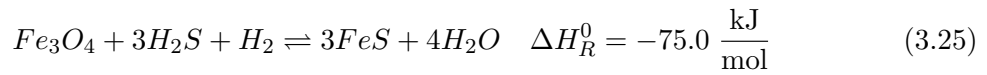
Many metals catalyze the WGSR but most of them lack a high selectivity. Fe_3O_4 is sufficiently active and only has a negligible activity for the methanation reaction. It is the chemically stable form of Fe under the typical reaction conditions of the WGSR. A good stability is also obtained from a low susceptibility to sulfur poisoning. However, pure Fe_3O_4 is not sufficiently refractory. It has to be promoted with Cr_2O_3 to inhibit sintering of the small Fe_3O_4 crystallites which enables a lifetime of several years. The moderate activity of the HT-catalyst allows the use of rather large pellets (up to $8.5 \text{ mm} \times 11 \text{ mm}$) without a severe loss of activity from pore diffusion. This is beneficial for the physical stability and leads to a low pressure drop. The HT-WGS stage is usually operated between 350 and 400 °C. At 30 bar pore diffusion gets increasingly rate-limiting at temperatures higher than 350 °C. With the rise in temperature along the bed height of a HT WGS reactor the process moves from almost pure reaction control to substantial pore-diffusion control. The limitation by pore diffusion can be reduced by a smaller particle size. However, also the pressure drop has to be considered if the particle size is decreased. This is especially important for the operation at low pressures which require big catalyst volumes. The required volume of catalyst decreases inversely proportional to the square root of the pressure in a pore-diffusion limited reaction [111].

HT WGS catalysts are produced by a precipitation method using a solution of FeSO_4 and Na_2CO_3 . Subsequent calcination leads to the formation of Fe_2O_3 . A washing step is included to remove sulfur from the product. The delivered HT WGS catalyst also contains Cr_2O_3 and some CrO_3 . The catalyst has to be reduced for activation. The reduction of the catalyst can be achieved by means of the addition of CO or H_2 . Within this thesis, H_2 was used. The important reactions during the reduction procedure are shown in Equation 3.20 and Equation 3.21. The reduction of CrO_3 (3.21) is strongly exothermic. Care should be taken to avoid an overheating of the catalyst bed during the activation process. Steam has to be added to the reduction mixture in order to avoid an over-reduction of magnetite according to the Equations 3.22 and 3.23. Rhodes et al. presented a convenient tool which helps to avoid an over-reduction of the catalyst. It is suggested to keep the reduction factor (R, calculated according to Equation 3.24) of the present reduction mixture smaller than 1.2. Values bigger than 1.6 may cause an over-reduction of the catalyst [99]. Prior to the application of a reducing atmosphere, the reactor should be purged free from O_2 . The reduction of haematite starts at 150 °C and is completed at 400 °C. The exothermic reactions during the reduction of phase should not cause a temperature rise above 500 °C to avoid sintering on the catalyst surface.



$$\text{Reduction factor} = \frac{p_{CO} + p_{H_2}}{p_{CO_2} + p_{H_2O}} \quad (3.24)$$

During the operation of the HT WGS, it is important to operate the catalyst above the dew point in order to avoid leaching of the catalyst. The inlet temperature should be set to the minimum which still enables the desired CO concentration at the outlet. Thereby the thermal stress on the catalyst is reduced and its lifetime can be increased. Generally, HT WGS catalysts are robust and can withstand a high degree of maltreatment [111]. Coke formation was observed in the presence of acetylenes, dienes, and other coke precursors (see Chapter 3.4.1). They are not especially susceptible to poisoning and are tolerant to chlorine and sulfur compounds [78]. However, if exposed to H₂S, FeS is formed according to the reversible reaction in Equation 3.25.

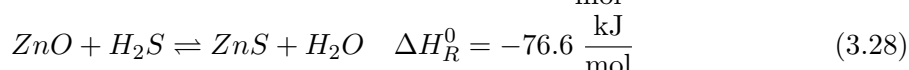
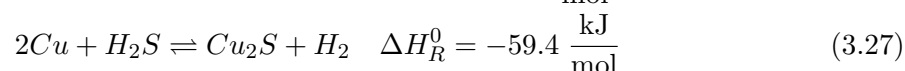
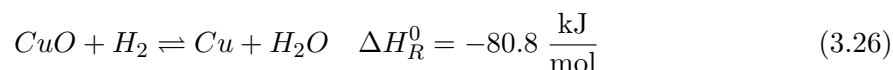


The equilibrium of the reaction is shifted toward the formation of FeS at lower temperatures. The activity of FeS toward the catalysis of the WGS is reported to be reduced by 50 % compared to magnetite. The catalyst volume has to be increased appropriately if a sulfur removal prior to WGS catalysis is not desired. The HT WGS catalyst also catalyzes the conversion of COS to H₂S according to Equation 3.10 [111].

LT WGS catalysts (Cu/Zn-based)

Cu/Zn-based catalysts for a LT WGS stage were first implemented in 1963. Compared to the Fe/Cr-based catalysts, much higher catalyst activities are required as the LT WGS stage is only operated at 200–250 °C and much lower partial pressures of CO. Among the active metals, copper is the only one which does not catalyze the methanation reaction. The delivered catalyst contains CuO and has to be reduced with H₂ to form the active Cu crystallites (Equation 3.26). Provided that the catalyst is sufficiently active, the inlet temperature of the LT WGS is only set slightly above the dew point of the present gas mixture, which strongly depends on the operating pressure. Deactivation of copper crystallites due to thermal sintering, halides (especially Cl-compounds), or sulfur components is almost inevitable which explains why the volume of catalyst is designed larger than required during commissioning of the plant. To increase the stability of the Cu-particles they are promoted with ZnO and stabilized with Al₂O₃. LT WGS catalysts are produced by precipitation. The precipita-

tion of mixed Cu/Zn-carbonates leads to the formation of very small and well dispersed Cu crystallites. ZnO also acts as an absorbant for catalyst poisons which extends the lifetime. Smaller-sized catalyst pellets are used to minimize the effect of pore diffusion limitation of this more active catalyst [111]. LT WGS catalysts are very sensitive to chlorine poisoning. Also sulfur components are a powerful poison for Cu/Zn-based catalysts. The sulfidation of the catalyst with H₂S occurs according to Equation 3.27 and Equation 3.28.



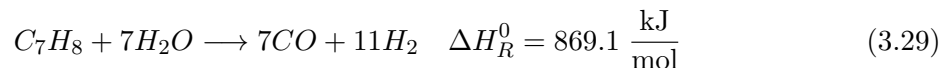
Sour shift catalysts (Co/Mo-based)

The formulation of Co/Mo-based catalysts for "sour shift" applications is very similar to HDS catalysts (see Chapter 3.3.1). Alumina is used as a catalyst support in order to provide a hydrothermal stability. Frequently alkali promoters (K and Cs) are used to enhance the activity. "Sour shift" catalysts are used in some plants where the feed contains high loads of the acid gas H₂S (mostly coal derived product gas) [78]. Usually between 1000–13000 vol.ppm of H₂S are contained in coal derived product gas (strongly depending on the sulfur content in the feedstock) [51, 64]. "Sour shift" catalysts only achieve full activity when properly sulfided. Provided that the catalyst activity is sufficiently high to allow inlet temperatures as low as 230 °C, the CO content at the outlet can be reduced down to 1 vol.% [111].

3.3.3 Catalytic tar removal

Many types of catalysts have been investigated to reduce tar more efficiently than by thermal, oxidative, or steam reforming atmosphere. Catalytic conversion methods are very attractive because they enable a complete destruction of tar and at the same time increase the amount of generated synthesis gas. However, they require high temperatures and therefore a considerable energy supply. A series of different catalysts have been tested for their tar conversion potential. It can be distinguished between Ni-based catalysts, non Ni-based catalysts (noble metals: Rh, Ru Pt, Ir, Pd; as well as Fe- and Mo-based catalysts), alkali metal based catalysts (like K₂CO₃, NaCl, LiCl, KCl) basic catalysts (dolomite, olivine, clay minerals, and alkaline earth metals like MgO, CaO, Ca(OH)₂), acid catalysts (zeolite, silica-alumina) and activated carbon. The effect of these catalysts is reviewed in [7]. Commercial Ni-based steam reforming catalysts are very effective because of their ability to attain complete tar reforming at around 900 °C. Additionally, methane and small hydrocarbons are reformed which leads to increased yields of H₂ and CO. However, these catalysts are easily deactivated by sulfur, which requires a preconditioning of the feed. The noble metals Rh, Pt, and Pd are reported to be even more active than Ni and less susceptible to coking (see Chapter 3.4.1), but high

costs limit their application. Alkali metal-based catalysts and basic catalysts can be added into the gasification zone by direct feeding, dry mixing with the biomass or wet impregnation. The measure leads to an increased ash formation and might cause disposal problems [7]. Generally, the catalytic tar removal is achieved by means of the catalysis of the steam reforming reaction (with H₂O) and the dry reforming reaction (with CO₂). Both reactions are catalyzed by Ni. Experimental investigations of these reactions are often carried out with toluene as a model compound for biomass tar. The corresponding reactions are strongly endothermic and are shown in Equations 3.29 and 3.30 [22, 118].



Within this work, two different WGS catalysts (active species Fe₃O₄ and MoS₂) were investigated. Only few literature can be found with respect to the tar removing potential of these catalysts. Nordgreen et al. [88] tested the capability of metallic iron and iron oxides to catalytically reform tar contained in wood gas derived from oxygen-blown fluidized bed gasification. A fixed bed of the catalysts was implemented downstream the gasifier. At 800 °C the metallic iron represented an effective catalyst for the decomposition of tar components. Fe₂O₃ and a mixture of Fe₃O₄ and FeO did not show a significant catalytic activity toward tar reforming. No literature could be found with respect to the influence of MoS₂-based catalysts on the catalytic tar conversion.

3.4 Catalyst deactivation

All catalysts will decay with respect to their activity or selectivity. This process of activity reduction in the course of lifetime is illustrated in Figure 3.9. Figure shows that the initial period of catalyst operation usually involves a strong change in catalyst activity. This can be due to the activation or the equilibration of the catalyst. The start up period with a strong change of the performance is usually followed by a steady state period with a slow decrease in catalyst activity. Finally, the catalyst deactivates rapidly in the "End of run" period [26].

A frequently applied measure to compensate for the decrease in activity is temperature ramping aiming to keep a constant conversion rate. By means of this measure, some industrial catalysts can be operated for more than 10 years [111]. Generally, the type of deactivation can be either chemical, thermal, or mechanical. Table 3.3 describes the different deactivation mechanisms, structured with respect to the type of deactivation. The deactivation of a catalyst via poisoning and / or fouling can be reversible. The other mechanisms described are usually irreversible [13]. Within this thesis, catalyst fouling via coking or carbon deposition as well as catalyst poisoning were considered to be the most important deactivation mechanisms. Together with the thermal degradation of catalysts, these deactivation mechanisms are discussed in more detail.

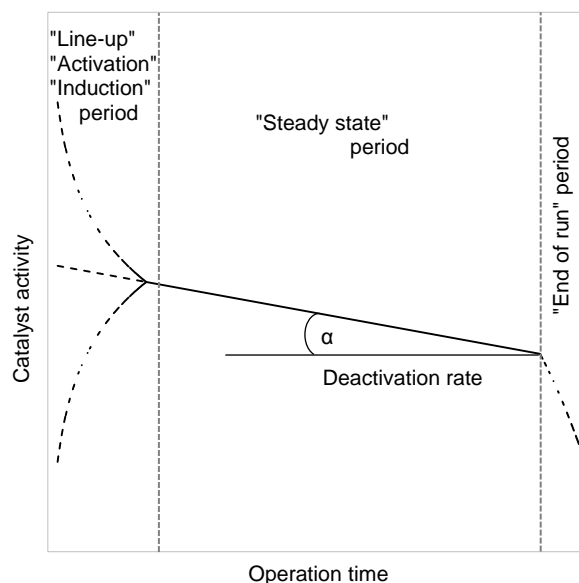


Figure 3.9: Life cycles of a catalyst, based on [26].

Table 3.3: Mechanisms of catalyst deactivation, reviewed in [13].

Mechanism	Type	Description
Poisoning	Chemical	Strong chemisorption of species on catalytically active sites, blocking or change in geometric and electronic structure
Vapor formation	Chemical	Reaction of gas phase with catalyst to produce a volatile component (f.ex.: metal carbonyl formation with CO)
Vapor-solid and solid-solid reactions	Chemical	Reaction of fluid, support, or promoter with catalytic phase to produce inactive phase
Thermal degradation	Thermal	Loss of catalytically active surface due to sintering of active phase (crystallite growth) or catalyst support
Fouling	Mechanical	Physical deposition of species on the catalytic surface/pores (coking, carbon formation)
Attrition/crushing	Mechanical	Loss of catalytic material due to abrasion, loss of internal surface area due to mechanical-induced crushing of the catalyst particle

3.4.1 Fouling via coking and carbon deposition

A catalyst can be deactivated mechanically by the deposition of solids on the catalyst surface, which results in the reduction of the active surface via blocking of active sites or even pores. This important process of deactivation is called fouling and includes the deposition of carbon and coke on the catalyst surface. The deposits can be derived from the upstream equipment or can be produced inside the converter [111]. Carbon- and coke-forming processes also include chemisorption, which explains why fouling can not be seen uniquely as a physical deactivation process. The carbon or coke-formation leading to a reduction of the available catalytically active surface of the catalyst is illustrated in Figure 3.10.

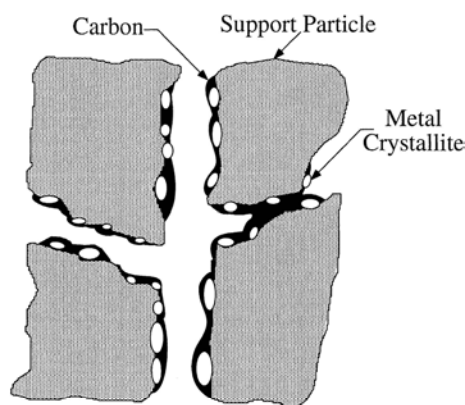


Figure 3.10: Conceptual model of fouling; crystallite encapsulation and pore plugging of a supported metal catalyst due to coking or carbon deposition; from [13].

Carbon and coke can be composed similarly and are therefore defined according to their origin. Coke is derived from the decomposition or condensation of hydrocarbons. Depending on the conditions under which coke was formed, its composition varies from graphite to high molecular weight hydrocarbons (composition range: C to CH). Coke formation can be catalyzed by supported metals as well as metal oxides and metal sulfide catalysts. Some catalytic processes lead to the formation of coke species which can easily be removed by gasification reactions (coke-insensitive reactions). Coke-sensitive processes lead to the formation of stable coke. Examples for coke sensitive reactions are the hydrogenolysis and the catalytic cracking [13]. Within this thesis a metal oxide and metal sulfide catalyst were investigated. On these catalysts, the formation of coke is mainly the result of cracking reactions of typical coke precursors like olefins or aromatics. Different mechanisms lead to the coke formation catalyzed by the acid sites of these catalysts:

- Polymerization of olefins
- Cyclization from olefins
- Formation of polynuclear aromatics from benzene

The order of reactivity for coke formation is clearly structure dependent. A rough order of the risk of various hydrocarbons toward coke formation can be stated as follows: polynuclear

aromatics > aromatics > olefins > branched alkanes > normal alkanes. Coke yields generally increase with an increased acidity of the active sites and an increased pore size [13].

Carbon is derived from CO disproportionation according to the reverse Boudouard reaction in Equation 3.2. Carbon deposits can also be derived indirectly from CO₂ and CH₄. CO₂ can be shifted to CO according to the WGSR in 3.5. CH₄ can be converted to CO according to the methanation reaction in 3.6. From equilibrium calculations of these three reactions it is possible to draw a ternary diagram (triangle diagram of the molar ratio of C-H-O) which can be split into an area which is prone to carbon formation and an area where the carbon formation is thermoc illustrates the carbo

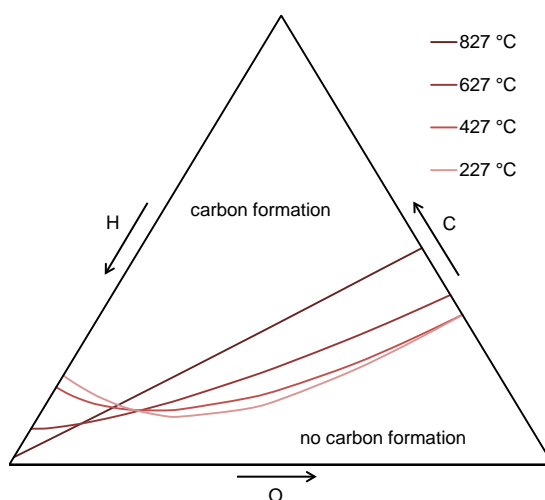


Figure 3.11: Ternary diagram of a gas mixture containing C, H, and O; C-H-O diagram; area of thermodynamically favored carbon formation; in atomic mol.%; atmospheric pressure; from [103, 102].

This presented diagram can be used to estimate the carbon formation potential of the present process condition. The equilibrium carbon deposition boundaries are pressure and temperature dependent. The carbon forming boundaries are more sensitive to the carbon fraction, than to the hydrogen or oxygen fraction. Addition of H₂ or H₂O decreases the probability of carbon deposition. The carbon formation tendency decreases with increasing temperature, increasing pressure and an increased steam to carbon ratio. The addition of steam however is often undesired because of the huge demand of energy required for steam production. It must be pointed out, that even if the current process conditions do not favor the formation of carbon, coke formation may occur as a consequence of the presence of olefins or aromatics as discussed earlier [12].

The fouling of catalysts via coking or carbon formation is sometimes reversible. HT WGS catalysts partly deactivated by coking or carbon deposition can be reactivated at 450 °C under steam atmosphere containing 1–2 vol.% of O₂ [111].

3.4.2 Poisoning

Poisoning is the strong chemisorption of reactants, products or impurities on the active sites of the catalyst. Most frequently the catalyst poison is present as an impurity in the feed. The chemisorption of a catalyst poison leads to the physical blocking of an adsorption site of the catalyst. Besides, a change in the electronic configuration or geometric structure of the active particle may occur. A physical blocking of active sites only leads to the reduction of the activity, whereas a modification of the structure may also affect the selectivity of a catalyst. Typical catalyst poisons have a very strong interaction with the active metal. As an example, if H_2S is present in the feed of Ni-based catalysis, the formation of nickel sulfides is strongly favored thermodynamically which explains why poisons can be very effective in even small concentrations (< 1 vol.ppm H_2S in that case). The chemisorption of sulfur is illustrated in Figure 3.12 [13, 111].

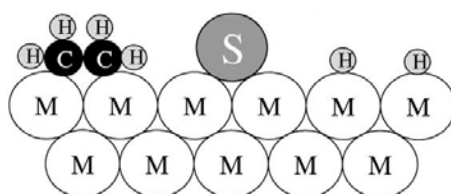


Figure 3.12: Conceptual model of poisoning by sulfur atoms (S) of a metal surface (M) during ethylene hydrogenation, from [13].

The poisoning mechanism is usually diffusion-rate limited as the concentration of the impurities is usually very low and the poisoning reaction very fast. As a consequence, the catalyst poisons are preferentially absorbed at the inlet of the reactor. After the saturation of the inlet, a deactivation front slowly progresses through the catalyst bed which usually leads to a change of the temperature profile of the reactor over time [111]. This process is illustrated in Figure 3.13 for sulfur poisoning of an industrial LT WGS unit. In the course of time, the temperature increase according to the exothermic WGSR is retarded over the bed height because of the sulfidation procedure which starts at the reactor inlet. After a long operation time, the inlet temperature of the LT WGS unit had to be increased in order to maintain a high conversion rate. To prevent poisons from entering the main reactor, a catalyst guard bed is frequently installed which can be replaced easily [111].

3.4.3 Thermal degradation

Thermally induced deactivation of catalysts generally results from a loss of catalytically active surface area. This "sintering" process can be caused by the crystallite growth of the active phase or the collapse of the catalyst support. The growth of crystallites can be either induced by crystallite migration (which involves the migration of entire particles over the support material and the subsequent collision and coalescence) as well as atomic migration (which involves the detachment of metal atoms from crystallites, their transport over the support surface and their capture by larger particles). Sintering reactions take place at high reaction

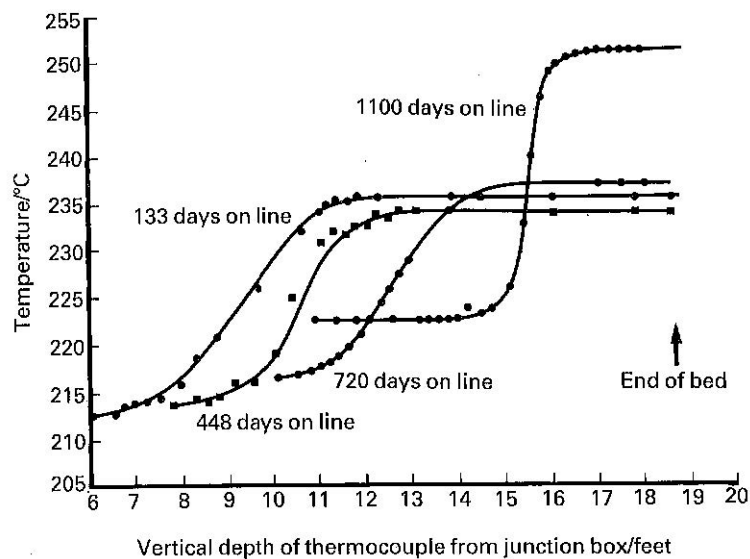


Figure 3.13: Variation of temperature profile with time for the poisoning of a LT WGS catalyst; the deactivation front progresses through the reactor, from [111].

temperatures and are generally accelerated by water vapor. At moderate temperatures, the sintering processes are kinetically slow. The sintering rate increases exponentially with the temperature. The crystallite stability generally decreases with decreasing metal melting temperatures. Promoters or impurities affect sintering by increasing or decreasing the metal mobility on the support. The processes can generally be considered as irreversible. However, in some cases a redispersion can be achieved [13].

Sintering of the catalyst support (usually an oxide carrier) may be caused by a series of different mechanisms. Alumina and silica carriers are thermally stable in an oxidizing atmosphere. In reducing atmospheres carbon is thermally very stable. Analogous to the sintering of crystallites, also the thermal degradation of the support material is affected by additives or impurities [13].

3.5 Reaction mechanisms and kinetics of the WGSR

Designing of a WGS reactor requires the prediction of the rate of reaction which in turn is determined by the kinetics of the reaction. The knowledge of the reaction kinetics is required for the prediction of the reactor performance. This can be desired for plant design or the improvement of an existing plant [106, 111]. Reaction kinetics of the catalyzed reaction are described as kinetic models. The reaction itself is comprised of a series of elementary steps under which each one can be rate limiting.

3.5.1 Reaction mechanisms

The knowledge about the elementary steps that are involved in the reaction can be obtained from isotope exchange data and stoichiometric number analysis [78]. The detailed chemistry

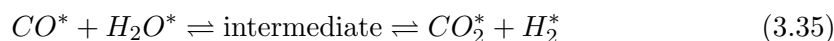
of the reaction is explored, providing the accurate pathway and prediction of the reaction. The approach is computationally intensive and requires an accurate knowledge of the composition of the catalyst [106]. Regarding the mechanism of the WGS over different catalyst, a series of reaction pathways are presented in literature. Some degree of controversy exists in the literature with respect to the suggested mechanisms. However, different elementary steps of the WGS seem to occur on surface of the available catalysts based on Fe/Cr, Cu/Zn, or Co/Mo [78]. By means of the investigation of the precise reaction routes and the kinetics of the elementary reaction steps, a more systematic catalyst design is desired [19].

Basically, the presented reaction mechanisms of the WGS can be divided into two approaches [106].

- Regenerative mechanisms (Redox mechanism, reduction and oxidation cycle on the catalyst surface responsible for the reaction)



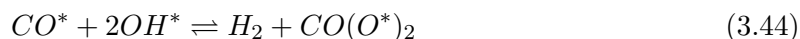
- Associative mechanisms (adsorption/desorption model including the formation of one or more intermediates, the symbol * denotes an active site of the catalyst which is accessible for adsorption.)



For the HT WGS catalysis over an Fe/Cr-based catalyst, an associative reaction mechanism involving 5 elementary steps (Equations 3.38 – 3.42) was suggested by Hakkarainen et al. [42]. The desorption of CO₂ and H₂, (Equations 3.39 and 3.42) were found to be the rate-limiting steps of this reaction pathway [42]. Other suggested HT WGS reaction mechanisms involve the formation of formate (COOH) as an intermediate [23, 78].



A different associative reaction mechanism is suggested by the same authors for the catalyzed WGSR over a Co/Mo-based catalyst. This pathway is illustrated in the Equations 3.43 – 3.45 with 3.44 and 3.45 being rate limiting [43].



However, in practice heterogeneous catalysis seems to be even more complex than presented for HT WGSR in Equations 3.38 – 3.42 and for "sour shift" catalysis in Equations 3.43 – 3.45. Callaghan et al. stated 17 elementary steps which are possible on the surface of a Cu-based LT WGS catalyst. Every elementary step has its own kinetics (including activation energies and pre-exponential factors). These elementary steps can be combined to form 70 possible reaction routes of the WGSR. Only some of them occur to a significant extent; some reaction routes are more important at elevated temperature, some are favored at lower temperatures. The final microkinetic model can be formed by the sum of the most important reaction routes [19]. Finally, it can be concluded that there is no undisputed conclusive microkinetic model of the WGSR available [106].

3.5.2 Kinetic models and the power law rate model

A broad range of kinetic models (Oxidation-Reduction Model, Hulburt-Vasan Model, Kodama Model, Moe Kinetic Model, Eley-Rideal Model, Langmuir Hinshelwood Model, Power Law Rate Model etc. [111, 106]) was developed by different authors for the description of the reaction rate r of the catalyzed WGSR. Smith et al. provide a review of this huge variety of models [106]. Frequently Langmuir Hinshelwood models, Eley-Rideal type models, and power law rate models are encountered [106, 111]. Podolski and Kim examined a number of different models and found that only the theoretically derived Langmuir-Hinshelwood expression and empirical power law models could adequately describe the reaction behavior over Fe/Cr-based HT WGS catalysts regarding their own experimental data as well as existing data from literature [94].

Most authors express their experimental data in the form of empirical power law rate models according to Equation 3.46. All symbols used are defined precisely in Table 3.4. The term β of the model is described in Equation 3.47. It reflects the reverse reaction or the approach to equilibrium. β values approaching zero indicate that the reaction occurs far from equilibrium which is usually desired for catalyst testing (see Chapter 3.6). The equilibrium constant of the WGSR was calculated according to Equation 3.49 (T in K, see Figure 3.7). It should be pointed out, that the unit of the pre-exponential factor A and therefore also the unit of the reaction rate constant k depend on the reaction orders a, b, c, d . The reaction

orders have to be adjusted at different levels of operating pressure [78]

$$r_{wt.} = k p_{CO}^a p_{H_2O}^b p_{CO_2}^c p_{H_2}^d (1 - \beta) \quad (3.46)$$

$$\beta = \frac{1}{K_p} \frac{p_{CO_2} p_{H_2}}{p_{CO} p_{H_2O}} \quad (3.47)$$

$$k = A \cdot e^{-\frac{E_A}{R \cdot T}} \quad (3.48)$$

$$K_p = e^{\frac{4577.8}{T} - 4.33} \quad (3.49)$$

Table 3.4: Power law rate model of the WGSR: List of symbols, explanation and units.

Symbol	Explanation	Unit
$r_{wt.}$	Reaction rate on a weight base	$\frac{mol}{g_{cat} \cdot s}$
k	Reaction rate constant	$\frac{mol}{g_{cat} \cdot s} kPa^{-(a+b+c+d)}$
K_p	Equilibrium constant of the WGSR at constant pressure	–
p_i	Partial pressures of gases	kPa
a, b, c, d	Apparent reaction order with respect to component i	–
A	Pre-exponential factor	$\frac{mol}{g_{cat} \cdot s} kPa^{-(a+b+c+d)}$
E_A	Apparent activation energy	$\frac{kJ}{mol}$
R	Universal gas constant	$8.314 \cdot 10^{-3} \frac{kJ}{mol \cdot K}$
T	Temperature	K

The power law rate model can be considered as an empirical approach to describe the activity (makrokinetics) of the catalyst. This model does not take into consideration the different elementary steps of the reaction but provides an overall model. Empirical models are based on experimental results and are typically expressed in accordance with the Arrhenius law (Equation 3.48). They provide an easy and computationally light way to predict the rate of reaction r . This simple empirical expression is considered as a useful tool for reactor design, which explains why this approach was chosen within this thesis [52, 106].

With respect to this PhD thesis, power law rate models for the modeling of the WGSR are mostly established for product gases derived from coal gasification. In this context, especially the work from Hla et al. has to be pointed out. The applied procedures for the generation of power law rate models within this work (see Chapter 5.2.2) are strongly based on his publications [49, 50, 51, 52].

3.6 Catalyst testing

To determine the chemical properties of a catalyst mostly elemental analysis, X-ray diffraction and electron microscopy are employed. Analytical standard techniques are applied to determine the physical standard properties like compression strength and attrition loss [111].

Within this thesis it was of more interest to assess the performance of the catalyst. Laboratory testing of the performance always aims to determine the activity of the catalyst itself (point 4 of the 7 stages of heterogeneous catalysis in Chapter 3.3) without an influence of

mass transfer or heat transfer phenomena. If there is a directly proportional dependence of the catalyst activity and the number of active sites, it can be concluded that the chemical kinetics are the rate limiting step [111]. In other words if everything is done properly, the reaction rate of a sample is given by the specific activity of each active site (turnover frequency per active site) multiplied by the number of present sites. The turnover frequency is an important figure if the intrinsic activity of different catalysts should be tested. However, for industrial applications it is more important to investigate the activity per volume of catalyst [23].

Testing of heterogeneously catalyzed gas phase reactions is mainly carried out in two different types of fixed bed reactors: Continuous stirred tank reactors (CSTR) and plug flow reactors (PFR). Preferably a CSTR should be used for catalyst testing, as there are no temperature or concentration gradients along the reactor which simplifies the data treatment. This type also allows the usage of full sized catalyst pellets. In Figure 3.14 the basic setup of a PFR and a CSTR is illustrated [111].

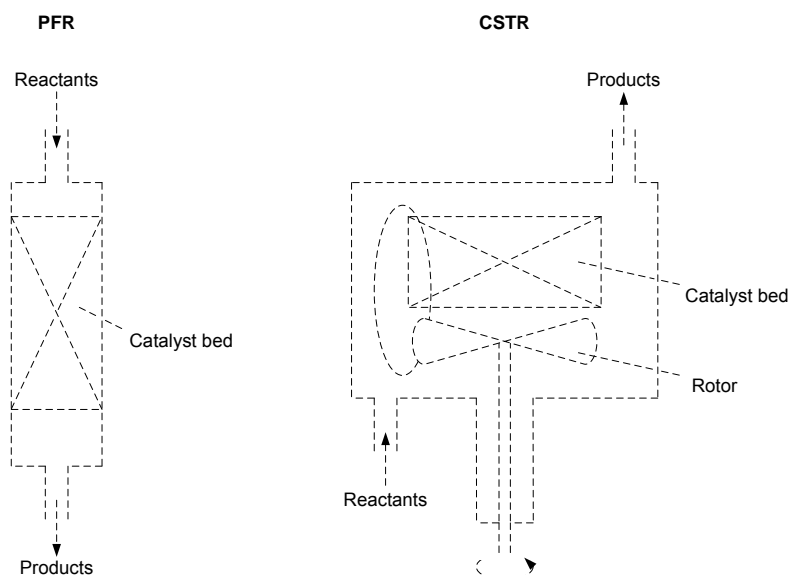


Figure 3.14: Basic setup of the two most common configurations for catalyst testing, Plug Flow Reactor (PFR) and Continuous Stirred Tank Reactor (CSTR) in the "Berty" configuration, based on [111].

Sigmund M. Csicsery provides a comprehensive guide for catalyst testing [26]. He states a series of guidelines how to test (and how not to test) a catalyst. Together with the recommendations for catalyst testing given in [23] the following points were summarized:

- Specify the purpose of the test.
- Provide a homogeneous feed at an even flowrate (proper mixing of reactants, even evaporation), an uneven feed may be detected by connecting the feed directly to the thermal conductivity detector (TCD) of a gas chromatograph (GC) .
- Avoid transport limitations, establish ideal flow patterns for ideal mixing: avoid the strong influence of the reactor wall and axial gradients by small catalyst particles (less

than one tenth of the reactor diameter, less than one hundredth of the length of the catalyst bed), apply high GHSV, operate at rather low temperatures to avoid diffusion rate limiting.

- Pay attention to the long memory time of feeding systems, especially if catalyst poisons such as sulfur have been used previous to catalyst testing.
- Measure during steady state operation at isothermal and isobaric conditions.
- Minimize the temperature gradient by the addition of inert material, small reactor diameters, high flow rates, turbulent flow, and/or low conversion rates.
- Avoid concentration gradients (CSTR, low conversion rates).
- Carry out blank tests to determine thermal reactions and catalytic effects of the reactor wall.
- Pay attention to sampling and analysis.
- Be aware of equilibrium limitations.
- Check reproducibility.
- Compare selectivities of two catalysts at the same operation conditions at equal conversion levels.
- Determine catalyst deactivation with the onstream time.
- Do not extrapolate.

Continuous PFR are between 5–15 *mm* wide and 50–1000 *mm* long. They should be operated in down flow, using less than 10 mL of catalyst [26]. A PFR should be operated in the differential mode which is defined as an operation at low conversion rates (0–5 %). This avoids results that are influenced by thermodynamic constraints, like the equilibrium between reactants and products. In the differential mode, the conversion rate does not change strongly over the catalyst bed. It can therefore be simplified that the reaction rate follows the Equation given in 3.50 with the symbols defined in Table 3.5 [23, 26]. High conversion rates should rather be used for the development stage of catalysis system [26].

$$r_{vol.} = \frac{c_{i,0} \cdot X_i}{\frac{V_{cat}}{F}} \quad (3.50)$$

If it is desired to analyze the reaction rate of the surface reaction itself, it is important to avoid mass transfer limitation. Mass transfer becomes rate limiting when the surface reaction is faster than the supply of reactants or the removal of the products by diffusion steps. At lower temperatures the overall rate is usually limited by the surface reaction. At higher temperature, however the catalysis can become diffusion rate limited, as the chemical reaction

Table 3.5: Differential reactor: List of symbols, explanation and units.

Symbol	Explanation	Unit
$r_{vol.}$	Reaction rate on a volumetric base	$\frac{mol}{L_{cat} \cdot h}$
$c_{i,0}$	Initial concentration of the component i in the feed	$\frac{mol}{L}$
X_i	Conversion rate of component i	–
V_{cat}	Volume of catalyst	L
\dot{F}	Volumetric feed flow rate	$\frac{L}{h}$

rate increases exponentially with the temperature, whereas the diffusion rate increases linearly with an increase in temperature. This can be especially problematic with highly exothermic reactions. Generally, mass transfer limitations are increasingly problematic with small pore catalysts, large catalyst particles, high rate constants, high temperatures, and high pressures. If mass transfer by diffusion is rate limiting, the conversion rate of the reaction will increase with a decrease of the particle size, provided that the other reaction parameters are held constant [26].

Regarding the different life cycles of a catalyst (illustrated in Figure 3.9) it has to be ensured, that the catalyst testing is carried out in the steady state period of the catalyst life cycle. This can be problematic, as the induction period of a catalyst is sometimes inconveniently long. The activity of a catalyst may be expressed as [26]:

- Rate constants (k)
- Turnover frequency per active site (TOF, activity per active site)
- Reaction rate on a weight base ($r_{wt.}$)
- Reaction rate on a volumetric base (r_v)
- Conversion of component i (X_i) reached at constant parameters
- Temperature required for a target conversion at constant parameters
- Space velocity required for a target conversion at constant parameters

Chapter 4

The DFB steam gasification technology with particular focus on the CHP plant Oberwart

The biomass power plant in Oberwart (Austria) employs the dual fluidized bed (DFB) steam gasification technology which was mainly developed at Vienna University of Technology [53]. Wood gas generated at this plant was used as a feedstock for the experimentation within this thesis. Prior to the description of this combined heat and power (CHP) plant, the DFB steam gasification technology is described. Also the sorption enhanced reforming (SER) operation of a DFB system is discussed which represents a further development of this technology.

4.1 DFB and SER

Since 1993, DFB systems for biomass gasification are studied extensively at the Institute of Chemical Engineering of the Vienna University of Technology. In the technical laboratory on site, the 4th generation of a pilot DFB gasifier is currently under construction. The scale of these pilot gasifiers in Vienna is usually 100 kW feed power [98]. At this scale, the influence of various gasification parameters (bed material, temperature, pressure, fuel, steam/fuel ratio, feeding point etc.) on the DFB process was studied extensively. An overview of the released literature is provided in [28]. On a bigger scale (8 MW feed power), the DFB steam gasification technology was proved first at the well-known and well-documented demonstration plant in Güssing (Austria) which was already subject to a series of publications ([6, 10, 54, 55, 65] etc.). The CHP plant Güssing started operation in 2002 [45]. In Figure 4.1 the conceptual schematic of the DFB technology is illustrated.

Basically, this process was developed to avoid the addition of inert N₂ to the generated wood gas in order to increase its heating value. If air is used as a gasification agent, the heating value of wood gas is usually in the range of 3.0–6.5 $\frac{MJ}{m_n^3}$. If steam is used as a gasification agent the heating value can be increased up to 12–14 $\frac{MJ}{m_n^3}$ [61]. Elevated heating values enable a more compact design and higher electric efficiencies in gas engines [62]. The

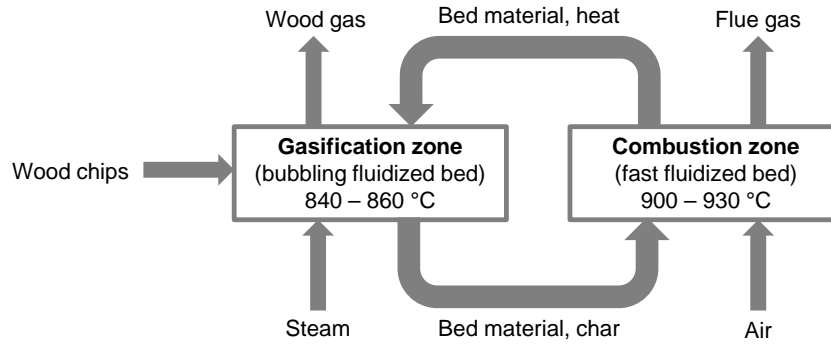


Figure 4.1: Schematic diagram of the dual fluidized bed (DFB) steam gasification technology, based on [53].

absence of N_2 in wood gas also enables its usage as synthesis gas to produce synthetic biofuels or "green" chemicals [97].

The system consists of a gasification zone and a combustion zone which are both operated as fluidized beds. Bed material (olivine, quartz sand, limestone, etc.) circulates between the two reaction chambers operated at different temperatures. The operating temperature in the combustion zone is usually 50–150 °C higher than in the gasification zone [61]. The bed material serves as a heat carrier which provides the energy for the endothermic steam gasification process. Wood chips are fed into the gasification zone which is fluidized with steam. Char is formed during the pyrolysis of the wood chips which is not completely gasified. Together with the cooled bed material, remaining char particles are transported to the combustion zone of the DFB system. Air is used as a fluidizing agent in the combustion zone to burn the char. This leads to a temperature increase and the regeneration of the bed material. Fluidized loop seals can be used to avoid gas transport between the two reaction chambers.

The DFB steam gasification of biomass is an interesting technology for medium scale hydrogen generation because it provides wood gas rich in H_2 and low in N_2 . The obtained hydrogen content can be further increased by means of the SER operation of a DFB gasifier. This process can be regarded as a further development of the technology. A schematic diagram of the SER process is shown in Figure 4.2.

The SER concept allows the selective transport of CO_2 from the gasification zone to the combustion zone. Limestone is used as a bed material which is carbonated ($CaO + CO_2 \rightarrow CaCO_3$) and calcinated ($CaCO_3 \rightarrow CaO + CO_2$) in a cyclic sequence. This results in the generation of a gas mixture rich in H_2 (up to 75 vol.%). Limestone is a catalytically very active bed material which enables the production of wood gas with a low tar content. Besides, the active material allows a reduced operating temperature in the gasification chamber which in turn leads to an increased efficiency of the energy conversion [95]. The efficiency of a gasification system is usually described by means of the cold gas efficiency of the gasifier (η_G) which is calculated according to Equation 4.1.

$$\eta_G = \frac{\dot{m}_{wood\ gas} \cdot LHV_{wood\ gas}}{\dot{m}_{wood} \cdot LHV_{wood}} \quad (4.1)$$

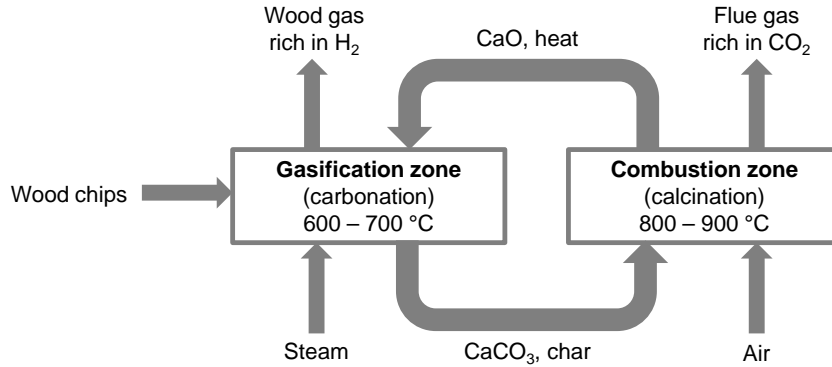


Figure 4.2: Schematic diagram of the dual fluidized bed (DFB) gasification technology operated as a sorption enhanced reformer (SER), based on [95].

Also the SER operation was studied extensively at the pilot gasifier of Vienna University of Technology ([29, 92, 93, 95] etc.). In Table 4.1 the typical composition of wood gas derived from conventional gasification (bed material olivine, according to Figure 4.1) and from SER gasification (bed material limestone, according to Figure 4.2) is compared. In 2008, the biomass CHP plant Güssing was operated in the mode of the SER process. Wood gas with an increased H₂ content (50.6 vol.%), and a decreased content of CO₂ (12.3 vol.%) and CO (16.5 vol.%) was generated. However, the existing plant in Güssing was not designed for SER operation and it has to be kept in mind that the H₂ content can be increased considerably, if the process is carried out under more optimized reaction conditions [68].

Table 4.1: Typical wood gas composition range in a DFB steam gasification process operated conventionally (olivine as bed material) and according to the SER concept (limestone as bed material); experimental data obtained from the 100 kW_{th} pilot plant at Vienna University of Technology; from [107].

Component	Conventional DFB	SER process	Unit
H ₂	36–42	55–71	vol.% _{db.}
CO	19–24	5–11	vol.% _{db.}
CO ₂	20–25	7–20	vol.% _{db.}
CH ₄	9–12	8–13	vol.% _{db.}
C ₂ H ₄	2.0–2.6	1.4–1.8	vol.% _{db.}
C ₂ H ₆	1.3–1.8	0.3–0.6	vol.% _{db.}
C ₃ fraction	0.3–0.6	0.1–1.0	vol.% _{db.}
N ₂	1.3–1.8	0.3–0.6	vol.% _{db.}
Gravimetric tar	4–8	0.3–3	$\frac{g}{m_{db}^3}$
Dust	10–20	20–50	$\frac{g}{m_{db}^3}$
H ₂ O	30–45	50–60	mol.% _{wb.}

To sum it up, wood gas derived from the SER process has a favorable composition regarding the downstream processing aiming at the generation of pure hydrogen. However, this technology did not reach a commercial state yet. This can be explained mainly by the low abrasion resistance of limestone which leads to high dust loads in the gas mixture and the

need for continuous addition of rather big amounts of fresh bed material.

4.2 CHP plant Oberwart

The CHP plant in Oberwart was the first DFB system which was designed as a commercial facility. It was ordered by Begas AG and Bewag AG, the former gas and electricity suppliers of the region of Burgenland, Austria. The history of the plant in relation to the plant in Güssing is described very well in [45]. In 2007 the plant was commissioned; the regular operation started in 2008 after a series of required modifications and improvements. According to the current operating company (Energie Burgenland AG) the power plant uses 24000 tons of wood chips annually to produce 21 *GWh* of electricity and 22.5 *GWh* of district heat [5]. Figure 4.3 shows a recent picture of the plant.



Figure 4.3: Picture of the DFB biomass steam gasification power plant Oberwart in 2014; from the left to the right: storage of wood chips, biomass feeding system, dryer, steel construction with gasification and gas cleaning, engine room, stack.

The design of the CHP plant is based on the well-documented biomass gasification plant in Güssing, Austria ([6, 10, 54, 55, 65] etc.). In both plants a high calorific gas mixture low in nitrogen is produced, which is cleaned by means of filters and scrubbers and subsequently burned in gas engines generating electricity and district heat. Both plants use the catalytically active bed material olivine. The basic design of the process can be seen in Figure 4.4.

In comparison to the demonstration plant in Güssing, several modifications have been implemented at the commercial facility in Oberwart. Generally, these modifications follow the suggestions for improvement given in the final report of the "Big power" project [73]. The main differences are an installed biomass dryer and an organic rankine cycle (ORC) process in order to increase the electric efficiency. Two gas engines are installed to increase

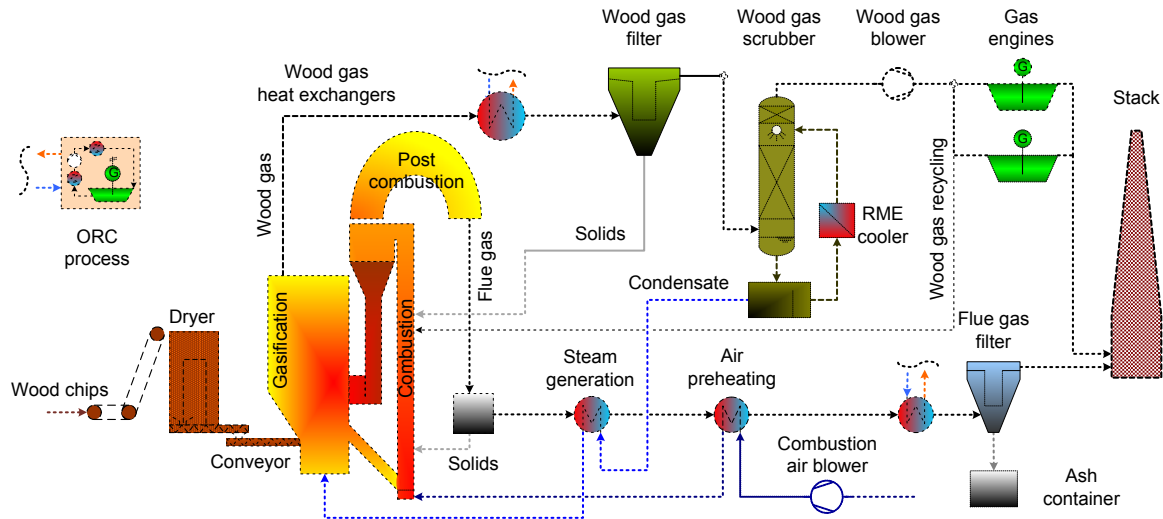


Figure 4.4: Flowchart of the DFB biomass steam gasification power plant Oberwart, based on [28].

the availability of the plant during engine maintenance. A main adjustment in comparison to the CHP plant Güssing was also the modified design of the heat exchangers and the reactor geometry which was aiming to improve the wood gas quality. The freeboard of the gasifier was designed bigger in order to enable an increased tar reforming by means of longer residence times. Also, the size of the combustion chamber, and the post combustion chamber was increased to improve char oxidation, and CO oxidation, respectively [70]. Compared to the demonstration plant in Güssing, less publications related to the CHP plant Oberwart can be found in literature [28, 36, 45, 66, 70, 115].

At the CHP plant Oberwart, the generated wood gas is cooled from about 850 °C to about 160 °C in a series of heat exchangers. The heat is mainly used for the operation of the ORC process but also the delivery of district heat. A baghouse with cylindrical polytetrafluoroethylene (PTFE) bags is used to remove particles from the wood gas stream. Flue gas from the combustion zone is used to convey these particles pneumatically to the combustion chamber of the DFB system. A wet gas scrubber is applied downstream which is operated with rapeseed oil methyl ester (RME) at a temperature of about 40 °C. Higher hydrocarbons are condensed and dissolved in the organic solvent reducing considerably the tar content of the gas. At the same time, process steam is partly condensed as well. It can be considered that the product gas exits the RME-scrubber with an equilibrium humidity corresponding to its temperature and pressure at the outlet. The condensing water also leads to the desired coabsorption of NH_3 [96]. The condensate (mostly water) formed during the quenching in the gas scrubber is partly evaporated and used as the fluidizing agent for the gasification zone.

A gas blower provides the required operating pressure of the two gas engines from GE Jenbacher GmbH which are finally operated with the cleaned and dried wood gas. The sensible heat of the flue gas generated in the combustion zone of the gasifier and the post-combustion chamber is used for the steam production, the preheating of combustion air and

the delivery of district heat [28]. A small part of the tar-loaded RME is continuously recycled into the combustion zone of the DFB system. 20–40 $\frac{kg}{h}$ of fresh bed material (olivine) have to be added. High CH₄ contents in the wood gas indicate a low steam reforming activity in the gasifier and are therefore used as an indicator for a high tar load in the wood gas. High tar loads are highly undesired because of the risk of tar condensation in the downstream equipment which might lead to plugging. A low degree of tar reforming in the gasifier can often be explained by a low catalytic activity of the bed material [65]. As a consequence, catalytically active limestone is added if high CH₄ contents are measured. N₂ is used for the dedusting of the pulse jet baghouse filter. It is also required to avoid backfiring on the biomass feeding. A more detailed description of the plant can be found in [70].

The plant is designed for a fuel power of 8 MW_{th} (about 3 tons/h). Each of the two gas engines used to provide an electrical power of 1080 kW . At the end of the year 2013, the electrical power of the gas engines was increased from 1080 to 1125 kW . At maximum power the ORC process has an electric output of 400 kW . About 1.5 MW_{th} of district heat can be delivered at maximum electricity production. If less heat is used for the electricity production in the ORC process, up to 3.9 MW_{th} of district heat can be produced [70]. The design data of the plant can also be reviewed in Table 4.2. Currently, the ORC process is mostly operated during the summer months. During the winter months, more district heat has to be produced, which does not allow an economic operation of the ORC process. The most important commercial consumers of district heat are the hospital and the commercial center of the community. Under full load of the CHP plant about 1650 $\frac{m^3_{db.}}{h}$ of wood gas are produced of which about 250 $\frac{m^3_{db.}}{h}$ are recycled into the combustion chamber of the gasifier. This value strongly fluctuates with the water content of the biomass.

In calendar week 47 of the year 2013, the actual mass and energy balances of the CHP plant Oberwart have been calculated. The obtained data are shown in Table 4.2 and in Figure 4.5 which illustrates the results in a Sankey diagram. During this operation period, the ORC process was not used because of an elevated demand for district heat. The data obtained from this closed mass balance can be compared directly with the design data of the CHP plant which are given in [70].

Table 4.2: Comparison of the key data of the performance of the CHP plant Oberwart during calendar week 47, 2013, based on [115]; and the design data of the plant, based on [70].

	Calendar week 47 (2013)	Design data (2006)	Unit
Biomass feeding	8206	8000	kW
Cold gas efficiency	77.9	73.5	%
Gas engine 1	1080	1150	kW
Gas engine 2	1080	1150	kW
ORC	0	0–400	kW
District heat	1998	1500–3900	kW
Electric efficiency	26	26.6–31.2	%
Thermal efficiency	24	18.1–41.5	%
Total efficiency	51	49.3–68.1	%

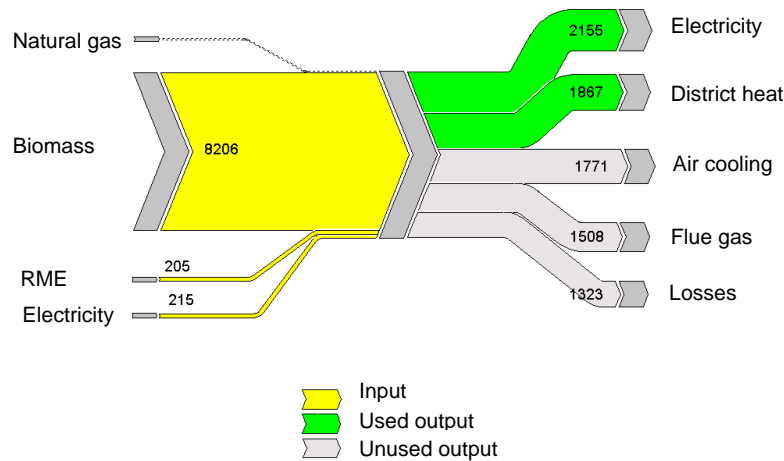


Figure 4.5: Sankey diagram of the energetic flows of the CHP plant Oberwart, based on [115].

Generally, it can be seen that a high overall efficiency of the CHP plant can only be achieved if there is an important demand for district heat. The operation of the ORC process leads to a rather small increase in the electric efficiency of the plant. This is only justified during the summer months, when there is only a small demand for district heat.

Finally, the designed wood gas composition and the designed flue gas composition of the power plant are given in Table 4.3. The design wood gas composition can be compared with the measured gas compositions that were measured within this thesis (see Chapter 6.1).

Table 4.3: Design gas compositions of the CHP plant Oberwart; Wood gas: given values of dust load and tar load at sampling point before wood gas filter; Flue gas: composition for combined flue gas derived from the combustion zone of the gasifier and the gas engines, dust load given for the combustion zone at the sampling point before flue gas filter; from [70].

Component	Wood gas	Unit	Component	Flue gas	Unit
CO	25	vol.% _{db.}	N ₂	78	vol.% _{db.}
CO ₂	21	vol.% _{db.}	CO ₂	15.4	vol.% _{db.}
H ₂	38	vol.% _{db.}	O ₂	2.4	vol.% _{db.}
CH ₄	11	vol.% _{db.}	NO	170	vol.ppm% _{db.}
C _{≤3} H _{≤8}	3.5	vol.% _{db.}	SO ₂	1.9	vol.ppm% _{db.}
N ₂	1.5	vol.% _{db.}	CO	150	vol.ppm% _{db.}
H ₂ O	35	mol.% _{wb.}	H ₂ O	13.2	mol.% _{wb.}
"Tar"	2.5	$\frac{g}{m^3_{db.}}$			
Dust	50	$\frac{g}{m^3_{db.}}$	Dust	45	$\frac{g}{m^3_{db.}}$

4.3 Research site Oberwart

Next to the CHP plant Oberwart, two 2 x 20' containers were placed one on top of the other. The container located on bottom mainly housed the gas chromatograph described in Chapter 5.3.5 as well as the analytical devices of the CHP plant Oberwart. The container

located on top housed a series of test facilities from the Vienna University of Technology and Bioenergy 2020+ which were designed and assembled within the framework of different research projects. The research projects involved in the research site Oberwart are listed below. Some projects are already finished, some projects are currently carried out, some projects have been submitted for the future:

- "Simple SNG"
- "Polygeneration I"
- "Polygeneration II"
- "Polygeneration III - Potential of Thermal Steam Biomass Gasification" (submitted)
- "Decentral Green H₂"
- "InnoGasClean"

In Figure 4.6 a recent picture of the research containers next to the CHP plant Oberwart can be seen.



Figure 4.6: Picture of research containers next to the DFB biomass steam gasification power plant Oberwart in 2014; in the container on bottom a series of analytical devices were placed; in the container on top a series of pilot plants for wood gas processing were realized.

The available operation units for wood gas processing in Oberwart are listed below. The test rigs are mainly placed in the research containers (except for the gas scrubber).

- Membrane separation unit
- Pressure swing adsorption; PSA unit
- Polymer electrolyte membrane fuel cell; PEM FC unit

- Gas scrubber; Scrubber unit (located at the steel construction of the CHP plant)
- Pilot plant for catalytic wood gas processing; WGS unit

This PhD thesis was realized within the research project "Simple SNG" which was finished in February 2014. In the framework of this project, the pilot plant for catalytic wood gas processing (see Chapter 5.3) was designed and assembled. In the course of this thesis the WGS unit was also combined with the other test rigs available in order to establish process chains aiming at the production of pure hydrogen (see Chapter 7).

Chapter 5

Experimental

This chapter describes the experimentation within this thesis. First, the applied catalysts are presented. Second, the "Test rig for chemical kinetics" is described which was used for kinetic investigations of the samples. Finally, the "Test rig for catalytic wood gas processing" or WGS unit is characterized which was realized within this PhD thesis.

5.1 Applied catalysts

Two commercially available catalysts were used to investigate the catalysis of the WGS. Both samples were fabricated on Al_2O_3 as a support material. The key data of both catalysts are summarized in Table 5.1. The presented data were obtained from the corresponding safety data sheets. More information regarding the composition was not available. Catalyst 1 was considered as a "sour shift" catalyst. Catalyst 2 (HT WGS catalyst) was usually combined with a LT WGS catalyst in a "sweet shift" operation. General properties of commercial catalysts based on Co/Mo or Fe/Cr are presented in Table 3.2.

At the "Pilot plant for catalytic wood gas processing" (Chapter 5.3) the original shape of the delivered catalyst samples was not changed. Pictures of the raw samples are shown in Figure 5.1 (a) and (b). The bulk density of Catalyst 1 was $0.78 \frac{\text{g}}{\text{cm}^3}$. The bulk density of Catalyst 2 was $1.24 \frac{\text{g}}{\text{cm}^3}$.

At the "Test rig for chemical kinetics" (Chapter 5.2) milled samples of the catalysts were used. A particle size range of 500–800 μm was chosen. Therefore the raw pellets were milled in a ball mill and subsequently fractionated in a sieve tower. Pictures of the milled catalysts are presented in Figure 5.1 (c) and (d). The bulk density of the milled samples differed from the original density of the raw pellets: Catalyst 1 milled: $0.73 \frac{\text{g}}{\text{cm}^3}$, Catalyst 2 milled: $1.06 \frac{\text{g}}{\text{cm}^3}$.

Table 5.1: Investigated commercial catalysts for the catalysis of the WGSR.

	Formulation	Active species	Promotor	Support material	Shape
Catalyst 1	CoO/MoO ₃	MoS ₂	Co ₉ S ₈	γ-Al ₂ O ₃	Pellets (diameter: 3 mm, length: 3–10 mm)
Catalyst 2	Fe ₂ O ₃ /Cr ₂ O ₃	Fe ₃ O ₄	Cr ₂ O ₃ (2.5 wt.%) CuO (10 wt.%)	γ-Al ₂ O ₃	Disks (diameter: 6 mm, width: 3 mm)



(a) Catalyst 1: Co/Mo raw



(b) Catalyst 2: Fe/Cr raw



(c) Catalyst 1: Co/Mo milled



(d) Catalyst 2: Fe/Cr milled

Figure 5.1: Samples of the tested commercial WGS catalysts; raw catalysts: shape of pellets and disks according to Table 5.1, bulk density Catalyst 1: $0.78 \frac{g}{cm^3}$, Catalyst 2: $1.24 \frac{g}{cm^3}$; milled catalysts: particle range 500–800 μm , bulk density Catalyst 1: $0.73 \frac{g}{cm^3}$, Catalyst 2: $1.06 \frac{g}{cm^3}$.

Catalyst 1 had to be sulfided at a temperature ramp of 150–320 °C in order to form the active MoS₂ phase. According to the producer, the heating rate of the catalyst should not exceed 50 $\frac{^{\circ}\text{C}}{\text{h}}$. The maximum operating temperature of the catalyst should be limited to 510 °C in order to minimize the extent of the exothermic methanation reaction which could be catalyzed as a side reaction. More than 100 vol.ppm of H₂S should be present in the feed in order to maintain a good performance of the catalyst. During the initial phase of operation the catalyst was reported to exhibit a high degree of activity so that it can be operated below the design inlet temperature. In the course of time, the inlet temperature could be increased in order to maintain the same conversion level. Sulfided Co/Mo-based catalysts are pyrophoric and care had to be taken during unloading. Catalysts which were deactivated by coking or carbon deposition, could be regenerated by means of small amounts of O₂ which burn the carbon deposits and a subsequent resulfidation [1].

Catalyst 2 had to be reduced at a similar temperature range as Catalyst 1 in order to form the active magnetite (Fe₃O₄). The heating rate of the catalyst should not exceed 100-150 $\frac{^{\circ}\text{C}}{\text{h}}$. According to the producer, the inlet temperature of this catalyst is usually set to 315–380 °C. Some loss of activity was possible if the catalyst was heated above 540 °C. The catalyst was delivered in the oxidized state (Fe₂O₃/Cr₂O₃) and had to be reduced prior to operation. Cr served as a matrix stabilizer to minimize deactivation. Some Cr was reported to be present in the form of CrO₃. The reduction of CrO₃ according to Equation 3.21 is strongly exothermic. The catalyst also contained CuO which served as a promoter. Similar to LT WGS catalysts, CuO had to be reduced according to Equation 3.26 to form Cu-crystallites. The reduction procedure should be carried out at a GHSV of at least 200 h⁻¹. The reduction was reported to lead to a temperature wave of up to 100 °C proceeding through the bed. H₂S could be produced during this procedure. Different gas mixtures containing CO and/or H₂ were suitable for the reduction of the catalyst (including process gas from partial oxidation reactors or steam reformers). Analogous to Catalyst 1, the activity of the fresh catalyst was reported to be higher than the design activity. The inlet temperature could therefore be set below the design value which was useful to increase the lifetime of the catalyst [2].

5.2 Test rig for chemical kinetics

Initially, the "Test rig for chemical kinetics" was used to obtain important design values for the "Pilot plant for catalytic wood gas processing" that will be discussed later (Chapter 5.3). Thereby, catalyst samples were investigated in a series of pre-tests. The main aim was to determine the later design volume of the reactors by means of estimating the required GHSV of the catalysis.

Later, the "Test rig for chemical kinetics" was used to establish empirical power law rate models of the available catalysts. The test rig enabled catalyst testing under comparable conditions using synthetic gas mixtures. Also, the influence of hydrogen sulfide on both catalysts was investigated by means of this apparatus.

The "Test rig for chemical kinetics" was placed in the technical laboratory of the Institute

of Chemical Engineering (Vienna University of Technology). Synthetic gas mixtures simulating the wood gas composition were passed over small amounts of catalyst. Figure 5.2 shows a picture of the laboratory test rig. Within this PhD thesis, the already existing device was improved and extended in order to meet the requirements of experimentation. Therefore, three mass flow controllers (MFC), a steam generating system, a trace heated steam line, and an additional thermocouple were installed.



Figure 5.2: Picture of the setup of the "Test rig for chemical kinetics"; left: gas supply with gas cylinders; central: electrical cabinet with mass flow controllers and evaporator, visualization of the experiment, the glass reactor was placed at the backside of the electrical cabinet; right: gas analyzer.

5.2.1 Design

Figure 5.3 shows a flowchart of the employed test rig. Five different mass flow controllers (MFC) from BronkhorstTM and MKSTM were used to set defined volumetric gas flow rates of H₂, CO, CO₂, N₂ and H₂S. The maximum flow rates of the MFC varied between $3 \frac{L_n}{h}$ and $300 \frac{L_n}{h}$. Sulfur addition was achieved over a corrosion resistant MFC suitable for H₂S. It was operated with a calibration gas mixture composed of 1.013 vol.% of H₂S in N₂ in order to enable the feeding of small volumetric flow rates of sulfur. A CEMTM (Controlled Evaporator Mixer) system from BronkhorstTM was capable of providing up to $30 \frac{g}{h}$ of process steam. The water supply was achieved over a pressurized tank (N₂ pressure from the gas cylinder) filled with demineralized water. A pressure reducer was used to adjust a pre-pressure of 1.0 barg in the tank in order to provide a driving force for the water supply. A mass flow controller for liquids (LiquiFlowTM from BronkhorstTM) was used to provide a defined mass flow rate of water. Upstream the mass flow adjustment a particle filter from SwagelokTM with a pore size of 0.5 μm was applied. H₂ was used as a carrier gas for steam generation within the CEM system. Electrical trace heating was implemented to avoid condensation in the steam

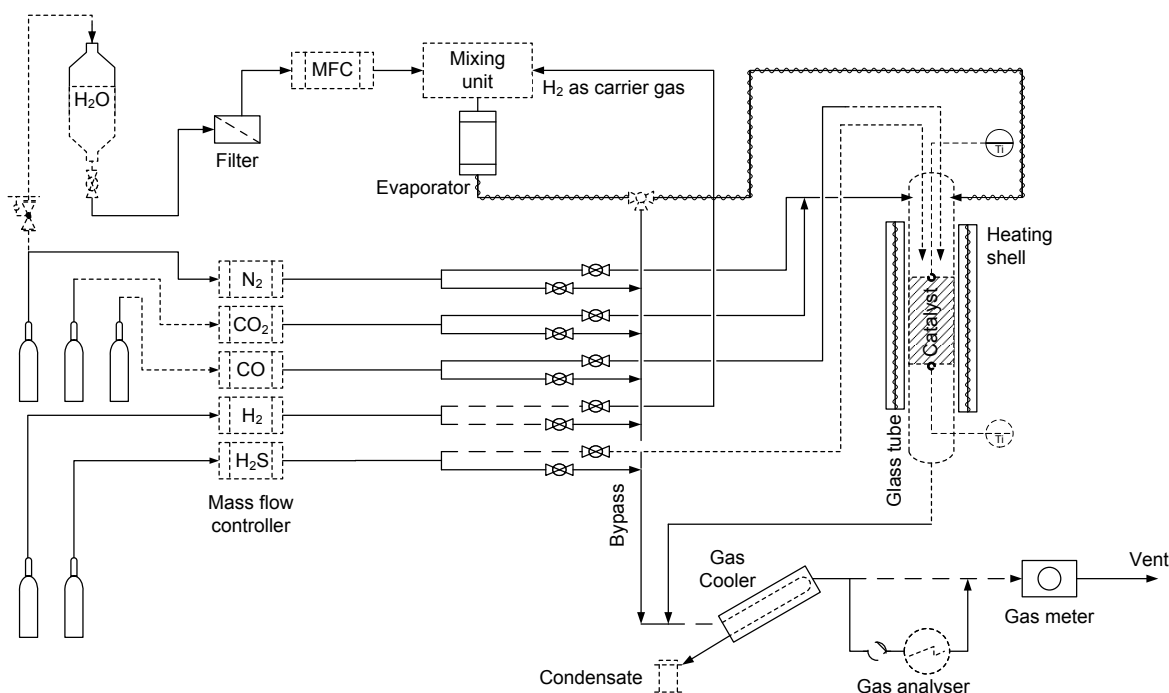
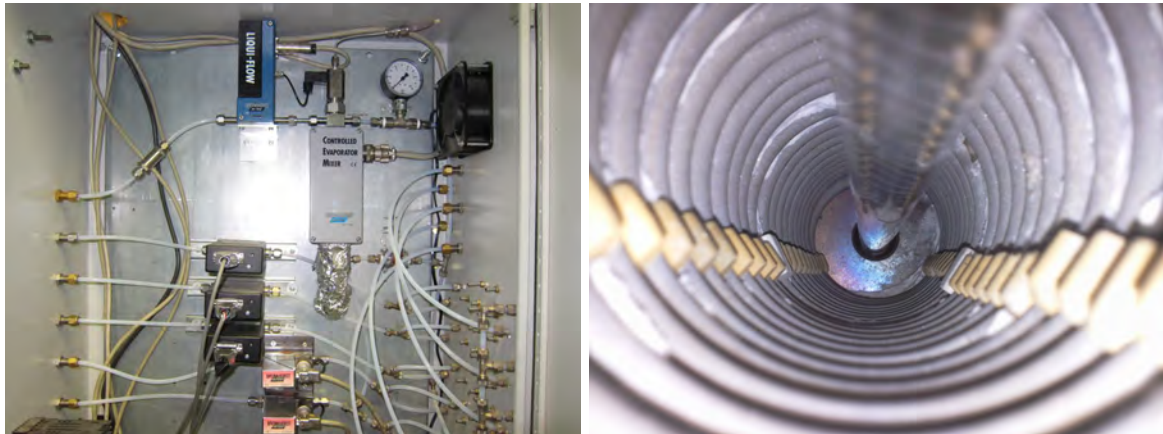


Figure 5.3: Flowchart of the "Test rig for chemical kinetics" used for catalyst testing on a small scale.

containing piping. Each gas channel was provided with two parallel valves directing either to the bypass or to the reactor. The reactor itself was a quartz glass tube with a length of 1000 *mm* and an inner diameter of 10 *mm*. In the middle, the reactor was lead through an electric heating shell with a height of 220 *mm* and an electric power of 860 *W*. The catalyst was placed inside the glass tube on quartz glass wool. The temperature of reaction was set with a digital temperature controller in combination with a type K thermocouple touching the outer surface of the glass reactor at the catalyst containing part of the tube. Two additional type K thermocouples measured the inside temperature at the inlet and at the outlet of the catalyst bed. The temperature of reaction was referred to as the average of the inlet and outlet temperature. Figure 5.4 shows pictures of the inside of the electric cabinet of the test rig as well as the quartz glass reactor inside the electric heating shell.

On-line gas analysis of the gas mixture exiting the reactor or the bypass gas mixture was carried out. Prior to gas analysis, water was removed in a Graham condenser. The condensate was collected in a reservoir. The dry gas stream was finally quantified with a bellows-type gas meter from KromschroderTM (BKG2.5). A temperature compensation of the obtained flow rate in actual $\frac{L}{h}$ was required. The ambient temperature was measured with a mercury thermometer. The volumetric flow rate at standard conditions (0 °C and atmospheric pressure) was calculated with the first law of Gay-Lussac. A bypass loop was installed to provide the employed on-line gas analyzer (see Chapter 5.2.3) with a partial flow of the gas stream. The gas meter was installed downstream the gas analyzer in order to attain a short response time of the analysis due to a small amount of dead volume.

Data acquisition was achieved over two data loggers from National InstrumentsTM (NI



(a) Electric cabinet of the laboratory test rig (b) Quartz glass reactor in the electric heating shell

Figure 5.4: Pictures of the "Test rig for chemical kinetics".

USB-6009). The software LabVIEW™ was used to set and control mass flow rates and evaporation temperatures. Also, the current flow rates, the reaction temperatures and the measured gas compositions were visualized and registered by means of this software. Different gases could be applied for each MFC by choosing the appropriate gas correction factor. A screenshot of the LabVIEW™ user interface can be seen in Figure 5.5.

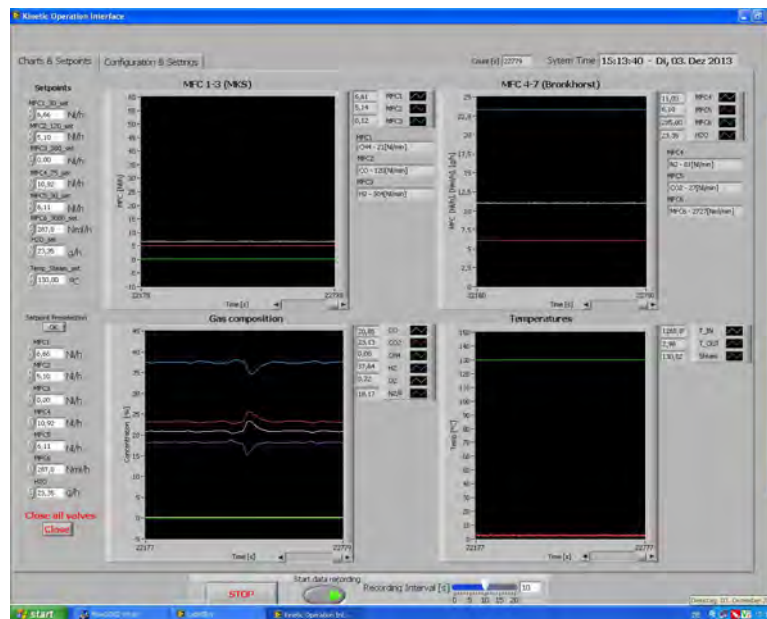


Figure 5.5: Screenshot of the operation surface of the test rig for chemical kinetics.

5.2.2 Experimentation

To ensure a proper operation of the MFC they were operated at 10–90 % of their maximum capacity. In preparation of the experiments, a soap film bubble flowmeter was used for MFC calibration. The accumulated water in the reservoir was quantified gravimetrically. Before

exposing an adjusted gas stream to the catalyst, it was led through the bypass. After achieving steady state, the inlet gas composition and the volumetric gas flow rate were measured for 15 minutes. Thereby the mass balance of the system inlet was defined. After the characterization of the inlet, the gas was exposed to the catalyst and the outlet was characterized identically.

Catalyst testing with the aim of establishing empirical power law rate models was generally carried out according to the guidelines listed in Chapter 3.6. A down flow reactor was used and operated in the differential mode. The CO conversion rate (Equation 3.17) was kept in the range of 5 % in order to minimize temperature and concentration gradients over the bed height. The height of the fixed bed of milled catalyst was adjusted to 50 mm. The catalysts were ground to a particle size range of 500–800 μm in order to avoid diffusion-rate limited operation [26]. The influence of the reactor wall was reduced by adjusting the ratio between the inner reactor diameter to the particle diameter (d_p) to be > 10 . The ratio of the fixed bed height and d_p was set > 50 to avoid axial gradients [23]. To facilitate isothermal operation, the bed height was not set higher than 50 mm. High GHSV (Equation 3.12) were adjusted to assure a turbulent flow and to avoid radial concentration gradients. The same catalyst volume of both samples was used. Also, equal volumetric flow rates were adjusted which resulted in equal GHSV. However, the bulk density of the tested catalysts differed (see Chapter 5.1) and therefore also the mass of used catalyst. A blank experiment was carried out prior to catalyst testing. At the applied GHSV and temperatures, no significant conversion of CO could be observed in the absence of a catalyst. The catalyst testing was carried out at atmospheric pressure.

The establishment of a power law rate model (Equation 3.46) requires mainly the variation of the feed composition and the variation of the temperature of reaction. A variation of the feed composition allows an estimation of the apparent reaction orders (a, b, c, d) with respect to each reacting agent. The temperature variation enables the generation of an Arrhenius plot and therefore the estimation of the apparent activation energy E_A and the pre-exponential factor A [52]. The applied gas compositions were generally based on the wood gas composition derived from DFB steam gasification of biomass. Wood gas components not taking part in the WGSR (mainly hydrocarbons) were subsumed as N_2 .

During the investigation of the reaction order of one reacting agent, only the partial pressure of this component was varied. The total flow rate ($58 \frac{\text{L}_n}{\text{h}}$) and the GHSV_{wb} (16000 h^{-1}) were kept constant by adjusting the N_2 flow rate. In the Chapter "Results and discussion", tables are presented which list the adjusted partial pressures during the investigation of the reaction orders (Table 6.5 for Catalyst 1 and Table 6.9 for Catalyst 2). Usually 5 different compositions were applied per reacting agent.

The influence of sulfur on the activity of the catalyst was expressed in the form of a simple power law model which is stated in Equation 5.1. The symbols of the equation are described in Table 5.2. The obtained reaction rate r_{wt} depended strongly on the factor S which was related to the catalyst and the experimental conditions including the gas composition and the reaction temperature. The factor e was defined as the apparent reaction order with respect

to H_2S .

$$r_{wt.} = S p_{H_2S}^e \quad (5.1)$$

Table 5.2: Power law rate model with respect to sulfur: List of symbols, explanation and units.

Symbol	Explanation	Unit
$r_{wt.}$	Reaction rate on a weight base	$\frac{mol}{g_{cat} \cdot s}$
S	Factor representing the catalyst and the experimental conditions	$\frac{mol}{g_{cat} \cdot s} \cdot kPa^{-e}$
p_{H_2S}	Partial pressure of H_2S	kPa
e	Apparent reaction order with respect to H_2S	-

The apparent activation energies E_A and the pre-exponential factors A for the power law rate model in Equation 3.46 were obtained from temperature variation studies at a fixed GHSV and a fixed gas composition of the feed (see Table 5.3). The adjusted gas mixtures contained 100 vol.ppm_{db.} of H_2S in order to simulate the sulfur load in real wood gas. The Fe/Cr-based catalyst was also tested under H_2S -free feed. For the Co/Mo-based catalyst, the temperature was increased from 320–470 °C. The Fe/Cr-based catalyst was tested from 220–305 °C. Arrhenius plots were drawn with the obtained CO conversion rates. The apparent activation energies E_A were calculated based on the slopes of these lines. The pre-exponential factors could be calculated from the intercept of these lines with the y axis.

Table 5.3: Adjusted gas composition to obtain Arrhenius plots for both catalysts (Catalyst 1: Co/Mo-based; Catalyst 2:Fe/Cr-based).

CO	CO ₂	H ₂	N ₂	H ₂ S
vol.% _{db.}	vol.% _{db.}	vol.% _{db.}	vol.% _{db.}	vol.ppm _{db.}
23.91	22.91	37.55	15.62	100

5.2.3 Chemical analysis

On-line gas analysis was carried out with a measurement device from Rosemount™ (Analytical model NGA 2000) which was equipped with an internal gas pump. This pump steadily provided the analyzer with a volumetric sampling stream of 50 $\frac{L_n}{h}$. Measurement of CO, CO₂ and CH₄ was achieved by a nondispersive infrared detector. The wavelength of an infrared absorption band is characteristic for a type of gas. The height of the absorption peak enables quantification. H₂ was detected by a thermal conductivity sensor within a Wheatstone bridge. O₂ was detected paramagnetically. The total error of the gas analyzer is reported to be less than 1 % related to the full scale [101].

5.2.4 Data treatment

The mass balance over the WGS reactor was basically overdetermined. For one set of parameters (one gas composition according to Tables 6.5 and 6.9), the dry volumetric gas flow

rate and the gas composition were measured during bypass operation (characterization inlet) and during catalyst operation (characterization outlet). Therefore, the proper functioning of every single MFC was only helpful for a precise setup of the experiment. The data evaluation and the calculation of the CO conversion rate were based on the measured volumetric gas flow rates. The mass flow controller for liquids was calibrated gravimetrically, whereby a proper functioning was revealed. Small water drops in the piping were necessitating a long period of measurement for a precise quantification of condensate. Therefore, the set value of the water addition was used directly for the quantification of water at the inlet of the reactor. The flow rate of water after reaction was estimated via mass balance using the change of the gas composition.

5.3 Pilot plant for catalytic wood gas processing

Catalyst testing on a bigger scale using real wood gas was carried out next in a laboratory container next to the CHP plant Oberwart which was described in Chapter 4. Within this thesis the "Pilot plant for catalytic wood gas processing" was designed, assembled, commissioned and optimized. Finally, this unit was linked to other operation units in order to produce pure hydrogen based on wood gas (see Chapter 7). Depending on the applied catalyst and the adjusted operating conditions, this pilot plant basically enabled the heterogeneous fixed bed catalysis of different chemical reactions. In the commissioning phase, noble metal catalysts were tested in order to enable the catalysis of the methanation reaction and the simultaneous medium temperature steam reforming of tar components. The tested catalysts turned out to be vulnerable to sulfur poisoning. In the course of this project, the research focus was therefore set on the WGS as its catalysis can be carried out with sulfur tolerant catalysts. As a consequence the pilot plant for catalytic wood gas processing was also called WGS unit. Figure 5.6 shows pictures of the finally realized experimental setup in Oberwart, Austria.

The WGS unit enabled the processing of real wood gas derived from the commercial biomass steam gasification power plant. The test rig could be operated with a feed extracted either after the filter or after the scrubber of the CHP plant Oberwart. 1 inch (DN 25) tubes were laid directing wood gas from the CHP plant to the pilot plant. Two optional feeding pipes and one recirculation pipe with a length of about 12 m each were installed. The wood gas extracted after the scrubber contained less steam and less tar components (see Chapter 4). The process temperature downstream the wood gas filter was approximately 140 °C. The process temperature downstream the wood gas scrubber was about 40 °C. The tubing (stainless steel, type 1.4571 according to EN 10027-2) was equipped with electrical trace heatings in order to avoid tar condensation. Electrical heating cables with a power of 30 $\frac{W}{m}$ (HKPT from HorstTM) in combination with temperature controllers (MC1-10A from HorstTM) were installed to maintain at least the process temperature at the corresponding point of gas extraction. Each cable, mounted back and forth, was equipped with two Pt-100 sensors for temperature control and emergency shutdown, respectively. The pipes were isolated with 40 mm of rock wool and covered in a steel shell. Figure 5.7 illustrates the integration of the pilot plant with its core elements (gas pump, water pump and 3 fixed bed reactors) into the CHP plant.

The generated water gas shifted gas mixture (raffinate) was recycled back into the power plant. For clarity reasons this is not plotted in Figure 5.7. In order to facilitate the recirculation, the raffinate was fed back upstream the wood gas blower of the power plant at a pressure of approximately -40 mbarg. Table 5.4 lists the interfaces of the WGS unit and the CHP plant including the present operation condition and the content of water and impurities.

5.3.1 Design of pilot plant

The basic flowchart of the realized pilot plant is given in Figure 5.8. A three-dimensional engineering drawing of this test rig is shown in Figure 5.9. In accordance to the connection



Figure 5.6: Pictures of the realized "Pilot plant for catalytic wood gas processing" (WGS unit); top: picture prior to heat insulation 2012; bottom: picture of the final setup in 2013, including heat insulation, sampling for gas analysis, etc.

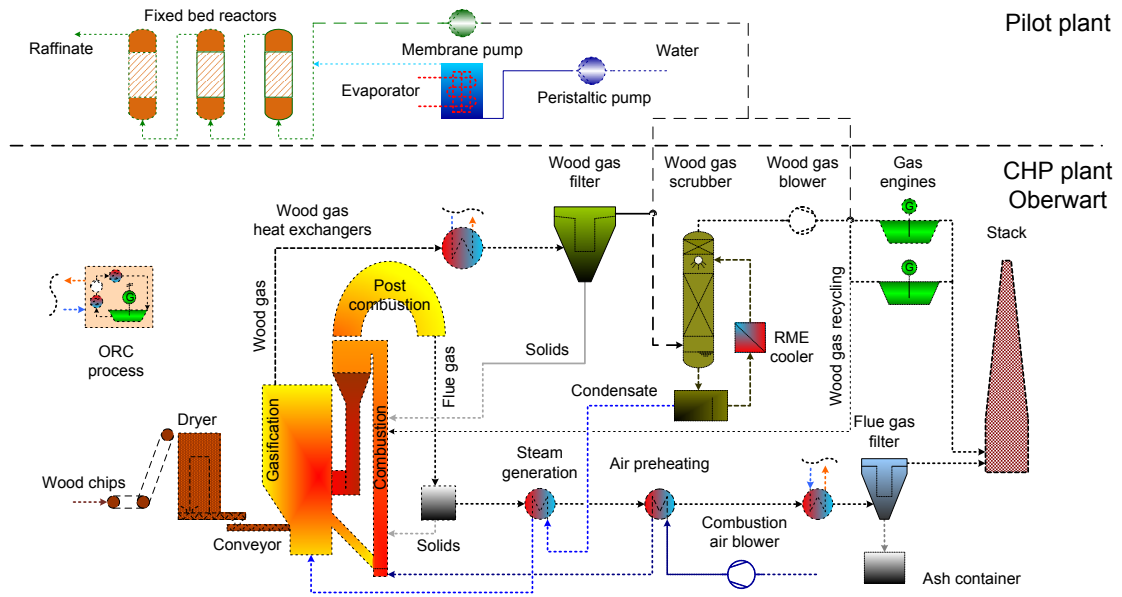


Figure 5.7: Connection of the "Pilot plant for catalytic wood gas processing" (WGS unit) to the CHP plant Oberwart.

Table 5.4: Process conditions at the interfaces of the WGS unit and the CHP plant Oberwart, temperatures and pressures from CHP plant operation calendar week 29 (2013), water content after gas filter from [70], water content after scrubber calculated based on the saturation with steam at the corresponding outlet temperature of the scrubber, NH_3 after filter from [96], NH_3 after scrubber measured in calendar week 2 (2014), Tar contents from [70].

	Raw gas	Cleaned gas	Recycle	Unit
Sampling point	After gas filter Before gas scrubber	After gas blower Before gas engines	After gas scrubber Before gas blower	
Temperature	153.4 ± 2.2	36.2 ± 2.9	35.8 ± 3.0	$^{\circ}\text{C}$
Pressure	-38.3 ± 5.8	82.0 ± 3.2	-38.3 ± 5.8	<i>mbarg</i>
Water content	35	5.5–7.6	5.5–7.6	$\text{mol.}\%_{wb.}$
NH_3	1100–1700	954	954	$\text{vol.ppm}_{db.}$
Gravimetric tar	1.54–1.87	0.08–0.27	0.08–0.27	$\frac{g}{m_n^3}$
GC-MS tar	6.865–7.076	0.204–0.327	0.204–0.327	$\frac{g}{m_n^3}$

to the CHP-plant, the standard dimension of the pilot plant were 1 inch (DN 25) pipes. Type 1.4571 stainless steel was used as the standard material. The pilot plant was designed within this thesis. The basic construction of the plant was carried out by the industrial project partner Binder Industrieanlagenbau GmbH.

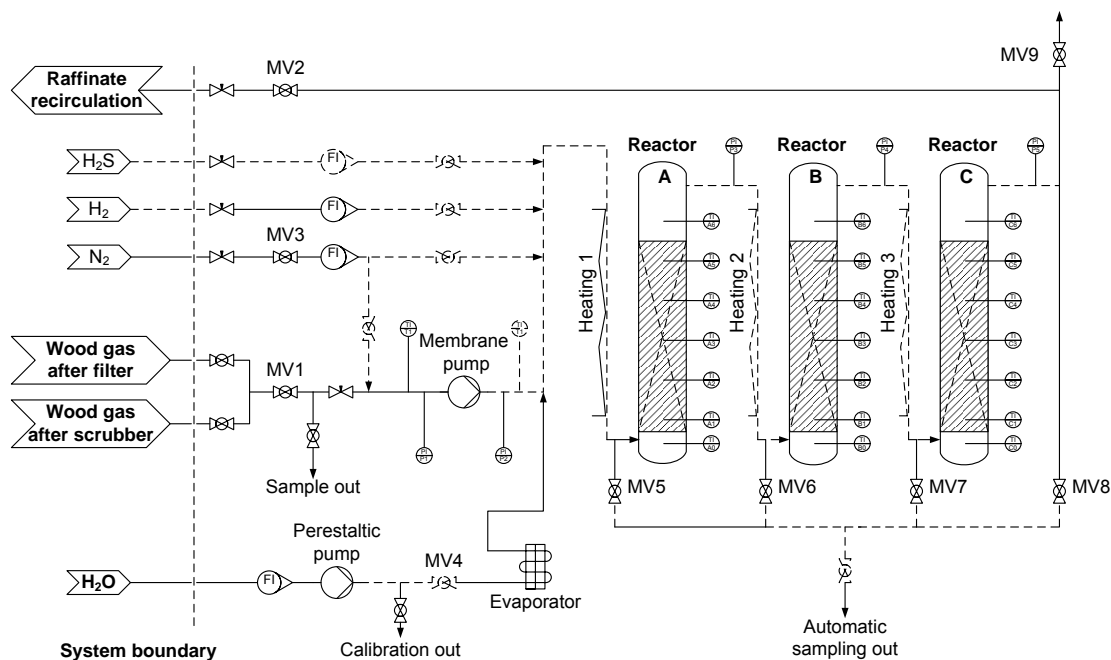


Figure 5.8: Flowchart of the pilot plant for catalytic wood gas processing (WGS unit).

Wood gas was extracted from the power plant with a heated and flow controlled membrane pump (KNFTM, N 036.0ST.11E). Trace heating of both stainless steel pump heads was achieved electrically in order to avoid tar condensation inside the pump. The membranes and the valves in contact with wood gas were manufactured out of the chemically resistant PTFE. A frequency converter (DanfossTM VLT 2803) was enabling the rotation speed control of the gas pump. According to the manufacturer, the maximum capacity of the pump was $3.5 \frac{m^3}{h}$. The recorded performance curve of the gas pump as an integral part of the system is presented in Figure 5.19. Frequency control at low rotation speed could lead to an overheating of the membrane pump motor. Therefore, the motor was additionally cooled with an external ventilation. Steam was added to the gas mixture to enhance the WGSR and to prevent carbon formation at the catalyst surface (see Chapter 3.4.1 and [75]). A water barrel with a capacity of 200 L was placed next to the test rig. Water addition was achieved by means of a flow controlled peristaltic pump (IsmatecTM, Reglo analog ISM 830) in combination with a flexible hose (Ismaprene, Inner diameter ID 2.06 mm). The liquid flow rate was monitored by means of a variable area flow meter (VAF Fluid-Technik) with a range of 2–80 $\frac{mL}{min}$. Evaporation was achieved in a stainless steel tube with an ID of 10 mm and a length of 3000 mm. The tube was bent into a coil and a heating rod with a length of 2440 mm and an electrical power of 2.3 kW was installed in between the loops. The evaporator was equipped with two different type J thermocouples. One was measuring the steam temperature at the

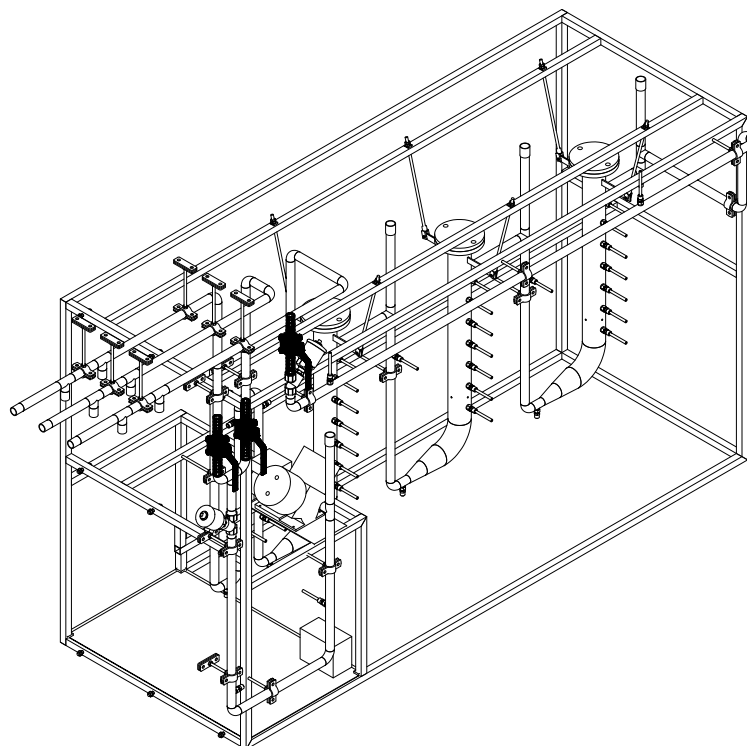
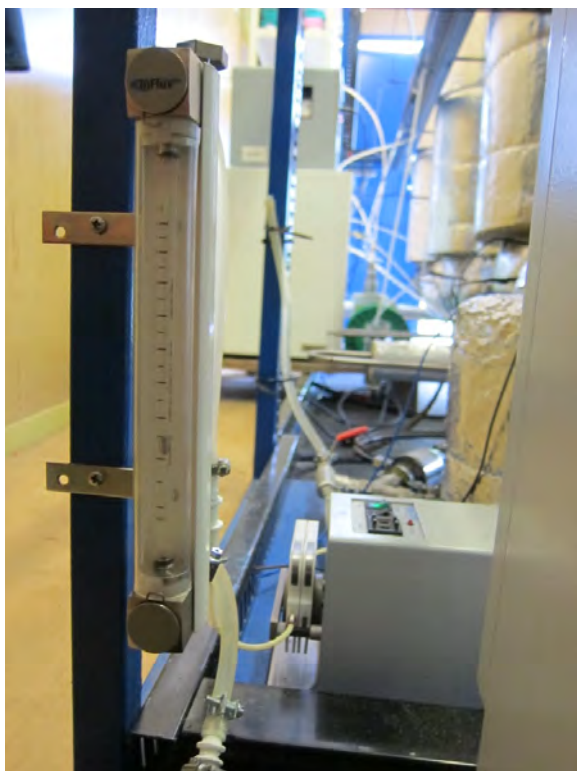


Figure 5.9: Three-dimensional engineering drawing of the pilot plant for catalytic wood gas processing (WGS unit).

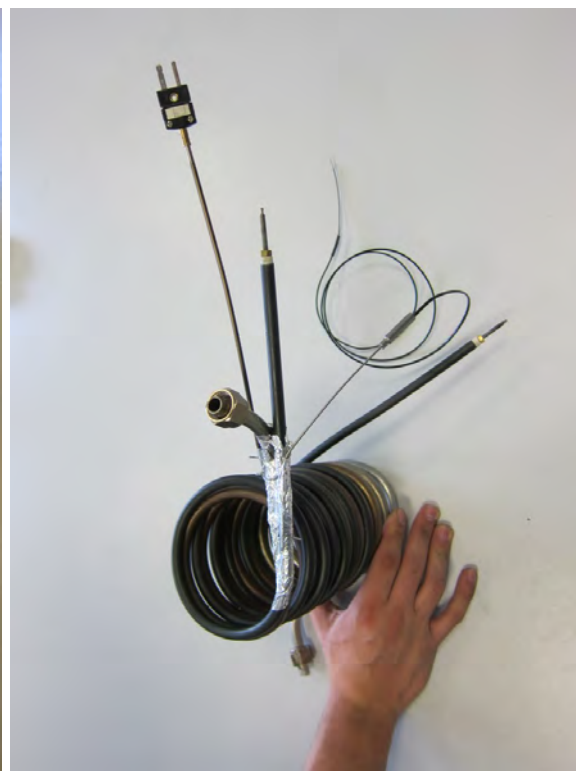
outlet of the evaporator. The other thermocouple measured the surface temperature of the heating rod. The entire unit was coated with aluminum foil in order to improve the heat transfer. Figure 5.10 illustrates the steam addition line of the pilot plant. The GHSV and the $\frac{H_2O}{CO}$ ratio could be adjusted by choosing an appropriate combination of flow rates of the membrane gas pump and the peristaltic water pump.

After the steam addition the gas mixture was heated up electrically to the desired reaction temperature. Gas preheating was achieved in a DN 25 pipe with a length of about 2 meters. A heating rod (length 2440 mm, power 1.5 kW) was attached to the surface of the pipe. Two thermocouples were directly related to this heating element. One was measuring the gas temperature at the inside, the other one was measuring the surface temperature of the heating rod. An overall of 7 identically constructed heating elements (length 2440 mm, power 1.5 kW) were installed along the system in order to enable a precise temperature control of the entire system. The temperature control based on this setup is described in more detail in Chapter 5.3.3. Additionally, each reactor was provided with 2 identical heatings resulting in an overall number of 13 heating elements and 26 related type J thermocouples. The reactor heatings were mostly used during preheating of the system. During steady state operation, these heating rods were usually turned off to avoid an influence on the temperature profile of the reactor. The most important heating rods were therefore the preheating elements at the inlet of each reactor. These are the only heatings which are illustrated in Figure 5.8.

The pilot plant was equipped with a series of variable area flow meters in order to add



(a) Flow meter and peristaltic pump



(b) Evaporator coil with heating rod

Figure 5.10: Steam addition including the variable area flow meter, the peristaltic pump, the evaporator tube with the heating rod and the type J thermocouples.

defined volumetric flow rates of N_2 , H_2 , or H_2S to the system (Flow indicators FI in Figure 5.8). These devices from VAF Fluid-Technik also included a needle valve. N_2 could be added in range of $10\text{--}100 \frac{L_a}{min}$; H_2 could be added in the range of $1\text{--}15 \frac{L_a}{min}$; and H_2S could be added with two different flow meters via a range of $10\text{--}100 \frac{L_a}{h}$ and $5\text{--}60 \frac{mL_a}{min}$. These flow meters were mainly used for the activation of the catalysts but also the simulation of wood gas with an increased sulfur load.

An engineering drawing of one example reactor is shown in Figure 5.11 (a). Stainless steel sieve plates with a hole diameter of 3 mm were placed inside the reactors to provide a basis for the catalyst beds. Each reactor was provided with 7 type J thermocouples. One thermocouple measured the gas temperature underneath the sieve plate. Subsequently, 5 thermocouples registered the temperature profile every 100 mm of the fixed bed. The top level thermocouple measured the gas temperature at the outlet of the reactor and was not in contact with catalyst any more (see Figure 5.11 (b) which shows a picture of the inside of the reactor filled with catalyst). The average temperature of reaction was referred to as the average temperature of the thermocouples which were in contact with catalyst (TA1–TA5, TB1–TB5, TC1–TC5). The inner diameter of the reactors was 80.8 mm (DN 80 tubes). The height of each catalyst bed was set to approximately 500 mm representing an overall bed volume of about 8 L . The GHSV could be calculated with respect to each sampling point of the process (changing catalyst volume). The overall GHSV was referred to as the GHSV after the last reactor (MV 8) and therefore the complete catalyst volume. The reactors were mounted in a hanging position to avoid temperature related tension problems.

5 pressure sensors (TecsisTM, type P3251B-067) were detecting the operating pressure at the most relevant points of the process:

- P1 Pressure at the inlet of the gas pump (membrane pump)
- P2 Pressure at the outlet of the gas pump (membrane pump)
- P3 Pressure at the outlet of reactor A
- P4 Pressure at the outlet of reactor B
- P5 Pressure at the outlet of reactor C

The pressure sensors were operating in a pressure range from $-0.3\text{--}0.3 \text{ barg}$. Generally, the test rig was designed for an operation around ambient pressure. Needle valves at the system inlet and outlet were enabling a fine pressure regulation over the process.

9 pneumatic valves were integrated into the system. A list of these valves is provided in Table 5.5. Each valve was controlled with pressurized nitrogen. The control pressure was regulated with magnetic valves (MV) directly integrated into the process control system (PCS). MV 3 and MV 9 were designed normally open. The aim was to assure an immediate inertization with nitrogen as a consequence of a power blackout. The outlet of nitrogen flushing (controlled by MV 9) was directed to the roof of the container.

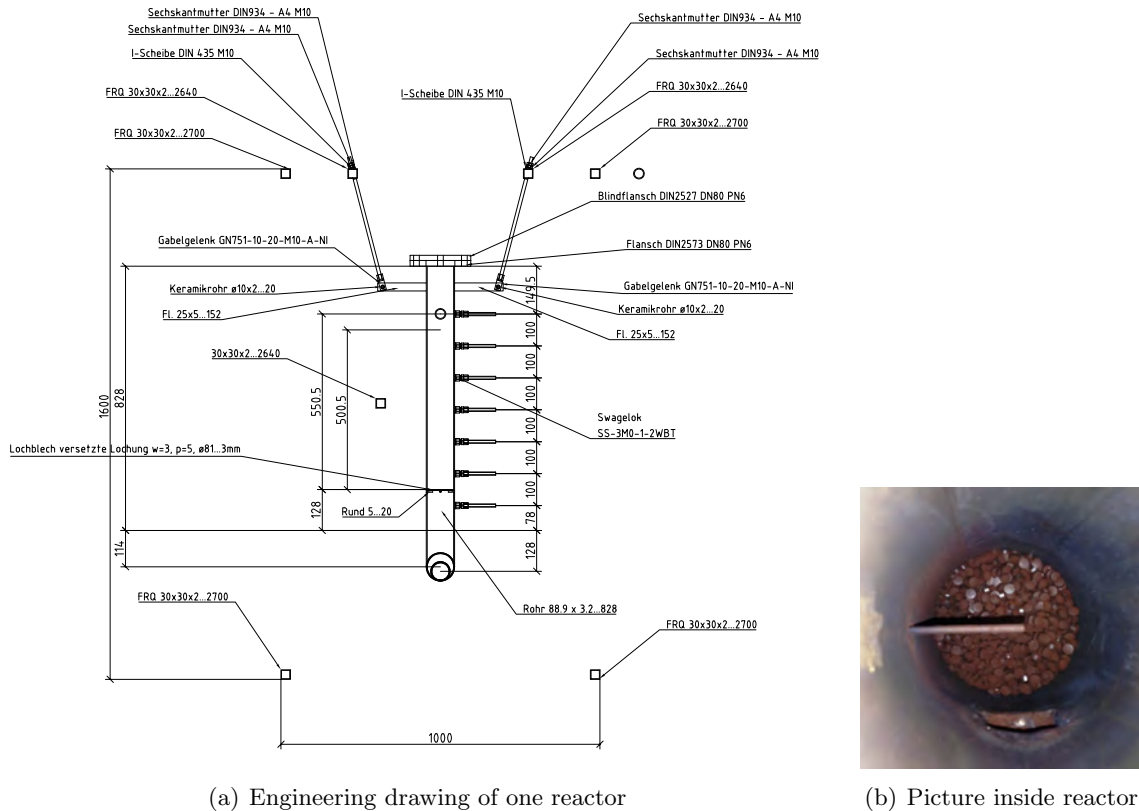


Figure 5.11: Fixed bed reactor of the pilot plant for catalytic wood gas processing (WGS unit).

Table 5.5: List of pneumatic valves integrated into the "Pilot plant for catalytic wood gas processing" (WGS unit), the pneumatic valves were controlled by means of magnetic valves (MV) and are labeled according to these valves, MV 3 and MV 9 were designed normally open.

	Position	Function
MV 1	Inlet wood gas	Feeding wood gas
MV 2	Outlet raffinate	Recycling raffinate into the CHP plant
MV 3	Inlet nitrogen flushing	Inertization for startup and shutdown
MV 4	Inlet water addition	Avoiding carbon formation, enhancing WGSR
MV 5	Sampling raw wood gas	Chemical analysis upstream catalysis
MV 6	Sampling after reactor A	Chemical analysis downstream reactor A
MV 7	Sampling after reactor B	Chemical analysis downstream reactor B
MV 8	Sampling after reactor C	Chemical analysis downstream reactor C
MV 9	Outlet nitrogen flushing	Inertization for startup and shutdown

Figure 5.12 shows pictures of the electric control panel of the pilot plant. Top down 5.12 (a) shows the interface to the peripheral devices, the process control system (PCS), the circuit breakers, the power supply unit, and the contactors of the heating rods. Top down 5.12 (b) shows the frequency converter of the pump, the supply of control pressure, the magnetic valves to operate the pneumatic valves, the high voltage power supply and the interface pins for the heating rods.

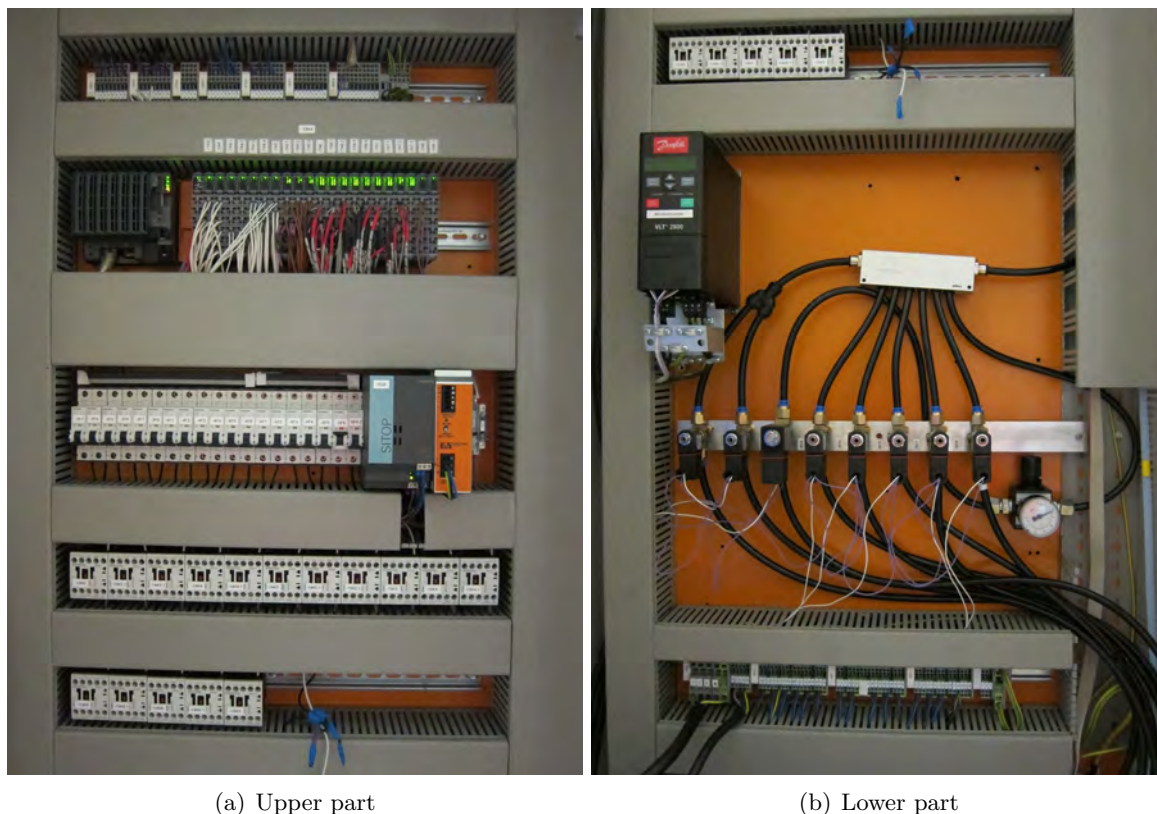


Figure 5.12: Pictures of the electric control panel of the pilot plant for catalytic wood gas processing (WGS unit).

5.3.2 Automation and visualization

The automation of the pilot plant was programmed by the project partner CTS GmbH (Competence for technical solutions) based on the requirement specification that was prepared within this thesis. The process control system (PCS) of the pilot plant was arranged with the X20 system from the automation company Bernecker und Rainer (B&RTM). The programming of the PCS was carried out with the automation software Automation StudioTM provided by B&RTM. The CPU of the system was connected to a series of analogous and digital input and output modules for the communication with the peripheral devices. Table 5.6 provides a list of all signals included into the PCS.

The communication of the process computer and the PCS was achieved with a virtual network computing software (VNC ViewerTM). All peripheral devices (Pumps, pneumatic

Table 5.6: Overview of signals integrated into the process control system (PCS) of the "Pilot plant for catalytic wood gas processing" (WGS unit); DI (digital input), DO (digital output), AI (analogous input), AO (analogous output), TI (thermocouple input).

Type	Amount	Function	Signal
DI	9	Position indicator pneumatic valve	24 VDC
DO	9	Control current for magnetic valve (MV 1–MV 9)	24 VDC
DO	6	Control current for the reactor heating rod	24 VDC
DO	8	Control current for the peripheral heating rod	24 VDC
DO	1	Control current for the evaporator heating rod	24 VDC
TI	21	Reactor temperature	Thermo voltage
TI	8	Peripheral gas temperature (T_{Gas})	Thermo voltage
TI	8	Peripheral heating rod temperature (T_{Del})	Thermo voltage
TI	1	Evaporator heating rod temperature (T_{Del})	Thermo voltage
TI	1	Steam temperature	Thermo voltage
TI	1	"Cooling box 2" temperature	Thermo voltage
AI	5	Pressure sensor	4–20 mA
AI	2	CO detector	4–20 mA
DI	2	Error report of pump	24 VDC
DO	2	Switch for pump	24 VDC
AO	2	Set value of rotation speed of pump	4–20 mA
DO	1	Electrical heating of the membrane pump	24 VDC
DO	1	External ventilation of membrane pump	24 VDC
DO	1	Switch for "Cooling box 2"	24 VDC
DI	1	Gas chromatograph ready	24 VDC
DI	1	Operation CHP plant Oberwart	24 VDC
AI	3	CH ₄ , CO ₂ , H ₂ S signals, biogas analyzer	4–20 mA

valves and heating rods) could be triggered manually from the user interface. Screenshots of this interface are presented in Figure 5.13. The process overview of the interface is shown in Figure 5.13 (a). The measured data of operating temperature and pressure were linked to alarm limits. These alarm limits (low low, low, high, high high) were defined within the setpoints sheet of the interface illustrated in 5.13 (b).

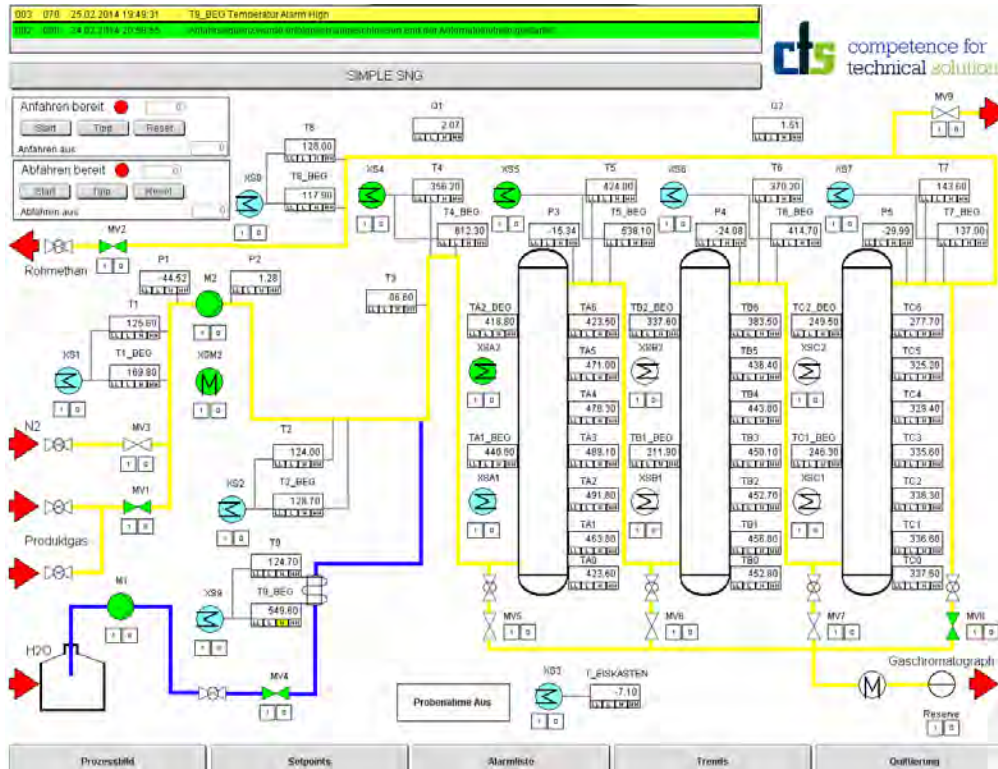
A shortfall of the low low limit or an exceeding of the high high limit led to the automatic shutdown of the pilot plant. This procedure included the closure of the pneumatic valve for wood gas supply (MV 1) and an inertization of the system by opening MV 3 and MV 9 (see Figure 5.8). For safety reasons the WGS unit was also equipped with two CO detectors from AdosTM (TOX 592). The devices were parameterized for an operation range between 0–300 vol.ppm of carbon monoxide. The maximum admissible workplace concentration of CO (30 vol.ppm [9]) was used as the alarm limit high. 100 vol.ppm of CO were defined as the alarm limit high high and induced a shutdown of the system.

Furthermore, the automation program included a sequencer for the simplification of the startup procedure. The aim of the automatic sequence illustrated in 5.14 was to avoid operating errors during startup. A series of preconditions had to be fulfilled initially (on top of Figure 5.14). Preheating was carried out under N₂ atmosphere. During Step 4 of the procedure, the different setpoint temperatures were increased manually according to the stated heating ramp provided by the catalyst producer. Water addition was initiated prior to the wood gas supply in order to operate at any time at a steam to carbon ratio without the risk of carbon formation (compare Figure 3.10). Finally, the N₂ supply was stopped and the corresponding valve for wood gas supply (MV 1) was opened.

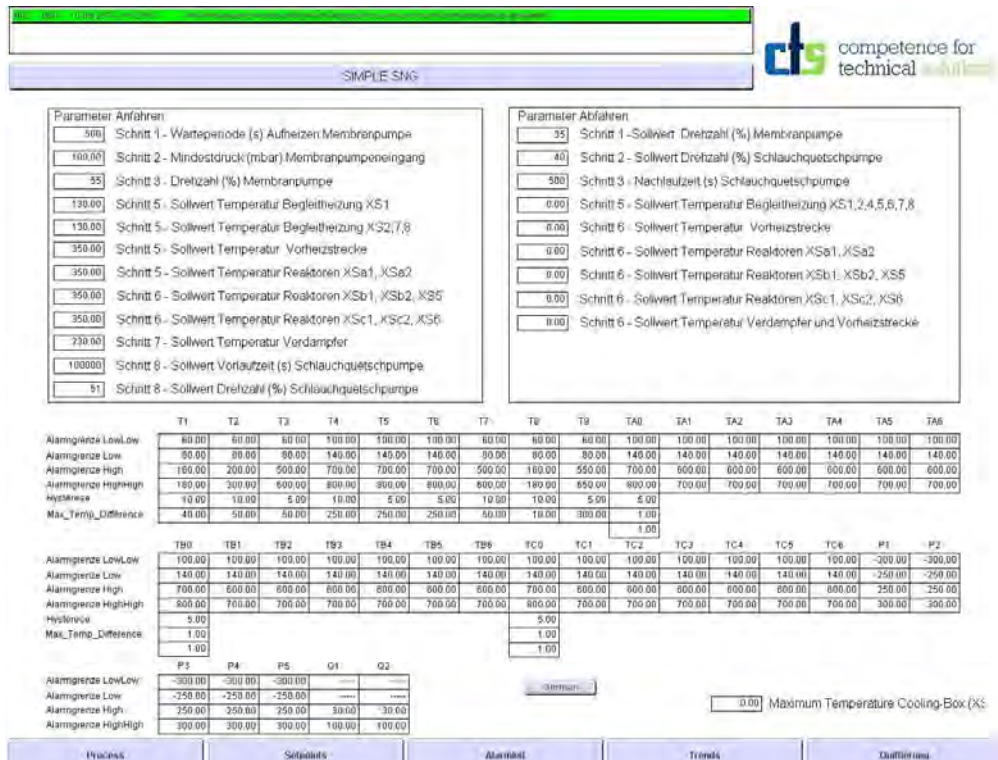
The visualization of the process parameters (temperatures, pressures, etc.) was achieved by means of the graphical programming software LabVIEW. The interface of LabVIEW and the PCS was created by means of an OPC server. LabVIEW was also used to register and save the process data continuously in a MS Excel sheet. Usually, all process variables were transferred to the MS Excel sheet once per hour. Figure 5.15 shows a screenshot of the process visualization window where the process gas temperatures were plotted. Also, the operating pressures P1–P5, the temperatures of the heating rods at the inlet of each reactor, the temperature of the evaporator, the automatic sampling sequence described in Chapter 5.3.5, the signals of the biogas analyzer, and the temperature of the "Cooling box 2" (described in Chapter 5.3.5) were visualized.

5.3.3 Temperature control

Each heating rod was provided with two thermocouples. One was measuring the corresponding temperature of the gas inside the piping (T_{Gas}). Another thermocouple registered the surface temperature of the heating rod. This delimiter thermocouple (T_{Del}) was installed in order to avoid an overheating of the element and to avoid the overshooting of the gas temperature T_{Gas} which should be controlled. Figure 5.16 illustrates the installation of one heating rod and the associated thermocouples.



(a) Process overview



(b) Setpoints

Figure 5.13: Screenshots of the graphical user interface of the pilot plant for catalytic wood gas processing (WGS unit).

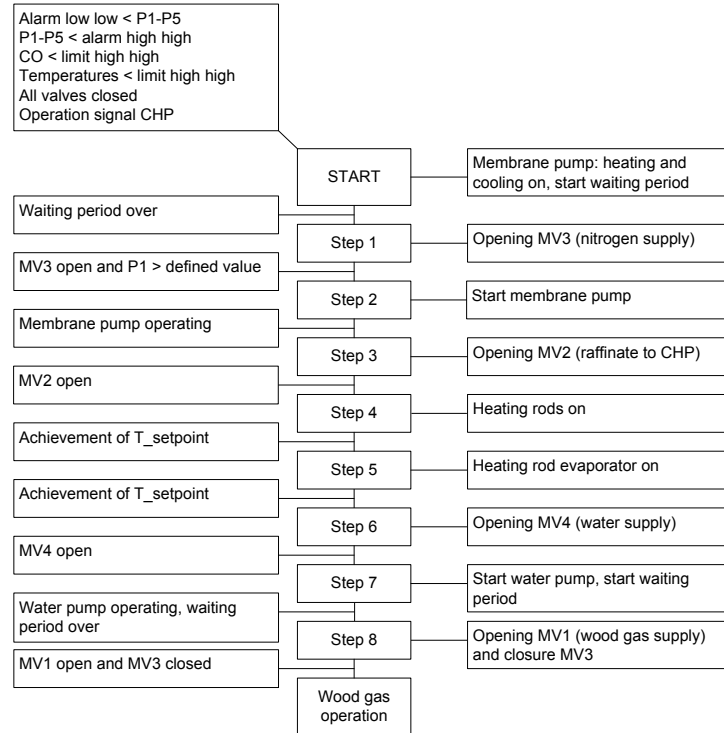


Figure 5.14: Startup sequencer of the "Pilot plant for catalytic wood gas processing" (WGS unit).

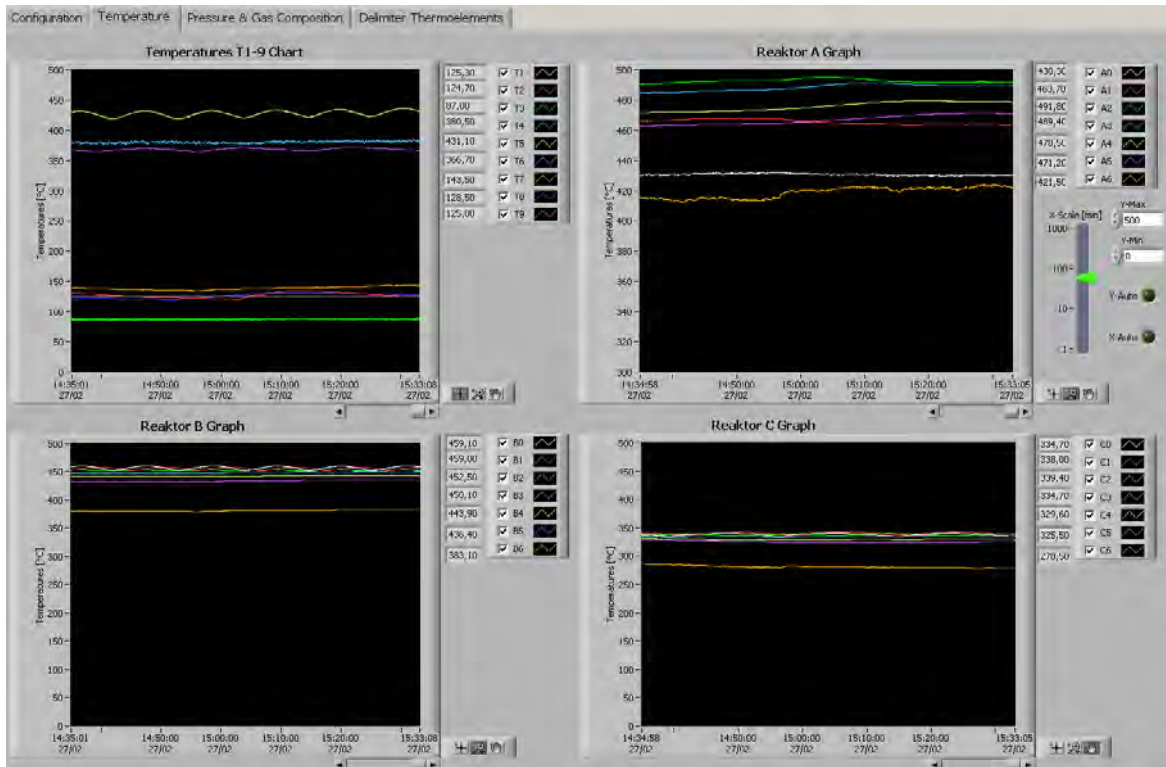


Figure 5.15: Screenshot of the installed process visualization with LabVIEW during operation of the WGS unit; top left: peripheral thermocouples, top right: reactor A, bottom left: reactor B, bottom right: reactor C.

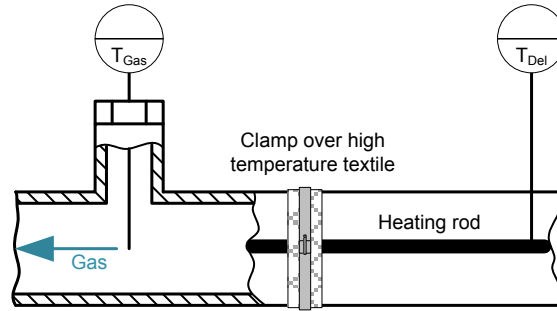


Figure 5.16: Hardware setup of one heating rod attached to the piping of the WGS unit, from [14].

Based on this hardware setup the finally realized temperature control of one heating rod was arranged in a control loop which is schematically illustrated in Figure 5.17.

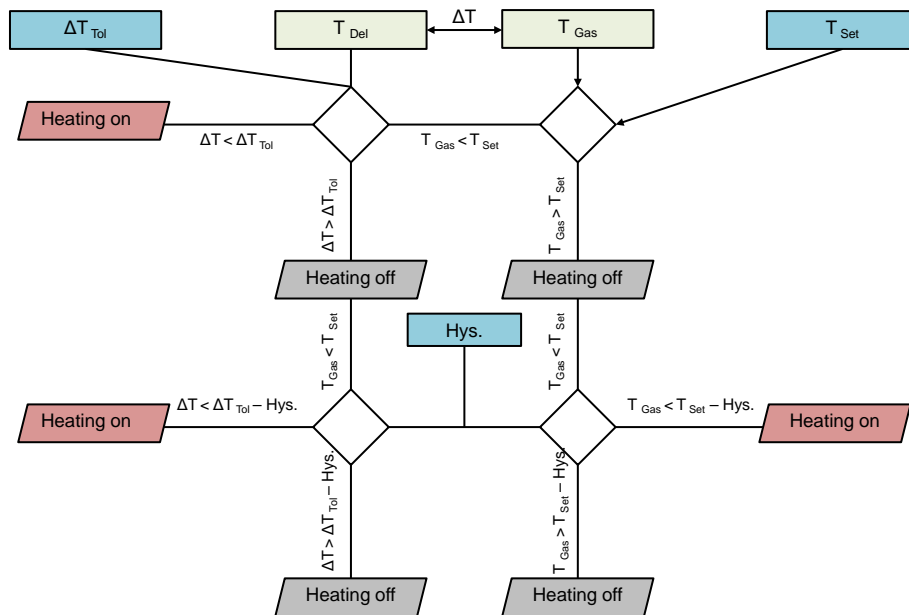


Figure 5.17: Flowchart of the temperature control of one heating rod installed at the "Pilot plant for catalytic wood gas processing".

The temperature control was defined by means of 3 set values: the set value (T_{Set}) of the gas temperature (T_{Gas}), the maximum tolerated difference (ΔT_{Tol}) between T_{Set} and T_{Gas} and the Hysteresis ($Hys.$). A more precise temperature control could be achieved by the decrease of the set values ΔT_{Tol} and $Hys.$. However, the excessive switching of the mechanic contactors controlling the heating rods should be avoided. A compromise between these factors (smooth temperature profile at few switching cycles) had to be found for the proper operation of the temperature control. The temperatures of the process relevant delimiter thermocouples (T_{Del} , heating rods at the inlet of each reactor) were registered and plotted in the LabVIEW™ trend visualization. Figure 5.18 shows a screenshot of the evolution of the delimiter thermocouples during wood gas operation. The graph illustrates the temperatures

of the heating rods of the preheating pipe ($T_{4_{Beg}}$, delimiter of reactor A), of the piping in between reactor A and reactor B ($T_{5_{Beg}}$, delimiter of reactor B), of the piping in between reactor B and C ($T_{6_{Beg}}$, delimiter of reactor C) as well as the temperature of the evaporator heating ($T_{9_{Beg}}$, delimiter of evaporator coil). It can be seen that $T_{9_{Beg}}$ is always swinging with the hysteresis $Hys.$ around the sum of T_{Set} and $\Delta T_{Tolerated}$ without reaching the desired T_{Set} of the evaporation temperature T_{Gas} . This was desired in order to allow a smooth evaporation. The heating rods of the reactor heatings performed similarly, but after a couple of heating cycles, T_{Gas} reached the corresponding T_{Set} and the heating rods cooled down until T_{Gas} fell below $T_{Set} - Hys.$. In Figure 5.18, also the temperature of the "Cooling box 2" (T_{KB}) is illustrated.

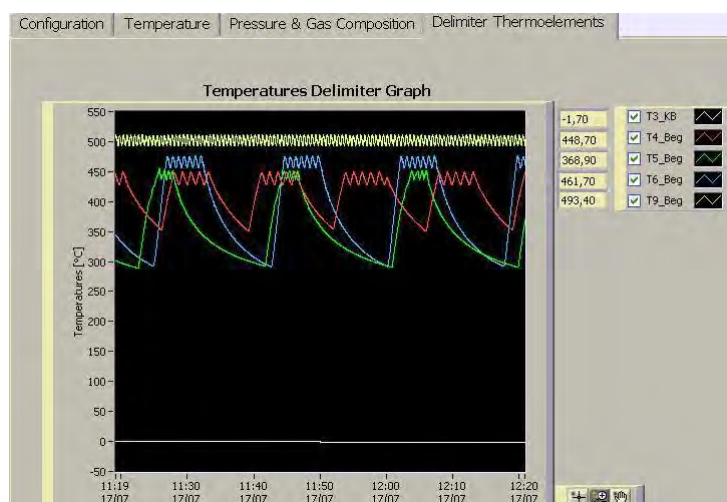


Figure 5.18: Screenshot of the LabVIEW™ visualization window of the most important delimiter thermocouples (T_{Del}) measuring the current surface temperature of the heating rods ($T_{4_{Beg}}$ preheating pipe before reactor A; $T_{5_{Beg}}$ heating before reactor B; $T_{6_{Beg}}$ heating before reactor C; $T_{9_{Beg}}$ heating of the evaporator).

5.3.4 Experimentation

In theory the reaction was carried out adiabatically. Usually, the reactor heatings were not used during steady operation and no cooling was installed. However, the heat losses of the WGS reactors did not allow an adiabatic operation. Small test rigs with a high surface to volume ratio frequently face this problem.

The characteristic numbers for the assessment of the operation conditions of the WGSR were already defined in Chapter 3.3.2. The key figure for the evaluation of each test run was the CO conversion rate (X_{CO}) defined in equation 3.17. The preparation of an experiment necessitated the estimation of the rotation speed of the gas pump (membrane pump) and the water pump (peristaltic pump). Provided that the catalyst volume and the wood gas composition of the CHP plant was fixed, the combination of the flow rate of wood gas and steam addition defined the steam to carbon, the steam to carbon monoxide, the steam to dry gas ratio, and also the GHSV on a wet and on a dry base. As a consequence, the membrane

pump and the peristaltic pump had to be calibrated prior to the first experiments.

First, the membrane pump was characterized with air at ambient conditions. The inlet and the outlet of the cold test rig (with catalyst inside) were opened to the ambient. At the outlet of the test rig a temperature compensated bellows-type gas meter from Kromschroder (BKG2.5T) was installed in order to measure the volumetric air flow rate over the rotation speed of the pump. The obtained pump characteristic curve is illustrated in Figure 5.19. The supplier of the membrane pump reported a maximum flow rate of $3.5 \frac{m^3}{h}$. Under the applied conditions the maximum flow rate was found to be $2.8 \frac{m^3}{h}$. A pressure drop over the catalyst bed of 15 mbar could be observed at the maximum load. The molar flow rate over the membrane pump depended strongly on the operating temperature, the operating pressure, and the pressure difference between the inlet and the outlet of the pump. During wood gas operation, the heated membrane pump was usually operated at 130 °C in order to avoid tar condensation. The volumetric flow rate of the pump at standard conditions could easily be calculated by means of the first law of Gay-Lussac. The pressure influence could be compensated by means of the installed needle valves at the inlet and at the outlet of the system. A pressure difference over the pump was usually avoided and the system was operated at atmospheric pressure.

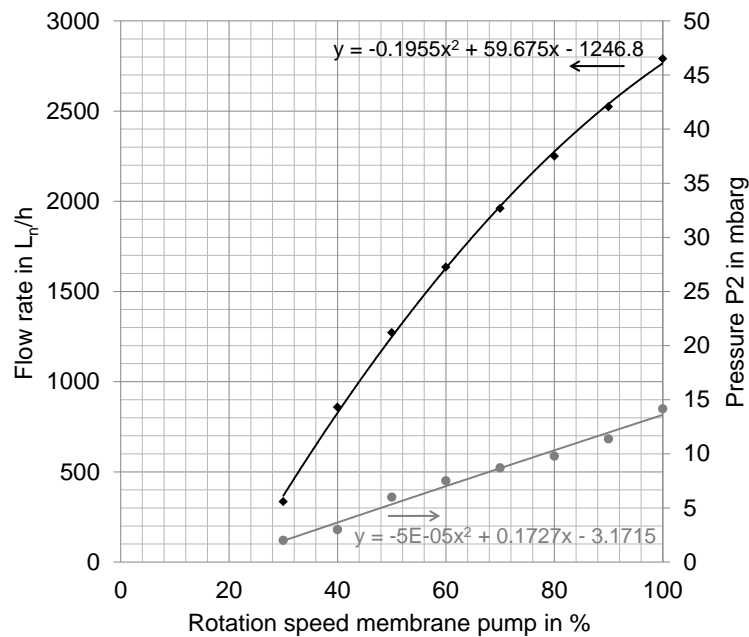


Figure 5.19: Calibration of the gas pump (membrane pump) from KNF™ for wood gas feeding.

Prior to the commissioning of the pilot plant with wood gas, also the water addition was calibrated. A calibration outlet was installed after the variable area flow meter and the peristaltic pump illustrated in Figure 5.8 and Figure 5.10. By means of this outlet a gravimetric calibration of the pump was carried out. The obtained pump characteristic curve is illustrated in Figure 5.20. It was observed, that the meter reading of the flow meter was not consistent with the actual flow rate determined gravimetrically. Also, the pump response

was not linear what could already be observed at the membrane pump. During long-term wood gas operation it was sometimes necessary to slightly increase the rotation speed of the peristaltic pump in order to maintain a constant water addition. Over the time, the flexible hose of the pump lost its elasticity.

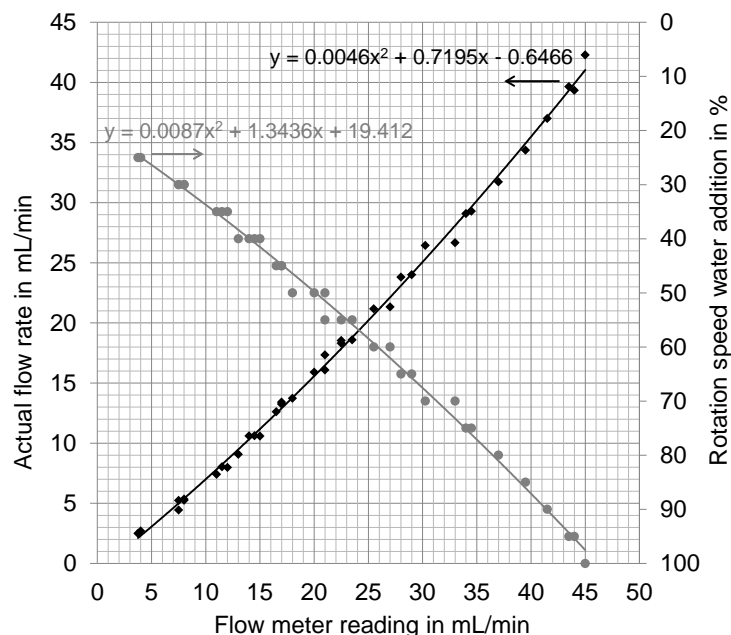


Figure 5.20: Calibration of the peristaltic pump for water addition and calibration of the variable area flow meter for the online control of water feeding.

Another parameter influencing the dry GHSV and the steam content in the adjusted gas mixture was the water content in the wood gas extracted from the power plant. If the wood gas was extracted after the gas filter of the CHP plant, the water content of the feed was measured according to the procedure explained in Chapter 5.3.5. The water content in the wood gas was fluctuating and strongly depended on the operation of the CHP plant and the water content of the gasified biomass. If the wood gas was extracted after the scrubber, the steam content could also be estimated by means of the vapor saturation of the gas with respect to the present temperature at the outlet of the scrubber. The water saturation is illustrated in 5.21.

Based on the pump characteristic curves and the water saturation curve, a spreadsheet was prepared. The aim of this calculation was to estimate the rotation speed of both pumps which is required to operate the system at a desired GHSV and a defined steam content in the gas. The volume of catalyst, the desired GHSV, the desired steam content in the gas, the operating temperature of the membrane pump, and the outlet temperature and pressure of the CHP plant scrubber had to be entered into the spreadsheet. As a result, the two rotation speeds were calculated which should accomplish operating conditions near to the desired process parameters. This spreadsheet also included a feature plotting the current process condition in the carbon formation diagram in Figure 3.10. If the current operation condition was in the area of a possible carbon deposition, the steam content in the gas mixture had to

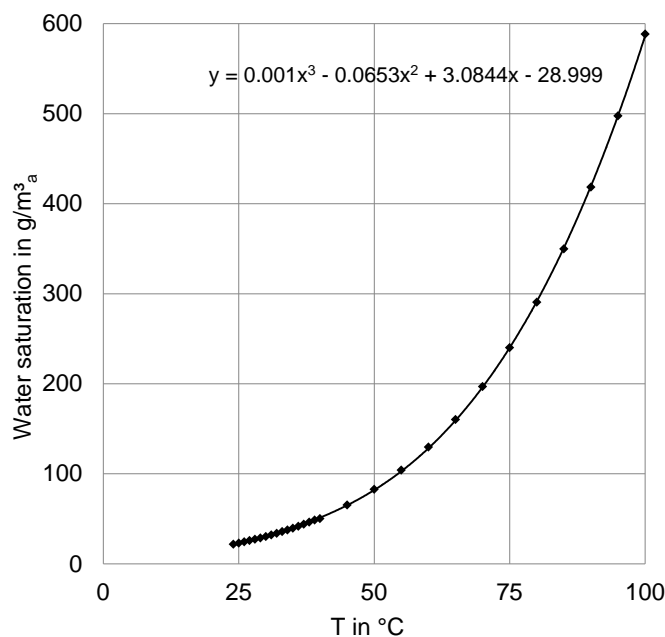


Figure 5.21: Water saturation of wood gas extracted after the CHP scrubber depending on the temperature, values from [72].

be increased.

Basically, the test rig was designed for a long term operation. This was necessary to test the long term stability of the catalyst but also to achieve steady state operation which was very time demanding. Heating up of the test rig (according to the suggested heating ramp of the catalyst) and attaining steady temperature profiles in the reactors took almost one working day. The PCS with the defined alarm limits and an automatic shutdown sequence, even enabled an unmanned operation over the weekend.

5.3.5 Chemical analysis

Basically, the main gas components, the water content, the sulfur components, and the tar compounds in the wood gas were analyzed. The sampling of wood gas for these measurements is illustrated in Figure 5.22. Electrical trace-heating was installed to avoid tar condensation in the piping. Standard analysis of the main gas components necessitated the removal of water from the sampling stream which was carried out along the bottom path of the sampling flowchart ("Standard analysis" in Figure 5.22). The gas was cleaned and dried over two impinger bottles filled with ethylene glycol at -3 °C. The gas scrubbing bottles were placed in a cooling bath inside of an ordinary refrigerator ("Cooling box 2") which was temperature controlled, by means of its integration into the PCS of the WGS unit. This turned out to be a very cheap and robust alternative to an expensive cryostat.

Downstream to gas quenching, another impinger bottle was placed which was filled with quartz wool to remove aerosols from the sampling stream. Subsequently, a needle valve combined with a variable area flow meter and a vacuum pump were installed. By means of

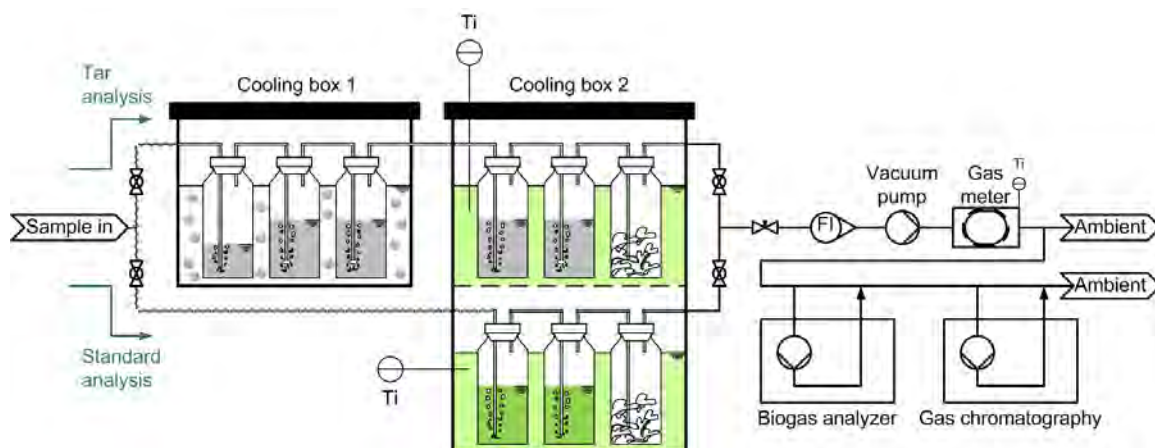


Figure 5.22: Flowchart of the installed sampling line for chemical analysis of wood gas components; tar analyses were carried out over the sampling line on top, the temperature of cooling box 1 was 0 °C (ice bath); the temperature of regulated cooling box 2 was adjusted to -8 °C; standard gas analyses were carried out over the bottom path, during these analyses the temperature of the cooling box 2 was adjusted to -3 °C.

adjusting the needle valve, the desired sampling flow rate could be regulated. Downstream the pump, a bellows-type gas meter from Elster[®] (BK-G2.5) was installed for the quantification of the stream. The outlet of the gas meter was opened to the ambient. It was considered that the gas temperature inside the gas meter corresponded to the ambient temperature. The ambient temperature was measured with a mercury thermometer what enabled the calculation of the dry volumetric flow rate at standard conditions (0 °C).

Neglecting the tar content in the wood gas, the increase in weight of the ethylene glycole filled flasks and the simultaneous measurement of the corresponding dry gas volume enabled the calculation of the molar water content of the wet gas (according to Equation 3.13). Results from water analysis according to this procedure and the water saturation method (according to Figure 5.21) of wood gas extracted after the scrubber of the CHP plant generally agreed very well. Prior to water analysis of a new sampling point, the sampling line had to be flushed with wood gas in order to remove condensate.

The most important analytical device was a two-channel gas chromatograph (GC - Clarus 500TM) from Perkin ElmerTM. The main gas components (CO₂, N₂, CO, O₂, CH₄, C₂H₆, C₂H₄ and C₂H₂) were separated in a combination of two different columns (7' HayeSep N, 60/80 1/8" SF and 9' Molecular Sieve 13x 45/60, 1/8" SF). A thermal conductivity detector (TCD) was used for quantification. The sulfur components (H₂S, COS, thiophene C₄H₄S, ethanethiol CH₃CH₂SH and methanethiol CH₃SH) were separated in a different column (Rt-XL Sulfur 1 m x 0.95 mm OD) and quantified by a flame photometric detector (FPD). A more detailed description of the applied GC methods can be found in [28]. The H₂ content was determined via mass balance.

Also an online measurement device was integrated into the sampling line of wood gas. The installed gas analyzer (InCa Bio04 from Union Instruments GmbH) was originally designed for the online analysis of biogas. It was recovered from a completed research project and

integrated into the PCS of the WGS unit. The system was capable of detecting H₂S, CH₄, CO₂ and O₂. However, it was only used to detect O₂ with an electrochemical detector [39]. The online O₂ measurement was very useful to detect possible leaks in the sampling line. This was especially important during tar sampling. The biogas analyzer can be seen on the picture of the WGS unit in Figure 5.6.

For long-term experimentation and night operation, an automatic sampling sequence was realized to achieve a semi-continuous analysis of the gas composition (main gas and sulfur components) at each sampling point of the process (MV 5, MV 6, MV 7, and MV 8 in Figure 5.8). The sequence was started with the analysis of the gas composition at the inlet of the first reactor (MV 5). Subsequently, gas was sampled after each of the three fixed bed reactors and finally the sequence was started again. The automatic sampling included three elementary steps: the opening of one sampling valve, the start of the analytical vacuum pump (after the impingers in Figure 5.22), and the start of the internal pump of the GC. The pumps were started simultaneously with the opening of the sampling valve. The realization of the automatic sampling sequence required the integration of the GC into the PCS of the WGS unit. The GC was capable of providing a digital signal (24 VDC) at definable time events. In this context it was useful to program the GC so that it provided this signal 5 minutes before an injection onto a separation column of the GC. The signal was detected by the PCS and the corresponding valve was opened. Furthermore, this signal was used as a control circuit for an electromagnetic two-port relay which was used to activate both pumps. By means of this measure, the accumulation of condensate in the impingers could be reduced considerably enabling an automatic sampling over night and even over weekend. The minimum sampling duration was the time of complete flushing of the sampling line to the GC. The sampling sequence could also be adjusted so that one sampling point was repeatedly analyzed.

For selected experiments, also tar analysis was carried out. Tar sampling was performed over 6 impinger bottles filled with a total of about 500 mL of toluene. This sampling procedure is illustrated in the upper path of Figure 5.22 ("Tar analysis"). A combination of two cooling boxes at different temperature levels was designed. The sampling line directing to the toluene filled impinger bottles was electrically heated to 130 °C in order to avoid tar condensation inside the tube. In the first cooling box ("Cooling box 1") a cooling bath was placed which was filled with a mixture of water and ice. 3 impinger bottles filled with toluene were placed in the first cooling box. In the first impinger bottle the majority of steam was condensed, leading to a temperature increase because of the high enthalpy of water condensation. The last three impinger bottles were placed in the temperature controlled "Cooling box 2" equipped with a cooling bath of ethylene glycol adjusted to a temperature of -8 °C. Two of these bottles were filled with toluene, the last flask was filled with quartz wool to remove aerosols from the sampling stream. The impingers were partly equipped with porous plates to enable a fine dispersion of the gaseous phase. For each tar analysis a sampling stream of $2 \frac{L_n}{min}$ was taken over a period of up to 8 hours. Generally, the sampling period was set longer for the analysis of cleaned wood gas and a minimum of $0.5 m_n^3$ were passed over the flasks. After tar sampling, the two phase sample including dissolved tar in toluene and condensate

was analyzed by the Test Laboratory for Combustion Systems at the Vienna University of Technology. The amount of water and toluene was determined. 2 mL of the organic phase were taken as a sample for GC-MS analysis. For detection of the tar components in toluene a gas chromatograph from Perkin ElmerTM (XL GCTM) coupled with a mass spectrometer from Perkin ElmerTM (Turbo Mass MSTM) was used to analyze 50 different tar species in this sample. GC-MS analysis could only detect tar components with a boiling point between 0 and 450 °C. Components with a higher boiling point remained in the column. Besides the GC-MS tar procedure, tar was also quantified gravimetrically. Therefore, the organic phase of tar sampling was inserted into a rotating evaporator where the solvent but also tar components with a low boiling point were evaporated. The solid residue was resolved in 30 mL of toluene, put in a petri dish and dried in an oven at 105 °C. Therefore, only tar components with a boiling point below 105 °C were quantified gravimetrically. A detailed description of the applied methods for tar analysis can be found in [116].

5.3.6 Data treatment

The data treatment of a test run was usually carried out after the experiment. The aim of the data treatment was to generate the complete mass balance of the WGS unit and to calculate the relevant characteristic figures. The main challenge of this task was that no flow measurement of wood gas was designed. The hot wood gas had a fluctuating composition and contained water, tar and other impurities. Condensation of wood gas components did not allow cooling of the gas prior to a flow measurement. An orifice plate was not desired because of the generated pressure drop, and an assumed low accuracy at the rather low volumetric gas flow rates. Other techniques were considered as too expensive or not very precise. Therefore, a water spike method was established to calculate the volumetric dry gas flow rate and to generate the mass balance of the system. The molar balance of the WGS unit is illustrated in Figure 5.23.

The molar water content of the wood gas before water addition ($y_{H_2O,G}$) was measured gravimetrically. This was achieved by means of the sampling procedure illustrated in Figure 5.22 ("Standard analysis"). The water content of cleaned wood gas could also be estimated by means of the outlet temperature of the CHP plant scrubber which was provided by the operating company. With the peristaltic pump a defined amount of water (\dot{W} with $y_{H_2O,W} = 1$) was added to the gas stream. This water addition ("spike") was monitored with the already discussed variable area flow meter. Analysis of the steam content in the wet gas stream after the steam addition (sampling point MV 5) could be used to quantify the dry gas volumetric flow rate at the inlet of the WGS unit ($\dot{G}_{db.}$) and to close the mass balance. In the course of this thesis it turned out, that the water content measured at this sampling point was too high which could be explained by the sampling which was not carried out under isokinetic conditions. Obviously wet steam containing small water droplets was present at this sampling point. The droplets were preferably directed into the sampling line which resulted in analyzed water contents which were too high. As a consequence, the water measurement

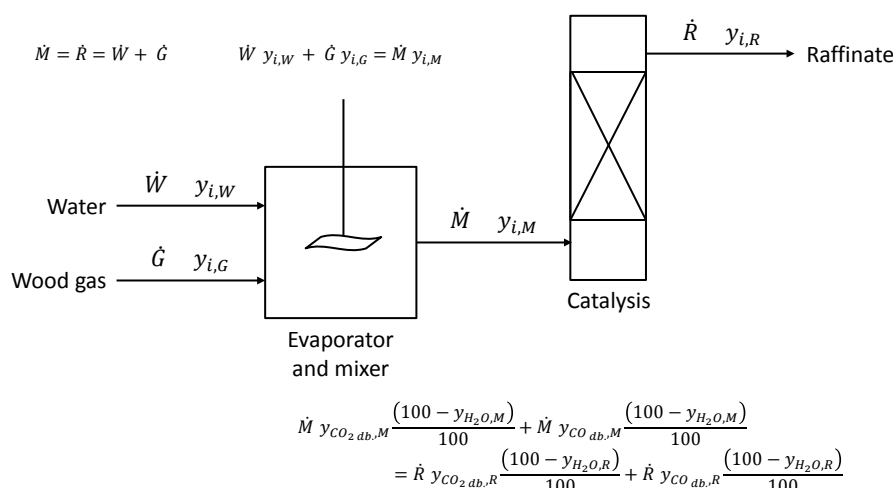


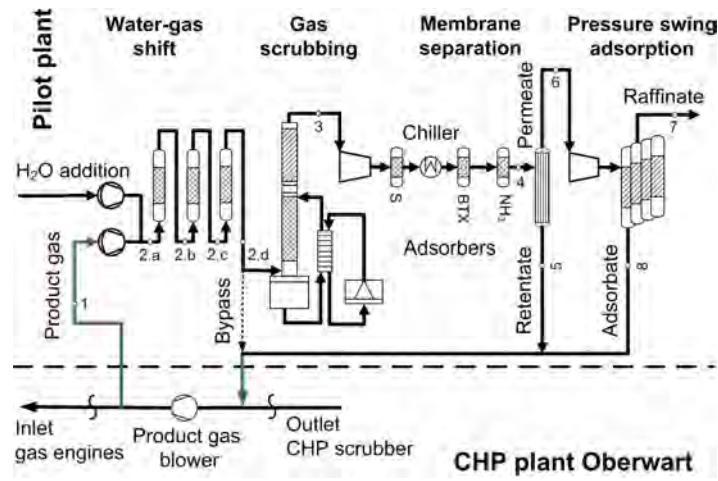
Figure 5.23: Molar balance of the WGS unit, and the most important formulas for the determination of the global mass balance.

was carried out after the reactors ($y_{H_2O,R}$) at the sampling point MV 8. By means of the formula at the bottom of Figure 5.23, the water content at the inlet of the catalysis ($y_{H_2O,M}$) could be calculated. The molar balance over the "Evaporator and mixer" in Figure 5.23 enabled the closure of the overall mass balance. Atomic mass balances were calculated based on the obtained molar flow rates which closed very well. Also, the "water-spike" method was verified during the experimentation of process chain 2 (see Chapter 7.2) where the gas at the outlet of the WGS unit was cleaned and dried in a scrubber and finally quantified volumetrically by means of a bellows-type gas meter.

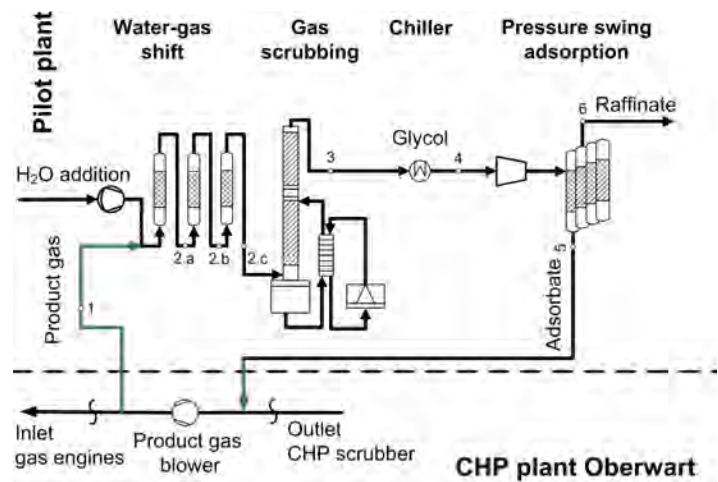
5.4 Process chains for the production of pure hydrogen

During this thesis, the "Pilot plant for catalytic wood gas processing" was integrated into two different process chains for the production of pure hydrogen. These configurations are illustrated in Figure 5.24 showing the flowcharts of process chain 1 (a) and process chain 2 (b).

Both process chains included a low temperature gas scrubber operated with RME and a PSA unit. These test rigs are described in detail in [28]. The experimental setup of process chain 1 as well as the basic results were published in a conference paper which was created within the thesis [36]. This conference paper is also included into this work and can be found in Chapter 7.1. The experimental setup of process chain 2 as well as the basic results were summarized in a journal paper and submitted to the "ACS Journal of Sustainable Chemistry and Engineering". This journal paper [35] was accepted on the 13th of October, 2014. It was also created within this thesis and can be found in Chapter 7.2.



(a) Process chain 1



(b) Process chain 2

Figure 5.24: Flow charts of the two different process chains which involved the operation of the "Pilot plant for catalytic wood gas processing".

Chapter 6

Results and discussion

As the WGS unit was designed, assembled and commissioned within this thesis, the proper operation of the pilot plant (described in Chapter 5.3) can be seen as the first result of this thesis. The hot gas commissioning of the "Pilot plant for catalytic wood gas processing" with N₂ took place in February 2012. Ever since, the pilot plant was steadily optimized in order to meet the requirements of experimentation. The most important measures of optimization were already described in the Chapter 5.3. These measures include the already described temperature control process, the automatic sampling sequence, the visualization of the process parameters, and the final versions of the installed analytical sampling lines in Figure 5.22.

The results are structured in 4 sections. First, the obtained results of the wood gas composition of the CHP-plant Oberwart are presented and equilibrium considerations are carried out. Second, the results of the Co/Mo-based catalyst are presented including its kinetic investigation at the "Test rig for chemical kinetics" as well as its performance at the "Pilot plant for catalytic wood gas processing". Third, the performance of the Fe/Cr-based catalyst at both test rigs is discussed. Finally, a theoretical approach for the estimation of the optimum operating temperature is presented.

6.1 Wood gas composition CHP plant Oberwart

The wood gas composition of the CHP plant Oberwart was mainly influenced by the process parameters in the gasifier. The gasification parameters (bed material activity [65], possible addition of limestone, residence time at part load operation, steam addition, gasification temperature, moisture content, particle size, composition of the biomass, etc.) were always subject to fluctuations and therefore also the gas composition varied over time. However, the power plant generally provided a reliable operation and a good availability. The site represented a very suitable environment for long term experimentation.

Besides the operating conditions of the gasifier, the tar content of the cleaned wood gas was also influenced by the operating conditions of the CHP plant scrubber.

The wood gas composition of the CHP plant Oberwart was analyzed together with each

test run of the WGS unit. In September 2013 the pilot plant was continuously operated for more than 350 hours with cleaned wood gas extracted after the RME scrubber. During this period, the automatic sampling sequence (described in Chapter 5.3.5) was activated. Besides the gas composition after each reactor, also the wood gas composition (sampling point MV 5) was measured once every 2.5 hours. Figure 6.1 illustrates the trend of the wood gas composition during this period.

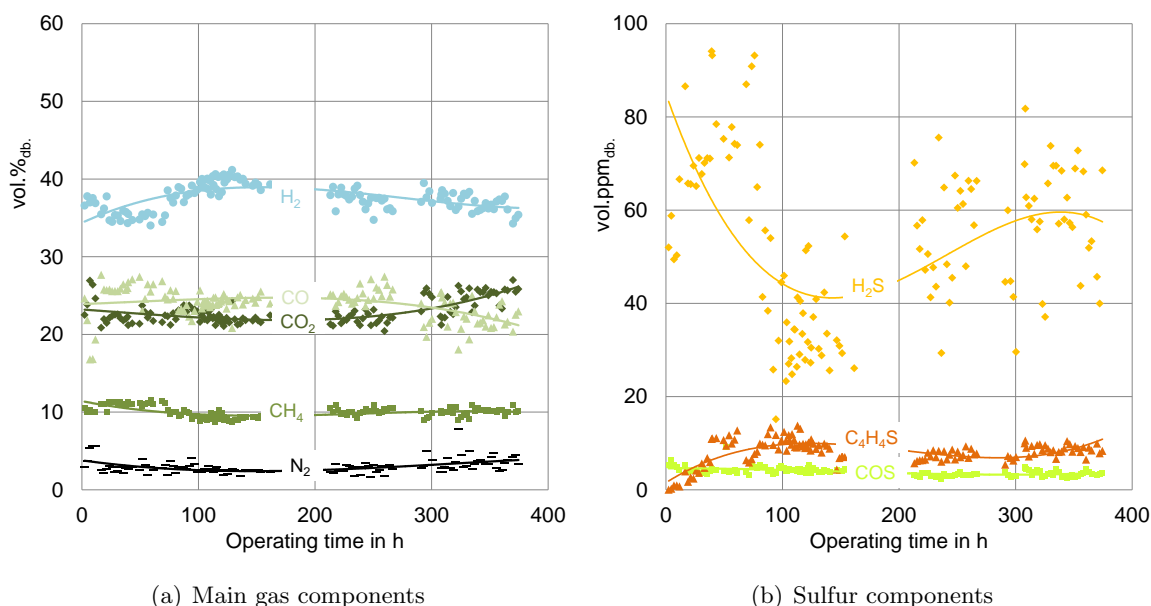


Figure 6.1: Trend of wood gas composition September 2013.

During the presented period in Figure 6.1 the amount of generated wood gas was reduced significantly after 270 hours. Operating problems of the CHP plant forced the plant operators to reduce the feeding rate of biomass which reduced the overall production of wood gas. An increased residence time of the wood gas in the freeboard of the gasifier was assumed to lead to an increased equilibration of the WGSR after these 270 hours. Also the N₂ content increased which could be explained by the unchanged dedusting of the wood gas filter with N₂ at a lower overall wood gas production. Within his PhD thesis, Nicolas Diaz also analyzed the wood gas composition of the CHP plant Oberwart several times between 2012 and 2013 [28]. Basically, the obtained values within this thesis were in the same order of magnitude. The average gas composition during the presented period was used for the theoretical examinations which are presented later. Table 6.1 summarizes the wood gas composition during the operation in Figure 6.1. Regarding the sulfur content it can be seen that the H₂S content was rather low during this period. Besides H₂S, also thiophene (C₄H₄S) and carbonyl sulfide (COS) could be analyzed. Methanethiol (MeSH) and ethanethiol (EtSH) could not be detected in the wood gas.

The values in Table 6.1 are derived from analysis of the cleaned wood gas extracted after the CHP plant scrubber. The RME scrubber mainly affects the dry gas composition with

Table 6.1: Averaged wood gas composition and standard deviation of cleaned wood gas on a dry base measured in September 2013, methanethiol (MeSH), ethanethiol (EtSH), thiophene (C₄H₄S), below detection limit (BDL).

CO ₂	C ₂ H ₄	C ₂ H ₆	C ₂ H ₂	O ₂	
22.91±1.53	2.21±0.26	0.18±0.06	0.13±0.03	0.17±0.14	vol.% _{db.}
N ₂	CH ₄	CO	H ₂		
2.96±0.88	9.99±0.69	23.91±2.04	37.56±1.72		vol.% _{db.}
H ₂ S	COS	MeSH	EtSH	C ₄ H ₄ S	
53.19±17.69	3.88±0.88	BDL	BDL	8.09±2.68	vol.ppm _{db.}

respect to ammonia, BTEX (benzene, toluene, ethylbenzene, and xylene) and tar components. The content of ammonia and BTEX in the cleaned gas was only analyzed for selected experiments (mainly the operation of process chains for H₂ production which are explained in Chapter 7) [36, 35]. In the framework of the research projects "Polygeneration I and II", Nicolas Diaz carried out some BTX analyses in Oberwart. The results are published in his Phd thesis [28]. Table 6.2 summarizes the obtained values of the analyses of NH₃ and BTEX which were carried out at the CHP plant Oberwart during 2013 and 2014. Cleaned gas was analyzed. Corresponding NH₃ and BTEX analysis of raw wood gas extracted after filter (before the scrubber) are not available.

Table 6.2: Results of the analysis of ammonia and benzene, toluene, ethylbenzene, xylene (BTEX); cleaned gas after filter; detection limit 1 vol.ppm_{db.}); n.a. (not analyzed); from [28, 36, 35].

	NH ₃	Benzene	Toluene	Ethylbenzene	Xylene	
Mar 2013	1460±200	6183	388	n.a.	15	vol.ppm _{db.}
Apr 2013	1500±200	6000	400	n.a.	8	vol.ppm _{db.}
Jan 2014	954	3296±36	201±5	1.3±0.6	1.1±0.6	vol.ppm _{db.}

A series of tar analyses were carried out in the course of this thesis. Table 6.3 provides an overview of the tar analyses of cleaned wood gas that were carried out within this thesis. It can be seen that naphthalene was by far the most important tar component to be detected in the gas mixtures. Also, important amounts of styrene, indene, phenylacetylene, and acenaphthylene were analyzed. The total amount of GC-MS tar varied between 1.6–4.6 $\frac{\text{g}}{\text{Nm}^3_{\text{db.}}}$. The total amount of gravimetric tar varied between 0.08–0.16 $\frac{\text{g}}{\text{Nm}^3_{\text{db.}}}$. It was already discussed, that the tar content in the cleaned wood gas depended strongly on the operating parameters in the gasifier (most of all the addition of limestone) and the operation of the RME scrubber. The tar separation efficiency of the CHP plant scrubber was strongly influenced by the addition of fresh RME and its operating temperature (tar is not only dissolved chemically but also condensed physically). Table 6.4 summarizes the results of the two tar analyses of raw wood gas that were carried out within this thesis. Compared to previous results, much lower tar contents in the raw wood gas after filter were analyzed recently (February 2014). The measured tar content is even lower than for single measurements of cleaned wood gas obtained before.

During 2008 and 2009 a series of wood gas analyses were carried out at the CHP plant

Table 6.3: Results of the tar analysis of cleaned wood gas after scrubber from the CHP plant Oberwart; detection limit $1 \frac{\text{mg}}{\text{Nm}^3_{db}}$; including results from [36, 35].

	Feb 2013	Mar 2013	Jul 2013	Jan 2014	$\frac{\text{mg}}{\text{Nm}^3_{db}}$
Naphthalene	1515	3376	1662	1139	$\frac{\text{mg}}{\text{Nm}^3_{db}}$
Styrene	317	456	270	247	$\frac{\text{mg}}{\text{Nm}^3_{db}}$
Indene	268	462	240	191	$\frac{\text{mg}}{\text{Nm}^3_{db}}$
Phenylacetylene	41	43	27	25	$\frac{\text{mg}}{\text{Nm}^3_{db}}$
Mesitylene	1	BDL	BDL	BDL	$\frac{\text{mg}}{\text{Nm}^3_{db}}$
Benzofuran	8	14	BDL	2	$\frac{\text{mg}}{\text{Nm}^3_{db}}$
Dibenzofuran	4	7	BDL	1	$\frac{\text{mg}}{\text{Nm}^3_{db}}$
1-Benzothiophene	3	5	2	2	$\frac{\text{mg}}{\text{Nm}^3_{db}}$
2-Methylnaphthalene	13	31	9	5	$\frac{\text{mg}}{\text{Nm}^3_{db}}$
1-Methylnaphthalene	8	18	5	3	$\frac{\text{mg}}{\text{Nm}^3_{db}}$
Biphenyl	7	19	4	1	$\frac{\text{mg}}{\text{Nm}^3_{db}}$
Acenaphthylene	48	150	45	13	$\frac{\text{mg}}{\text{Nm}^3_{db}}$
Acenaphthene	3	5	5	2	$\frac{\text{mg}}{\text{Nm}^3_{db}}$
Anthracene	3	6	2	2	$\frac{\text{mg}}{\text{Nm}^3_{db}}$
Flouranthene	BDL	4	2	1	$\frac{\text{mg}}{\text{Nm}^3_{db}}$
Pyrene	BDL	4	3	1	$\frac{\text{mg}}{\text{Nm}^3_{db}}$
Flourene	4	7	BDL	1	$\frac{\text{mg}}{\text{Nm}^3_{db}}$
Quinoline	3	5	BDL	BDL	$\frac{\text{mg}}{\text{Nm}^3_{db}}$
Phenol	4	5	BDL	BDL	$\frac{\text{mg}}{\text{Nm}^3_{db}}$
Isoquinoline	BDL	3	BDL	BDL	$\frac{\text{mg}}{\text{Nm}^3_{db}}$
Cresol	12	BDL	BDL	BDL	$\frac{\text{mg}}{\text{Nm}^3_{db}}$
Phenanthrene	BDL	5	BDL	1	$\frac{\text{mg}}{\text{Nm}^3_{db}}$
Total GC-MS	2259	4625	2276	1635	$\frac{\text{mg}}{\text{Nm}^3_{db}}$
Gravimetric tar	170	190	160	80	$\frac{\text{mg}}{\text{Nm}^3_{db}}$

Table 6.4: Results of the tar analysis of raw wood gas after filter from the CHP plant Oberwart; detection limit $1 \frac{\text{mg}}{\text{Nm}^3 \text{ db}}$; results from tar analysis Apr 2014 published with permission from DI Robert Bardolf.

	Aug 2013	Feb 2014	Apr 2014	
Naphthalene	6999	2855	6209	$\frac{\text{mg}}{\text{m}^3 \text{ db}}$
Styrene	401	202	249	$\frac{\text{mg}}{\text{m}^3 \text{ db}}$
Indene	403	292	147	$\frac{\text{mg}}{\text{m}^3 \text{ db}}$
Phenylacetylene	29	32	31	$\frac{\text{mg}}{\text{m}^3 \text{ db}}$
Mesitylene	BDL	BDL	BDL	$\frac{\text{mg}}{\text{m}^3 \text{ db}}$
Benzofuran	6	BDL	BDL	$\frac{\text{mg}}{\text{m}^3 \text{ db}}$
Dibenzofuran	56	14	8	$\frac{\text{mg}}{\text{m}^3 \text{ db}}$
1-Benzothiophene	7	6	9	$\frac{\text{mg}}{\text{m}^3 \text{ db}}$
2-Methylnaphthalene	84	62	28	$\frac{\text{mg}}{\text{m}^3 \text{ db}}$
1-Methylnaphthalene	49	40	20	$\frac{\text{mg}}{\text{m}^3 \text{ db}}$
Biphenyl	105	41	34	$\frac{\text{mg}}{\text{m}^3 \text{ db}}$
Acenaphthylene	1570	383	320	$\frac{\text{mg}}{\text{m}^3 \text{ db}}$
Acenaphthene	68	32	35	$\frac{\text{mg}}{\text{m}^3 \text{ db}}$
Anthracene	527	60	11	$\frac{\text{mg}}{\text{m}^3 \text{ db}}$
Flouranthene	46	6	BDL	$\frac{\text{mg}}{\text{m}^3 \text{ db}}$
Pyrene	40	6	BDL	$\frac{\text{mg}}{\text{m}^3 \text{ db}}$
Flourene	118	31	8	$\frac{\text{mg}}{\text{m}^3 \text{ db}}$
Quinoline	11	3	BDL	$\frac{\text{mg}}{\text{m}^3 \text{ db}}$
Phenol	2	2	BDL	$\frac{\text{mg}}{\text{m}^3 \text{ db}}$
Isoquinoline	3	BDL	BDL	$\frac{\text{mg}}{\text{m}^3 \text{ db}}$
Cresol	BDL	BDL	BDL	$\frac{\text{mg}}{\text{m}^3 \text{ db}}$
Phenanthrene	45	4	1	$\frac{\text{mg}}{\text{m}^3 \text{ db}}$
4,5-Methylphenanthrene	14	2	BDL	$\frac{\text{mg}}{\text{m}^3 \text{ db}}$
Indole	5	1	BDL	$\frac{\text{mg}}{\text{m}^3 \text{ db}}$
Total GC-MS	10588	4073	7110	$\frac{\text{mg}}{\text{m}^3 \text{ db}}$
Gravimetric tar	240	150	180	$\frac{\text{mg}}{\text{m}^3 \text{ db}}$

Oberwart. The results were published in an internal report [69] and also in a PhD thesis [70]. On the 20th of June, 2008 between 20–24 $\frac{g}{m_n^3 db.}$ of GC-MS tar was detected in the raw wood gas before filter. The gravimetric tar content was between 13.5–15.5 $\frac{g}{m_n^3 db.}$. At that time the plant was still facing many problems and the process was far from being optimized. Measured CO contents were higher than 30 vol.% and the content of CH₄ was higher than 12 vol.%. Both values denote an operation far from the equilibrium composition and therefore also indicate high tar contents which was proven by means of the tar analysis. High CH₄ contents indicate low steam reforming activity for the conversion of short hydrocarbons and tar. High CO contents usually indicate a low activity of the WGSR. About one month later (23rd of July, 2008) the content of GC-MS tar was lowered to 12.8 $\frac{g}{m_n^3 db.}$ and a gravimetric tar content was lowered to 8.4 $\frac{g}{m_n^3 db.}$. At the same time, lower CO and CH₄ contents were measured. This shift in the gas composition was explained by an activation of the bed material in combination with the ash components of the biomass (according to [65]). In the wood gas before filter, some tar components are usually adsorbed on the present particles. The removal of particles via the wood gas filter led to a simultaneous decrease in tar (around 30 %). It was also demonstrated that the application of dolomite as an alternative bed material can reduce the tar content significantly. However, the measured dust load was very high (up to 400 $\frac{g}{m_n^3 db.}$) if dolomite was used as a bed material. During co-feeding of CaO into the gasifier, gravimetric tar contents of the raw gas before filter between 1.74–2.08 $\frac{g}{m_n^3 db.}$ and gravimetric tar contents of cleaned gas after filter between 0.17–0.25 $\frac{g}{m_n^3 db.}$ were measured [70]. Currently 10 $\frac{kg}{h}$ of CaO are fed into the gasifier. Generally, it can be concluded that the wood gas composition of the CHP plant Oberwart was improved over time. The tar contents that were measured during this thesis are basically lower than during 2008 and 2009. At the same time, lower CH₄ and CO concentrations were measured.

Figure 6.2 shows the ternary coking diagram that was already shown in Chapter 3.4.1. This time the wood gas composition in Table 6.1 with different water contents is plotted into the diagram. 6 mol.%_{wb.} H₂O represents the steam content according to the water saturation of the gas at 35 °C (usual operating temperature of the RME scrubber). 35 mol.%_{wb.} H₂O can be considered as an average steam content in the wood gas upstream the gas scrubber [70]. Both operating points are clearly in the carbon formation region of the plot. This explains why it was necessary to add steam to the wood gas mixture prior to the catalysis of the WGSR. Figure 6.2 illustrates, why the steam to dry gas ratio (Equation 3.15) was usually set higher than 1 which represented a water content of 50 mol.%_{wb.}.

Besides the position of the wood gas mixture in the carbon formation diagram it was also interesting to examine the equilibrium composition of the wood gas. The equilibrium considerations were carried out by means of the chemistry software HSC ChemTM minimizing the Gibbs free energy. Figure 6.3 illustrates the obtained equilibrium results using the wood gas mixture in Table 6.1 as an initial composition. The steam to dry gas ratio was adjusted to 1 representing a steam content of 50 mol.%_{wb.}. In Figure 6.3 (a), methane and the methanation reaction were included into the equilibrium calculations. In that case, the equilibrium composition of the gas at lower temperatures was strongly on the side of CH₄ and

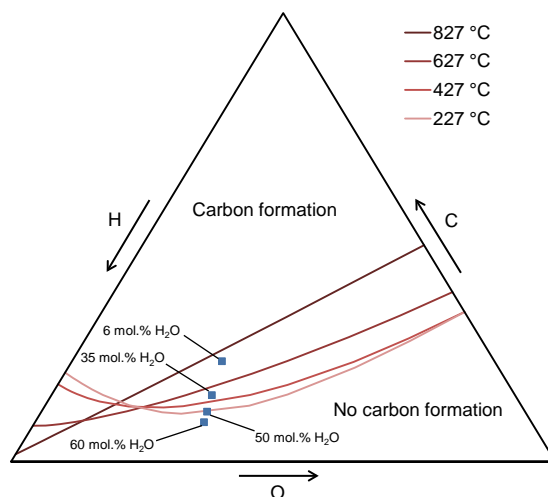
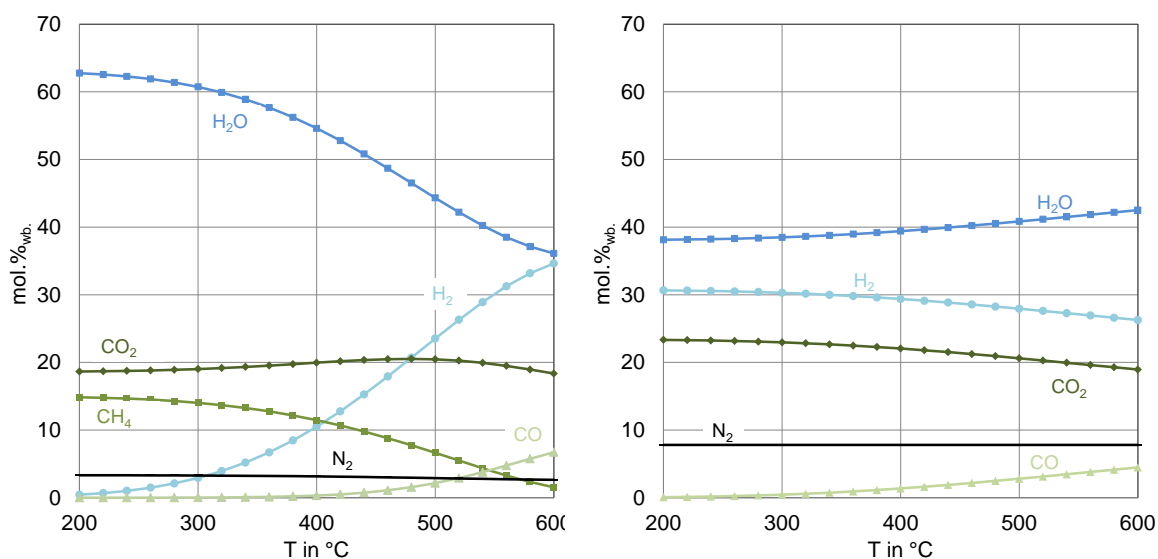


Figure 6.2: Ternary diagram of a gas mixture containing C, H, and O; in atomic mol.%, from [103, 102]; wood gas composition from Table 6.1, 6 mol.% H₂O cleaned wood gas after scrubber, 35 mol.% H₂O raw wood gas after, 50–60 mol.% typical operation of the WGS unit.

CO₂. This is especially interesting, as biogas derived from fermentative digestion of biomass is composed similarly. Therefore, wood gas derived from thermochemical conversion can be regarded as unequilibrated biogas. Commercial methanation catalysts are usually based on nickel and are therefore sensitive to sulfur poisoning [111]. As a consequence, it is difficult to attain these equilibrium conditions in wood gas which contains sulfur impurities. In Figure 6.3 (b) the methanation reaction and methane at the inlet were excluded. The CH₄ present at the inlet was compensated by N₂. Excluding CH₄, hydrocarbons and the methanation reaction from the equilibrium calculations reveals a different result. H₂ generated by means of the equilibration of the WGSR is not converted further to CH₄. At the usual operating temperature (300–500 C) more H₂ is generated if the methanation reaction is not catalyzed.

The SER technology has already been discussed in Chapter 4.1 as a possible improvement of the gasification process aiming at the production of H₂. During this work, the question arose if the catalysis of the WGSR is still of interest if the SER technology is used within a DFB steam gasifier. This question could also be answered by means of an equilibrium consideration of the WGSR. The results of this calculation are illustrated in Figure 6.4. Only reaction agents of the WGSR were considered and hydrocarbons as well as N₂ were subsumed under "no WGS". The steam to dry gas ratio was set to 1. Figure 6.4 (a) shows the results of the equilibrium calculation of the gas mixture obtained during SER operation of the CHP plant Güssing [68]. In Figure 6.4 (b) a more optimized gas composition for H₂ production was taken as a starting point for the equilibrium calculation. This gas composition was achieved at the 100 kW pilot DFB gasifier at Vienna University of Technology [86]. It can be seen that the equilibrium content of CO is even lower than in Figure 6.3 (b) and higher H₂ contents can be achieved. On a dry base, the CO content can be reduced from 5–15 vol.% to less than 1 vol.%. The question if the operation of a WGS unit is still economic if SER is carried out, should not be answered within this thesis. However, the carbon formation in SER gas is not



(a) Including CH₄ at the inlet and the formation of CH₄ by means of the methanation reaction. (b) Excluding CH₄ at the inlet (N₂ compensation) and the formation of CH₄ by means of the methanation.

Figure 6.3: Equilibrium composition of the wood gas mixture in Table 6.1 over the temperature, atmospheric pressure, hydrocarbons subsumed as N₂, 50 mol.% of H₂O in the wet gas.

likely which means that no steam would have to be added upstream the catalysis. It can also be expected, that the H₂ production according to the WGSR would enhance the overall H₂ yield of the process as well as the specific H₂ yield of the hydrogen purification facility.

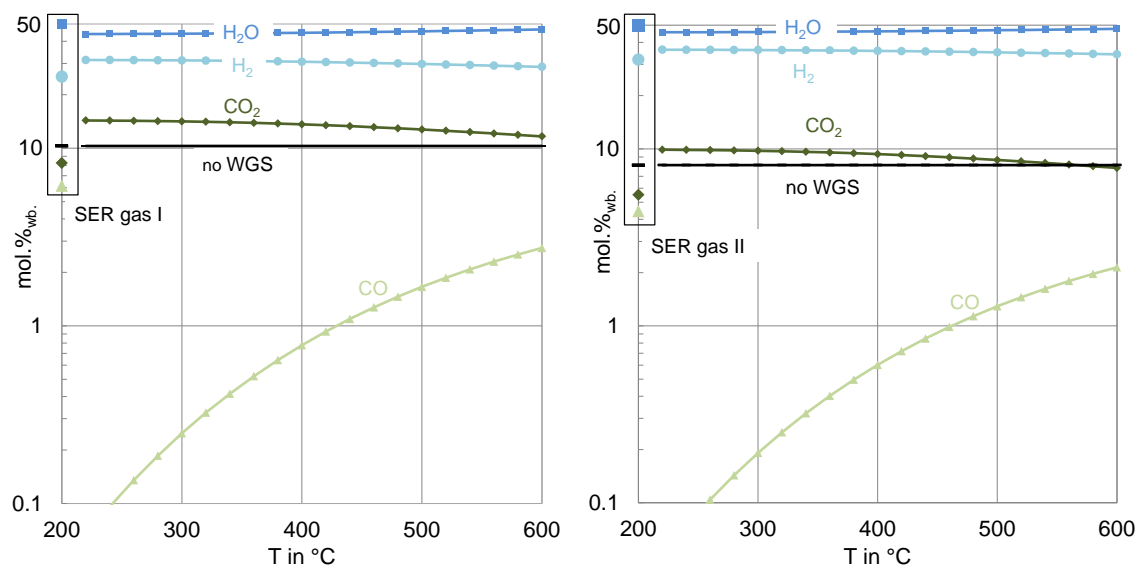
6.2 Co/Mo-based catalyst

Catalyst 1, based on a Co/Mo formulation was already described in Chapter 5.1. The catalyst was tested at the "Test rig for chemical kinetics" and the "Pilot plant for catalytic wood gas processing". In both cases, the catalyst had to be activated by means of a sulfidation procedure in order to form MoS₂.

6.2.1 Test rig for chemical kinetics

The activation of the milled catalyst at the "Test rig for chemical kinetics" was carried out by means of a synthetic mixture composed of N₂, H₂ and H₂S. Prior to sulfidation of the catalyst, the system was purged free from O₂ using N₂. During sulfidation the GHSV was set to 5000 h⁻¹. After attaining a temperature of 150 °C, 20 vol.% of H₂ was added to the N₂ flow. At about 200 °C, 0.1 vol.% of H₂S was added to the system. H₂S addition and the temperature were steadily increased to 0.81 vol.% and at about 300 °C the sulfidation was stopped. Care was taken to provide enough sulfur for a complete sulfidation.

After the activation of the catalyst, basically three different test runs were carried out. The first run aimed at the determination of the apparent reaction orders by means of a variation of the reacting agents. The second test run aimed at the investigation of the



(a) SER gas 1: gas composition achieved during SER operation of the CHP plant Güssing [68].

(b) SER gas 2: gas composition achieved during SER operation at the 100 kW pilot gasifier [86].

Figure 6.4: Equilibrium composition of different two SER wood gas mixtures with the temperature, wet inlet gas composition plotted on the y-axis, all gas components not taking part at the WGSR are subsumed as "no WGS", 50 mol.% of H₂O in the wet gas.

effect of sulfur on the catalyst activity. Finally, the pre-exponential factors and the apparent activation energies were determined based on a temperature variation experiment.

The apparent reaction orders were detected at an operating temperature of 380 °C and a GHSV_{wb.} of 16000 h⁻¹. At this temperature the equilibrium constant K_p of the WGSR was 14.57 (according to Equation 3.49). The adjusted gas compositions were generally based on the wood gas composition at the CHP plant Oberwart. During each test run, the amount of one single component was varied. Table 6.5 lists the applied inlet partial pressures of each test run, which were detected with the online gas analyzer during bypass operation. In a separate test run, also the H₂S content in the feed was varied in order to investigate the influence of sulfur on the catalyst. The varied component of each set is printed in bold. The GHSV was kept constant by means of adjusting a corresponding N₂ flow rate. By means of the measured partial pressures, the β values could be calculated according to Equation 3.47. After the bypass operation which aimed at the definition of the inlet flow, the reactants were passed over the catalyst. The dry gas volumetric flow rate was increased via the catalysis of the WGSR. Therefore, also the flow rate of the gas mixture at the outlet was quantified. The CO conversion rate (X_{CO}) and the reaction rate on a weight base ($r_{wt.}$) were calculated for each mixture. These values are also shown in Table 6.5.

The temperature of reaction was adjusted in order to achieve an operation in the differential mode (conversion rate around 5 %) [26]. Especially during sulfur experimentation, this level was exceeded because of the strong influence of H₂S on the catalyst activity. The values obtained for β were in the range of 0.016–0.032 which represented the desired opera-

Table 6.5: Catalyst 1: Co/Mo-based; variation of partial pressures at the inlet of the reactor to obtain the reaction orders of each reacting agent; applied temperature for catalyst testing: 380 °C, $GHSV_{wb}$, 16000 h⁻¹, CO conversion rate (X_{CO}), reaction rate (r).

P_{CO} kPa	P_{CO_2} kPa	P_{H_2} kPa	P_{H_2O} kPa	P_{H_2S} kPa	P_{N_2} kPa	β -	X_{CO} %	r mol g _{cat} ⁻¹ s ⁻¹
8.97	11.36	18.85	50.66	0.005	11.47	0.0324	5.26	8.225E-07
10.52	11.31	18.86	50.66	0.005	9.97	0.0275	5.44	1.005E-06
12.03	11.31	18.63	50.66	0.005	8.69	0.0237	5.74	1.203E-06
13.53	11.26	18.87	50.66	0.005	7.00	0.0213	5.92	1.414E-06
15.03	11.24	18.76	50.66	0.005	5.63	0.0190	6.02	1.609E-06
12.05	8.87	19.04	50.66	0.005	10.70	0.0190	6.12	1.292E-06
12.00	10.33	18.88	50.66	0.005	9.46	0.0220	6.02	1.276E-06
11.94	11.78	18.76	50.66	0.005	8.18	0.0251	5.99	1.245E-06
11.90	13.23	18.77	50.66	0.005	6.75	0.0283	5.95	1.226E-06
11.85	14.70	18.51	50.66	0.005	5.59	0.0311	5.83	1.213E-06
12.03	11.31	15.35	50.66	0.005	11.97	0.0196	6.25	1.329E-06
12.00	11.31	16.47	50.66	0.005	10.88	0.0210	6.17	1.305E-06
11.96	11.28	17.63	50.66	0.005	9.79	0.0225	5.98	1.266E-06
11.94	11.27	18.80	50.66	0.005	8.64	0.0240	5.88	1.231E-06
11.96	11.30	19.91	50.66	0.005	7.50	0.0255	5.83	1.209E-06
13.21	12.47	20.81	45.60	0.006	9.24	0.0296	5.20	1.182E-06
12.26	11.56	19.33	49.40	0.005	8.77	0.0253	5.54	1.193E-06
11.32	10.69	17.89	53.20	0.005	8.23	0.0218	6.14	1.204E-06
10.37	9.80	16.41	57.00	0.004	7.75	0.0187	6.57	1.209E-06
9.43	8.87	14.87	60.80	0.004	7.35	0.0158	7.35	1.214E-06
11.82	11.10	19.14	50.66	0.005	8.58	0.0244	4.19	8.593E-07
11.97	11.24	18.89	50.66	0.010	8.54	0.0240	4.85	9.974E-07
11.96	11.22	18.87	50.66	0.020	8.59	0.0240	5.84	1.197E-06
11.91	11.17	18.85	50.66	0.030	8.70	0.0240	6.33	1.341E-06
11.90	11.16	18.83	50.66	0.041	8.73	0.0239	6.97	1.469E-06
11.85	11.10	18.86	50.66	0.051	8.80	0.0239	7.69	1.611E-06
11.88	11.13	18.82	50.66	0.061	8.77	0.0239	8.35	1.768E-06
11.90	11.14	18.93	50.66	0.071	8.62	0.0240	8.86	1.864E-06
11.85	11.09	18.76	50.66	0.081	8.88	0.0238	9.31	1.970E-06

tion far from equilibrium. Based on Table 6.5 a "log-log" plot was drawn. Revealing linear relations, the natural logarithm (ln) of the term $\frac{X_{CO}}{1-\beta}$ was plotted versus the ln of the partial pressures of CO, H₂O, CO₂ and H₂. The obtained curves for each reacting agent are illustrated in Figure 6.5. The slope of each line in the plot was taken as the corresponding reaction order with respect to the component. The obtained slopes are summarized in Table 6.6. The apparent reaction orders of the reactants CO and H₂O were positive. An increase in the concentrations of the products (CO₂ and H₂) caused a decrease in the conversion rate, represented by negative slopes of the corresponding reaction orders. Especially, the conversion rates were enhanced with an increase in the CO concentration. Few data of apparent reaction orders of Co/Mo-based catalysts could be found in literature. The available data are strongly based on experiments with simulated coal gas. Other authors also consider CO as the most important reaction partner, but generally smaller slopes are documented. Hla et al. established a power law rate model for a Co/Mo-based catalyst at a sulfur load of 1000 vol.ppm_{db}. and found a reaction order of 0.75 with respect to CO and an order of 0.31 with respect to H₂O [50]. Besides the properties of the catalyst, this difference of the catalysts performance could basically be explained by the lower sulfur content that was used during this study (100 vol.ppm_{db}).

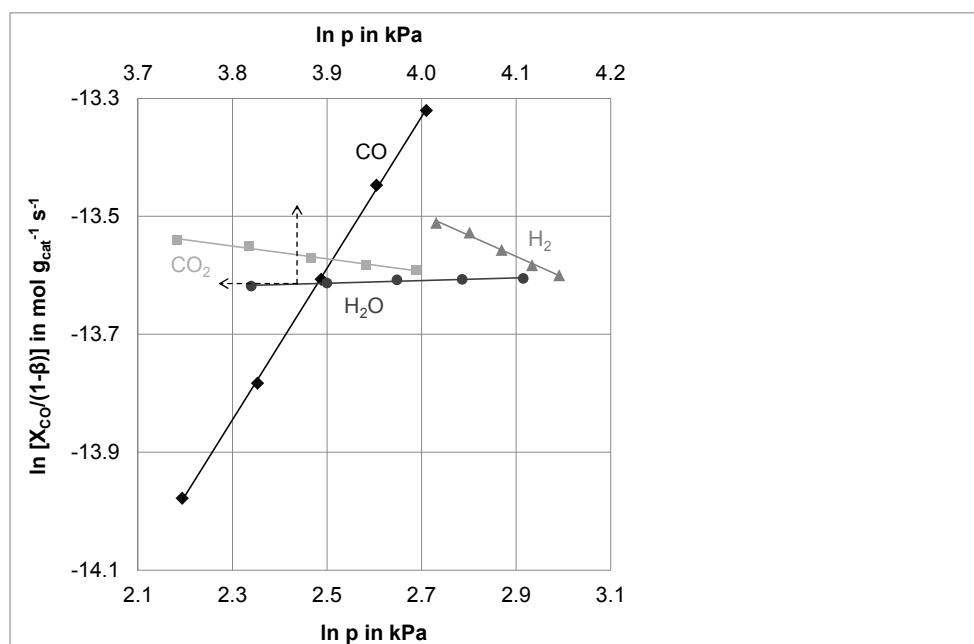


Figure 6.5: Catalyst 1: Co/Mo-based; determination of apparent reaction orders; "Log-log" plot of the influence of the partial pressures of CO, CO₂, H₂ and H₂O on the reaction rate; operating temperature 380 °C, ambient pressure, GHSV_{wb}. 16000 h⁻¹.

Table 6.6: Catalyst 1: Co/Mo-based; obtained apparent reaction orders of each reacting agent; applied temperature for catalyst testing: 380 °C, GHSV_{wb}. 16000 h⁻¹.

Catalyst 1	a [CO]	b [H ₂ O]	c [CO ₂]	d [H ₂]
Co/Mo	1.28	0.05	-0.11	-0.36

To investigate the effect of sulfur on the performance of the Co/Mo-based catalyst, a series of H₂S concentrations ranging from 100–1600 vol.ppm_{db}. were tested at a fixed temperature of 380 °C (see Table 6.5). For each sulfur concentration the achievement of steady state was awaited. The sulfur load strongly influenced the activity of the catalyst. The results of the sulfur variation on the Co/Mo-based catalyst are shown in Figure 6.6. In this figure, the ln of X_{CO} was plotted versus the ln of the partial pressure of H₂S. In the investigated range of H₂S variation the catalyst activity was doubled which can also be seen in Table 6.5. A linear relation with a slope of 0.3 was estimated. Similar results were given in [50], reporting an H₂S slope of 0.5 for another commercial Co/Mo-based catalyst operated at 450 °C. The apparent reaction order of H₂S could not be included into the overall power law rate model of the catalyst. It could be expected, that sulfur has an influence on the apparent reaction orders of the reacting agents, the apparent activation energy and the pre-exponential factor of the model. Therefore, the simple power law model in Equation 6.1 for sulfur addition at 380 °C was established according to the general Equation 5.1.

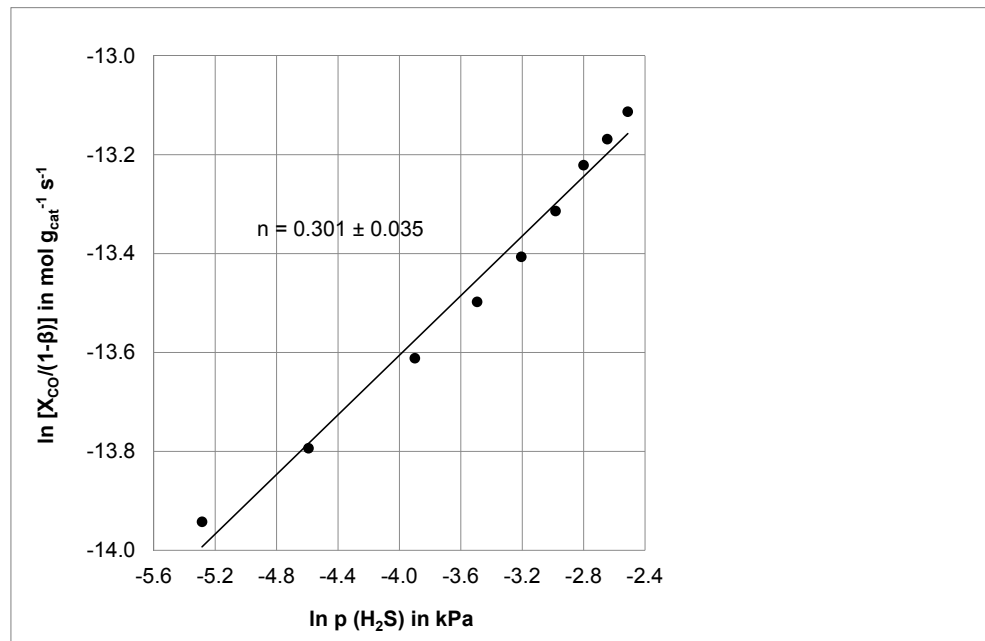


Figure 6.6: Catalyst 1: Co/Mo-based; Log-log plot of the effect of the H₂S partial pressure on the reaction rate, 380 °C, atmospheric pressure, GHSV_{wb}. 16000 h⁻¹.

$$r_{wt.} = -12.40 p_{H_2S}^{0.301} \quad (6.1)$$

The results of the temperature variation of Catalyst 1 are shown in Figure 6.7. The graph shows an Arrhenius plot where the ln of the rate constant k was plotted against the reciprocal temperature ($\frac{1}{T}$) revealing a linear relation. From the slope of this line ($\frac{-E_a}{R}$) the apparent activation energy was found to be 66.3 $\frac{kJ}{mol}$ which is in good agreement with [50], who reported an apparent activation energy of 60.3 $\frac{kJ}{mol}$ for another commercial Co/Mo-based catalyst. Calculated from the intercept of the plotted line at the ordinate, the pre-exponential factor A was found to be 0.034.

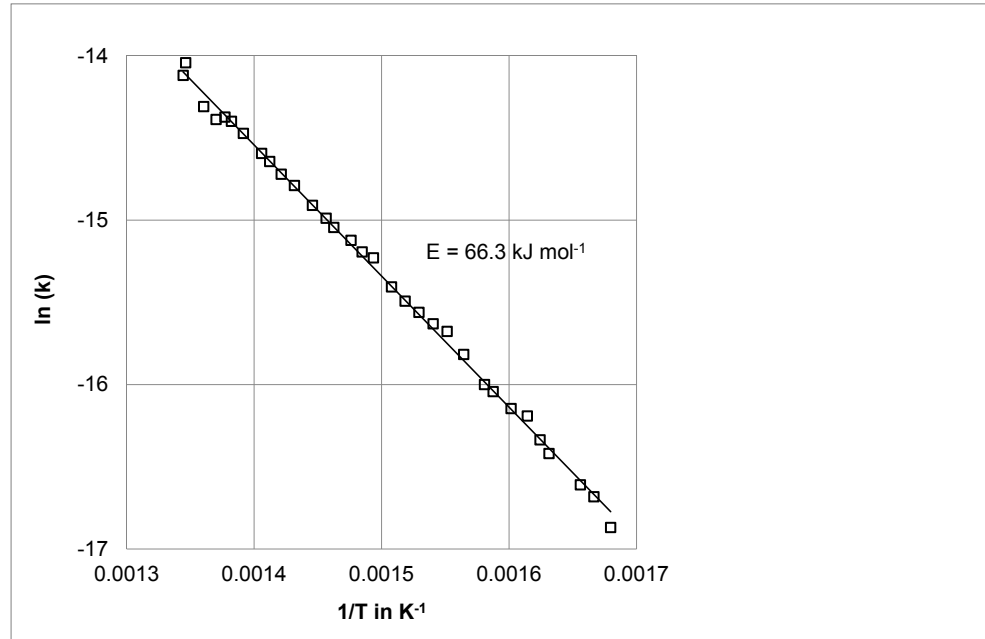


Figure 6.7: Catalyst 1: Co/Mo-based; Arrhenius plot of the catalyzed WGSR, gas composition in Table 5.3, 320–470 °C, atmospheric pressure, GHSV_{wb} . 16000 h^{-1} .

After the estimation of all apparent factors of the model, the power law rate model of the Co/Mo-based catalyst was expressed as Equation 6.2. The model is only valid for a H_2S content of about 100 vol.ppm._{db.}.

$$r_{wt.(Co/Mo)} = 0.034 \exp\left(\frac{-66.3}{R T}\right) p_{CO}^{1.28} p_{H_2O}^{0.05} p_{CO_2}^{-0.11} p_{H_2}^{-0.36} \left(1 - \frac{1}{K_p} \frac{p_{CO_2} p_{H_2}}{p_{CO} p_{H_2O}}\right) \quad (6.2)$$

At the "Test rig for chemical kinetics" the Co/Mo-based catalyst was also investigated in another experiment. That time, the aim was basically to estimate the design catalyst volume of the "Pilot plant for catalytic wood gas processing". A more practical approach was followed to estimate the influence of the main reaction parameters on the catalysis of the WGSR. The catalyst was not milled for these test runs. The catalyst pellets were introduced into a bigger quartz glass reactor which enabled an operation at lower GHSV_{wb} . (550–2500 h^{-1}). CO conversion rates up to 80 % were reached which means that the catalysis was not carried out in the differential mode. The catalyst performance of the raw catalyst and the sulfided catalyst were compared, revealing the strong importance of the catalyst activation by means of sulfidation. Subsequently, the influence of the temperature, the GHSV , and the steam content on the CO conversion rate was investigated. It could be seen that GHSV_{wb} as low as 500 h^{-1} should be designed for the "Pilot plant for catalytic wood gas processing" in order to enable high conversion rates also at moderate operating temperatures which are useful for the longterm stability of the catalyst. The obtained results of these investigations were published within a short conference communication [37] and a bachelor thesis [109]. This simple parameter study was carried out prior to the more sophisticated kinetic investigation aiming at the establishment of a power law rate model.

6.2.2 Pilot plant for catalytic wood gas processing

Before the commissioning with wood gas, the catalyst had to be activated by means of a sulfidation procedure. Subsequently, an extensive parameter study was carried out, where the influence of the operating temperature, the GHSV, and the steam content was investigated. Besides the CO conversion according to the WGS, also the influence of the catalyst on C₂ components, sulfur components, and tar was investigated. In contrast to the kinetic investigations, high CO conversion rates were desired at the "Pilot plant for catalytic wood gas processing". 8.19 L of the catalyst were evenly distributed over the three reactors of the WGS unit (2.73 L per reactor).

Activation of the CoMo-based catalyst

The principles of the sulfidation procedure of a Co/Mo-based catalyst were already discussed in 3.3.1. The activation of Catalyst 1 at the WGS unit is illustrated in Figure 6.8. The sulfidation procedure was carried out at a GHSV_{wb.} of 200 h⁻¹. First, only N₂ was passed over the catalyst. At a catalyst temperature of about 180 °C, 20 mol.% of H₂ were added to the activation mixture. The temperature was raised steadily and also increasing amounts of H₂S were added to the gas mixture. At about 300 °C, the maximum sulfur load of 3.5 mol.% was applied. Discharged Co/Mo-based catalysts usually contain up to 3 wt.% of sulfur [111]. The duration of the sulfidation procedure was calculated in order to enable a sulfur uptake of 5 wt.% assuming that only half of the sulfur is chemisorbed. Sulfur analysis at the outlet was not possible as the analytical method of the GC was not designed for high sulfur loads. During the sulfidation of the catalyst, the outlet of the WGS unit was connected to a barrel filled with 20 kg of activated charcoal. By means of this measure, both the input of H₂S into the power plant, as well as the emission of sulfur into the atmosphere could be avoided.

During the commissioning of the pilot plant with wood gas after scrubber it could be seen that the (old) temperature control of the process did not work properly. The process control was therefore modified and realized according to Figure 5.17.

Parameter study- Temperature

After this modification, the first parameter study was carried out at the "Pilot plant for catalytic wood gas processing". The rotation speed of both pumps was adjusted in order to achieve an operation at a GHSV_{wb.} of 300 h⁻¹ and a water content of 50 mol.%_{wb.}. Based on the already described "water spike" method, the mass balance was established and the GHSV_{wb.} was calculated to be 289 h⁻¹. A water content of 51 mol.%_{wb.} was measured at the inlet. The setpoint temperature at the inlet of all 3 reactors was steadily increased (20 °C steps) and only the gas composition at the outlet of the last reactor was measured (MV 8). The results of this temperature variation are illustrated in Figure 6.9. The CO conversion rate is plotted over the average temperature of all 3 fixed bed reactors. Initially, the rate increased strongly with the increase in temperature. At the present operating parameters,

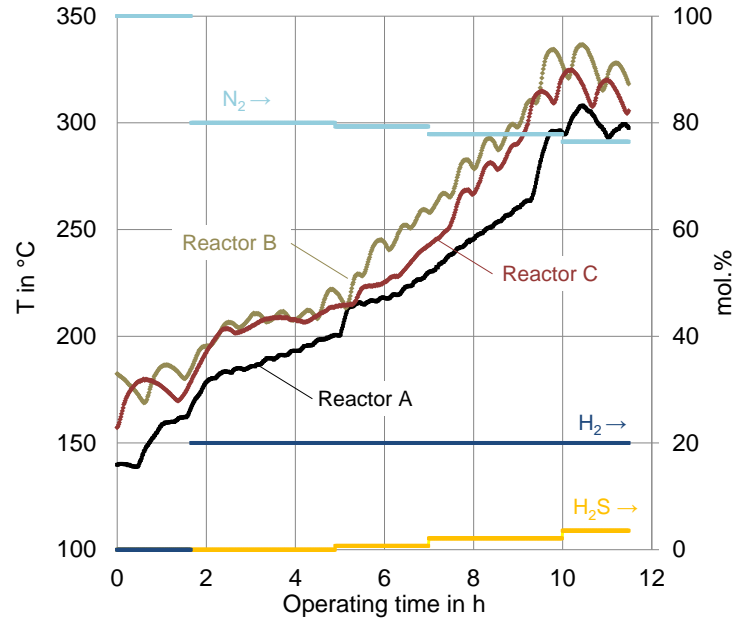
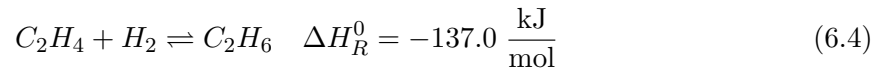
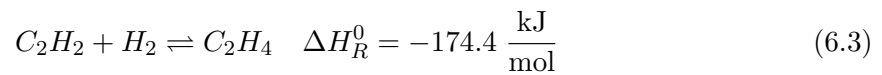


Figure 6.8: Catalyst 1: Co/Mo-based, sulfidation procedure at the "Pilot plant for catalytic wood gas processing".

the maximum CO conversion rate of about 85 % was recorded at temperatures between 380–410 °C. Subsequently, the conversion rate decreased without attaining equilibrium. This unusual behaviour could be explained via the influence of sulfur on the catalyst. At higher temperatures the equilibrium of the sulfidation reaction in Equation 3.11 is shifted toward the removal of H₂S and therefore it was assumed that the amount of active MoS₂ on the catalyst surface was reduced. At that time sulfur analysis was not yet available. Besides the conversion of CO according to the WGSR, also a complete removal of C₂H₂ was observed. This could be explained by its hydrogenation to ethylene according to Equation 6.3. Also, it could not be excluded that acetylene undergoes polymerization reactions on the catalyst surface leading to coke formation [111] (see Chapter 3.3.1 and Chapter 3.4.1). With an increase in temperature also an increasing amount of ethylene was hydrogenated to ethane according to Equation 6.4.



Parameter study- GHSV

In the following, the influence of the GHSV was investigated. Thereby, three different operating conditions were set up. The rotation speed of the gas pump and the water pump was adjusted to achieve an overall GHSV_{wb.} of 200, 300, and 400 h⁻¹ over all 3 reactors (total amount of catalyst) at a constant water content of 50 mol.%_{wb.} at the inlet. The inlet

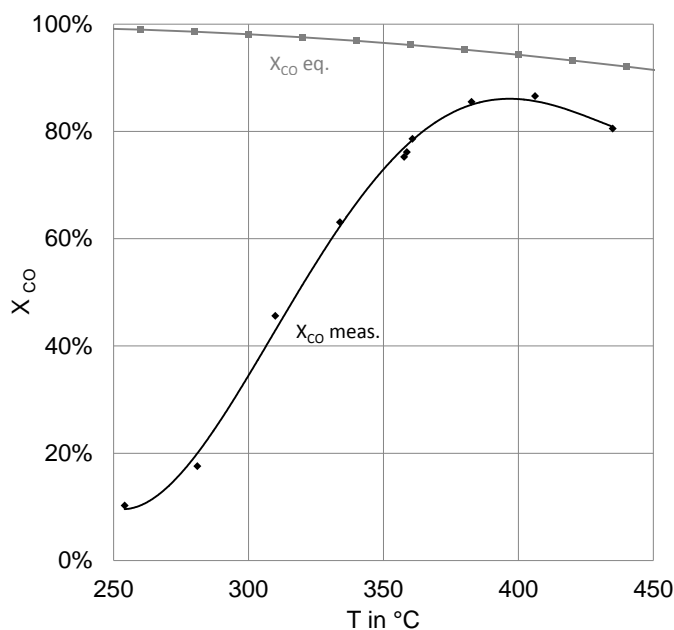


Figure 6.9: Temperature variation of Catalyst 1 at the "Pilot plant for catalytic wood gas processing"; cleaned wood gas; water content at the inlet 51 mol.%_{wb.}; GHSV_{wb.} 289 h⁻¹.

temperature of all 3 reactors was set to 370 °C, which resulted in averaged temperatures of all 3 reactors between 377–389 °C. This temperature could be considered as the optimum temperature with respect to the operating conditions applied before (see Figure 6.9, GHSV_{wb.} 289 h⁻¹, 51 mol.%_{wb.}). However, it had to be kept in mind that the optimum temperature of reaction depends on the GHSV. The gas composition was analyzed after each reactor which resulted in 9 different GHSV. The results of the investigation of the influence of the GHSV on the CO conversion rate are plotted in Figure 6.10. It can be seen that a GHSV_{wb.} lower than 400 h⁻¹ was basically required to reach a CO conversion rate higher than 80 %. The fluctuations of the obtained values were explained by deviations of the operating temperature. Besides the conversion of CO, a complete removal of C₂H₂ and a partly hydrogenation of C₂H₄ to C₂H₆ were observed again.

Performance of the WGS unit during the operation of process chain 1

The next experiment that was carried out at the WGS unit was the operation of process chain 1. An overall of 4 operation units was operated to produce pure hydrogen based on generated wood gas of the CHP plant Oberwart. Besides the WGS unit, this experiment also involved a gas scrubber, a membrane separation unit, and a PSA unit. The results of this process chain were summarized in a conference paper [36] which is included in Chapter 7.1 of this work. At this point, only the operation of the WGS unit is summarized in more detail.

Regarding the obtained results of this process chain it can be distinguished between two test runs. During the first test run, only the WGS unit, the gas scrubbing unit, and the membrane separation unit were operated. These results have not been published yet. The

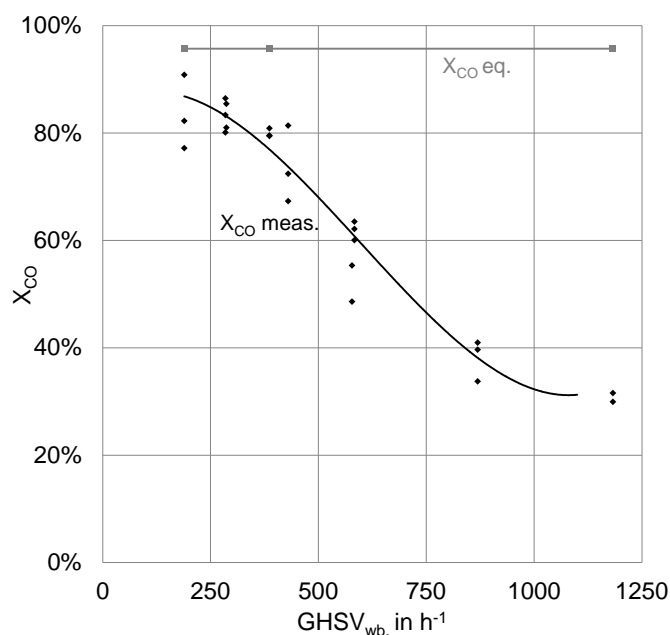


Figure 6.10: $GHSV_{wb}$ variation of Catalyst 1 at the "Pilot plant for catalytic wood gas processing"; cleaned wood gas; water content at the inlet 47–53 mol.% $_{wb}$.; T_{set} at the inlet of each reactor: 370 °C; average temperature over all reactors 377–389 °C.

second test run included the final purification of the product by means of the PSA unit. The corresponding results of the second test run were published in [36]. The basic operating conditions together with the obtained results of both test runs are summarized in Table 6.7. In both cases the WGS unit was operated continuously for about 100 hours. Table 6.7 shows that the performance of the WGS unit during the 1st test run was better than during the 2nd test run. This could be explained by means of the lower $GHSV$, the higher $\frac{H_2O}{CO}$ ratio, and the higher temperature in the last reactor - applied during the operation of the 1st test run. The influence of the Co/Mo-based catalyst on sulfur components, BTX, tar, and ammonia is discussed in Chapter 7.1 and [36].

Parameter study- $GHSV$ and Temperature

The next studies aimed to investigate the influence of the reaction temperature at different $GHSV$. First, the overall $GHSV_{wb}$. (full amount of catalyst, sampling point MV 8) was adjusted to 165 h^{-1} at a water content of 60.4 mol.% $_{wb}$. The temperature was varied between 350–420 °C and the gas composition was analyzed after each reactor. Sampling after each reactor could be used to investigate the performance of the catalysis at three different $GHSV$. The results are shown in Figure 6.11. The CO conversion rate in the first reactor increased strongly with the temperature. An Arrhenius relation was imagined. Regarding the overall CO conversion rate at the sampling point MV 8 it can be seen that the equilibration of the WGSR was almost achieved. The influence of a further temperature increase diminished with an approach to the equilibrium condition. The graph illustrates perfectly that high reaction

Table 6.7: Basic operating conditions and results of the WGS unit during operation of process chain 1.

	1 st test run	2 nd test run	Unit
Volume Catalyst 1	8.2	8.2	<i>L</i>
Water content wood gas	9.2	9.5	mol.% _{wb.}
Water content inlet WGS unit	63.9	58.6	mol.% _{wb.}
Water content outlet WGS unit	56.6	51.2	mol.% _{wb.}
CO content inlet	25.4	23.6	vol.% _{db.}
CO content outlet	2.9	5.6	vol.% _{db.}
Volumetric flow rate dry	1.37	1.92	$\frac{m_n^3}{h}$ db.
Volumetric flow rate wet	3.79	4.63	$\frac{m_n^3}{h}$ wb.
$\frac{H_2O}{CO}$ ratio	6.9	6.1	-
Pressure	140	120	<i>mbar</i> g
Temperature setpoint RA	370	370	°C
Temperature setpoint RB	370	370	°C
Temperature setpoint RC	370	330	°C
Overall GHSV _{wb.}	463.8	565.4	h ⁻¹
X _{CO}	86.4	72.5	%

temperatures are required to compensate for short residence times or high GHSV. However, it was already discussed, that high operating temperatures might reduce the lifetime of the catalyst due to thermal sintering of the active particles.

Subsequently, the same approach was repeated with an extended temperature variation. Compared to the operation in Figure 6.11 the GHSV was increased and the water content at the inlet was reduced to 52.1 mol.%_{wb.}. To obtain the presented results in Figure 6.12, the WGS unit was continuously operated for almost 3 weeks. The obtained results in Figure 6.12 (a) and are basically comparable with the results given in Figure 6.11. The obtained CO conversion rates were slightly lower, which could be explained by an increased GHSV and a reduced water content during the operation of the extended temperature variation. Besides the catalysis of the WGSR, also an increased hydrogenation of ethylene to ethane could be observed at higher temperatures which is shown in Figure 6.12 (b). To improve clarity, only the results of MV 8 (outlet WGS unit) are plotted. It can be seen that up to 40 % of C₂H₄ were converted to C₂H₆. Table 6.8 summarizes the basic operating conditions and results of this test run during the operation at an inlet temperature of 420 °C.

The measured H₂S content at the outlet of the WGS unit changed strongly with the operating temperature of the reactors. At higher temperatures (see Table 6.8) sulfur was desorbed from the catalyst according to the reversible reaction in Equation 3.11. An equilibration of the sulfur content at the inlet and at the outlet was very time consuming because of the low GHSV applied. An almost complete removal of COS was observed which was explained by the catalysis of the COS hydrolysis in Equation 3.10. Thiophene was not removed completely according to Equation 3.8 described in Figure 3.6. This was not expected as the composition of the catalyst was very similar to commercial HDS catalysts. At the present operating conditions, the equilibrium of this reaction was strongly on the side of the

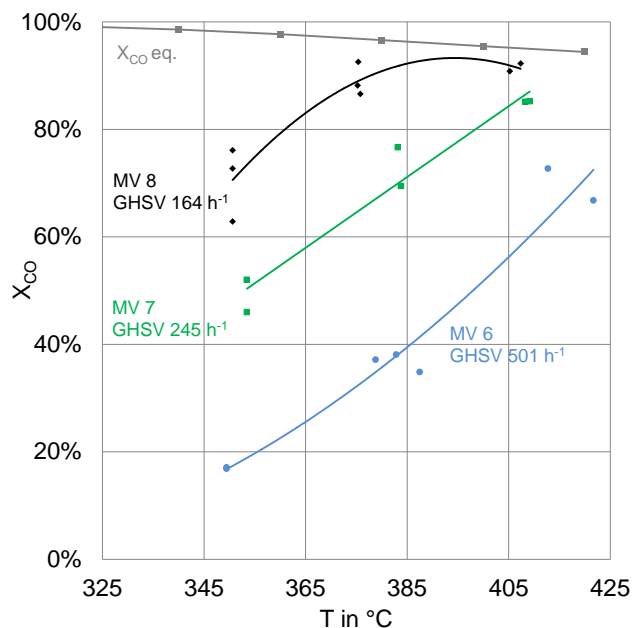


Figure 6.11: Temperature variation of Catalyst 1 at the "Pilot plant for catalytic wood gas processing"; cleaned wood gas; water content at the inlet 60.4 mol.%_{wb.}, average temperatures are plotted, gas sampling was carried out after each reactor (MV 6, MV 7, MV 8).

formation of butane. The low activity toward this reaction was explained by the atmospheric operating pressure. HDS catalysis is usually carried out at 30 bar [100]. Surprisingly, at low operating temperatures the content of thiophene measured at the outlet was higher than at the inlet which was already observed in [36]. At higher temperatures (see Table 6.8), the thiophene content increased in the first reactor and subsequently decreased over the downstream reactors. Therefore, it was assumed that thiophene was generated from a conversion of furan or other tar components in the presence of H₂S [77]. Furan was not analyzed within this thesis.

The basic operating conditions (GHSV and water content) during this study were similar to the temperature study in Figure 6.9. It can be seen that at that time higher CO conversions could be reached at more moderate temperatures. This could be explained by higher sulfur loads on the catalyst (time consuming equilibration of the sulfur load after sulfidation). Also, a partial deactivation of the catalyst was possible (see Chapter 3.4). Formation of coke due to acetylene and tar components was highly probable.

Influence of the catalyst on the tar composition

During the parameter investigation in Figure 6.12 also the tar content was measured at 3 different setpoint temperatures. The tar contents at the outlet of the WGS unit were measured at 300, 380 and 420 °C. Together with the inlet composition, the achieved results are summarized in Figure 6.13. The overall performance at 420 °C was already described in Table 6.8. It was shown that the dry gas volume was increased by 25 % at the outlet of

Table 6.8: Measured gas composition, temperatures, and key figures of the operation at an inlet temperature of 420 °C.

	CO ₂	C ₂ H ₄	C ₂ H ₆	C ₂ H ₂	O ₂		
Reactor A in	21.31	2.28	0.20	0.11	0.07	vol.% _{db.}	
Reactor A out	28.91	2.05	0.28	0.00	0.04	vol.% _{db.}	
Reactor B out	33.93	1.57	0.54	0.00	0.03	vol.% _{db.}	
Reactor C out	34.72	1.28	0.79	0.00	0.03	vol.% _{db.}	
	N ₂	CH ₄	CO	H ₂			
Reactor A in	1.69	9.73	25.41	37.56		vol.% _{db.}	
Reactor A out	1.51	8.88	13.04	47.83		vol.% _{db.}	
Reactor B out	1.47	8.29	5.03	50.19		vol.% _{db.}	
Reactor C out	1.95	8.09	3.29	50.64		vol.% _{db.}	
	H ₂ S	COS	MeSH	EtSH	C ₄ H ₄ S		
Reactor A in	61.6	2.3	BDL	BDL	5.1	vol.ppm _{db.}	
Reactor A out	81.9	0.4	BDL	BDL	10.61	vol.ppm _{db.}	
Reactor B out	116.9	0.2	BDL	BDL	7.6	vol.ppm _{db.}	
Reactor C out	134	0.2	BDL	BDL	5.3	vol.ppm _{db.}	
	T0	T1	T2	T3	T4	T5	
Reactor A	415	420	427	435	427	419	°C
Reactor B	420	427	438	442	437	429	°C
Reactor C	418	422	423	417	408	398	°C
	$\frac{H_2O}{CO}$	Y _{H₂O}	$\frac{\dot{V}_{db,out}}{\dot{V}_{db,in}}$	H _{2 rec}	X _{CO}		
	-	mol.% _{wb.}	-	-	-		
Reactor A in	4.3	52.1	-	-	-		
Reactor A out	6.7	46.7	1.16	1.42	42.8		
Reactor B out	14.8	42.6	1.23	1.60	76.3		
Reactor C out	21.6	41.6	1.26	1.66	84.1		

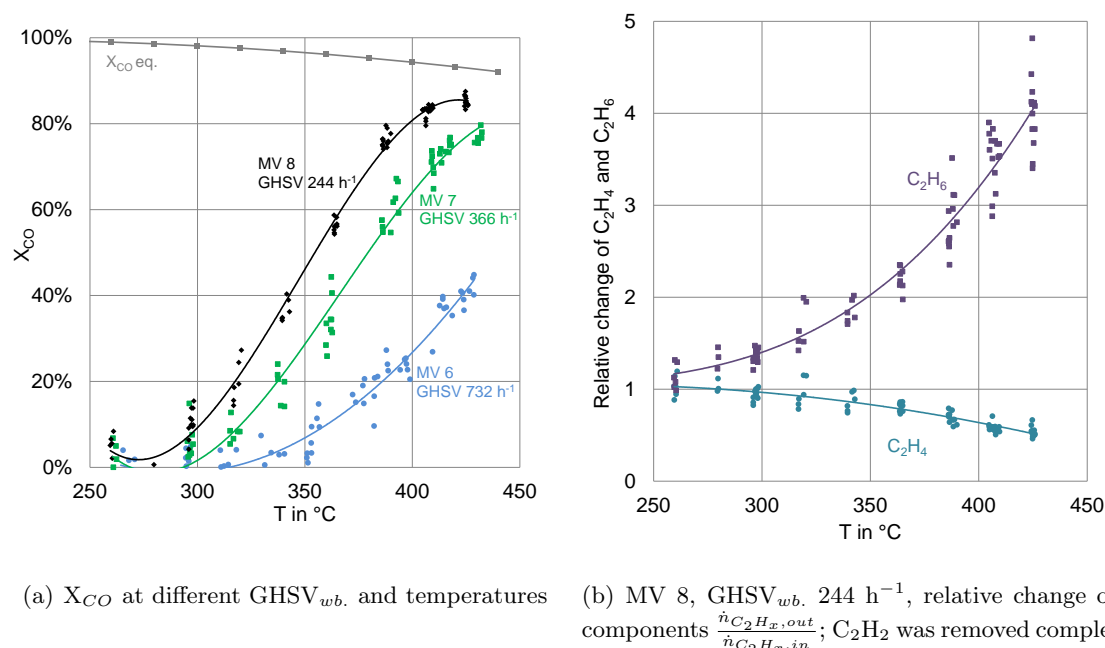


Figure 6.12: Temperature variation of Catalyst 1 at the "Pilot plant for catalytic wood gas processing"; cleaned wood gas after scrubber; water content at the inlet 52.1 mol.%_{wb.}, overall $GHSV_{wb}$ 244 h^{-1} ; average temperatures over all concerned reactors are plotted.

the last reactor. This caused a general dilution effect of the present tar components. The dilution effect was more pronounced at higher operating temperatures (higher X_{CO}) which explained the reduction of naphthalene over the temperature. It could therefore be assumed, that naphthalene as the most important tar component was not seriously affected by the catalyst. As discussed in [36] phenylacetylene and styrene were most probably hydrogenated to ethylbenzene. Indene was assumed to be reduced to indane, which was not analyzed. Acenaphtylene was also hydrogenated forming acenaphtene. The total amount of GC/MS tar was not presented here as tar components like ethylbenzene and indane were not analyzed. The gravimetric tar at 420 °C was reduced from 160 $\frac{mg}{m_n^3}$ to 130 $\frac{mg}{m_n^3}$ which was also explained by the volume change according to the WGSR.

After the operation of Catalyst 1 with cleaned gas after scrubber, raw wood gas was passed over the reactors. Basically, similar operating conditions were adjusted and the set-point temperature was varied. The obtained results of the tar analyses during raw wood gas operation were summarized in Figure 6.14. More tar components were present at concentration levels above the detection limit. Again, the most important tar component analyzed was naphthalene. The heavy tar components (naphthalene, acenaphtylene, and anthracene) were present in much higher concentrations compared to the operation with cleaned wood gas. In the RME-scrubber of the CHP plant, the lighter compounds indene and styrene were obviously removed to a smaller extent. Basically, the same influence of the catalyst on the tar composition was observed as with cleaned gas. However, the heavy tar components were mostly reduced stronger than it could be explained by the general dilution effect. In

literature no tar reforming activity is described for MoS₂ based catalysts. Therefore, it was possible that a tar induced coke formation was responsible for the decrease of the stable tar components naphthalene, acenaphtylene, and anthracene. The gravimetric tar was reduced from 240 $\frac{mg}{m_n^3}$ to 170 $\frac{mg}{m_n^3}$ at 420 °C which was also mainly explained by the increase of the dry gas volume.

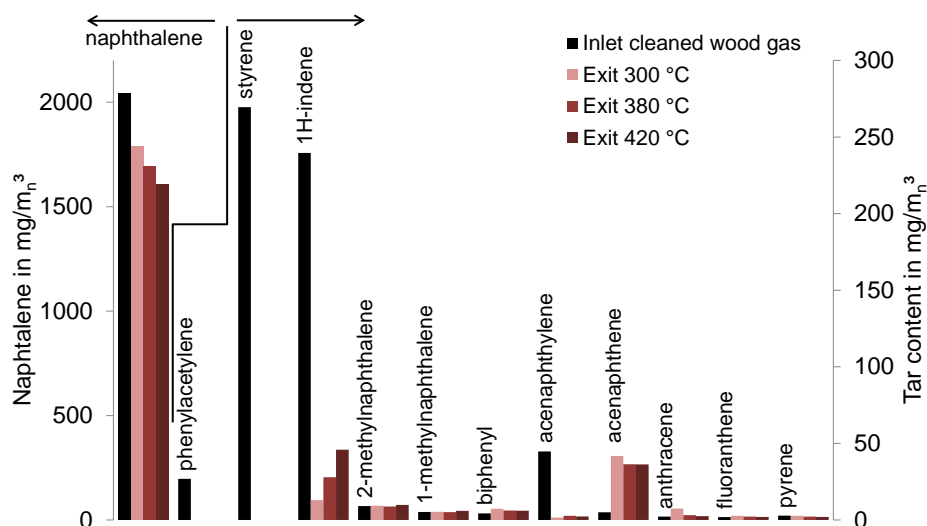


Figure 6.13: Tar analysis at different operating temperatures, cleaned wood gas after scrubber, sampling during the operation in Figure 6.12.

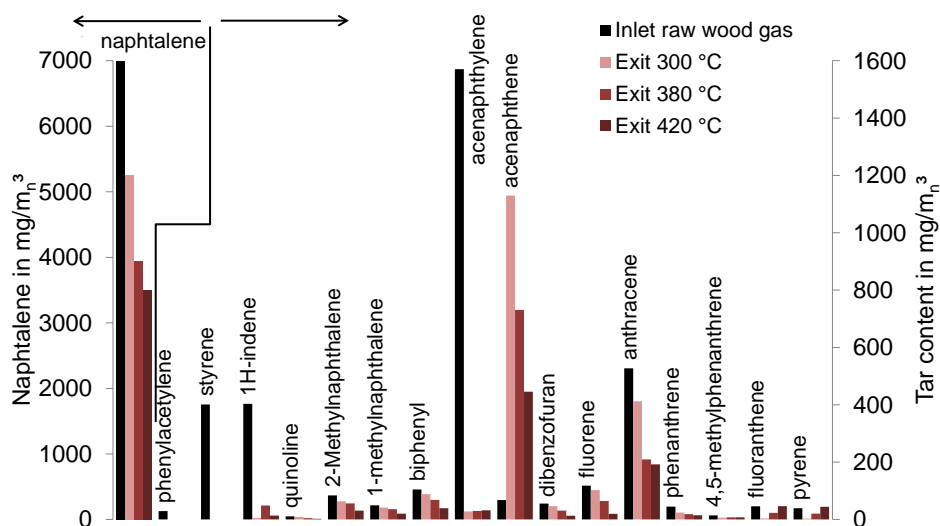


Figure 6.14: Tar analysis at different operating temperatures, raw wood gas after filter.

Parameter study- Sulfur addition

Finally, it was aimed to investigate the influence of sulfur on the performance of the Co/Mo-based catalyst. The same operating conditions (same combination of rotation speed of both pumps) were adjusted as in Figure 6.12. The inlet temperature of all three reactors was set

to 330 °C. At this temperature, a CO conversion rate of less than 30 % could be achieved at the outlet of the WGS unit. Usually about 60 vol.ppm_{db} of H₂S were present in the wood gas at the inlet. Four test runs were carried out, where 10, 20, 30, and 40 $\frac{mL_m}{min}$ of H₂S were added to the feed by means of a variable area flow meter. The effect of the addition of sulfur on the CO conversion rate is illustrated in Figure 6.15. The activity of the catalyst was strongly increased with the addition of H₂S which was in perfect accordance to [50] and the presented results of the catalyst at the "Test rig for chemical kinetics".

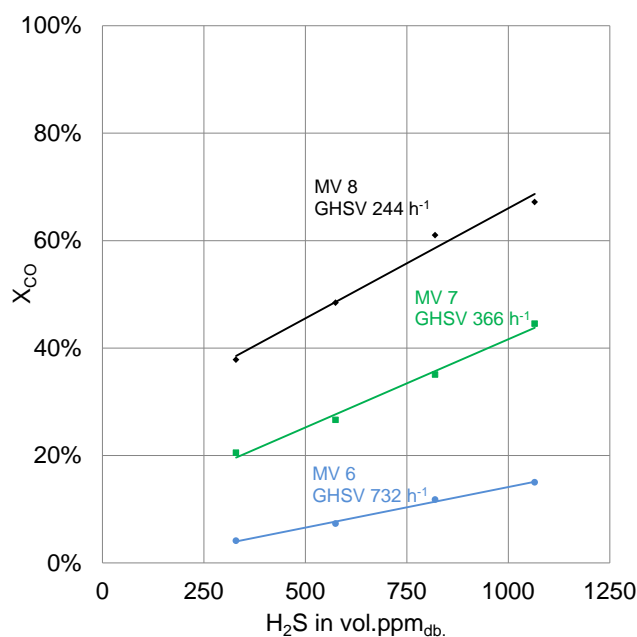


Figure 6.15: Sulfur addition at the inlet of the "Pilot plant for catalytic wood gas processing"; operation according to Figure 6.12; setpoint temperatures of all 3 reactors 330 °C, gas sampling was carried out after each reactor (MV 6, MV 7, MV 8).

Within this PhD thesis, the CoMo-based catalyst was operated for more than 1500 hours. In order to achieve CO conversion rates of about 85 %, rather low GHSV_{wb} (300 h⁻¹) and rather high temperatures (400–420 °C) were required. The low activity was mainly explained by the low sulfur content in the wood gas but also by the atmospheric operating pressure. An olefin/tar-induced deactivation of the catalyst by coke formation was possible but not verified.

6.3 Fe/Cr-based catalyst

Catalyst 2, based on a Fe/Cr formulation was already described in Chapter 5.1. The catalyst was tested at the "Test rig for chemical kinetics" and the "Pilot plant for catalytic wood gas processing". In both cases, the catalyst had to be activated by means of a reduction procedure in order to form the active magnetite.

6.3.1 Test rig for chemical kinetics

Analogous to Catalyst 1, also a milled sample of Catalyst 2 was tested at the "Test rig for chemical kinetics" with the aim of establishing an empirical power law rate model. According to [111], a gas mixture containing N_2 , H_2 and H_2O was applied to reduce the catalyst and to form the active Fe_3O_4 . The reduction was carried out at a $GHSV_{wb.}$ of 10000 h^{-1} and the temperature was steadily increased from ambient temperature to $300\text{ }^\circ\text{C}$. At the same time the N_2 content was steadily decreased from $90\text{ vol.}\%_{db.}$ to $50\text{ vol.}\%_{db.}$. Care was taken to keep a $\frac{H_2O}{H_2}$ ratio of 0.25 in order to avoid an overreduction of the catalyst to FeO or metallic iron. The reduction started at $150\text{ }^\circ\text{C}$ and could be detected by means of a small temperature increase (moderation by high N_2 flow rate) and a decrease in the partial pressure of H_2 at the outlet.

The gas compositions in Table 6.9 were used to determine the apparent reaction orders of Catalyst 2. During startup with synthetic wood gas, it turned out that the activity of Catalyst 2 (Fe/Cr-based) was much higher than the activity of Catalyst 1 (Co/Mo-based). Therefore, the operating temperature of these test runs was set to $300\text{ }^\circ\text{C}$ in order to keep a CO conversion rate of less than 5% (at a $GHSV_{wb.}$ of 16000 h^{-1}). During the investigation of the apparent reaction orders of Catalyst 1 the operating temperature had been set to $380\text{ }^\circ\text{C}$. At $300\text{ }^\circ\text{C}$ the equilibrium constant K_p of the WGSR was 38.75 (according to Equation 3.49). During experimentation, the β values were in between 0.006–0.012 (see Table 6.9) which indicated the desired operation far from equilibrium. The investigation was carried out at a H_2S content of 100 vol.ppm. In a separate test run, also the sulfur content was varied (last set of composition variation in Table 6.9. Figure 6.16 illustrates the results of the composition variation in Table 6.9 for Catalyst 2. The slope of each line in the plot was taken as the corresponding reaction order for the empirical power law model. The obtained apparent reaction orders from the plot are summarized in Table 6.10.

The reaction orders of the reactants CO and H_2O were positive. Especially, the conversion rate was enhanced drastically with increasing CO concentrations. Other authors also consider CO as the most important reaction partner, but generally smaller slopes are documented for Fe/Cr-based catalysts(0.9–1.0 [52], 0.74–1.1 [106]). On the one hand this could be explained by a different composition of the reaction partners. The present study, based on wood gas, was carried out at considerably lower partial pressures of CO and higher concentrations of CO_2 . On the other hand, the reported apparent reaction orders in the literature were usually estimated in a sulfur free feed, whereas this study was carried at an H_2S concentration of 100 vol.ppm_{db.}. The reaction order obtained of H_2O was 0.23 which was found to be in good

Table 6.9: Catalyst 2: Fe/Cr-based; variation of partial pressures to obtain the reaction orders of each reaction partner; applied temperature for catalyst testing: 300 °C, $GHSV_{wb}$. 16000 h^{-1} .

P_{CO} kPa	P_{CO_2} kPa	P_{H_2} kPa	P_{H_2O} kPa	P_{H_2S} kPa	P_{N_2} kPa	β -	X_{CO} %	r $mol\ g_{cat}^{-1}\ s^{-1}$
9.18	11.16	18.88	50.66	0.005	11.43	0.0117	2.57	4.050E-07
10.84	11.13	18.88	50.66	0.005	9.80	0.0099	3.15	5.829E-07
12.37	11.12	18.93	50.66	0.005	8.24	0.0087	3.28	7.214E-07
13.90	11.11	18.90	50.66	0.005	6.75	0.0077	3.56	8.711E-07
15.47	11.10	18.73	50.66	0.005	5.35	0.0068	3.83	1.040E-06
12.02	9.10	18.98	50.66	0.005	10.55	0.0073	4.84	1.024E-06
11.98	10.53	18.91	50.66	0.005	9.23	0.0085	4.72	9.754E-07
11.92	11.91	18.84	50.66	0.005	7.98	0.0096	4.57	9.755E-07
11.88	13.32	18.75	50.66	0.005	6.72	0.0107	4.52	9.404E-07
11.81	14.71	18.66	50.66	0.005	5.48	0.0118	4.44	9.368E-07
11.90	10.86	15.48	50.66	0.005	12.42	0.0072	4.73	9.853E-07
11.89	10.85	16.58	50.66	0.005	11.34	0.0077	4.68	9.790E-07
11.91	10.87	17.69	50.66	0.005	10.18	0.0082	4.63	9.658E-07
11.91	10.87	18.82	50.66	0.005	9.05	0.0087	4.60	9.624E-07
11.91	10.88	19.91	50.66	0.005	7.96	0.0093	4.54	9.541E-07
13.23	12.13	20.76	45.60	0.006	9.60	0.0108	3.83	8.779E-07
12.31	11.28	19.31	49.40	0.005	9.02	0.0092	4.12	8.816E-07
11.35	10.40	17.87	53.20	0.005	8.51	0.0079	4.58	9.037E-07
10.41	10.89	16.43	57.00	0.004	6.59	0.0078	4.98	9.135E-07
9.47	8.70	14.98	60.80	0.004	7.38	0.0058	5.72	9.441E-07
12.33	11.11	18.72	50.66	0.000	8.50	0.0086	3.91	8.573E-07
12.41	10.86	18.70	50.66	0.005	8.68	0.0083	3.74	7.865E-07
12.41	11.18	18.82	50.66	0.010	8.24	0.0086	3.42	7.302E-07
12.27	11.05	18.83	50.66	0.020	8.49	0.0086	2.79	6.068E-07
12.32	11.10	18.78	50.66	0.030	8.43	0.0086	2.48	5.233E-07
12.33	11.11	18.94	50.66	0.041	8.25	0.0087	2.09	4.458E-07
12.31	11.10	18.91	50.66	0.051	8.29	0.0087	1.93	4.190E-07

Table 6.10: Catalyst 2: Fe/Cr-based; obtained apparent reaction orders of each reacting agent; applied temperature for catalyst testing: 300 °C, $GHSV_{wb}$. 16000 h^{-1} .

Catalyst 1	a [CO]	b [H ₂ O]	c [CO ₂]	d [H ₂]
Co/Mo	1.77	0.23	-0.17	-0.12

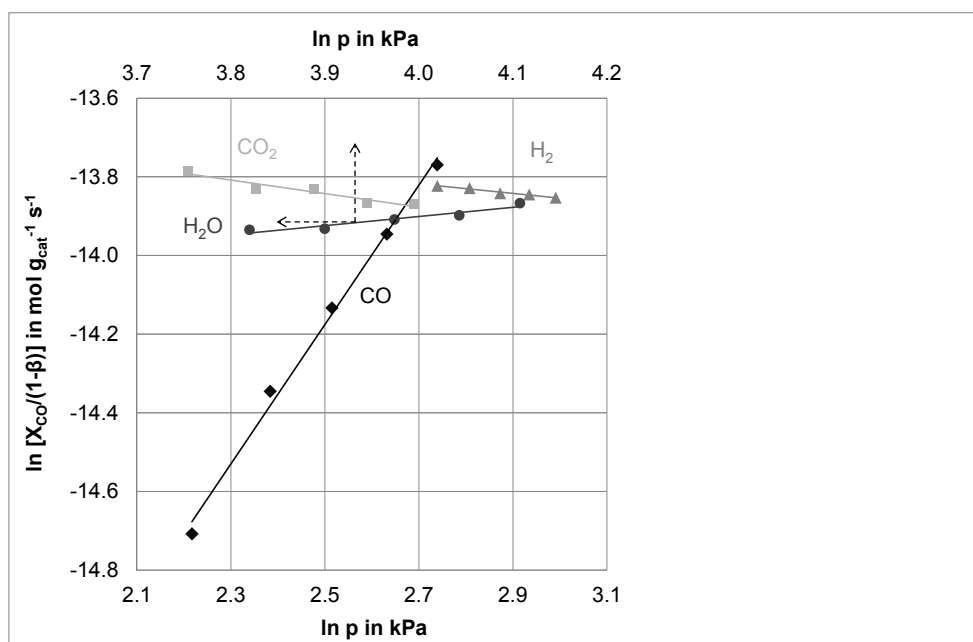


Figure 6.16: Catalyst 2: Fe/Cr-based; determination of power law rate model reaction orders; Log-log plot of the effect of CO, CO₂, H₂ and H₂O partial pressure on the reaction rate; operating temperature: 300 °C, GHSV_{wb}, 16000 h⁻¹.

agreement with the literature [52, 106]. An increase in CO₂ and H₂ concentrations caused a decrease in the conversion rate, represented by negative slopes of the corresponding reaction orders. Also, the obtained reaction rates of CO₂ and H₂ are in good agreement with the literature [52, 106].

The sulfur study of the more active Fe/Cr-based catalyst was also carried out at 300 °C. The H₂S concentration was varied between 0 and 1000 vol.ppm_{db}. (see Table 6.9). The effect of the sulfur variation on the activity of Catalyst 2 is shown in Figure 6.17.

Unlike the sulfur response of Catalyst 1, the activity of Catalyst 2 was reduced with increasing H₂S concentrations. This was found to be in accordance to [111], reporting that the FeS formed according to Equation 3.11 exhibits an activity reduced by 50 % compared to Fe₃O₄. At 1000 vol.ppm_{db}. of H₂S in the feed gas, the catalyst activity was reduced practically by 50 % compared to sulfur-free operation. The reaction order of the Fe/Cr-based catalyst with respect to H₂S was calculated to be -0.28 whereas a linear relation might not be justified in that case. Also non-linear activity responses to sulfur addition have been reported in the literature for Fe-containing catalysts [84]. The simple power law model in Equation 6.5 for sulfur addition at 300°C was established according to the general Equation 5.1.

$$r = -15.48 p_{H_2S}^{-0.284} \quad (6.5)$$

The Arrhenius graph which was obtained from the temperature variation (220–305 °C) of Catalyst 2 is shown in Figure 6.18. One temperature variation was carried out with the standard gas composition in Table 5.3 including 100 vol.ppm_{db}. of H₂S. The other line was obtained from temperature variation using the same gas mixture without H₂S.

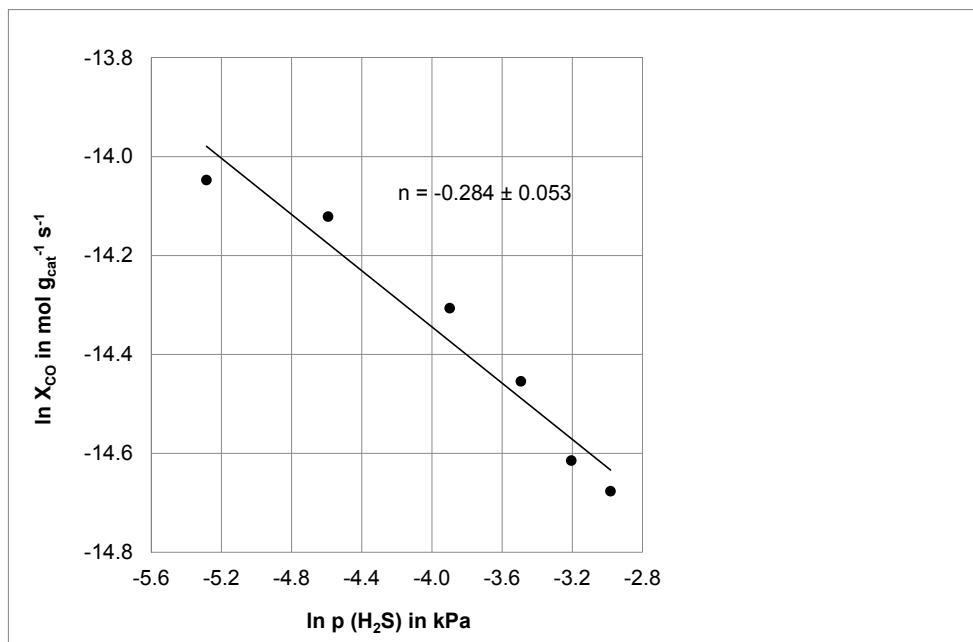


Figure 6.17: Catalyst 2: Fe/Cr-based; Log-log plot of the effect of the H₂S partial pressure on the reaction rate, 300 °C, atmospheric pressure.

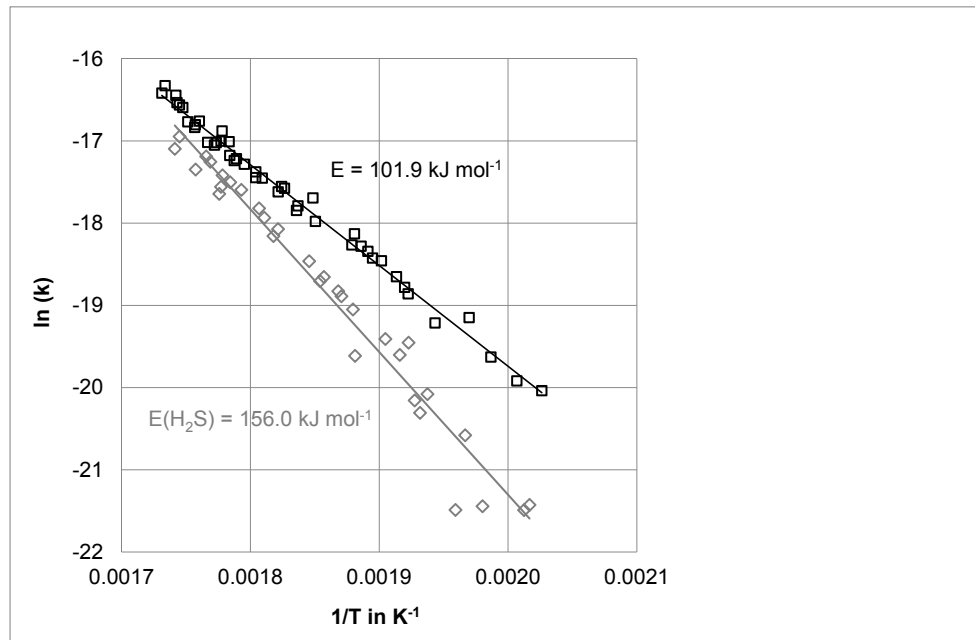


Figure 6.18: Catalyst 2: Fe/Cr-based; Arrhenius plot of the catalyzed WGSR, E: gas composition in Table 5.3 without H₂S, E(H₂S): gas composition in Table 5.3 with a H₂S load of 100 vol.ppm_{db.}, 220–305 °C, atmospheric pressure.

Especially at lower temperatures, the obtained rate constants were higher during H₂S-free operation. An apparent activation energy of 101.9 $\frac{kJ}{mol}$ was calculated in the absence of H₂S. The same value was found to be 156.0 $\frac{kJ}{mol}$ for the gas mixture including 100 vol.ppm_{db.} of H₂S. For sulfur-free operation with small catalyst particles, the activation energy is generally in the range of 100–113 $\frac{kJ}{mol}$ [63], which is in good agreement with the achieved results. The effect of a partial deactivation due to the formation of FeS was more pronounced at lower temperatures. Based on the obtained apparent reaction orders, the activation energy, and the exponential factor the power law rate model in Equation 6.6 was established. Because of the strong influence of the presence of sulfur on the activation energy, the pre-exponential factors, and the assumed influence on the apparent reaction orders, this model is only valid for an operation at a H₂S load of 100 vol.ppm_{db.}. It should not be extrapolated to higher temperatures.

The Arrhenius plot in Figure 6.18 suggests that the activity of the catalyst during H₂S addition (100 vol.ppm_{db.}) approaches the activity of the same catalyst during sulfur-free operation. Above 320 °C the activity of the catalyst is assumed to be almost independent from the present sulfur concentration of 100 vol.ppm_{db.}. HT WGS processing is usually carried out at more elevated temperatures. It can therefore be considered that the model in Equation 6.7 achieves better results at higher temperatures.

$$r_{wt.(Fe/Cr)} = 2.967 \cdot 10^6 \exp\left(\frac{-156.0}{R T}\right) p_{CO}^{1.77} p_{H_2O}^{0.23} p_{CO_2}^{-0.17} p_{H_2}^{-0.12} \left(1 - \frac{1}{K} \frac{p_{CO_2} p_{H_2}}{p_{CO} p_{H_2O}}\right) \quad (6.6)$$

$$r_{wt.(Fe/Cr)} = 117.8 \exp\left(\frac{-101.9}{R T}\right) p_{CO}^{1.77} p_{H_2O}^{0.23} p_{CO_2}^{-0.17} p_{H_2}^{-0.12} \left(1 - \frac{1}{K} \frac{p_{CO_2} p_{H_2}}{p_{CO} p_{H_2O}}\right) \quad (6.7)$$

6.3.2 Pilot plant for catalytic wood gas processing

7.8 L of the Fe/Cr-based catalyst were evenly distributed over the three fixed bed reactors (2.6 L per reactor) in order to test the performance of Catalyst 2 in combination with real wood gas derived from the CHP plant Oberwart.

This chapter is basically structured in four sections. First, the activation of the catalyst is described which represented a critical stage of the usage of the catalyst within the WGS unit. Second, the "Induction period" (also "Line-up period", see Figure 3.9) of the catalyst is presented where the catalyst was operated steadily with cleaned wood gas after scrubber. During this period, the catalyst was exposed to sulfur which led to the formation of FeS according to Equation 3.25. Subsequently, the performance of the WGS unit during the operation of process chain 2 (Chapter 7.2) is reviewed. Finally, the full load of the WGS unit was achieved with the two available extraction points of wood gas (cleaned wood gas after filter and raw wood gas after scrubber).

Activation of the Fe/Cr-based catalyst

The activation of the Fe/Cr-based catalyst at the "Pilot plant for catalytic wood gas processing" is illustrated in Figure 6.19. Prior to the reduction of the catalyst, a N₂ flow was applied to purge the system free from O₂. The reduction was carried out in an atmosphere containing H₂, H₂O and N₂. The graph shows the temperature profile in reactor A and the applied gas composition over the activation time. Generally, the $\frac{H_2}{H_2O}$ ratio was set to 0.25 and the procedure was started at a GHSV_{wb.} of 250 h⁻¹. As reported in [111] the exothermic reduction process (Equations 3.20 and 3.21) started at a temperature of about 150 °C. Subsequently, a wave of temperature increase (up to 300 °C) proceeded through the bed. To avoid an even more stringent temperature increase, the N₂ addition was increased over the activation time and therefore also the GHSV. The same trend as in reactor A was also observed in reactor B and C. After this strong temperature increase, the N₂ addition was steadily decreased and higher partial pressures of H₂ and H₂O were applied. The $\frac{H_2}{H_2O}$ ratio was kept constant in order to avoid an overreduction of the catalyst. The inlet temperature of each reactor was steadily increased to reach 300 °C. Subsequently, the WGS unit was commissioned with cleaned wood gas which is described in the next chapter.

Induction period of the Fe/Cr-based catalyst

After the activation of the catalyst, its long-term operation with wood gas after scrubber was started instantly. In the presence of H₂S, Fe₃O₄ was converted to FeS according to the reversible sulfidation reaction in Equation 3.25. The aim was to achieve an equilibrium sulfidation of the catalyst. The same sulfur content at the inlet and at the outlet indicated equilibrium conditions with respect to the operating conditions and the sulfur content in the feed. The equilibrium of the exothermic sulfidation reaction is shifted toward the formation of FeS at lower operating temperatures of the catalyst. FeS is reported to exhibit only half of the activity of Fe₃O₄ [111]. Together with the activation of the catalyst, this sulfur equilibration

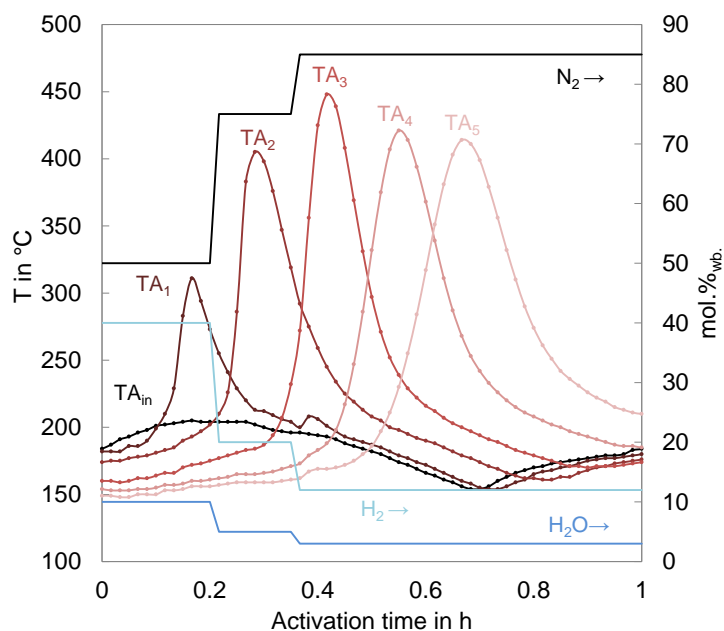


Figure 6.19: Temperature profile of reactor A and gas composition during activation of the Catalyst 2.

can be seen as part of its "Induction period" or "Line-up period" (according to Figure 3.9) where a rather strong change of the catalyst activity occurs. The equilibration was carried out for almost 400 hours at the basic operating conditions summarized in Table 6.11. The temperature and pressure profiles over the WGS unit are illustrated in Figure 6.20. The inlet temperature of all three reactors was set to 350 °C what can be referred to as the standard inlet temperature of a HT WGS stage [111]. Inside the first reactor, the exothermic WGSR led to a rather strong temperature increase in the range of 80 °C. During the operation with the Co/Mo-based catalyst, this temperature increase was much less pronounced what was indicating a higher activity of the Fe/Cr-based catalyst. At the present conditions summarized in Table 6.11, the main part of the reaction was already completed after the first half of the catalyst bed height of reactor A. Subsequently, temperatures dropped because of heat losses. The temperature control of the WGS unit was capable of providing a constant temperature at the inlet of the first reactor. However, the other thermocouples TA₁–TA₅ showed rather strong fluctuations. Generally, this was explained by the varying wood gas composition. Strong deviations of the temperature profiles indicated operating problems of the CHP plant Oberwart. The two strong temperature increases were caused by the presence of oxygen in the wood gas and oxidation reactions of wood gas components. The temperature drops were caused by the dilution of wood gas with N₂ which occurred during short shut downs of the CHP plant. The temperature profiles of reactor B and C were more stable because of the buffering effect of reactor A. Also, the temperature increase due to the exothermic WGSR was less pronounced because of the lowered CO contents. During the induction period, the automatic sampling sequence TA₁ was operated which allowed the gas analysis at the available sampling points (MV 5, MV 6, MV 7, and MV 8). The obtained results of the main gas

composition over the operating time are illustrated in 6.21. No significant change of the composition over time could be observed apart from the varying wood gas composition. At the present operating conditions, the sulfidation of the catalyst did not lead to a significant change of the main gas composition. The average composition of the wood gas and the outlet composition of each reactor is also summarized in Table 6.12. This table also includes the analysis of the C₂ components. Acetylene was hydrogenated to ethylene. Also, some ethylene was hydrogenated to ethane. The overall balance of the C₂ components closed very well and acetylene is not reported to cause coke formation on HT WGS catalyst [111]. Apart from the general dilution effect of the increased dry flow rate, CH₄ was not affected by the catalyst. The sulfur trends are illustrated in Figure 6.22. It can be seen, that the sulfur content in the generated wood gas varied strongly over the time. The sulfur composition was flattened by the reactors. A steady increase in the sulfur content at the outlet of each reactor was observed. However, during this experiment the sulfidation was only completed in the first reactor. Anyway, also the performance of the first reactor did not decrease in the course of the experiment. The main results of the induction period are summarized in Table 6.12 and 6.13. In accordance to the temperature profile of the first reactor, most of the CO was converted in reactor A. An overall CO conversion rate of 90.5 % was reached which represented a CO concentration of about 1.85 vol.%_{db.} at the outlet of the WGS unit.

Table 6.11: Induction period of the Fe/Cr-based catalyst, basic operating conditions.

Volume Catalyst 2	7.8	<i>L</i>
Water content wood gas	7.0	mol.% _{wb.}
Water content inlet WGSR	49.23	mol.% _{wb.}
Volumetric flow rate dry	1.19	$\frac{m^3}{h}$ _{db.}
Volumetric flow rate wet	2.36	$\frac{m^3}{h}$ _{wb.}
$\frac{H_2O}{CO}$ ratio	4.06	-
Pressure	0–50	<i>mbarg</i>
Temperature setpoint	350	°C
Overall GHSV _{wb.}	303	<i>h</i> ⁻¹

Table 6.12: Induction period of the Fe/Cr-based catalyst, averaged gas composition of Figure 6.21 at the inlet and at the outlet of each reactor of the WGS unit, measured in September 2013.

	CO ₂	C ₂ H ₄	C ₂ H ₆	C ₂ H ₂	O ₂	
Reactor A in	22.91	2.21	0.18	0.13	0.17	vol.% _{db.}
Reactor A out	34.81	1.88	0.16	0.01	0.06	vol.% _{db.}
Reactor B out	36.16	1.80	0.19	0.00	0.06	vol.% _{db.}
Reactor C out	36.49	1.77	0.22	0.00	0.07	vol.% _{db.}
	N ₂	CH ₄	CO	H ₂		
Reactor A in	2.96	9.99	23.91	37.56		vol.% _{db.}
Reactor A out	2.45	8.63	4.17	47.83		vol.% _{db.}
Reactor B out	2.49	8.43	2.34	48.55		vol.% _{db.}
Reactor C out	2.52	8.44	1.85	48.63		vol.% _{db.}

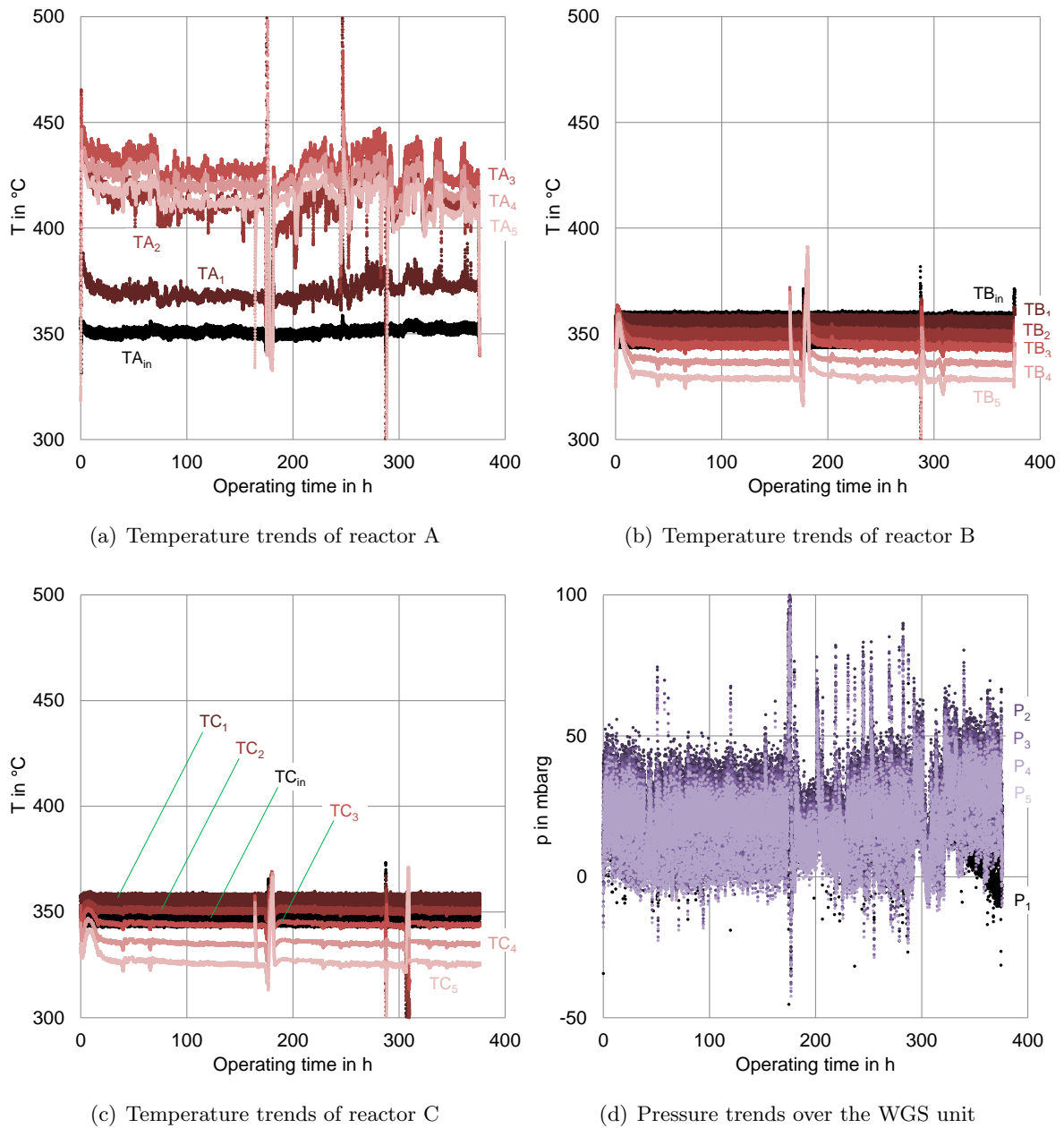


Figure 6.20: Induction period of the Fe/Cr-based catalyst, temperature and pressure trends over the WGS unit.

Table 6.13: Induction period of the Fe/Cr-based catalyst, key results, operation according to Table 6.11.

	GHSV _{wb.}	$\frac{H_2O}{CO}$	CO vol.% _{db.}	H ₂ O mol.% _{wb.}	Increase $\dot{V}_{db.}$	H ₂ rec	X _{CO}
Reactor A in	-	4.06	23.91	49.23	-	-	-
Reactor A out	908	15.59	4.17	39.02	1.20	1.53	79.05
Reactor B out	454	26.72	2.34	37.79	1.24	1.64	88.12
Reactor C out	303	33.10	1.85	37.50	1.25	1.65	90.48

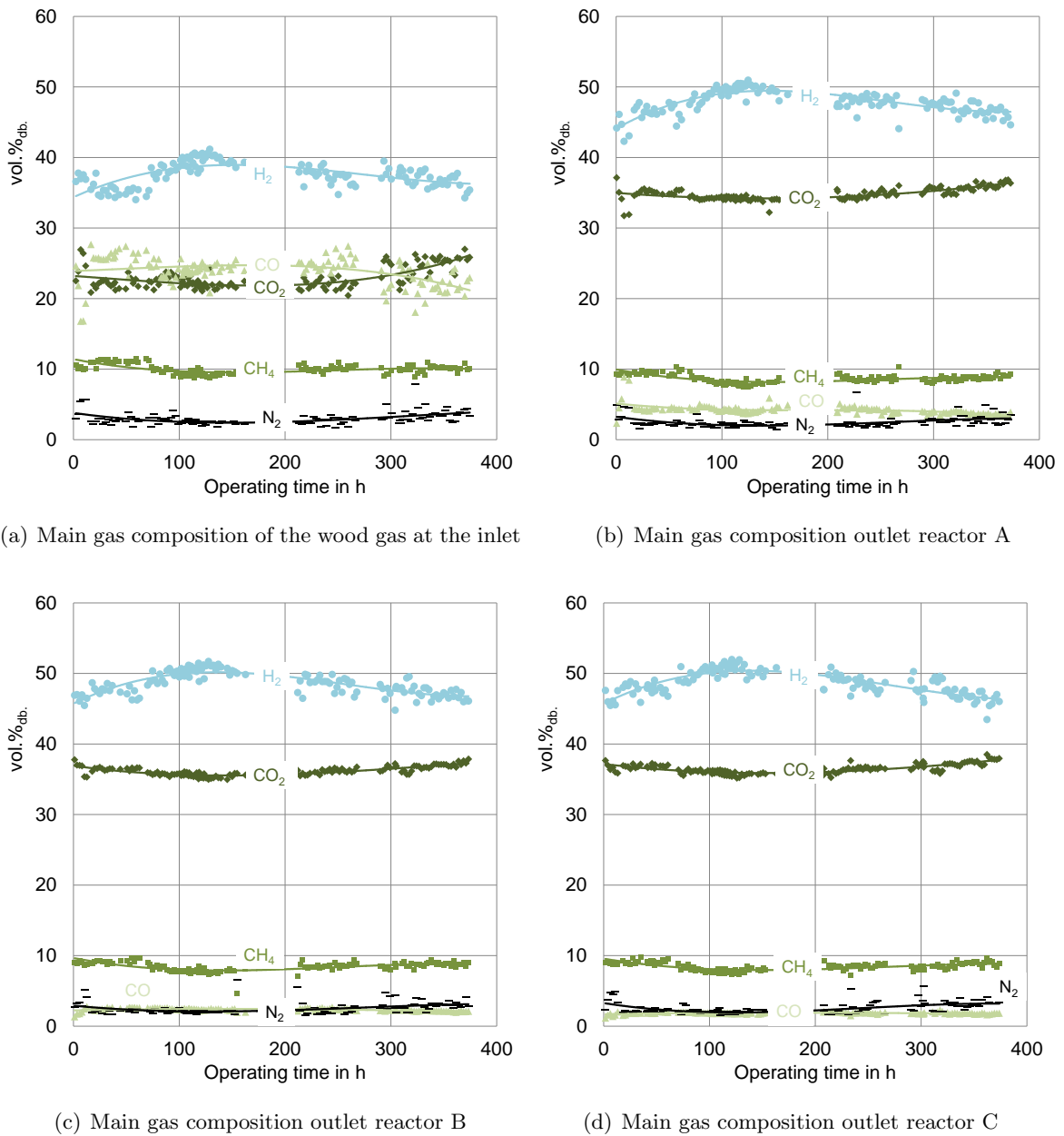


Figure 6.21: Induction period of the Fe/Cr-based catalyst, main gas composition over the operating time.

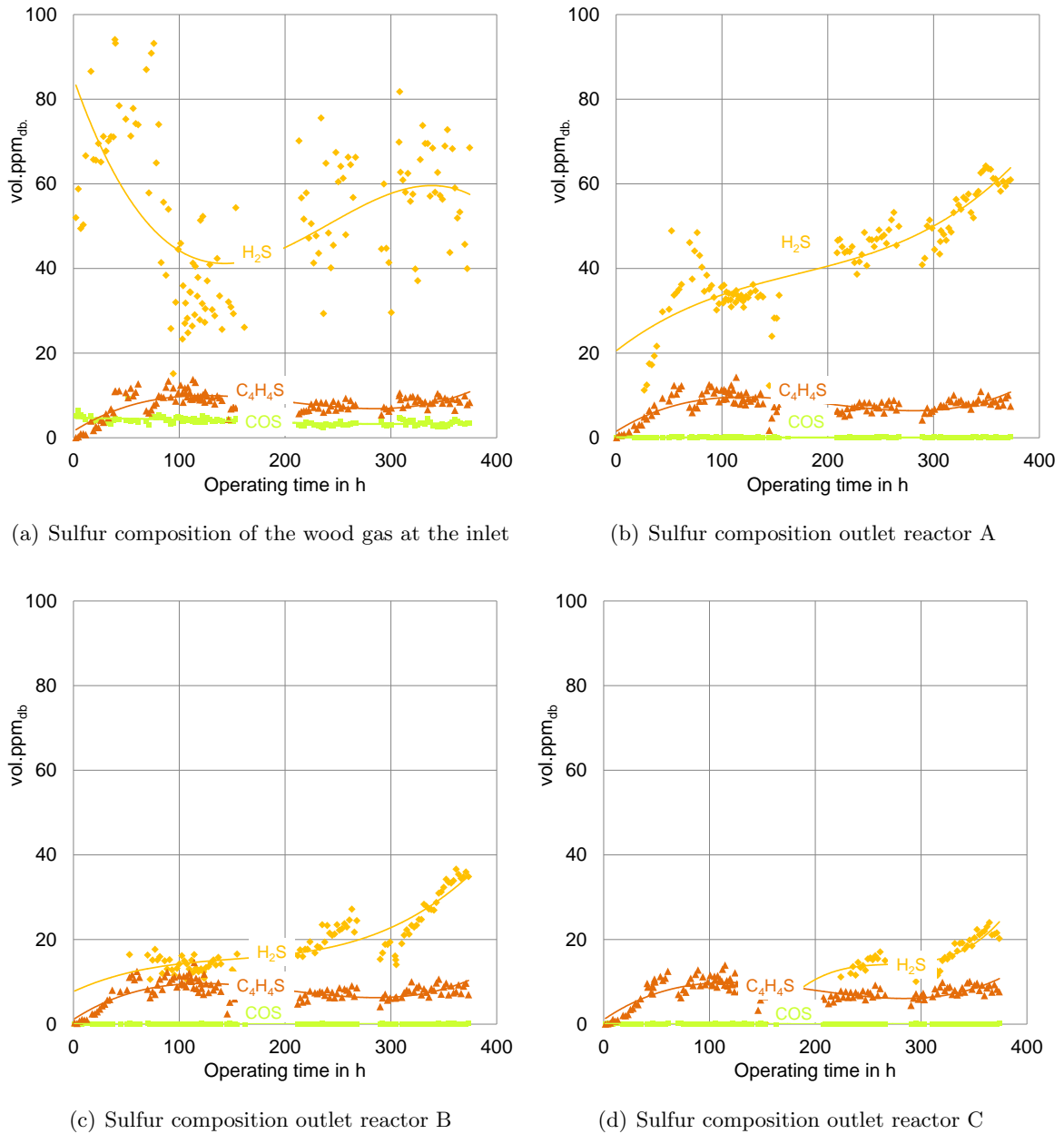


Figure 6.22: Induction period of the Fe/Cr-based catalyst, sulfur composition over the operating time.

Performance of the WGS unit during the operation of process chain 2

The next experiment that was carried out at the WGS unit was the operation of process chain 2. An overall of 3 operation units was operated to produce pure hydrogen based on generated wood gas of the CHP plant Oberwart. Besides the WGS unit, this experiment also involved a gas scrubber, and a PSA unit. At the end of the experimental test run (250 hours of operation), the generated hydrogen was fed into a PEM fuel cell in order to demonstrate the high quality of the generated product. The results of this process chain were summarized in a journal paper [35] which is included in Chapter 7.2 of this work (ACS Journal "Sustainable Chemistry and Engineering", paper accepted on the 13th of October 2014). At this point, only the operation of the WGS unit is summarized in more detail.

The basic operation conditions are summarized in Table 6.14. This process chain was operated for almost 250 hours. During the experiment the GHSV in the WGS unit was very low which provided good conditions for the achievement of a high overall CO conversion rate. Also a temperature profile was set with decreasing inlet temperatures of the reactors in order to harness from more favorable equilibrium conditions of the WGSR at lower temperatures. The trends of temperatures and pressures are illustrated in Figure 6.23. During this experiment, the membrane pump was turned off and the volumetric flow rate over the WGS unit was set by means of the rotation speed of the compressor of the PSA unit. The fluctuations of the temperature profiles were explained by deviations of the overall flow rate. The averaged gas compositions that were analyzed are summarized in Table 6.15. The given sulfur concentrations were detected at the end of the test run. The temperature in the last reactor was set considerably lower than during the induction experiment. Therefore, the sulfur content at the outlet of the WGS unit was very low even though the first two reactors were already equilibrated. The key results are summarized in Table 6.16. An overall CO conversion rate of about 95 % could be reached. The temperature profile of the reactor over the catalyst bed height is illustrated in Figure 6.24. The graph also shows the measured (meas.) gas compositions of the reacting agents which can be compared with their equilibrium (eq.) content with respect to the outlet temperature of each reactor. After the experiment, the optimum temperature (T_{opt}) of reaction was calculated according to Chapter 6.4 and plotted into Figure 6.24. It can be seen that the temperature was generally set too low. Anyway, much higher CO conversions can not be expected from a HT WGS catalyst but the same conversion rates can be achieved at higher GHSV if the temperature is increased.

Achieving full load with cleaned wood gas

The last test run that was carried out at the "Pilot plant for catalytic wood gas processing" aimed at the achievement of the maximum load of the pilot plant. Full load should be reached with both available sampling points of wood gas. The load was basically limited by the capacity of the membrane pump. Also, the heating capacity of the preheating pipe turned out to be limiting if high inlet temperatures of the first reactor were desired. Compared to the extraction point of raw wood gas after filter, a lower steam content was present in the cleaned

Table 6.14: Operation of process chain 2, basic operating conditions of the WGS unit.

Volume Catalyst 2	7.8	<i>L</i>
Water content wood gas	5.13	mol.% _{wb.}
Water content inlet WGSR	56.05	mol.% _{wb.}
Volumetric flow rate dry	0.56	$\frac{m^3}{h}$ _{db.}
Volumetric flow rate wet	1.28	$\frac{m^3}{h}$ _{wb.}
$\frac{H_2O}{CO}$ ratio	5.24	-
Pressure	70–85	<i>mbarg</i>
Temperature profile	460–260	°C
Overall GHSV _{wb.}	164	<i>h</i> ⁻¹

Table 6.15: Operation of process chain 2, averaged gas composition at the inlet and at the outlet of each reactor of the WGS unit.

	CO ₂	C ₂ H ₄	C ₂ H ₆	C ₂ H ₂	O ₂	
Reactor A in	22.7	2.3	0.17	0.15	0.10	vol.% _{db.}
Reactor A out	36.9	1.8	0.17	0.00	0.06	vol.% _{db.}
Reactor B out	37.0	1.8	0.17	0.00	0.08	vol.% _{db.}
Reactor C out	37.1	1.9	0.18	0.00	0.07	vol.% _{db.}
	N ₂	CH ₄	CO	H ₂		
Reactor A in	2.3	10.0	24.0	38.0		vol.% _{db.}
Reactor A out	1.8	8.2	1.9	49.2		vol.% _{db.}
Reactor B out	2.0	8.1	1.3	49.5		vol.% _{db.}
Reactor C out	1.9	8.2	1.0	49.6		vol.% _{db.}
	H ₂ S	COS	C ₄ H ₄ S			
Reactor A in	59	1	7.2			vol.ppm _{db.}
Reactor A out	49	BDL	2			vol.ppm _{db.}
Reactor B out	50	BDL	1			vol.ppm _{db.}
Reactor C out	4	BDL	1			vol.ppm _{db.}

Table 6.16: Operation of process chain 2, key results, operation according to Table 6.14.

	GHSV _{wb.}	$\frac{H_2O}{CO}$	CO vol.% _{db.}	H ₂ O mol.% _{wb.}	Increase $\dot{V}_{db.}$	H ₂ <i>rec</i>	X _{CO}
Reactor A in		5.24	24.0	56.05			
Reactor A out	492	45.35	1.9	46.41	1.22	1.58	90.45
Reactor B out	246	66.77	1.3	45.68	1.24	1.62	93.56
Reactor C out	164	84.73	1.0	45.66	1.25	1.63	94.94

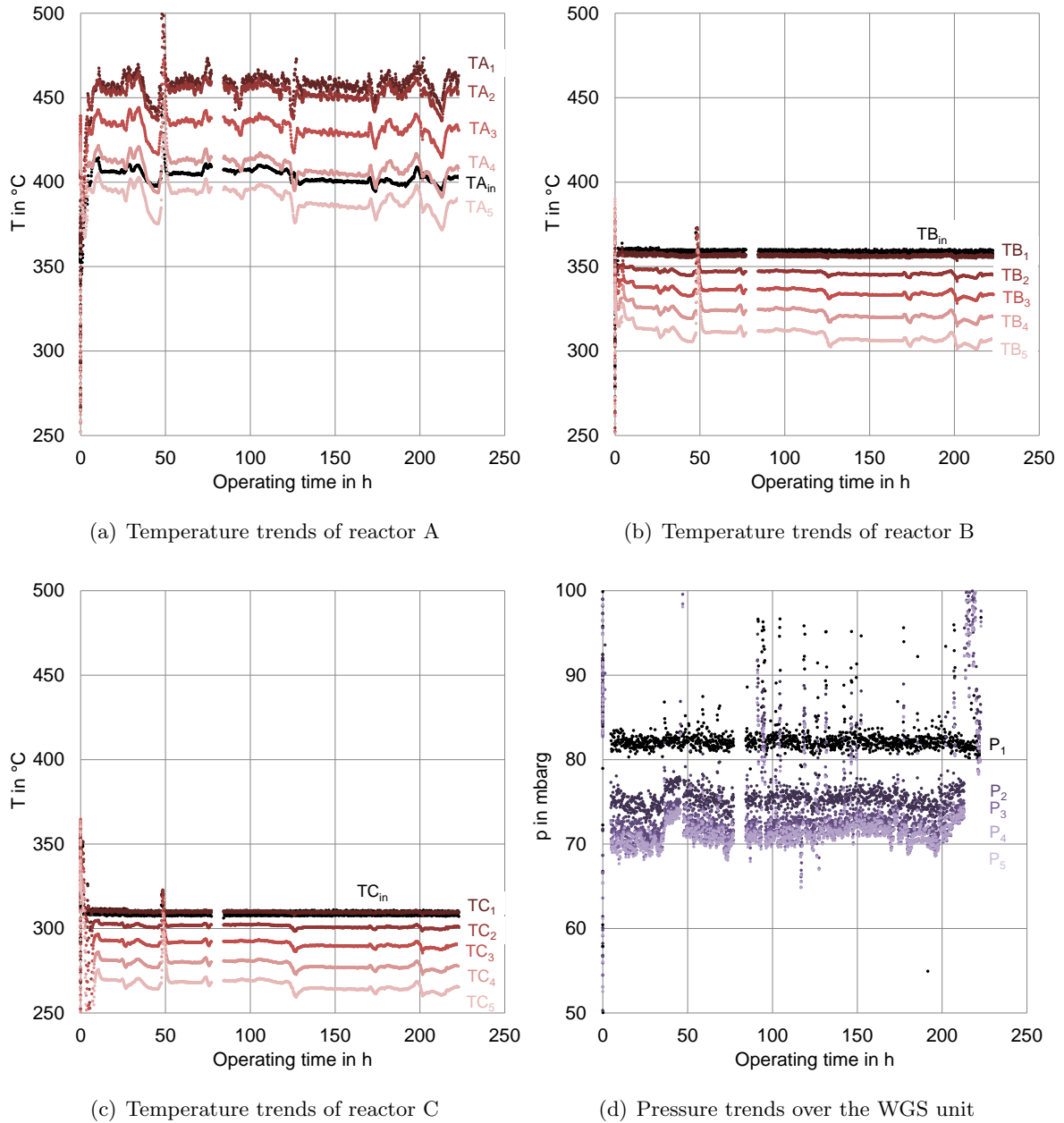


Figure 6.23: Operation of process chain 2, temperature and pressure trends over the WGS unit, operation according to Table 6.14.

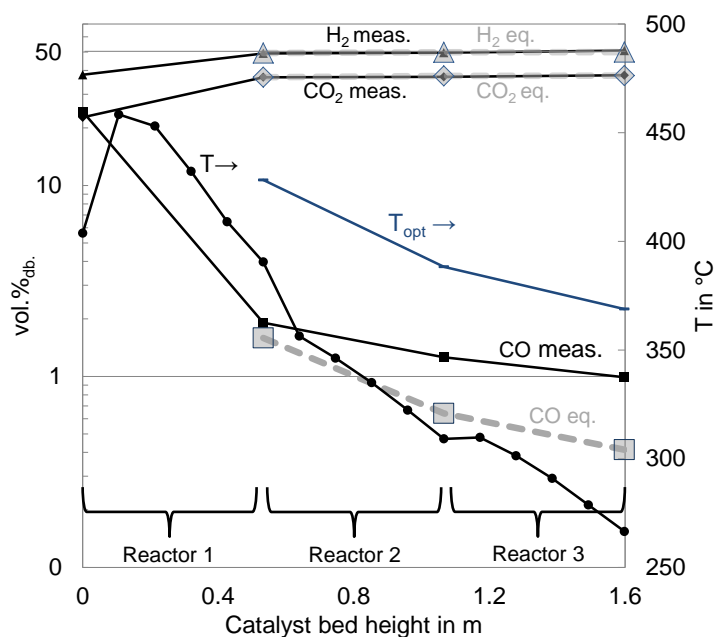


Figure 6.24: Operation of process chain 2, achieved composition and deviation from the equilibrium, optimum temperature to maximize the conversion rate with respect to the measured outlet composition.

wood gas after scrubber. Therefore, a higher dry volumetric flow rate could be achieved with the cleaned gas at the full rotation speed of the membrane pump.

First, the results of the operation with cleaned wood gas extracted after the CHP plant scrubber are presented. The basic operating conditions during this experimentation are summarized in Table 6.17. The given volumetric flow rates were calculated via the "water-spike" method explained in Chapter 5.3.6. This time, the WGS unit was operated at a GHSV which is in the range of operation of an industrial HT-WGS stage (400–1200 h⁻¹ [78]). The temperature trends in each reactor and the pressure trends of the system are illustrated in Figure 6.25. The inlet temperature of the first reactor was set to 400 °C which is rather high compared to the usual inlet temperature of a HT WGS stage (around 350 °C [111]). This was necessary in order to achieve a sufficiently high conversion rate in the first reactor. As a consequence of the exothermic WGS, the temperature in reactor A increased by about 80 °C. The fluctuating temperature profile in the first reactor could be explained by the varying gas composition extracted from the CHP plant Oberwart. The settings of the temperature control of the pilot plant enabled very stable temperature profiles over the operating time. After 2 hours of operation, the setpoint temperature of the inlet of reactor C was increased up to 400 °C. This measure was taken, as it was aimed to approach the operating temperature of the entire system to the optimum temperature for high conversion rates. This approach is described in Chapter 6.4. The higher inlet temperatures required were explained by the high heat losses of the pilot plant, the H₂S content in the gas, and the lower operating pressure than usually applied for "sweet shift" processes. The catalyst producer reports that some activity loss may occur if the catalyst is heated above 540 °C.

With respect to this reference, thermal sintering of the active crystallites was not likely at the present operating temperatures. However, it is reported that thermal stabilization of Fe_3O_4 with Cr_2O_3 is only possible to a limited extent. To maximise the long-term stability of the catalyst, the lowest temperature should be set at the reactor inlet which still enables the design conversion rate [111]. The measured gas compositions are summarized in Table 6.18. No trends of the main gas composition could be observed. The presented sulfur concentrations were measured at the end of the experiment. Due to the rather high temperature in the first reactor, H_2S was desorbed from the catalyst. The sulfur concentration at the exit was approaching the inlet concentration. COS was assumed to be converted according to Equation 3.10. Thiophene was not affected significantly. The effect of the WGS catalyst on the tar components is shown in Table 6.19. Basically, the same effects of Catalyst 2 on the tar composition were already observed during the operation of process chain 2 (these results are shown in Chapter 7.1). Due to the increased GHSV during this experiment, the observed effects in Table 6.19 were less pronounced. Styrene and indene were probably hydrogenated to form ethylbenzene and indane (which was not analyzed). The formation of ethylbenzene could already be proved by means of the BTEX analyses of process chain 2. Furthermore, the results indicate a hydrogenation of phenylacetylene to ethylbenzene as well as a hydrogenation of acenaphthylene to acenaphthene. Generally, it could be assumed that the overall tar load was not affected strongly by the catalyst. The most important and very stable molecules naphthalene (and benzene, see [35]) passed the WGS unit unchanged. The detected concentrations were reduced by about 25 % according to the increased dry gas volumetric flow rate at the outlet of the WGS unit. Exposed double bonds and triple bonds were hydrogenated. The desired effect of a simultaneous tar reforming activity of the Fe/Cr-based catalyst could not be proved. Figure 6.26 shows the temperature profile over the reactors, as well as the achieved gas composition which can be compared with the equilibrium composition with respect to the temperature at the outlet of each reactor. Also the optimum temperature curve is plotted in the graph. The key results of this test run are summarized in Table 6.20. Even at full load of the system, a CO conversion rate of more than 90 % could be reached.

Table 6.17: Catalyst 2: Fe/Cr-based; basic operating conditions for achieving full load with cleaned wood gas after scrubber.

Volume Catalyst 2	7.8	<i>L</i>
Water content	4.9	mol.% _{wb.}
Water content inlet WGSR	53.41	mol.% _{wb.}
Volumetric flow rate dry	1.99	$\frac{m_n^3}{h}$
Volumetric flow rate wet	4.27	$\frac{m_n^3}{h}$
$\frac{\text{H}_2\text{O}}{\text{CO}}$ ratio	4.83	-
Pressure	0–60	<i>mbarg</i>
Temperature profile	490–375	°C
Overall GHSV _{wb.}	547	<i>h</i> ⁻¹

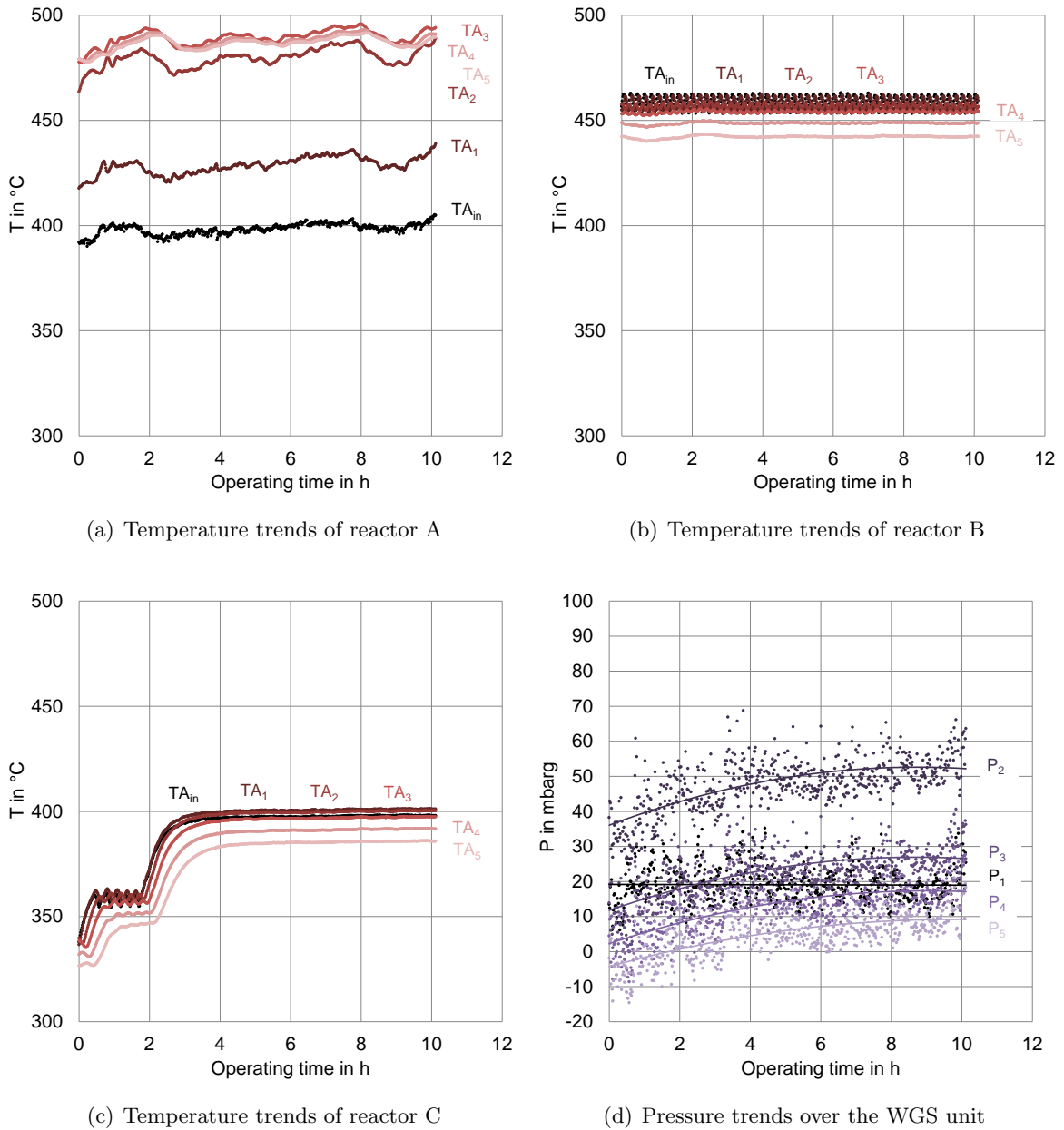


Figure 6.25: Achieving full load of the pilot plant with cleaned wood gas after scrubber, temperature and pressure trends over the WGS unit, operation according to Table 6.17.

Table 6.18: Achieving full load of the pilot plant with cleaned wood gas after scrubber, averaged main gas and sulfur composition at the inlet and after each WGS reactor, Catalyst 2 : Fe/Cr-based, February 2014.

	CO ₂	C ₂ H ₄	C ₂ H ₆	C ₂ H ₂	O ₂	Unit
Reactor A in	22.95	2.41	0.19	0.03	0.10	vol.% _{db.}
Reactor A out	34.55	1.99	0.17	0.00	0.05	vol.% _{db.}
Reactor B out	35.20	1.85	0.18	0.00	0.05	vol.% _{db.}
Reactor C out	36.06	1.87	0.20	0.00	0.07	vol.% _{db.}
	N ₂	CH ₄	CO	H ₂		Unit
Reactor A in	1.97	9.64	23.72	39.00		vol.% _{db.}
Reactor A out	1.52	8.14	4.06	49.52		vol.% _{db.}
Reactor B out	1.85	8.02	2.96	49.90		vol.% _{db.}
Reactor C out	1.70	8.01	1.81	50.29		vol.% _{db.}
	H ₂ S	COS	MeSH	EtSH	C ₄ H ₄ S	Unit
Reactor A in	52.34	1.05	0.0	0.0	9.41	vol.ppm
Reactor A out	63.22	0.14	0.0	0.0	8.51	vol.ppm
Reactor B out	53.41	0.12	0.0	0.0	8.67	vol.ppm
Reactor C out	31.39	0.01	0.0	0.0	7.63	vol.ppm

Table 6.19: Achieving full load of the pilot plant with cleaned wood gas after scrubber, tar analysis at the inlet and at the outlet of the WGS unit, detection limit $1 \frac{\text{mg}}{\text{Nm}^3_{db.}}$.

	Reactor A in	Reactor C out	
Naphthalene	1139	728	$\frac{\text{mg}}{\text{Nm}^3_{db.}}$
Styrene	247	13	$\frac{\text{mg}}{\text{Nm}^3_{db.}}$
Indene	191	53	$\frac{\text{mg}}{\text{Nm}^3_{db.}}$
Phenylacetylene	15	0	$\frac{\text{mg}}{\text{Nm}^3_{db.}}$
Mesitylene	BDL	5	$\frac{\text{mg}}{\text{Nm}^3_{db.}}$
Benzofuran	2	BDL	$\frac{\text{mg}}{\text{Nm}^3_{db.}}$
1-Benzothiophene	2	BDL	$\frac{\text{mg}}{\text{Nm}^3_{db.}}$
2-Methylnaphthalene	5	5	$\frac{\text{mg}}{\text{Nm}^3_{db.}}$
1-Methylnaphthalene	3	3	$\frac{\text{mg}}{\text{Nm}^3_{db.}}$
Biphenyl	1	1	$\frac{\text{mg}}{\text{Nm}^3_{db.}}$
Acenaphthylene	13	1	$\frac{\text{mg}}{\text{Nm}^3_{db.}}$
Acenaphthene	2	8	$\frac{\text{mg}}{\text{Nm}^3_{db.}}$
Anthracene	2	2	$\frac{\text{mg}}{\text{Nm}^3_{db.}}$
Flouranthene	1	2	$\frac{\text{mg}}{\text{Nm}^3_{db.}}$
Pyrene	1	2	$\frac{\text{mg}}{\text{Nm}^3_{db.}}$
Total GC-MS	1635	825	$\frac{\text{mg}}{\text{Nm}^3_{db.}}$
Gravimetric tar	83	100	$\frac{\text{mg}}{\text{Nm}^3_{db.}}$

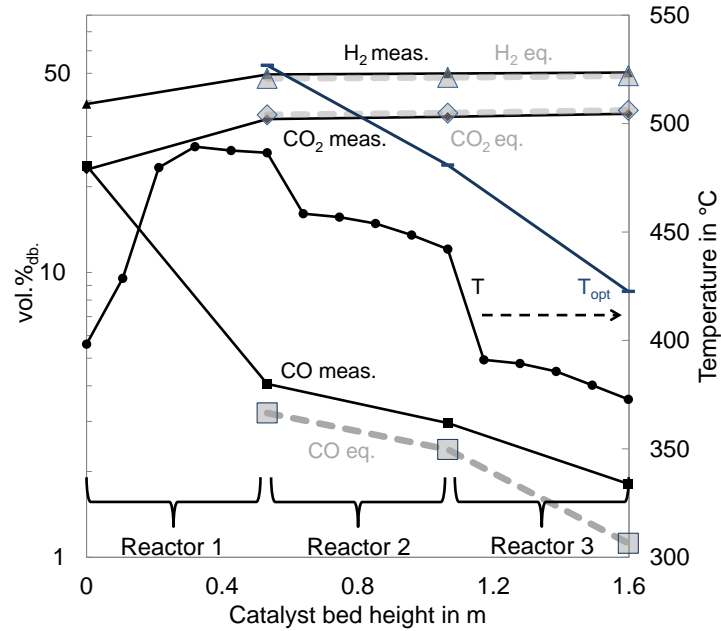


Figure 6.26: Achieving full load with cleaned wood gas after scrubber, average operating temperature over the height of the catalyst bed, achieved composition and deviation from the equilibrium, optimum temperature to maximize the conversion rate with respect to the measured outlet composition.

Table 6.20: Achieving full load with cleaned wood gas after scrubber, key results, operation according to Table 6.17.

	GHSV _{wb.}	$\frac{H_2O}{CO}$	CO vol.% _{db.}	H ₂ O mol.% _{wb.}	Increase $\dot{V}_{db.}$	H _{2 rec}	X _{CO}
Reactor A in		4.83	23.72	53.41	-	-	-
Reactor A out	1643	19.51	4.06	43.69	1.21	1.54	79.30
Reactor B out	821	26.12	2.96	43.03	1.22	1.57	84.74
Reactor C out	547	41.85	1.81	42.58	1.23	1.59	90.62

Achieving full load with raw wood gas

Finally, full load was also set with raw wood gas extracted after the CHP plant filter (before the scrubber). The basic operating conditions are summarized in Table 6.21. The dry volumetric flow rate was lower compared to the operation with dried gas after scrubber. The water addition was reduced but the water content at the inlet was higher compared to the other experiments. The temperature and pressure trends are illustrated in Figure 6.27. The temperature profile was similar to the full load operation with cleaned wood gas. The system was operated at a small underpressure as the wood gas was extracted upstream the wood gas blower of the CHP plant. The obtained gas compositions at the inlet and after each reactor are summarized in Table 6.22. Because of the enhanced steam content and the lower GHSV on a dry basis, lower CO contents could be achieved at the outlet of the system. Finally, the sulfur composition at the inlet was equal to the sulfur composition at the outlet. The results of the tar analysis are summarized in Table 6.23. The measured tar level was higher compared to the operation with cleaned wood gas. However, the same influence of the catalyst on the tar composition could be found. The results indicate that naphthalene was not affected by the catalyst. Tar components with exposed double bondings were hydrogenated.

Table 6.21: Catalyst 2: Fe/Cr-based; basic operating conditions for achieving full load with raw wood gas after filter.

Volume Catalyst 2	7.8	<i>L</i>
Water content	35.1	mol.% _{wb.}
Water content inlet WGSR	66.83	mol.% _{wb.}
Volumetric flow rate dry	1.25	$\frac{m_n^3}{h}$ _{db.}
Volumetric flow rate wet	3.79	$\frac{m_n^3}{h}$ _{wb.}
$\frac{H_2O}{CO}$ ratio	8.56	-
Pressure	-40–10	<i>mbar_g</i>
Temperature profile	490–375	°C
Overall GHSV _{wb.}	486	<i>h</i> ⁻¹

To sum it up, the activity of the Fe/Cr-based catalyst was much higher than the activity of the Co/Mo-based catalyst. This was already indicated during the test runs with synthetic wood gas at the "Test rig for chemical kinetics" and finally proved in long term experiments with real wood gas at the "Pilot plant for catalytic wood gas processing". At the present sulfur content in the wood gas derived from the CHP plant Oberwart (60–100 vol.ppm_{db.}) much higher CO conversion rates (up to 95 %) could be achieved at higher GHSV_{wb} with the Fe/Cr-based catalyst. So far, the catalyst was operated for more than 800 hours and no performance loss could be observed.

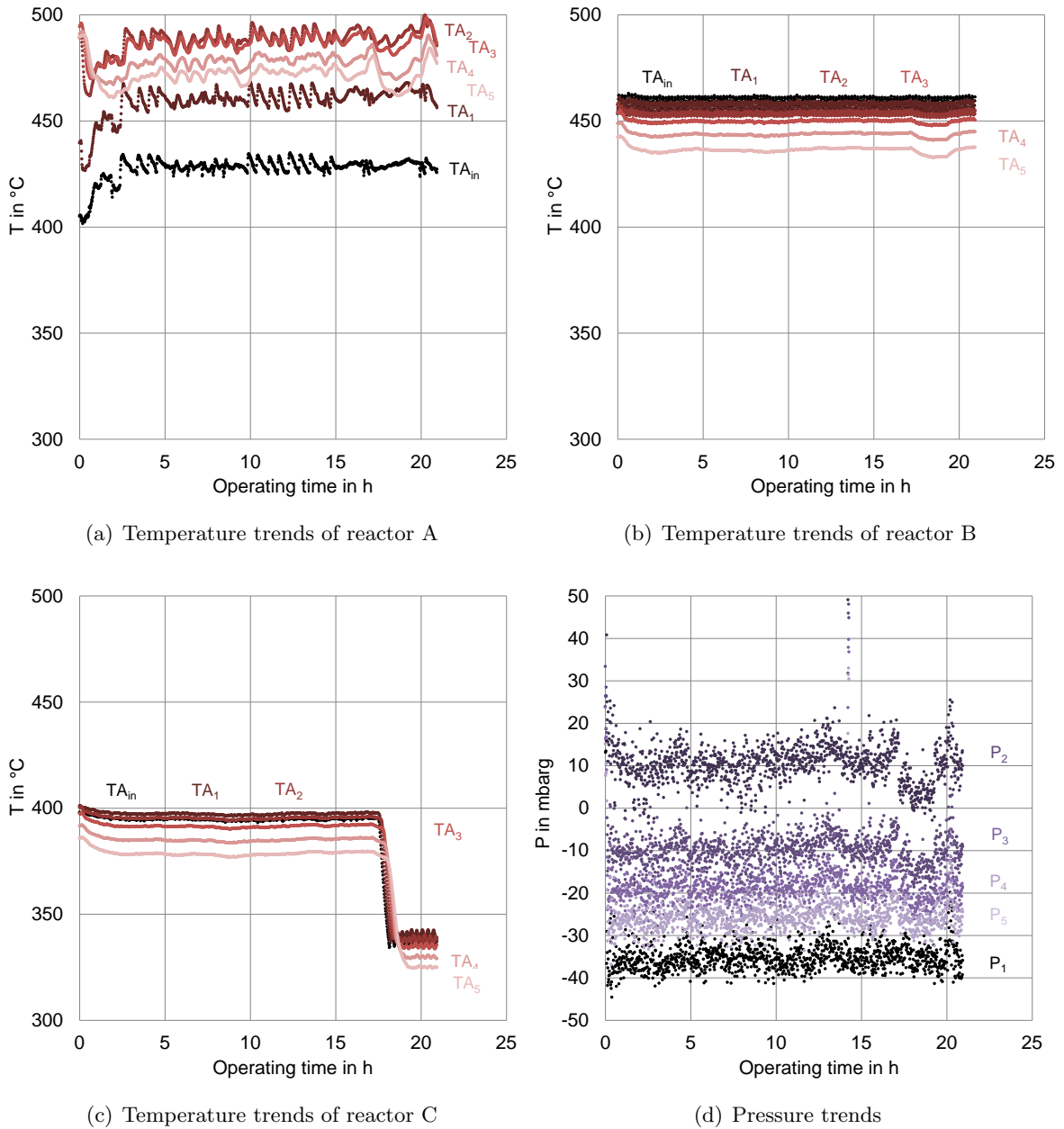


Figure 6.27: Achieving full load of the pilot plant with raw wood gas after filter, temperature and pressure trends over the WGS unit, operation according to Table 6.21.

Table 6.22: Achieving full load of the pilot plant with raw wood gas after filter, averaged main gas and sulfur composition at the inlet and after each WGS reactor, Catalyst 2 : Fe/Cr-based, February 2014.

	CO ₂	C ₂ H ₄	C ₂ H ₆	C ₂ H ₂	O ₂	Unit
Reactor A in	22.69	2.51	0.19	0.03	0.10	vol.% _{db.}
Reactor A out	36.37	2.05	0.17	0.00	0.04	vol.% _{db.}
Reactor B out	36.74	2.02	0.18	0.00	0.04	vol.% _{db.}
Reactor C out	36.91	1.98	0.18	0.00	0.04	vol.% _{db.}
	N ₂	CH ₄	CO	H ₂		Unit
Reactor A in	1.86	9.84	23.92	38.87		vol.% _{db.}
Reactor A out	1.28	8.29	1.75	50.05		vol.% _{db.}
Reactor B out	1.33	8.21	1.30	50.19		vol.% _{db.}
Reactor C out	1.20	8.14	0.91	50.64		vol.% _{db.}
	H ₂ S	COS	MeSH	EtSH	C ₄ H ₄ S	Unit
Reactor A in	55.08	1.3	0.0	0.0	4.95	vol.ppm
Reactor A out	80.27	0.0	0.0	0.0	7.13	vol.ppm
Reactor B out	79.69	0.0	0.0	0.0	6.95	vol.ppm
Reactor C out	53.85	0.0	0.0	0.0	6.77	vol.ppm

Table 6.23: Achieving full load of the pilot plant with raw wood gas after filter, tar analysis at the inlet and at the outlet of the WGS unit, detection limit $1 \frac{\text{mg}}{\text{Nm}^3_{db.}}$.

	Reactor A in	Reactor C out	
Naphthalene	2855	2641	$\frac{\text{mg}}{\text{Nm}^3_{db.}}$
Styrene	202	24	$\frac{\text{mg}}{\text{Nm}^3_{db.}}$
Indene	292	89	$\frac{\text{mg}}{\text{Nm}^3_{db.}}$
Phenylacetylene	32	0	$\frac{\text{mg}}{\text{Nm}^3_{db.}}$
Mesitylene	BDL	7	$\frac{\text{mg}}{\text{Nm}^3_{db.}}$
Benzofuran	BDL	BDL	$\frac{\text{mg}}{\text{Nm}^3_{db.}}$
1-Benzothiophene	6	2	$\frac{\text{mg}}{\text{Nm}^3_{db.}}$
2-Methylnaphthalene	62	47	$\frac{\text{mg}}{\text{Nm}^3_{db.}}$
1-Methylnaphthalene	40	55	$\frac{\text{mg}}{\text{Nm}^3_{db.}}$
Biphenyl	41	35	$\frac{\text{mg}}{\text{Nm}^3_{db.}}$
Acenaphthylene	383	11	$\frac{\text{mg}}{\text{Nm}^3_{db.}}$
Acenaphthene	32	206	$\frac{\text{mg}}{\text{Nm}^3_{db.}}$
Anthracene	60	43	$\frac{\text{mg}}{\text{Nm}^3_{db.}}$
Flouranthene	6	5	$\frac{\text{mg}}{\text{Nm}^3_{db.}}$
Pyrene	6	5	$\frac{\text{mg}}{\text{Nm}^3_{db.}}$
Dibenzofuran	14	7	$\frac{\text{mg}}{\text{Nm}^3_{db.}}$
Fluorene	31	22	$\frac{\text{mg}}{\text{Nm}^3_{db.}}$
Total GC-MS	4073	3203	$\frac{\text{mg}}{\text{Nm}^3_{db.}}$
Gravimetric tar	150	130	$\frac{\text{mg}}{\text{Nm}^3_{db.}}$

Table 6.24: Achieving full load with raw wood gas after filter, key results, operation according to Table 6.21.

	GHSV _{wb.}	$\frac{H_2O}{CO}$	CO vol.% _{db.}	H ₂ O mol.% _{wb.}	Increase $\dot{V}_{db.}$	H ₂ <i>rec</i>	X _{CO}
Reactor A in		8.56	23.92	66.83			
Reactor A out	1459	84.51	1.75	59.45	1.24	1.59	90.95
Reactor B out	729	113.30	1.30	59.36	1.24	1.60	93.27
Reactor C out	486	160.03	0.91	59.13	1.25	1.62	95.25

6.4 Optimum temperature for the catalysis of the WGSR

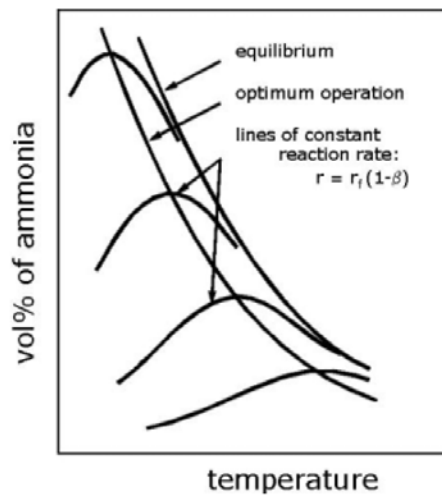
At low temperatures, the conversion of CO according to the WGSR is limited kinetically. At high temperatures, the conversion rate is limited by means of unfavorable equilibrium conditions of the WGSR. Also, the heat release of the exothermic WGSR leads to higher equilibrium partial pressures of CO (see Figure 3.7). These considerations result in a compromise for the operating temperature. It is desirable to operate the reactor at as low a temperature as possible while keeping the rate as high as possible. In the course of this thesis the question arose, which temperature has to be adjusted at the inlet of one WGS reactor in order to maximise the conversion rate per volume of catalyst. The solution was inspired from the synthesis of ammonia, which is also an exothermic reaction with an enthalpy of reaction in the same order of magnitude as the WGSR. In ammonia plants, the optimum temperature is calculated by means of the "Concept of optimal operating line" which is also called the "Concept of maximal rate line" [23]. The mathematical procedure to obtain this operating line, is described well in [76]. Generally, this concept has to be based on kinetic data of the applied catalyst, an initial gas composition, and equilibrium data of the investigated reaction.

Within this work, the reaction rate of the WGSR was described with the general power law rate model $r = k p_{CO}^a p_{H_2O}^b p_{CO_2}^c p_{H_2}^d (1 - \beta)$ which was already presented in Equation 3.46 (also Equations 3.47 and 3.48). The activation energies, the pre-exponential factors, and the apparent activation orders for both catalysts had already been estimated at the "Test rig for chemical kinetics" (Equation 6.2 and 6.7). The equilibrium constant K_p of the WGSR was calculated by means of Equation 3.49.

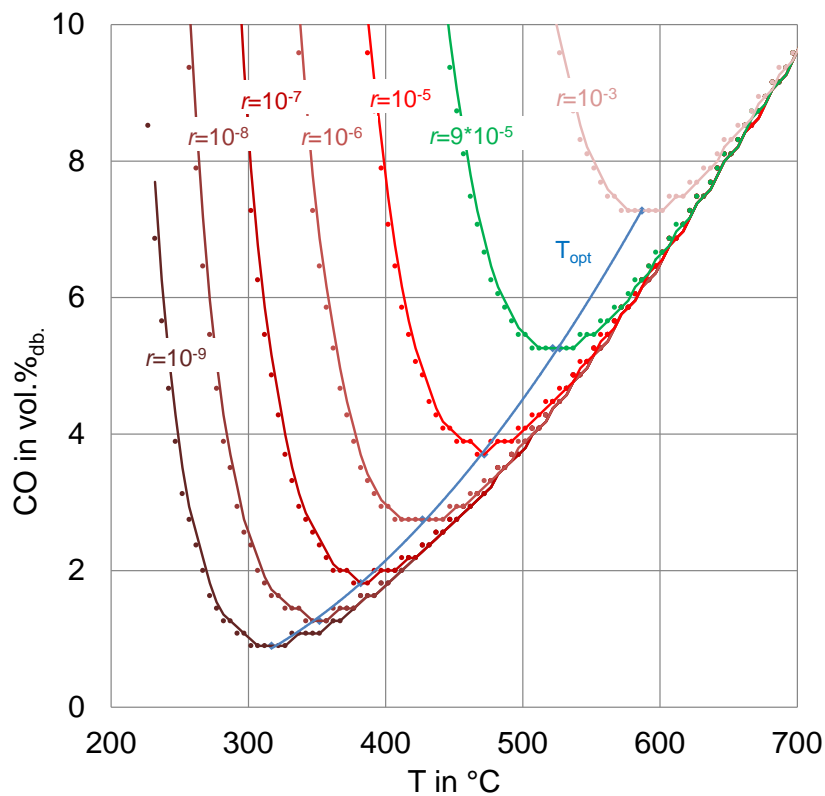
Based on these equations and the inlet gas composition in Oberwart, a mathematical model was created using the software MATLAB[®] in order to predict the optimum temperature of reaction with respect to the present gas composition. Fictitious values were set for the reaction rate $r_{wt.}$ (in $\frac{mol}{g_{cat} \cdot h}$). The concentration of one component (for example CO) was changed in defined intervals, which caused a corresponding change of the concentration of the other reacting agents (here: H₂, H₂O, and CO₂) according to the WGSR. For a given reaction rate, the corresponding temperature was calculated over the change of the gas composition. For a series of fictitious reaction rates, the generated lines of constant reaction rates $r_{wt.}$ were plotted into the graph. All lines converged at the equilibrium of the WGSR. The left wing of the lines was determined by the kinetics of the reaction (Arrhenius term). The right wing of the curves was determined by the term β which included the equilibrium constant K_p .

The optimum operating line with respect to the current concentration of CO went through the minimum of all of these curves. In accordance to the synthesis of ammonia (Figure 6.28 (a) from [23]), the optimum operation line was also found to run parallel to the equilibrium curve, shifted 20–40 °C toward lower temperatures.

Experimentally, this procedure of the optimum operation line was used for some selected experiments at the "Pilot plant for catalytic wood gas processing" using the Fe/Cr-based catalyst (see Figure 6.24 and Figure 6.26). At the very inlet of the catalysis, it was favorable to adjust very high operating temperatures. However, the temperature will increase further because of the exothermic WGSR and the maximum temperature of the catalyst has to be considered. Also, if the specified maximum temperature of the catalyst is not reached, the long term stability of the catalyst might be affected due to sintering of catalyst particles. With respect to the long-term catalyst stability, the temperature of reaction should be adjusted as low as possible [111]. Therefore, the inlet temperature of the first reactor at the WGS unit was usually not set higher than 400 °C. At the outlet of the first reactor the CO concentration was measured. This CO concentration could be plotted into Figure 6.28 and the optimum inlet temperature of the second reactor could be read. Analogous, the optimum inlet temperature could be estimated for the third reactor.



(a) Optimum operating temperature approach for the synthesis of ammonia; from [23].



(b) Optimum operating temperature of the Fe/Cr-based catalyst with respect to the current CO concentration (inlet gas composition from Table 6.17 and 6.18).

Figure 6.28: "Concept of optimal operating line"; (a): motivation from the literature [23] ; (b): result from this thesis, this plot was basically used for the estimation of the optimum reaction temperature in Figure 6.24 and Figure 6.26.

Chapter 7

Process chains for biohydrogen production

Few experimental data can be found in literature regarding the production of pure hydrogen based on wood gasification. In 2008, Corella et al. [25] investigated a process consisting of the fluidized bed gasification of wood chips, steam reforming with a commercial Ni-based catalyst, and catalysis of the WGSR ("sweet shift") using a commercial HT- and a commercial LT-shift catalyst. In the generated gas mixture a hydrogen content up to 73 vol.% could be reached which represented a hydrogen yield of $140 \frac{g}{kg_{wood,d.a.f.}}$ (d.a.f. dry ash free). Regarding the catalysis of the WGSR, a CO conversion rate of 90 % could be reached at GHSV of 1300–2700 h⁻¹ for the HT catalyst and 4600–5100 h⁻¹ for the LT catalyst. However, the given data are short term results and the deactivation of the catalysts due to sulfur components is not discussed.

In cooperation with other research projects, two different process chains for BioH₂ production were realized within this PhD thesis. Both process chains demonstrated the generation of pure hydrogen based on wood gas derived from the biomass gasification power plant in Oberwart. In both cases, the "Pilot plant for catalytic wood gas processing" (or WGS unit) was used as initial step for wood gas processing.

The first process chain was operated for about 100 hours using Catalyst 1 (Co/Mo-based) in the WGS unit. The results of this process chain 1 were published in a conference paper [36] which is subsequently included in Chapter 7.1.

The second process chain was operated for about 250 hours using Catalyst 2 (Fe/Cr-based) in the WGS unit. The results of this process chain 2 were published in a conference paper [35] which is later included in Chapter 7.2. The process chain 2 was also described in more detail in a Master thesis that was carried out at the Institute of Chemical Engineering (Vienna University of Technology) [14]. Energetically, this experimental setup was evaluated in another Master thesis also suggesting further improvements of the existing process [48].

7.1 Process chain 1: WGSR - Gas scrubbing - Membrane separation - Pressure swing adsorption

The first process chain to be presented included the operation of the WGS unit with Catalyst 1, gas cleaning and drying in a LT RME scrubber, hydrogen enrichment by means of a membrane separation unit, and hydrogen purification via pressure swing adsorption.

An Experimental Approach for the Production of Pure Hydrogen Based on Wood Gasification

S. Fail¹ and N. Diaz^{1,2}, D. Konlechner¹, M. Hackel³, E. Sanders⁴, R. Rauch^{1,2}, M. Harasek¹, K. Bosch⁵, F. Schwenninger⁵, P. Zapletal⁶, Z. Schee⁶ and H. Hofbauer^{1,2}.

1. Vienna University of Technology, Institute of Chemical Engineering, Vienna, Austria.
 2. Bioenergy 2020+ GmbH, Güssing, Austria.
 3. AIR LIQUIDE™ Forschung und Entwicklung GmbH, Frankfurt Research and Technology Center(FRTC), Germany.
 4. AIR LIQUIDE™ America, Delaware Research and Technology Center (DRTC), USA.
 5. Energie Burgenland AG. , Eisenstadt, Austria.
 6. Technical University of Ostrava, Department of Power Engineering, ENET, Ostrava, Czech Republic.
-

Abstract

In this experimental work, a unique process chain for hydrogen production based on biomass gasification has been investigated. For almost 100 hours, a pilot plant was operated continuously with 2 Nm³/h of dry product gas, derived from dual fluidized bed steam gasification at the combined heat and power plant in Oberwart, Austria. The implemented process chain consisted of four operation units: (1) sulfur resistant catalysis of the water gas shift reaction, (2) gas drying and cleaning in a chilled rapeseed methyl ester scrubber, (3) hydrogen enrichment via membrane separation and (4) generation of pure hydrogen by means of pressure swing adsorption. High hydrogen yields of all operational units were achieved, resulting in an overall hydrogen recovery of almost 70% (42g/kg dry biomass). The purity of hydrogen was above 99.85%vol.

1. Introduction

More than 100 million Nm³/h of hydrogen are currently produced worldwide. By far the most important application of hydrogen is the production of ammonia (50%), followed by various applications in refineries (22%) and the synthesis of methanol (14%) [1]. 96% of this hydrogen production is directly based on fossil fuels, 49% are derived from natural gas, 29% from liquid hydrocarbons and 18% from coal. The remaining 4% are generated as a by-product from electrolysis and other processes [2]. Large scale production of hydrogen is usually achieved by means of thermochemical oxidative processing of the mentioned fossil fuels. The most important industrial process for hydrogen production is steam reforming of hydrocarbons, especially methane. Besides, catalytic partial oxidation of hydrocarbons and coal gasification are

carried out for the generation of hydrogen rich gases [3, 4].

Since the invention of the Haber-Bosch process the hydrogen demand for ammonia production has been rising continuously [5]. Also the consumption of hydrogen in refineries is increasing, as heavy crudes are making up a steadily increasing proportion in refineries. This leads to a reduction of internally produced hydrogen required for hydroprocessing techniques. Finally, upcoming processing of oil sands, gas-to-liquid approaches and the synthesis of liquid hydrocarbons based on coal gasification increase the hydrogen demand in refineries [2].

The growing hydrogen demand, the dependency on fossil fuels with limited long-term availability, considerable amounts of greenhouse gas emissions due to hydrogen production, as well as the ongoing discussion about the replacement of fossil fuels by “green” hydrogen led to

numerous research activities aiming for a renewable production of hydrogen. These approaches can broadly be divided into electrochemical approaches, biological processes and thermochemical conversion of biomass (gasification or pyrolysis) [6, 4, 7]. This article addresses the production of H₂ via thermal biomass gasification.

The established routes for hydrogen production based on coal gasification cannot be applied directly for hydrogen production based on biomass gasification. From an economic point of view it is very difficult to predict the availability and the price of biomass for future energy production [8]. From a technological view, different structures and another chemical composition of biomass in contrast to coal have to be faced. This also results in a different composition of gasified biomass and gasified coal [9]. Anyway, coal or biomass gasification is assumed to be the cheapest way of hydrogen generation when natural gas prices are high [3, 7]. A promising technology for hydrogen production from aqueous biomass suspensions is gasification in supercritical water [10, 11]. For solid biomass however, the dual fluidized bed (DFB) steam gasification seems to be an appropriate technology, generating a high calorific gas mixture poor in nitrogen. In the following this gas mixture is referred to as product gas, whereas in literature it is also named synthesis gas or syngas. Especially when applying the sorption enhanced reforming (SER) concept, a hydrogen-rich product gas can be produced [12, 13, 14].

Pure hydrogen based on biomass gasification can only be obtained by means of further processing of the

product gas. Different configurations for hydrogen production based on biomass gasification are suggested in literature [15, 16, 17]. Most of the reported work on biomass based hydrogen production is process evaluation by means of simulation. Little experimental data of a complete process chain can be found in the open literature.

In this work, the process chain in Figure 1 is suggested for hydrogen production based on biomass gasification. Regarding an upscale of this experimental approach, this configuration should be considered as a polygeneration concept, aiming the simultaneous production of hydrogen, electricity and district heat. It is not the main purpose to maximize hydrogen yields per biomass input, but to achieve high overall efficiencies and thus economic benefits.

The process chain involves:

(1) CO conversion via sulfur resistant catalysis of the water gas shift (WGS) reaction;

(2) Gas drying and cleaning in a chilled rapeseed methyl ester (RME) scrubber;

(3) Hydrogen enrichment via membrane separation and

(4) Final generation of pure hydrogen by means of pressure swing adsorption (PSA).

(1) Prior to the application of gas cleaning and gas separation techniques, the catalysis of the water gas shift (WGS) reaction (a) was applied in order to produce additional H₂ from the conversion of CO.

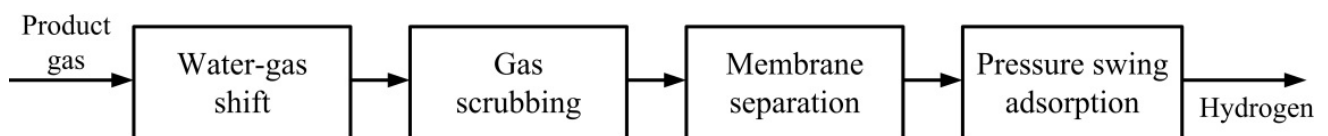
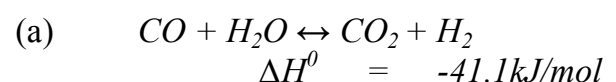


Figure 1: implemented process chain for the production of pure hydrogen starting from product gas based on DFB steam gasification of wood chips.

The surplus of hydrogen was also thought to increase the efficiencies of the subsequent operation units, resulting in higher overall hydrogen yields. Especially, an enhanced efficiency of the pressure swing adsorption unit was expected, as the adsorption of carbon monoxide on activated charcoal is inferior to the adsorption of carbon dioxide [18]. Catalysis of the WGS-reaction is a well-established key technology in industrial hydrogen production based on steam reforming of hydrocarbons. It is normally carried out in a two stage system with a desulfurized feed. A high temperature (HT) stage employing a $\text{Fe}_2\text{O}_3/\text{Cr}_2\text{O}_3$ based catalyst is usually followed by a low temperature (LT) stage with a Cu/Zn based catalyst. Especially the applied catalysts for LT catalysis are vulnerable to sulfur poisoning [19, 20]. At low temperatures the reaction rates diminish and the reaction becomes kinetically controlled [3]. As organic and inorganic sulfur components are present in the biomass-derived product gas, a CoO/MoO₃ based catalyst has been chosen for the suggested process chain in Figure 1. These catalysts require sulfur to be present in the product gas and are resistant to sulfur poisoning. For activation a sulphidation of the catalyst has to be performed in order to create MoS₂ as an active species. During sulphidation, also Co₉S₈ crystallites are formed which are said to act as promotor for the MoS₂ [21].

(2) Product gas from biomass gasification contains NH₃, H₂S and high molecular weight organic compounds (tars) which must be removed prior to further gas utilization. A highly effective approach toward the removal of tars is absorption in organic solvents. As a secondary effect, condensation of water takes place in the scrubber, allowing the removal of water-soluble gaseous trace components such as NH₃ and H₂S from

the gas stream. Both Austrian DFB gasification power plants (Güssing and Oberwart) employ gas scrubbing in rapeseed methyl ester (RME) prior to gas utilization in gas engines. Lowering the scrubbing temperature and increasing the amount of fresh solvent enhances the separation efficiency for tars with low boiling point, NH₃ and H₂S [22, 23, 24], respectively.

(3) Membranes are barriers which, by their physical nature, enable components to permeate selectively across them. For polymer membranes, gas separation is explained via a solution-diffusion mechanism. Separation is a product of solubility and mobility through a solid barrier [25]. Polymer membrane technology is a commercially viable separation process and especially efficient for the separation of CO₂, CH₄ (natural gas sweetening, biogas upgrading, and enhanced oil recovery [26]) and for hydrogen separation from gaseous mixtures consisting of nitrogen, carbon monoxide, or hydrocarbons [25]. It is also used for N₂ generation from compressed air. Providing an operation with a suitable feed composition on an appropriate scale, membrane-related processes are a promising technology for the production of high-purity hydrogen [25]. In the context of this work, a membrane was implemented to increase the efficiency of the subsequent PSA unit.

(4) The PSA process is based on physical binding of gas molecules to an adsorbent material. The forces acting between the gas molecules and the adsorbent material depend on the gas component, type of adsorbent material, partial pressure of the gas component and operating temperature. Highly volatile components with low polarity, such as hydrogen, are practically non-adsorbable in contrast to CO, CO₂, hydrocarbons and water vapor. Consequently, these impurities can be adsorbed from a

hydrogen-containing stream and high purity hydrogen is recovered [27]. Major commercial PSA processes include H₂ and CO₂ recovery, air separation, landfill gas separation and separation of hydrocarbons. The largest PSA processes are generally found in petroleum refineries. In a typical hydrogen purification process the product purity is commonly 99.995%vol. or higher [27].

The presented process chain was operated with real product gas from the commercial biomass steam gasification process in Oberwart, Austria (Figure 2). The equipment was placed in laboratory containers next to this combined heat and power (CHP) plant. The design of the CHP plant is based on the well documented biomass gasification plant in Güssing, Austria [28]. It is the second commercial plant implementing the innovative dual fluidized bed (DFB) steam gasification technology, proved first of its kind in Güssing, Austria. In both plants a high calorific gas mixture poor in nitrogen is produced, which is cleaned by means of filters and scrubbers and subsequently burned in gas engines

generating electricity and district heat. In comparison to Güssing, several modifications have been implemented in Oberwart. The main differences are an installed biomass dryer and an organic rankine cycle (ORC) process in order to increase the electric efficiency. Generally, these modifications follow the suggestions for improvement given in the final report of the “Big power” project [29]. Only few publications dealing with the CHP plant in Oberwart can be found in literature [30, 31, 32].

Starting from the chilled gas scrubber, a simplified configuration of the process chain in Figure 1 has already been operated for more than 1000 hours. This process will be subject to future publications. The scope of this 100 hours lasting experiment was to study the influence of a preliminary WGS unit on the overall performance of the process chain. The project also disposes of a 2.5kW Mobixane[®] fuel cell from AXANE[™]. The investigation of this fuel cell will also be subject to future publication.

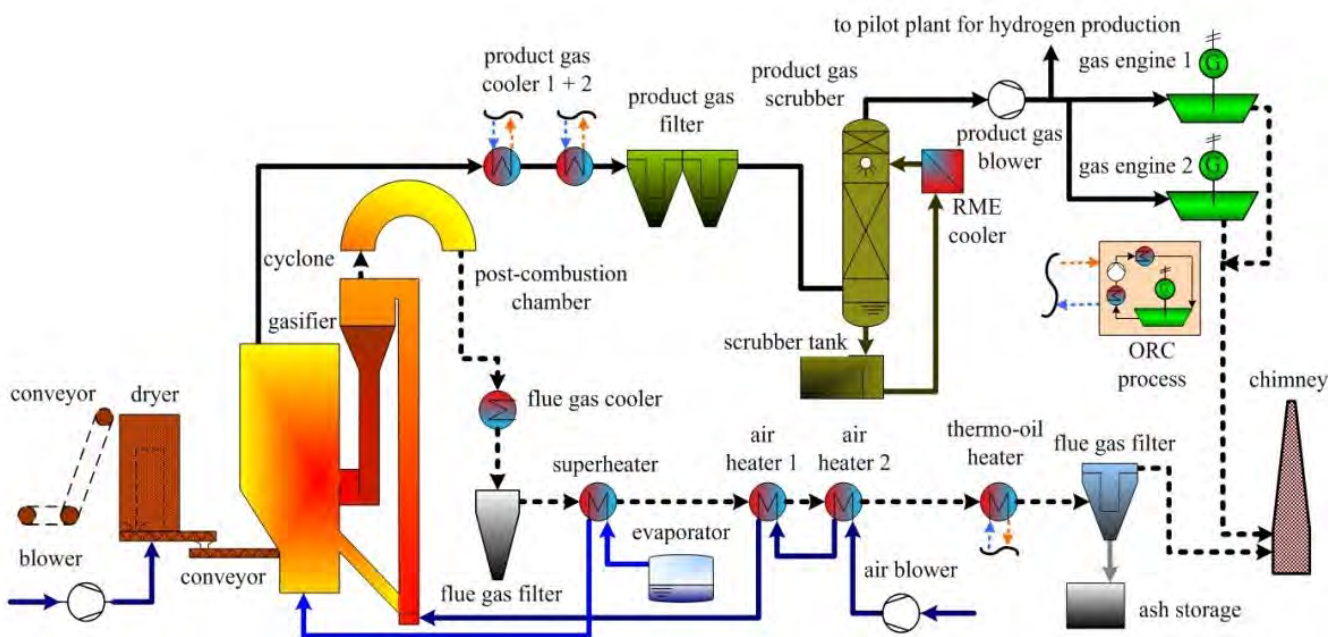


Figure 2: design of the combined heat and power plant in Oberwart (Austria), the process is based on dual fluidized bed steam gasification of biomass.

2. Concept and methodology

The product gas fed into the pilot plant was extracted after gas cleaning of the CHP plant Oberwart [31]. On the one hand, particles have been removed in industrial baghouse filters. On the other hand, the majority of heavy tars present in the product gas have been separated in a gas scrubber [22, 23]. Also, it can be considered that the product gas exits the RME-scrubber with an equilibrium humidity corresponding to its temperature and pressure at the outlet [24]. During experimentation, product gas left the RME scrubber of the CHP plant with a temperature of about 44°C, resulting in an average water content of 10%wt. in the product gas being fed into the pilot plant. With approximately 40% H₂, 24% CO, 21% CO₂ and 10% CH₄ the dry gas composition was typical for DFB biomass steam gasification. The detailed composition can be found in Table 6. Figure 3 presents an extended flow chart of the studied process chain described first in Figure 1. In terms of a

polygeneration concept, the side streams produced in the membrane permeation unit (retentate) and in the PSA unit (adsorbate) were fed back into the CHP plant. After analysis, also the PSA raffinate, composed of almost pure hydrogen, was recycled to the power plant.

2.1. WGS unit

High temperature WGS catalysis at about 375°C has been realized in three fixed bed reactors. A commercial CoO/MoO₃ based catalyst was implemented. Prior to product gas admission, the catalyst was activated by sulphidation.

The product gas was extracted from the power plant with a heated and flow controlled membrane pump (Figure 3). Before entering the catalyst bed, steam had to be added to enhance the water gas shift reaction and to prevent coking at the surface of the catalyst [33, 34]. Therefore, a peristaltic pump was used to feed water into an evaporator generating process steam. The flow rate of water could be

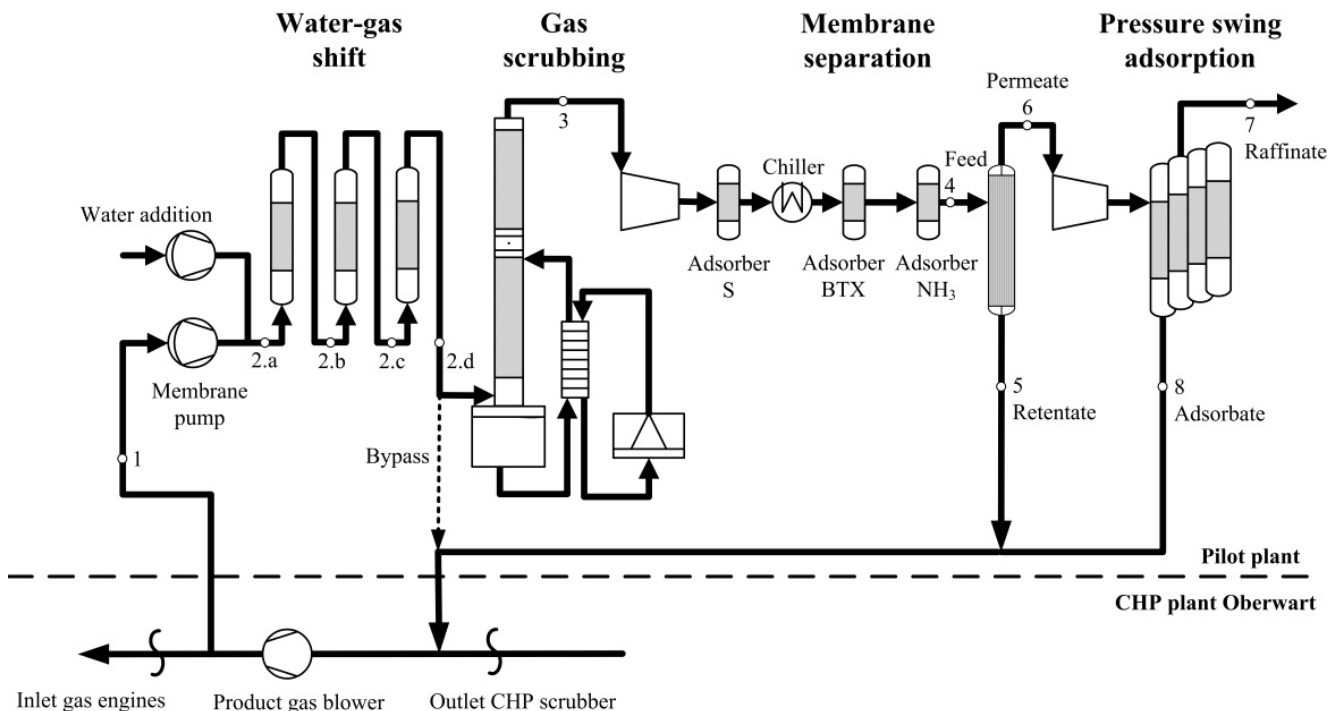


Figure 3: flow chart of the applied process chain for hydrogen production based on wood gasification, the test rigs have been operated with about 2Nm³/h of dry product gas from the CHP plant Oberwart, Austria.

adjusted by rotation speed control. A flow meter was used to control the actual flow rate of added water. Subsequently, the steam loaded gas was heated up to the desired reaction temperature and introduced into the three fixed bed reactors connected in series. Process control was achieved by several thermocouples and pressure sensors distributed over the system. Catalyst temperature inside the reactors was monitored every 10cm along the fixed bed. Gas hourly space velocity (GHSV) and the steam to carbon monoxide ratio (S/CO) were adjusted by choosing an appropriate combination of rotation speeds of both pumps.

The GHSV over the catalyst could be calculated according to a water balance over the WGS unit. The water content at the inlet was measured gravimetrically (condensation of water in cooled impinger bottles filled with glycol and subsequent quantification of dry gas in a gas meter) and was also validated by calculating the equilibrium steam content of the product gas at the outlet of the CHP scrubber. The water content at the outlet of the WGS reactors was measured gravimetrically, allowing a closure of the water balance and the total molar balance over this unit.

Table 1 provides the reaction conditions of the WGS unit.

Table 1: Operation conditions of the WGS unit.

WGS unit	Value	Units
Flow rate wet gas	4.6 ± 0.2	Nm ³ /h
GHSV wet basis	565 ± 20	h ⁻¹
Water content inlet	58 ± 2	% mol.
H ₂ O/CO	6 ± 0.4	-
Pressure	100 ± 25	mbar(g)
Temp. reactor 1	385 ± 17	°C
Temp. reactor 2	385 ± 7	°C
Temp. reactor 3	330 ± 6	°C

The CO conversion rate (X_{CO}) defined in equation (b) was used as a characteristic factor for the evaluation of the performance of the WGS catalysis.

$$(b) \quad X_{CO} = \frac{\dot{n}_{CO\ in} - \dot{n}_{CO\ out}}{\dot{n}_{CO\ in}}$$

2.2. Scrubber unit

The water gas (WG) shifted gas subsequently entered a cleaning and cooling stage. A chilled gas scrubber operated with rapeseed methyl ester (RME) was employed for gas drying and absorption of tars and ammonia from the gas stream. This gas scrubber was operated at lower temperatures than the RME scrubber from the CHP plant Oberwart. A countercurrent flow of the gaseous and liquid phase over a structured packed column (Sulzer Mellapak[®]) has been implemented, cooling down the gas stream and therefore condensing the majority of the process water. The flow of RME was arranged in a circuit. A centrifugal pump continuously charged the packed column with cooled RME. Cooling of RME was achieved in an external plate heat exchanger. Ethylene glycol was used as coolant liquid, which in turn was cooled in an external chiller (HAAKE Phoenix II C41P). For safety reasons, the chilled RME scrubber was connected in bypass processing only a partial flow of the WG shifted gas (Figure 3, Table 1, Table 2). Table 2 summarizes the steady state operation conditions of the chilled gas scrubber.

Table 2: Operation conditions of the chilled RME scrubber.

Scrubber unit	Value	Units
Flow rate (dry)	0.97 ± 0.01	Nm ³ /h
Temp. gas inlet	67 ± 1	°C
Temp. gas outlet	21 ± 1	°C
Mean pressure	35 ± 4	mbar(g)
RME circulation	700	L/h
Fresh RME input	1.5	L/h

2.3. Membrane permeation unit

After preliminary evaluation of three different membranes, a polymer based membrane module from Air Liquide™ was chosen for further enrichment of hydrogen in the gas mixture.

Entering the membrane unit, the pre-dried feed from the chilled RME scrubber was initially compressed to 13 bars (find Figure 3). After compression, H₂S present in the feed was removed on zinc oxide granulate. Subsequently, a heat exchanger cooled the gas down to 4°C in order to condense the remaining water. Two additional adsorbents have been used to remove undesired trace components. Activated charcoal has been implemented to adsorb residual tar components as well as benzene, toluene and xylenes (BTX). Activated carbon impregnated with phosphoric acid was used to remove NH₃. A particle filter was applied to prevent particles from entering the membrane module. Hydrogen preferentially permeated the membrane resulting in enhanced hydrogen concentrations in the low pressure permeate. Methane and carbon monoxide were accumulated in the high pressure retentate. The permeate was further used for final processing of pure hydrogen in the PSA unit. The retentate was expanded and recycled to the CHP plant. All relevant process parameters have been measured continuously and registered automatically at low time scale. A series of

thermocouples and pressure sensors were implemented to control the process. Gas meters were used to quantify the flow rates of feed and retentate. For process control, the main gas components were measured continuously via non-dispersive infrared (NDIR) for CO, CO₂ and CH₄ and a thermal conductivity sensor for quantification of H₂. The process conditions shown in Table 3 were chosen for membrane separation.

Table 3: Operation conditions of the membrane permeation unit.

Membrane unit	Value	Units
Feed flow rate	0.97 ± 0.09	Nm ³ /h
Feed pressure	12.0 ± 0.1	bar(g)
Temp. module	25 ± 5	°C

2.4. PSA unit

The membrane permeate was further processed by a pressure swing adsorption unit for hydrogen purification. The desired adsorption pressure was built up with a gas compressor (KNF® PM 25821-186). The unit was equipped with four 4.72L adsorber vessels, each filled with 2.5kg of activated charcoal (Norit RB2®). Desorption under vacuum was achieved using a diaphragm vacuum pump (Pfeiffer® MVP020-3AC). At the bottom, each vessel was connected to one control valve leading to the gas compressor (for feeding the vessel while adsorption) and one solenoid valve leading to the vacuum pump (for regeneration of adsorbent by desorption). At the top, each vessel was connected with one solenoid valve leading to a buffer vessel (for gas production) and one control valve leading to the other three absorbers (for pressure equalization and repressurization). A constant adsorption pressure was achieved by means of a back pressure valve situated at the exit of the buffer vessel.

Product purity and recovery were used to define the performance of the studied PSA system. These characteristic values are strongly dependent on the operation conditions. Table 4 summarizes the chosen operation parameters for pressure swing adsorption in the reported experiment. The cyclic operation of the four adsorbers is summarized in Figure 7 in the annex.

Table 4: Operation conditions of the PSA unit.

PSA unit	Value	Units
Adsorption pressure	6.5	bar(a)
Adsorption time/cycle	12.0	min
Desorption pressure	0.15	bar(a)
Equalization pressure	5.0	bar(a)
Purge/feed time ratio	$5 \cdot 10^{-3}$	-
Feed flow rate	0.40 ± 0.08	Nm ³ /h
Feed pressure	1.03 ± 0.01	bar(a)
Cyclic operation	Figure 7 in the annex	

The hydrogen recovery of each operation unit was calculated according to the equation given in (c).

$$(c) \quad H_{2\text{Recovery}} = \frac{\dot{n}_{H_2\text{ out}}}{\dot{n}_{H_2\text{ in}}}$$

In the case of the membrane permeation unit, the outlet was considered as the hydrogen flow in the permeate. For the PSA unit the referred outlet was the molar flow of the generated raffinate.

2.5. Analytics

As described in Table 5, an exhaustive analysis of all streams has been carried out in order to present a complete characterization of the entire process chain. The sampling points are also plotted in Figure 3.

Table 5: Gas sampling points and employed analytical techniques.

Nr.	Name	GC	GC/MS	HPIC
1	WGS entry dry	✓	✓	✓
2.b 2.c 2.d	WGS exit reactor 1(b), 2(c), 3(d)	✓ ✓ ✓	✓	✓
3	Scrubber exit	-	✓	✓
4	Membrane feed after adsorbers	✓	✓	✓
5	Membrane retentate	✓	✓	✓
6	Membrane permeate	✓	✓	✓
7	PSA raffinate	✓	✓	✓
8	PSA adsorbate	-	-	-

A Clarus 500[®] gas chromatograph from Perkin Elmer[®] was used on site to analyze the main gas components as well as the present organic and inorganic sulfur impurities at the sampling points 1 to 7. A thermal conductivity detector (TCD) was employed to detect CO, CO₂, CH₄, C₂H₂, C₂H₄, C₂H₆, CH₄, N₂ and O₂. An additional flame photometric detector (FPD) enabled the detection of the sulfur components H₂S, COS, CH₃SH, CH₃CH₂SH and C₄H₄S. Benzene, toluene and xylenes (BTX) were quantified by gas chromatography–mass spectrometry (GC-MS, Shimadzu QP2010 Plus[®]) from samples of the points 1 to 7 taken in sampling bags. The BTX analysis was carried out at the Vienna University of Technology directly after sampling. An absorption method was used for quantification of NH₃. For 30 min, a sampling stream of 3 NL/min was taken from the process and passed through three impinger bottles which were arranged in a cooling bath at 0 °C. The impinger bottles were filled with 0.05 M H₂SO₄, which solves NH₃ in the form of NH₄⁺ ions.

Subsequently NH_4^+ was detected by ion chromatography (Dionex ICS 5000[®]). Sampling for tar analysis was performed by means of impinger bottles filled with toluene. A gas chromatograph from Perkin Elmer[®] (XL GC[®]) coupled with a mass spectrometer from Perkin Elmer[®] (Turbo Mass MS[®]) was used subsequently to measure the content of 50 different tar species. A detailed description of the applied method for tar analysis can be found in [35]. Data reconciliation was carried out by applying the process simulation software

IPSEpro[®]. The software was provided with all available gas concentrations from GC analysis and the measured flow rates from membrane feed and retentate. The permeate flow rate was calculated by closing the mass balance over the membrane unit. The data reconciliation entailed small deviations of the measured values and the presented results in chapter 3. Equilibrium calculations for WGS catalysis have been accomplished using the chemistry software HSC[®] minimizing the Gibbs free energy.

3. Results and discussion

Table 6 depicts the mean gas concentrations over 100 hours of operation. Each sampling point of the process chain is defined in Table 5 and Figure 3. All dry gas compositions, except for adsorbate gas from the PSA unit, have been analyzed by means of gas phase chromatography. The presented

data are partly reconciled, closing the mass balances of the entire process chain. Besides, a comprehensive analysis of the sulfur components was carried out (Table 7). Sulfur measurements have not been reconciled and are plotted with the corresponding standard deviations. BTX analyses are shown in Table 8. Analysis of ammonia is presented in Table 9.

Table 6: Gas concentrations (dry) along the process chain, * Reconciled data, ** Calculated data from mass balance, below detection limit (BDL) : <0.0001%vol.

Component	Unit	H ₂	CO	CO ₂	CH ₄	C ₂ H ₂	C ₂ H ₄	C ₂ H ₆	N ₂	O ₂
1. Raw PG	%vol.	39.73	23.58	21.38	9.94	0.13	2.47	0.21	2.43	0.15
2d. WGS exit	%vol.*	49.99	5.63	32	8.13	BDL	2.13	0.4	1.7	0.03
5. Retentate	%vol.*	31.8	9.33	38.49	13.67	BDL	3.19	0.67	2.82	0.04
6. Permeate	%vol.*	76.08	0.3	22.67	0.17	BDL	0.06	0.01	0.08	0.09
7. Raffinate	%vol.	99.85	0.001	0.01	0.001	BDL	BDL	BDL	0.09	0.052
8. Adsorbate	%vol.**	37.76	0.78	59.27	0.44	BDL	0.03	0.01	0.131	0.002

Table 7: Measured concentrations of sulfur components along the process chain, below detection limit (BDL) : <0.2ppm_v, n/a* : not available, measurement was carried out during tar analysis over toluene filled impinger bottles, thiophene (C₄H₄S) is strongly absorbed in toluene.

Component	Unit	H ₂ S	C ₄ H ₄ S	COS	MeSH	EtSH
1. Raw PG	ppm _v	96 ± 7	9 ± 2	1.8 ± 0.4	BDL	BDL
2d. WGS exit	ppm _v	94 ± 7	19 ± 3	0.4 ± 0.1	BDL	BDL
3. Scrubber exit	ppm _v	80 ± 7	n/a*	0.3 ± 0.1	BDL	BDL
4. Membrane feed	ppm _v	BDL	0.2 ± 0.5	0.4 ± 0.1	BDL	BDL
5. Retentate	ppm _v	BDL	3 ± 1	0.9 ± 0.1	BDL	BDL
6. Permeate	ppm _v	BDL	BDL	BDL	BDL	BDL
7. Raffinate	ppm _v	BDL	BDL	BDL	BDL	BDL

Table 8: BTX analysis over the process chain, benzene (Ben.), toluene (Tol.), xylenes (Xyl.), BDL: <1ppm_v.

Component	Unit	Ben.	Tol.	Xyl.
1. Raw PG	ppm _v	6183	388	15
2d. WGS exit	ppm _v	5728	388	107
3. Scrubber exit	ppm _v	5009	162	14
6. Permeate	ppm _v	288	28	7
7. Raffinate	ppm _v	BDL	BDL	BDL

Table 9: Ammonia (NH₃) analysis along the process chain, BDL: <0.3ppm_v.

Component	Unit	NH ₃
1. Raw PG	ppm _v	1460 ± 200
2d. WGS exit	ppm _v	1010 ± 70
3. Scrubber exit	ppm _v	2.3 ± 0.6
4. Membrane feed	ppm _v	BDL
7. Raffinate	ppm _v	BDL

Tar analysis was carried out at three different sampling points of the process chain. The corresponding results are stated in Table 10.

Table 10: Tar composition (dry base) in the raw product gas (1), the outlet of the WGS unit (2d), and the exit of the chilled scrubber (3).

	1	2.d	3
	mg/ Nm ³	mg/ Nm ³	mg/ Nm ³
Total gravimetric tar	19	24	13
Total GC/MS tar	4625	3211	116
Naphtalene	3376	2923	81
1H-Indene	462	48	4
Styrene	456	3	3
Acenaphtylene	150	2	2
Phenylacetylene	43	0	0
2-Methylnaphthalene	31	28	2
Biphenyl	19	18	1
1-Methylnaphthalene	18	13	2
Benzofuran	14	7	4
Flourene	7	6	2
Dibenzofuran	7	6	2
Anthracene	6	6	0
Acenaphtene	5	104	1
Phenanthrene	5	5	0
Quinoline	5	4	0
Phenol	5	5	0
1-Benzothiophene	5	3	0
Pyrene	4	4	0
Flouranthene	4	3	0
Isoquinoline	3	3	0
Mesitylene	0	19	0

3.1. WGS unit

Figure 4 illustrates the effect of temperature on the equilibrium gas composition of the gas mixture entering the WGS reactors (Table 6). Only the equilibration of the WGS-reaction was taken into consideration. For simplification, all components not taking part in the WGS reaction were summarized as an unreactive species (“no WGS”). In this graph, the achieved gas composition after the WGS unit is plotted

at the outlet temperature of the last reactor (330°C).

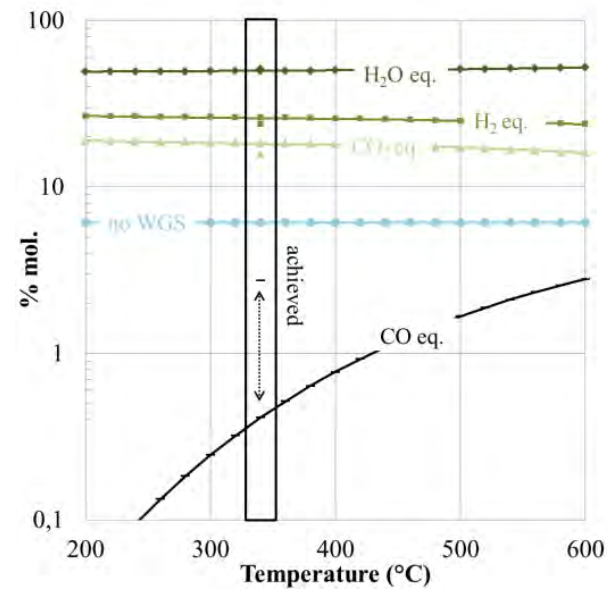


Figure 4: Temperature dependence of the WGS equilibrium of the wet gas entering the WGS unit; logarithmic scale; the achieved composition at the exit of the WGS unit was plotted at the outlet temperature of the last reactor.

The WGS-reaction is moderately exothermic ($\Delta H^0 = -41.1\text{kJ/mol}$), which leads to higher equilibrium concentrations of the reactants at elevated temperatures. Regarding the performance of the WGS unit, the CO content was lowered from ~24%vol. to ~6%vol. in the dry gas, representing a CO conversion rate of about 72% and an equilibration of the WGS-reaction up to 75% ($\dot{n}_{CO_{out}} / \dot{n}_{CO_{out,eq}}$). At the same time the water content was lowered from 58%mol. to 51%mol. and due to hydrogen production, the dry flow rate was increased from 1.92Nm³/h to 2.26Nm³/h. The observed conversion rate seems to be low, as it is reported in literature that Co-Mo catalysts are capable of reducing the CO content in a feed gas derived from coal gasification to less than 1% [20]. In this experiment the WGS reaction was carried out at a GHSV (wet basis) of about 600h⁻¹ which is in the range of operation of commercial high temperature WGS reactors employing Fe₂O₃/Cr₂O₃ catalysts (400-1200h⁻¹) [3]. Co-Mo

catalysts are said to be more active than $\text{Fe}_2\text{O}_3/\text{Cr}_2\text{O}_3$ catalysts [3] but less active than copper based catalysts applied for low temperature WGS catalysis [20]. These catalysts are usually operated at GHSV of 4800 to 24000h^{-1} , pressures between 5 and 27bar and temperatures between 250 and 300°C [3]. In [36, 37, 38] commercially available Fe-Cr catalysts and a commercial Co-Mo catalyst for hydrogen production have been investigated in a synthetic coal derived product gas. For the Co-Mo catalyst, high H_2S concentrations in the feed were found to enhance the conversion of CO. In the studied range from 330ppm_w to 2670ppm_w H_2S in the dry gas, the activity of the catalyst increased strongly [38]. In the present experiment the H_2S content in the feed of the WGS unit was below 170ppm_w in the dry gas. On the other hand, it is reported in literature that the CO conversion rate increases linearly with an increase in total pressure [37]. Pressure does not have a significant influence on the equilibrium of the WGS reaction but on kinetics [3]. With respect to these articles, the rather low conversion rate during this experiment could be explained by low H_2S concentrations in the feed ($<100\text{ppm}_v$ in the dry gas), as well as the low operation pressure ($\sim 100\text{mbar(g)}$). During experimentation of the coupled process chain, samples were taken after each reactor of the WGS unit. This allowed an investigation of the dependence of the CO conversion ratio on the GHSV. These results are illustrated in Figure 5.

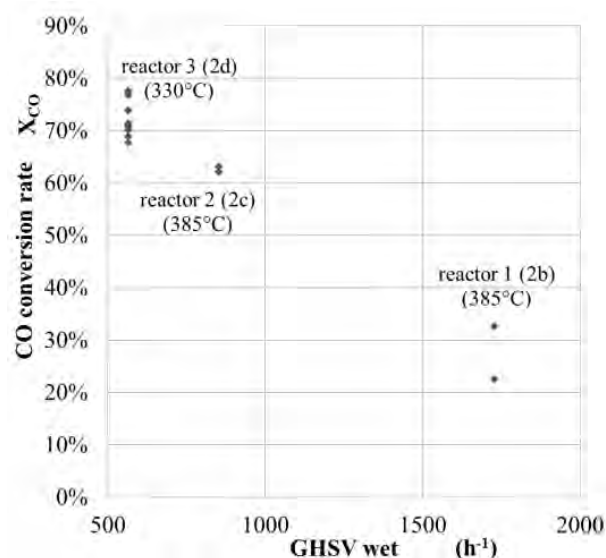
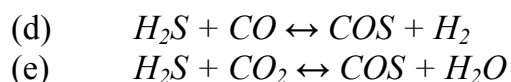
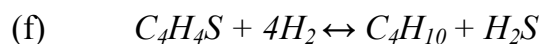


Figure 5: CO conversion rate (X_{CO}) depending on GHSV wet (h^{-1}).

Besides the catalysis of the WGS-reaction, a complete hydrogenation of acetylene as well as a partly hydrogenation of ethylene were observed. Regarding the influence of the WGS catalyst on the composition of the sulfur components, a reduction of the COS content at the reactor outlet was observed. This could be explained by the reactions (d) and (e) [39].



Furthermore, an increase in thiophene at the exit of the WGS unit was observed. The production could not be explained by the reaction of thiophene hydrogenolysis (f). The equilibrium of this reaction in the present gas mixture is strongly on the side of butane production [20].



Therefore, thiophene is suggested to be generated from a conversion of furan [40] (not analyzed) or other tars in the presence of H_2S . Regarding the BTX analysis, an increase in xylene content was observed over the WGS unit. In the WGS unit the detected GC/MS tar

content was lowered from 4.6 to 3.2 g/Nm³. Especially significant reductions of styrene and indene were observed. Acenaphthylene was hydrogenated to acenaphthene. Also, mesitylene could be detected after WGS catalysis, although it was not present in feed.

3.2. Scrubber unit

The WGS unit and the RME scrubber have been connected via 15m of trace heated stainless steel pipes. Due to controlled heat losses the WG-shifted gas, leaving the last reactor with 330°C, entered the scrubber with a temperature of 67°C. Gas temperature as well as the content of BTX and tars at the outlet, were characteristic for the performance of the scrubber. In the course of the experiment, the chiller turned out to be not suitable for the coupled process chain. Due to the high water content of the gas entering the scrubber unit (~51%) and the high enthalpy of water condensation, the targeted exit temperature of 5°C could not be reached. Tars were reduced from a total of 3211mg/m³ to 116mg/m³. Also at the exit of the scrubber, naphthalene turned out to be the most important tar component. High removal levels were accomplished for toluene and xylenes. However, benzene was not removed significantly. This could be explained with the low amount of fresh RME added and the relatively high operation temperature in the scrubber (above the melting point of benzene). Finally, the frequently reported efficient removal of ammonia by means of the condensed water in the scrubber could be observed [22, 23, 24].

3.3. Membrane unit

H₂S could not be detected in the feed of the membrane and was, therefore, removed efficiently with the employed

ZnO adsorber. Also, the phosphoric acid impregnated activated carbon reduced the NH₃ content in the membrane feed below the limit of detection. The only impurities which could still be detected in the feed of the membrane were less than 1ppm of thiophene and carbonyl sulfide and BTX components.

0.97Nm³/h of dry gas were further processed in the membrane unit. At the present operation conditions (12bar(g) and ambient temperature), the feed was separated according to Table 11.

Table 11: Partition of the membrane feed in the applied module.

Permeate flow rate	0.40 ± 0.08	Nm ³ /h
Retentate flow rate	0.57 ± 0.06	Nm ³ /h

The hydrogen content in the permeate could be enriched up to 76%vol. Especially the low CO content of 0.3%vol. in this gas mixture was representing a good condition for the subsequent pressure swing adsorption.

3.4. PSA unit

During the experiment, analysis of the main gas components at the outlet of the PSA unit was carried out continuously for almost 10 hours. The measured raffinate composition as a function of time is illustrated in Figure 6.

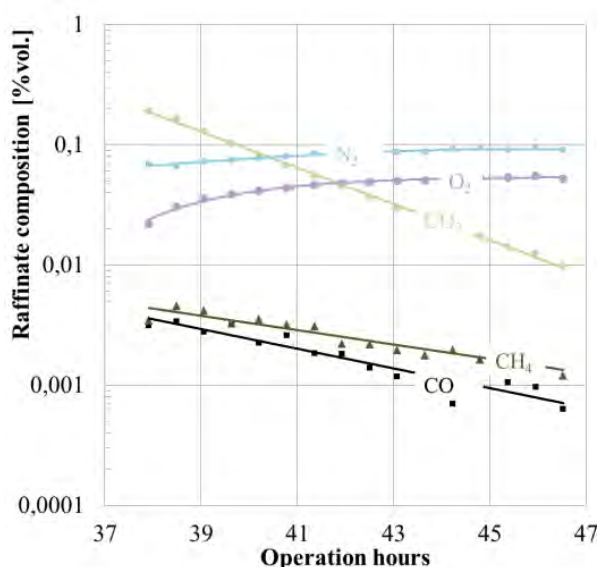


Figure 6: Continuous analysis of the raffinate composition at the exit of the PSA unit.

The increasing purity of the generated hydrogen flow could be explained by time-demanding flushing of the analytical sampling line. During this experiment an equilibration of the composition could not be achieved. The reported impurities in Table 6 are equivalent to the gas composition at the end of the continuous analysis in Figure 6, even though the content of undesired components (CO, CO₂ and CH₄) was probably lower as reported here. This assumption is also confirmed by more recent experiments, where the detection limit of CO, CO₂ and CH₄ could be reached with an improved analytical sampling line.

With the presented PSA unit, a hydrogen purity of 99.85%vol. as well as a hydrogen recovery of 76% could be achieved. This is within the range of similar PSA systems reporting hydrogen purity up to 99.99%vol. and hydrogen recoveries between 70 and 85% [41, 42, 43, 44].

No traces of sulfur compounds, benzene, toluene, xylenes or ammonia were detected in the raffinate (Table 7, Table 8 and Table 9).

The most important impurities were 0.09%vol. of N₂ and 0.05%vol. of O₂ (Table 6). These components have

already been contained in the feed gas and were not removed completely over the entire process chain. N₂ and O₂ in the product could have been removed in applying a multiple adsorbent bed involving a layer of zeolite with an enhanced capacity for these gases [43].

To facilitate the desorption process, only a single layer of activated carbon was preferred to a mixed bed with zeolite. Activated carbon has relatively moderate strengths of adsorption for the relevant gases, whereas CO₂ is adsorbed almost irreversibly on zeolite [18].

3.5. Hydrogen recovery

Table 12 gives an overview of the achieved hydrogen recoveries of each operation unit.

Table 12: Overview of the hydrogen recoveries of each operation unit.

Component	Unit	H ₂ recovery
WGS unit	-	1.38
Scrubber unit	-	1
Membrane unit	-	0.66
PSA unit	-	0.76
Overall	-	0.69

Based on cold gas efficiency, low heating values and the stated wood composition (19%wt. water content) by Wilk et al. [45] an overall hydrogen yield for the presented process chain of 42g/kg of dry biomass was calculated. Toonssen et al. simulated hydrogen production based on five different commercial or pilot scale gasification systems. Among various sceneries a hydrogen yield of 96g/kg of dry biomass was calculated for a 10 MW DFB steam gasification power plant including low temperature gas cleaning, reforming of hydrocarbons, two step WGS catalysis and a PSA process [15]. Comparable hydrogen yields are also presented by [46]. The next chapter

demonstrates a series of possible improvements of the presented configuration. A further approximation to simulated hydrogen yields in literature is feasible and desired. Anyway, values in the order of magnitude of 100g/kg of dry biomass are not possible due to the absence of a steam reforming unit.

4. Conclusion and Outlook

The accomplished hydrogen yield of about 70% over the entire process chain was a satisfactory result. Also the purity of the generated hydrogen came up to the expectations. During the reported 100h of operation including WGS catalysis, the raffinate did not meet the high standards from ISO 14687 and SAE J2719. Anyway it can be considered, that the operation of a proton exchange membrane (PEM) fuel cell is viable. N₂ as the most important impurity is only reported to entail a dilution effect. O₂ should be tolerated up to 500ppm_v [47].

With respect to the numerous operational units and their interactions it is apparent that the investigated process chain still has a big potential of optimization. A series of desirable improvements have been discovered during the presented experiment and isolated test runs of the single operation units. For instance, the catalysis of the WGS reaction has not yet been optimized for the presented process chain. It turned out that conversion rates at these GHSV would have been enhanced at more elevated operation temperatures. Especially it is favorable to operate the first WGS reactor near maximum temperature of the catalyst. High initial conversion rates would have been achieved due to the great influence of temperature on reaction kinetics. Temperature level in the subsequent reactors should be decreased deliberately, in order to benefit from the low equilibrium CO contents at reduced

temperatures. Also, the operation of the gas scrubber could be improved by lower operation temperatures.

The membrane permeation unit with a reconciled recovery of about 66% has been operated at conditions which turned out to be suitable for direct processing of product gas. For the WG shifted gas however, the optimum operation conditions are likely to be different. Therefore it is assumed, that also the hydrogen yield of the membrane unit can still be increased by adjusting the process parameters. Further improvements of the membrane separation unit could also include a multi-stage process with more than one membrane. Moreover it would be desirable to introduce a reverse selective membrane which could reduce the number of essential compression steps [48]. The implemented gas cleaning stages upstream the module were designed very carefully to avoid damage of the polymer membrane. With respect to an industrial application of similar approaches, present experiments are investigating the reduction of these measures to a minimum operating expense.

Especially, for the operation with water gas shifted feed, also more optimization work is necessary for the PSA system. The goal is to achieve hydrogen purities which allow an operation of the available PEM fuel cell from AXANETM. At the same time, the hydrogen yield of the PSA unit has to be maximized.

An overall hydrogen yield of 80% for the complete process chain could already be achieved in another test run with an incomplete characterization of the entire process chain.

5. Acknowledgements

The authors would like to thank all project partners involved. Especially we want to thank the research and

development division from AIR Liquide™. Furthermore we would like to thank the CHP-Oberwart and Energie Burgenland® for a stable supply of product gas and operation resources. Automation was carried out by cts® (competence for technical solutions) and the working group from Michael Harasek (Vienna University of Technology). Manufacturing was supported by Jörg Artner and Binder Industrieanlagenbau®. The coupling of both test rigs could only be achieved with the help of Michael Weitzer. Also, we would like to thank Ivan Bergamo, Martin Miltner, Aleksander Makaruk and Christian Jordan for their collaboration. Nicolas Diaz received financial support from Conicyt-Becas Chile. Bioenergy2020+ is funded within the Austrian COMET program managed by the Austrian Research Promotion Agency (FFG). The financial support of the funding association FFG and the Austrian Climate and Energy Fund is gratefully acknowledged.

6. References

- [1] A. DÜKER, Hydrogen-Production and Application in Industry, in *Presentation Süd-Chemie*, Süd-Chemie AG, 2011.
- [2] B. M. BIZZARI, S. N., Chemical Industries Newsletter CEH Marketing Research Report Abstract- Hydrogen, Technical report, SRI Consulting, 2007.
- [3] V. S. LIU, K.; CHUNSHAN SONG, *Hydrogen and Syngas Production and Purification Technologies*, Wiley, 2010.
- [4] IEA, Hydrogen Production and Distribution, International Energy Agency - Energy Technology Essentials, 2007.
- [5] C. FRANCESCO, D. KRAMER, and L. APODACA, Nitrogen (fixed) - ammonia statistics, 2010.
- [6] R. CHAUBEY, S. SAHU, O. O. JAMES, and S. MAITY, *Renewable and Sustainable Energy Reviews* **23**, 443 (2013).
- [7] M. NI, D. Y. LEUNG, M. K. LEUNG, and K. SUMATHY, *Fuel Processing Technology* **87**, 461 (2006).
- [8] M. HOOGWIJK, A. FAAIJ, R. VAN DEN BROEK, G. BERNDIS, D. GIELEN, and W. TURKENBURG, *Biomass and Bioenergy* **25**, 119 (2003).
- [9] S. KERN, C. PFEIFER, and H. HOFBAUER, Dual fluidized bed steam gasification of coal and biomass: influence of the state of pyrolysis on the process performance, in *Clean Coal Conference*, 2013.
- [10] Y. MATSUMURA, T. MINOWA, and B. POTIC, *Biomass and Bioenergy* **29**, 269 (2005).
- [11] Y. CALZAVARA, C. JOUSSOT-DUBIEN, G. BOISSONNET, and S. SARRADE, *Energy Conversion and Management* **46**, 615 (2005).
- [12] C. PFEIFER, B. PUCHNER, and H. HOFBAUER, *International Journal of Chemical Reactor Engineering* **5**, 1542 (2007).
- [13] S. KOPPATZ, C. PFEIFER, R. RAUCH, H. HOFBAUER, T. MARQUARD-MOELLENSTEDT, and M. SPECHT, *Fuel Processing Technology* **90**, 914 (2009).
- [14] T. PRÖLL and H. HOFBAUER, *Fuel Processing Technology* **89**, 1207 (2008).
- [15] R. TOONSEN, N. WOULDSTRA, and A. H. VERKOOIJEN, *International Journal of Hydrogen Energy* **33**, 4074 (2008).
- [16] M. STEINBERG and H. CHENG, *International Journal of Hydrogen Energy* **14**, 797 (1989).
- [17] S. MUELLER, M. STIDL, T. PROELL, R. RAUCH, and H. HOFBAUER, *Biomass Conversion and Biorefinery* **1**, 55 (2011).

- [18] S. SIRCAR, T. GOLDEN, and M. RAO, *Carbon* **34**, 1 (1996).
- [19] I. N. J. CHORKENDORFF, *Concepts of Modern Catalysis and Kinetics*, Wiley-VCH, 3rd reprint 2013 edition, 2013.
- [20] M. V. TWIGG, *Catalyst Handbook-Chapter 6: The Water-gas Shift Reaction*, Manson Publishing, 1989.
- [21] M. BRUNE, *Verfahren zur Entschwefelung von flüssigen handelsüblichen Brennstoffen*, Scientific Publishing, 2009.
- [22] H. HOFBAUER, R. RAUCH, and K. BOSCH, Zwischenbericht Wäscher, Report for Renewable Energy Network Austria 12, Technische Universität Wien, Insitut für Verfahrens-, Brennstoff- und Umwelttechnik, 2000.
- [23] H. HOFBAUER, R. RAUCH, K. BOSCH, and I. G. SIEFERT, Produktgasreinigung Lösungsmittel - Wäscher, Report for Renewable Energy Network Austria 34, Technische Universität Wien, Insitut für Verfahrenstechnik, Umwelttechnik und technischen Biowissenschaften, 2002.
- [24] T. PRÖLL, I. G. SIEFERT, A. FRIEDL, and H. HOFBAUER, *Industrial & Engineering Chemistry Research* **44**, 1576 (2005).
- [25] S. ADHIKARI and S. FERNANDO, *Industrial & Engineering Chemistry Research* **45**, 875 (2006).
- [26] Y. ZHANG, J. SUNARSO, S. LIU, and R. WANG, *International Journal of Greenhouse Gas Control* **12**, 84 (2013).
- [27] D. M. RUTHVEN, *Pressure Swing Adsorption*, VCH, 1994.
- [28] H. HOFBAUER, R. RAUCH, K. BOSCH, R. KOCH., and C. AICHERNING, *Biomass CHP Plant Güssing – A Success Story*, CPL Press, 2003.
- [29] E. KURKELA and M. KURKELA, Advanced Biomass Gasification for High-Efficiency Power, Publishable Final Activity Report of BiGPower Project, Technical report, VTT, TUV, Kokemäen Kaasutin, Carbona, RPT, MEL, Norta, GEJ, MTU, BKG, CERTH, TKK, Clear Edge, 2009.
- [30] F. KIRNBAUER, J. KOTIK, and H. HOFBAUER, Investigations on inorganic matter in DFB biomass steam-gasification plants in Güssing/Austria and Oberwart/Austria, in *19th European Biomass Conference and Exhibition*, p. 6, 2011.
- [31] J. KOTIK, *Über den Einsatz von Kraft-Wärme-Kopplungsanlagen auf Basis der Wirbelschicht-Dampfvergasung fester Biomasse am Beispiel des Biomassekraftwerks Oberwart ausgeführt*, PhD thesis, Technische Universität Wien, 2010.
- [32] H. HELLSMARK and S. JACOBSSON, *Energy Policy* **37**, 5597 (2009).
- [33] Y. SHIRATORI, T. IJICHI, T. OSHIMA, and K. SASAKI, *International Journal of Hydrogen Energy* **35**, 7905 (2010).
- [34] E. XUE, M. O'KEEFFE, and J. ROSS, *Catalysis Today* **30**, 107 (1996).
- [35] U. WOLFESBERGER, I. AIGNER, and H. HOFBAUER, *Environmental Progress & Sustainable Energy* **28**, 372 (2009).
- [36] S. S. HLA, D. PARK, G. DUFFY, J. EDWARDS, D. ROBERTS, A. ILYUSHECHKIN, L. MORPETH, and T. NGUYEN, *Chemical Engineering Journal* **146**, 148 (2009).
- [37] S. S. HLA, G. DUFFY, L. MORPETH, A. COUSINS, D. ROBERTS, and J. EDWARDS, *Catalysis Communications* **11**, 272 (2009).
- [38] S. S. HLA, G. DUFFY, L. MORPETH, A. COUSINS, D. ROBERTS, and J. EDWARDS, *International Journal of Hydrogen Energy* **36**, 6638 (2011).
- [39] L. LI and D. L. KING, *Catalysis Today* **116**, 537 (2006).
- [40] Q. LI, Y. XU, C. LIU, and J. KIM, *Catal Lett* **122**, 354–358 (2008).

- [41] J. YANG, S. HANA, C. CHOB, C.-H. LEE, and H. LEE, *Separations Technology* **5**, 239 (1995).
- [42] S. AHN, Y.-W. YOU, D.-G. LEE, K.-H. KIMB, M. OH, and C.-H. LEE, *Chemical Engineering Science* **68**, 413 (2012).
- [43] A. M. RIBEIRO, C. A. GRANDE, F. V. LOPES, J. M. LOUREIRO, and A. E. RODRIGUES, *Chemical Engineering Science* **63**, 5258 (2008).
- [44] J.-H. PARK, J.-N. KIM, and S.-H. CHO, *AIChE Journal* **46**, 790 (2000).
- [45] V. WILK, H. KITZLER, S. KOPPATZ, C. PFEIFER, and H. HOFBAUER, Gasification of residues and waste wood in a dual fluidised bed steam gasifier, in *ICPS Leipzig*, 2010.
- [46] S. MÜLLER, *Hydrogen from Biomass for Industry - Industrial Application of Hydrogen Production Based on Dual Fluid Gasification*, PhD thesis, Vienna University of Technology, 2013.
- [47] B. M. BESANCON, V. HASANOV, R. IMBAULT-LASTAPIS, R. BENESCH, M. BARRIO, and M. J. MØLNVIK, *International Journal of Hydrogen Energy* **34**, 2350 (2009).
- [48] C. H. LAU, P. LI, F. LI, T.-S. CHUNG, and D. R. PAUL, *Progress in Polymer Science* **38**, 740 (2013).

7. Annex

PSA automation

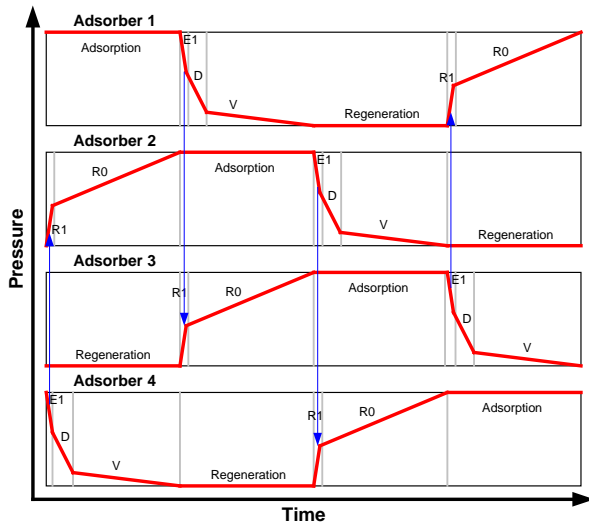


Figure 7: Cyclic sequence steps of the PSA test rig.

The pressure swing adsorption unit in the pilot plant was equipped with an automation system to control the cyclic operation of the adsorbers. Figure 7 illustrates the cyclic sequence of the PSA, which considers the following seven steps:

- (1) Adsorption at high pressure, with raffinate withdrawal to repressurize the next bed.
- (2) Pressure equalization (E1), cocurrent depressurization.
- (3) Dump step (D), countercurrent depressurization of the adsorber to produce the tail gas.
- (4) Vacuum (Regeneration), countercurrent regeneration of the bed by desorption at low pressure with.
- (5) Purging (Regeneration), countercurrent regeneration of the bed at low pressure with highly pure hydrogen from the adsorption step.
- (6) First repressurization (R1), countercurrent repressurization carried out by using pure hydrogen from the adsorber presently under depressurization (pressure equalization step).

- (7) Final repressurization (R0), countercurrent repressurization is carried out with a split stream from the hydrogen product line until the required pressure level is reached.

7.2 Process chain 2: WGSR - Gas scrubbing - Pressure swing adsorption

The second process chain to be presented included the operation of the WGS unit with Catalyst 2, gas cleaning and drying in a LT RME scrubber, and hydrogen purification via pressure swing adsorption.

Wood Gas Processing to Generate Pure Hydrogen Suitable for PEM Fuel Cells

Silvester Fail,^{*,†} Nicolas Diaz,^{*,†,‡} Florian Benedikt,[†] Michael Kraussler,[†] Julian Hinteregger,[†] Klaus Bosch,[¶] Marius Hackel,[§] Reinhard Rauch,^{†,‡} and Hermann Hofbauer^{†,‡}

Vienna University of Technology, Institute of Chemical Engineering, Vienna, Austria., Bioenergy 2020+ GmbH, Güssing, Austria., Energie Burgenland AG, Eisenstadt, Austria., and Air LiquideTM Forschung und Entwicklung GmbH, Frankfurt Research and Technology Center (FRTC), Germany.

E-mail: silvester.fail@tuwien.ac.at; nicolas.diaz@gmx.at

Phone: +43(0)158801 166353. Fax: +43(0)158801 9166388

Abstract

A test campaign was carried out to generate renewable hydrogen based on wood gas derived from the commercial biomass steam gasification plant in Oberwart, Austria. The implemented process consisted of four operation units: (I) catalyzed water gas shift (WGS) reaction, (II) gas drying and cleaning in a wet scrubber, (III) hydrogen purification by pressure swing adsorption and (IV) use of the generated biohydrogen (BioH₂) in a proton exchange membrane (PEM) fuel cell. For almost 250 hours, a

*To whom correspondence should be addressed

†Vienna University of Technology, Institute of Chemical Engineering, Vienna, Austria.

‡Bioenergy 2020+ GmbH, Güssing, Austria.

¶Energie Burgenland AG, Eisenstadt, Austria.

§Air LiquideTM Forschung und Entwicklung GmbH, Frankfurt Research and Technology Center (FRTC), Germany.

reliable and continuous operation was achieved. 560 $\frac{\text{L}_n \text{ dry basis (db)}}{\text{h}}$ of wood gas were extracted to produce 280 $\frac{\text{L}_n \text{ db}}{\text{h}}$ of BioH₂ with a purity of 99.97 vol.%_{db}. The catalyzed WGS reaction enabled a hydrogen recovery of 128 % $\frac{\dot{n}_{\text{BioH}_2}}{\dot{n}_{\text{H}_2, \text{wood gas}}}$ over the whole process chain. An extensive chemical analysis of the main gas components and trace components (sulfur, C_xH_y and ammonia) was carried out. No PEM fuel cell poisons were measured in the generated BioH₂. The only detectable impurities in the product were 0.02 vol.%_{db} of O₂ and 0.01 vol.%_{db} of N₂.

Keywords

biohydrogen, biomass, gasification, product gas, water gas shift, gas scrubbing, pressure swing adsorption, L^AT_EX

Nomenclature

Abbreviations & Acronyms

BDL Below detection limit

BioH₂ Biohydrogen, hydrogen produced by or out of biomass

BTEX Benzene, toluene, ethylbenzene, xylene

CHP Combined heat and power

C_xH_y Hydrocarbons

DFB Dual fluidized bed

DL Detection limit

FPD Flame photometric detector

GC Gas chromatography

GHSV Gas hourly space velocity
LHV Lower heating value
mol. Molar
ORC Organic rankine cycle
PEM Proton exchange membrane
PSA Pressure swing adsorption
RME Rapeseed oil methyl ester
S.pt. Sampling point
TCD Thermal conductivity detector
vol. Volumetric
WGS Water gas shift

Indices

cool Cooling
db Dry base
el Electric
eq Equilibrium
heat Heating
in Inlet
meas Measured
n Standard conditions (0 °C, atmospheric pressure)

out Outlet

rec Recovery

wb Wet base

Symbols

a Year (anno)

ΔH_R^0 Standard enthalpy of reaction (at 0 °C and 1 bar)

$\eta_{el\ gross}$ Gross electrical efficiency

L Liter

\dot{n} Molar flow rate

t Ton

\dot{V} Volumetric flow rate

X_{CO} CO conversion rate

Introduction

Hydrogen is required chiefly for the synthesis of ammonia and methanol as well as for various applications in refineries. In 2007, the world's installed capacity of production was about 65 million tons of hydrogen.¹ Its demand is growing especially because of the usage of heavier and dirtier feedstock in refineries which requires greater amounts of hydrogen for hydrotreating and hydrocracking.² Some authors consider a global hydrogen economy as the future perspective to cover the demands for electricity, heat, and transportation.^{3,4} This would require a further increase in the production capacity. 96 % of the current hydrogen production is directly based on fossil fuels, mainly natural gas (49 %).¹

Considerable research has been carried out in the field of renewable hydrogen production. It can be distinguished between thermochemical, electrochemical, and biological approaches.⁵ Especially the increasing number of power-to-gas concepts, which use the excess electricity from wind power and photovoltaics for the hydrogen production in electrolyzers, should be pointed out.⁶ This article deals with hydrogen production via the thermochemical processing of biomass, which is reported to be more costly than the conventional production methods but competitive with the electrolysis of water using renewable electricity.^{7,8} Life cycle assessment of gasification-derived biohydrogen shows reduced greenhouse gas emissions compared to steam reforming of natural gas and a low non-renewable energy demand.^{9,10}

The established process chain for biohydrogen (BioH_2 , here defined as hydrogen generated by or out of biomass) production was operated with a partial flow of wood gas (also product gas, producer gas, syngas, or synthesis gas) derived from the commercial biomass gasification plant in Oberwart, Austria. 8.7 MW of wood chip power ($23000 \frac{t_{wood}}{a}$) are converted to 2.5 MW of electrical power and 3.5 MW of district heat.¹¹ The flowchart of the gasification power plant Oberwart is illustrated in Figure 1.

The design of this combined heat and power (CHP) plant is based on the well documented plant in Güssing, Austria.¹³ Both plants employ the dual fluidized bed (DFB) steam gasification technology. Wood gas is generated, cooled down, filtered, cleaned, and finally burned in gas engines to generate electricity and district heat. Unlike the plant in Güssing, a biomass dryer and an organic rankine cycle (ORC) are employed in the CHP plant Oberwart.¹⁴ The investigated pilot plant for hydrogen production was operated with a partial flow of wood gas extracted after its gas cleaning units. Therefore, particles were already removed in a baghouse filter and the majority of the tar was already separated in a gas scrubber operated with rapeseed oil methyl ester (RME). The wood gas extraction point and the point of recycling are plotted in Figure 1 (Pilot plant inlet and outlet).

The applied unit operations for wood gas conditioning involved: (I) carbon monoxide conversion via sulfur tolerant catalysis of the water gas shift (WGS) reaction, (II) gas cleaning

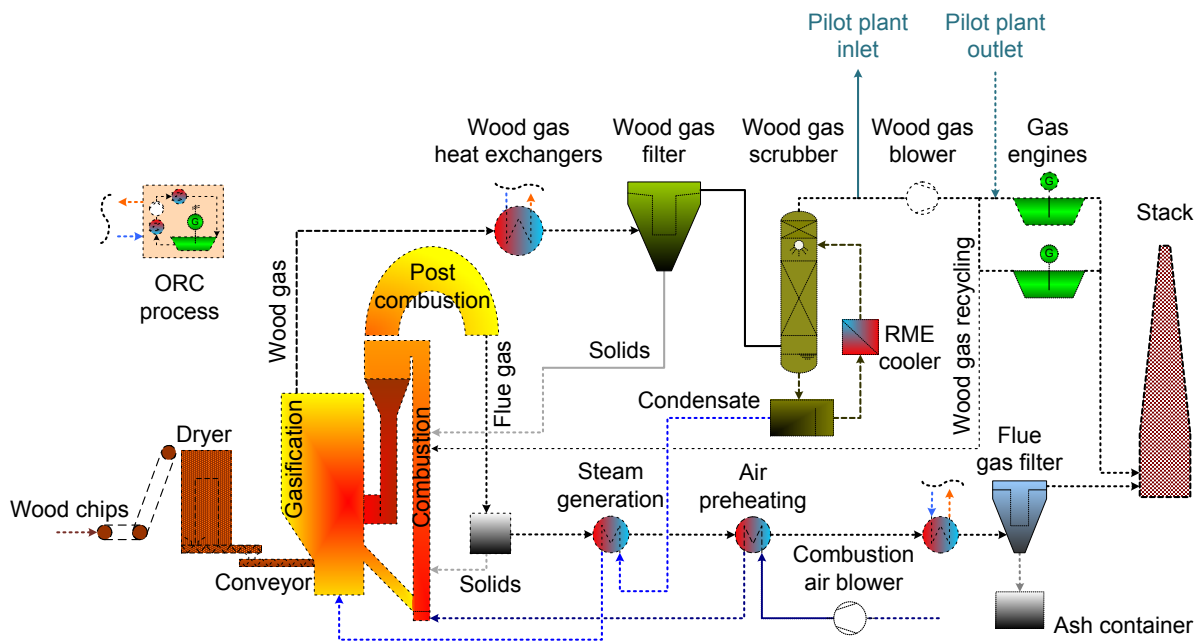
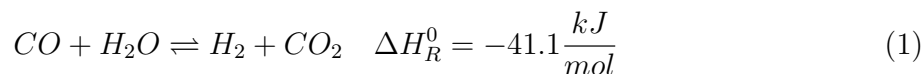


Figure 1: Flowchart of the biomass gasification plant Oberwart including the sampling point of wood gas of the investigated pilot plant; based on¹².

Reprinted with permission from Diaz, N. Hydrogen Separation from Producer Gas Generated by Biomass Steam Gasification. Ph.D. thesis, Vienna University of Technology, 2013., COPYRIGHT (2013) Nicolas Diaz

in a wet scrubber operated with RME, (III) pressure swing adsorption (PSA) for hydrogen purification, and (IV) application of the BioH₂ in a proton exchange membrane (PEM) fuel cell.

I Catalysis of the WGS reaction (Equation 1) is a state of the art technology. A two stage system with different catalysts is industrially applied in order to produce additional hydrogen by the conversion of carbon monoxide with steam.¹⁵



II Wood gas contains traces of ammonia, sulfur components, benzene, toluene, ethylbenzene, and xylene (BTEX), as well as condensable organic compounds (tar). A highly effective approach towards the removal of tar is the absorption in organic solvents (e.g. biodiesel or RME). In parallel, condensing water enables a removal of water soluble impurities like ammonia and hydrogen sulfide.¹⁶

III The PSA process is based on the physical binding of gas molecules to a solid adsorbent material. The interaction between the gas and the adsorbent depends mainly on the gas component, its partial pressure, the type of adsorbent, and the temperature. Hydrogen is a highly volatile compound with a low polarity and its adsorption capacity on activated carbon is very low.¹⁷

IV As a demonstration of the high quality of the product, its use in a PEM fuel cell was chosen. The principles of a PEM fuel cell are reviewed in.¹⁸ In order to meet the requirements of this fuel cell type, the presence of certain wood gas components in the generated BioH₂ had to be avoided. In the following, the influence of the relevant wood gas components on a PEM fuel cell are reviewed.

CO is adsorbed on the active surface of the platinum catalyst of a PEM fuel cell and

reduces the available area for H₂ oxidation. Concentrations as low as 0.5 to 4.5 vol.ppm have been reported to cause performance losses due to a voltage drop which is directly proportional to the CO concentration.¹⁹ CO₂ causes a more pronounced performance loss than inert components like N₂. The reason seems to be the formation of CO, either through the reverse WGS reaction or an electrochemical reduction reaction. Severe performance loss has been reported for CO₂ concentrations of about 20 vol.% and higher.²⁰ H₂S is also adsorbed on the catalyst surface and reduces the area for H₂ oxidation. This mechanism was even observed at concentrations as low as 0.25 vol.ppm. In contrast to CO poisoning, the adsorption of H₂S seems to be irreversible²⁰. Also carbonyl sulfide (COS) is reported to reduce the active surface of the catalyst.²¹ NH₃ is oxidized to NH₄⁺ ions which reduces the proton concentration at the catalyst layer and leads to a reduction of the performance of the anode. After long exposure times, NH₄⁺ ions migrate into the proton exchange membrane, resulting in a conductivity loss. These effects have already been observed at ammonia concentrations as low as 1 vol.ppm.²⁰ Inert components like N₂ reduce the partial pressure of the H₂, which leads to a potential loss according to the Nernst equation. Apart from this effect, even high CH₄ concentration show no negative effects on the performance of a PEM fuel.²² The O₂ content in the BioH₂ needs to be as low as possible in order to avoid the direct formation of water at the anode.²⁰

Experimental

The studied process chain shown in Figure 2 is the third configuration for BioH₂ production, which has been tested experimentally at Oberwart. A series of test campaigns, which included a membrane separation unit, were carried out in 2013: its results have been already published.^{12,23}

The current configuration can be seen as a polygeneration concept, aiming at the simultaneous production of H₂, electricity, and district heat. Electricity production can be

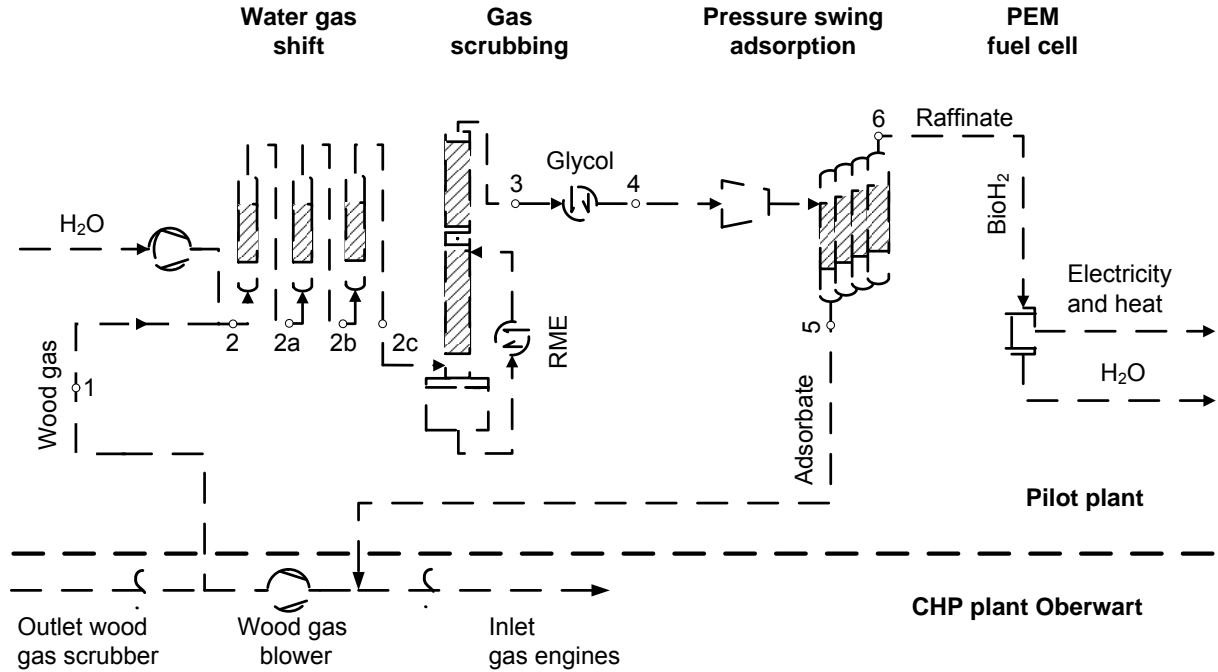


Figure 2: Flowchart of the investigated pilot plant for BioH₂ production including the applied sampling points (1–6) for chemical analysis.

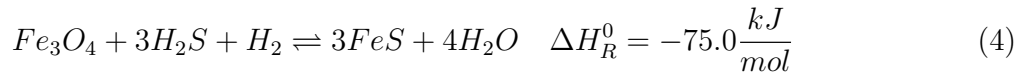
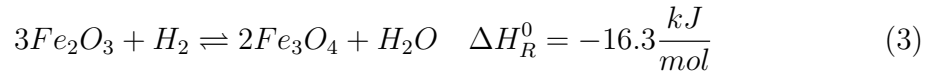
achieved via combustion of the adsorbate fraction of the PSA unit. The complexity, the costs of investment as well as the operating expense should be kept low, with high overall efficiencies and an acceptable H₂ recovery ($H_2 \text{ rec}$) calculated according to the molar flow rate of hydrogen at the inlet and at the outlet of the process chain (Equation 2). Therefore, a steam reformer for CH₄ and tar reforming was not desired although it enables an increased hydrogen yield per biomass input.

$$H_2 \text{ rec} = \frac{\dot{n}_{H_2, \text{out}}}{\dot{n}_{H_2, \text{in}}} \quad (2)$$

Water Gas Shift Unit

WGS catalysis was realized in three fixed bed reactors connected in series. A picture of the experimental setup for the catalysis of the WGS reaction can be found in the supporting information of this article. A commercial Fe₂O₃/Cr₂O₃ based catalyst was applied for heterogeneous fixed bed catalysis of the WGS reaction. Prior to the operation of the process

chain, the catalyst had been activated according to Equation 3 in order to form the catalytically active magnetite (Fe_3O_4). The overall hydrogen demand for this reduction process was negligible (about 1 m_n^3). After the activation of the catalyst, the WGS unit had been commissioned with real wood gas and operated continuously for almost 400 hours at an inlet temperature of each reactor of $350 \text{ }^\circ\text{C}$. During this conditioning phase, FeS had been formed according to the equilibrium reaction in Equation 4. This sulfiding reaction is reversible and H_2S will be released if the reaction temperature is increased or if the partial pressure of H_2S in the feed is decreased. With respect to the equilibrium constant of the reaction, it can be considered that the loading of FeS is increased by factor 6.5 if the temperature is decreased from $400 \text{ }^\circ\text{C}$ to $300 \text{ }^\circ\text{C}$. FeS is reported to exhibit an activity reduced by 50 % compared to magnetite.^{15,24}



Steam was added to the wood gas in order to enhance the shift reaction and to prevent carbon formation on the surface of the catalyst.²⁵ The wood gas flow rate over the WGS unit was set with the rotational speed of the compressor of the PSA unit. The gas at the inlet of each reactor was electrically heated and the temperature was monitored every 10 cm along the fixed bed. A temperature profile along the three reactors was set, attempting to optimize the overall CO conversion rate. Equilibrium calculations of the WGS reaction have been accomplished using the software HSCTM. Table 1 summarizes the operating conditions of the WGS unit. In the following, \pm denotes the standard deviation of the measured values. The CO conversion rate (X_{CO}) defined in Equation 5 was used to describe the performance of the WGS unit. The gas hourly space velocity (GHSV) was calculated using Equation 6.

Table 1: Operating conditions of the WGS unit.

	Value	Unit
Wood gas in	0.56 ± 0.02	$\frac{\text{m}^3}{\text{n}} \frac{\text{db}}{\text{h}}$
Water addition	0.55 ± 0.02	$\frac{\text{kg}}{\text{h}}$
T _{in} reactor 1	403 ± 5	°C
T _{in} reactor 2	358 ± 3	°C
T _{in} reactor 3	309 ± 3	°C
Pressure	76 ± 7	mbarg
GHSV _{wet}	170 ± 5	h ⁻¹
$\frac{\text{H}_2\text{O}}{\text{CO}}$ molar ratio	5 ± 0.2	-
$\frac{\text{H}_2\text{O}}{\text{C}}$ molar ratio	2 ± 0.1	-

$$X_{CO} = \frac{\dot{n}_{CO,in} - \dot{n}_{CO,out}}{\dot{n}_{CO,in}} \quad (5)$$

$$GHSV = \frac{\dot{V}_{gas}}{V_{catalyst}} \quad (6)$$

Scrubber Unit

The water gas shifted gas subsequently entered a wet scrubbing unit in order to be cleaned and dried for PSA operation. A pipe with a length of 22 m was installed to connect the outlet of the WGS unit with the inlet of the scrubber unit. The heat losses over this length resulted in a rather low inlet temperature of the scrubber. A counter current flow of wood gas and organic solvent (RME) was realized over a structured packed column. The RME was cooled with a plate heat exchanger provided with cold ethylene glycol from an external chiller. In order to assure complete gas drying, a gas washing bottle filled with ethylene glycol cooled to 0 °C was implemented afterwards. The operating conditions of the scrubbing unit can be seen in Table 2. A detailed description of the scrubber unit is provided in.¹² Tar components represent a potential risk for the WGS catalyst as they might serve as precursors for the formation of coke.²⁶ However, the scrubber was placed downstream the WGS unit in order to avoid an additional energy intensive cycle of condensation and evaporation.

Table 2: Operating conditions of the scrubber unit.

	Solvent	Value	Unit
T_{in} gas	RME	48.3 ± 2.4	$^{\circ}\text{C}$
T_{out} gas	RME	5.1 ± 0.2	$^{\circ}\text{C}$
Pressure	RME	58.5 ± 5.8	mbarg
Circulation rate	RME	700	$\frac{\text{L}}{\text{h}}$
Fresh addition	RME	0.5	$\frac{\text{L}}{\text{h}}$
T_{out} gas	Glycol	0	$^{\circ}\text{C}$

Pressure Swing Adsorption Unit

The cleaned gas was further processed in a PSA unit for H_2 purification. A picture of this setup can be found in the supporting information of this article. The unit consisted of four vessels with a capacity of 4.72 L each. Every reactor was filled with 2.5 kg of activated carbon (Norit, RB2) as adsorption agent. The volumetric flow rates of PSA feed and raffinate (BioH_2) were quantified with diaphragm gas meters enabling an accurate mass balance of the PSA unit. The adsorption pressure was built up with a gas compressor and the desired desorption pressure was achieved using a diaphragm vacuum pump. The PSA unit was operated in a cyclic sequence, which is described in detail in.¹² Raffinate was generated during the adsorption step of one vessel carried out over a variable time frame (adsorption time). During the pressure equalization step, the product of one loaded vessel was used to partly repressurize a currently regenerated adsorber. The equalization pressure (in bara) is defined as the value to which the pressure drops in the gas dispensing vessel. The applied adsorption time and equalization pressure for the long-term experiment were estimated in a previous parameter study. During this study the adsorption time per column was varied between 400 and 800 s, and the equalization pressure was set to the values 4.0 and 4.5 bara. Table 3 summarizes the basic operating conditions of the PSA unit which were chosen during the continuous long-term operation.

Table 3: Operating conditions of the PSA unit.

	Value	Unit
Adsorption pressure	6.5	bara
Desorption pressure	0.1	bara
Purge/feed time ratio	$5 \cdot 10^{-3}$	-
Feed flow rate	0.7 ± 0.04	$\frac{\text{m}^3_{\text{n}}}{\text{h}}$
Feed pressure	1000 ± 17	mbara
Adsorption time per column	650	s
Equalization pressure	4.5	bara

Fuel Cell Unit

A proton exchange membrane (PEM) fuel cell from AXANETM was operated with the generated BioH₂ to demonstrate its quality. A picture of the employed fuel cell can be found in the supporting information of this article. As a benchmark the PEM fuel cell was also operated with Alphagaz 1TM (H₂ purity > 99.999 vol.%). Key data of this PEM fuel cell are shown in Table 4 provided by²⁷.

Table 4: Key data of the PEM fuel cell unit, based on²⁷.

	Value	Unit
Nominal voltage DC	48	V
Nominal voltage AC	230	V
Minimum power _{el}	500	W
Maximum power _{el}	2500	W
H ₂ quality (ISO 14687)	99.99	vol.%
H ₂ operating pressure	250 ± 30	mbarg
H ₂ consumption at max. power	35.1	$\frac{L_n}{\text{min}}$
H ₂ peak consumption	60	$\frac{L_n}{\text{min}}$

Chemical Analysis and Mass Balance

This section describes the adopted methods of chemical analysis. Extensive analyses of main gas components, sulfur components, tar, water, BTEX and ammonia were carried out. The selected sampling points (S.pt.) of the process chain are illustrated in Figure 2. A matrix

of the analyzed components at the available sampling points is provided in the supporting information of this article. Prior to gas chromatography (GC) analysis, the water containing sampling streams were dried over two gas washing bottles filled with ethylene glycol, which were connected in series. The flasks were placed in a temperature controlled cooling box at -3 °C. A flask filled with glass wool was subsequently removing aerosols from the stream. The sampling flow rate was adjusted with a needle valve upstream to a vacuum pump. A gas meter from Kromschröder (BKG2.5T) was used to quantify the volumetric flow rate of the dry sampling gas at ambient pressure. A corresponding increase in weight of the ethylene glycol filled flasks enabled a parallel estimation of the water content. A figure of the sampling line can be found in the supporting information of this article.

The main gas components (CO₂, N₂, CO, O₂, CH₄, C₂H₆, C₂H₄ and C₂H₂) were separated in a combination of two different columns (7' HayeSep N, 60/80 1/8" SF and 9' Molecular Sieve 13x 45/60, 1/8" SF) in a GC (Clarus 500TM) from Perkin ElmerTM. A thermal conductivity detector (TCD) was used for quantification. The sulfur components (H₂S, COS, C₄H₄S, CH₃CH₂SH, and CH₃SH) were separated in a different column (Rt-XL Sulfur 1 m.x 0.95 mm OD) and quantified by a flame photometric detector (FPD).

Tar sampling is also illustrated in the supporting information. A combination of two cooling boxes was applied. Scrubbing bottles filled with 50 mL or 100 mL of toluene were applied to dissolve tar components. Three gas washing bottles were placed in an ice bath at 0 °C and two additional impingers were placed in a temperature controlled cooling box at -8 °C. For each tar analysis a sampling stream of $2 \frac{L_n}{\text{min}}$ was taken over a period of 8 hours. For detection of the tar components a GC from Perkin ElmerTM (XL GCTM) coupled with a mass spectrometer from Perkin ElmerTM (Turbo Mass MSTM) was used. A detailed description of the applied method for tar analysis can be found in²⁸.

BTEX were measured by gas chromatography - mass spectrometry (GC-MS, Shimadzu QP2010 PlusTM) at Vienna University of Technology. Six samples of each relevant point of the process were taken by means of gas sampling bags. For the quantification of NH₃ an

absorption method was used. A sample of $1 \frac{L_n}{min}$ was extracted from the process for three hours and passed through three gas washing bottles connected in series in a cooling bath at $0 \text{ }^\circ\text{C}$. The bottles were filled with $0.05 \text{ M H}_2\text{SO}_4$, which solves NH_3 in the form of NH_4^+ ions. NH_4^+ ions were quantified by ion chromatography (Dionex ICS 5000TM).

It could be considered that the wood gas fed into the pilot plant was saturated with water corresponding to the operation temperature and pressure of the CHP plant scrubber.¹⁶ The water addition upstream the catalyzed WGS reaction was quantified gravimetrically and monitored with a variable area flow meter. Additionally the flow rate of condensate formed in the scrubber was quantified volumetrically. The H_2 content in the dry gas was determined via mass balance. Volumetric flow rates of the dry PSA feed and the raffinate were quantified by diaphragm gas meters. The adsorbate flow rate and composition were calculated via mass balance. The flow rate of the wood gas at the inlet of the WGS unit was calculated via mass balance based on the feed flow rate of the PSA and the change of the gas composition according to the WGS reaction.

Results and Discussion

During the presented long-term experiment the CHP plant Oberwart was constantly generating an average of $2100 \frac{\text{m}^3_{\text{db}}}{\text{h}}$ of wood gas, of which $350 \frac{\text{m}^3_{\text{db}}}{\text{h}}$ were recycled back into the combustion zone of the DFB reactor. The outlet temperature of the CHP plant scrubber was $35 \pm 6 \text{ }^\circ\text{C}$. Assuming a relative humidity of $100 \text{ } \%$ at the outlet of this scrubber, a humidity of approximately $5 \text{ mol.}\%_{\text{wb}}$ could be calculated in the feed gas of the experimental setup.¹⁶

The pilot plant for H_2 production was successfully operated continuously for almost 250 hours. This section gives an overview of the performance of each operation unit as well as the results of the detailed chemical analysis of the entire process chain. The results of the chemical analysis are presented with respect to the analyzed substance class (main gas

components, sulfur components, BTEX components, tar components, and ammonia). Next, the mass balance of the process is presented and visualized in a Sankey diagram. Finally, the issue energy consumption is discussed and a brief outlook is given.

Water Gas Shift Unit

The performance of the WGS unit is illustrated in Figure 3, summarizing all three reactors. The measured gas compositions are plotted on a logarithmic scale and can be compared with the WGS equilibrium at the corresponding outlet temperature of each reactor. Within the first 10 cm of the catalyst bed in the first reactor, the temperature increased by about 60 °C due to the exothermic WGS reaction. The temperature profile demonstrates that the main share of CO was converted within this section of the catalyst bed. Subsequently, the temperature along the bed height decreased due to heat losses. The inlet temperatures of the reactors 2 and 3 were steadily lowered in order to harness lower equilibrium CO contents.

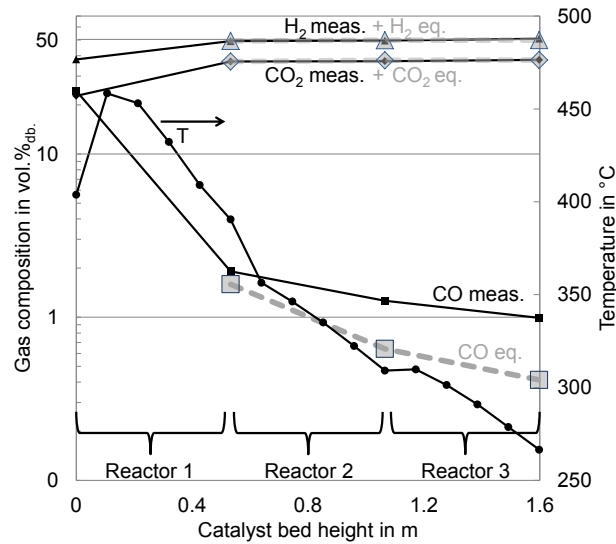


Figure 3: Results of the WGS unit, measured (meas.) and equilibrium (eq.) gas composition as well as temperature along the bed height; the sulfidation procedure (Equation 4) at the present operating temperature was only completed for Reactor 1 and Reactor 2 (also see Table 7).

At the outlet of the WGS unit the CO content could be reduced to about 1 vol.%_{db} (also

see Table 6), representing a CO conversion rate of 95 % and a H₂ recovery of 160 % within this unit. The dry volumetric flow rate was increased from 0.56 $\frac{\text{m}^3_{\text{db}}}{\text{h}}$ to 0.70 $\frac{\text{m}^3_{\text{db}}}{\text{h}}$ while the H₂O content was lowered from 56 to 45 mol.%_{wb}. Low GHSV, low sulfur loads in the feed gas (see Table 7), and the approach of temperature optimization enabled high overall conversion rates.¹⁵ However, especially in the reactors 2 and 3 a complete equilibration of the WGS reaction could not be reached. In order to further enhance the CO conversion in these reactors, the temperature should have been set higher. This is demonstrated by an increasing deviation of the equilibrium CO content and the measured CO content. By means of this, the amount of catalyst could have been reduced significantly maintaining the same CO conversion rate. Industrially applied FeO₃/Cr₂O₃ based catalysts are operated at GHSV of 400–1200 h⁻¹.²

Scrubber Unit

The scrubber unit was capable of cooling the shifted gas to 0 °C. Hence, it could be assumed that only a negligible amount of H₂O was present at the inlet of the PSA unit. A condensate flow rate of 0.32 $\frac{\text{L}}{\text{h}}$ was generated in the scrubber, which corresponded to the overall water balance of the process chain. The performance of the scrubber in terms of tar separation and removal of other undesired gas components is shown in Tables 7–10.

Pressure Swing Adsorption Unit

A parameter study of the PSA unit was carried out previous to the long-term experiment. During the study, a steady state operation of the upstream equipment was maintained. The operation parameters adsorption time and equalization pressure were varied, revealing a trade-off between the purity of the product and the H₂ recovery. At a fixed equalization pressure (4.5 bara) the effect of a variation in adsorption time on the content of the impurities is shown in Figure 4. Increasing amounts of contaminants were analyzed at longer adsorption times. Similar results were achieved at an equalization pressure of 4.0 bara.

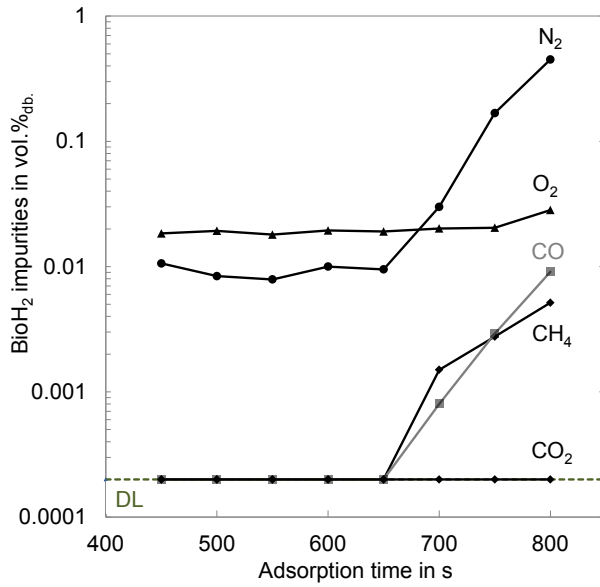


Figure 4: Results of PSA parameter study: BioH₂ impurities over adsorption time at an equalization pressure of 4.5 bara, DL = Detection Limit = 2 vol.ppm.

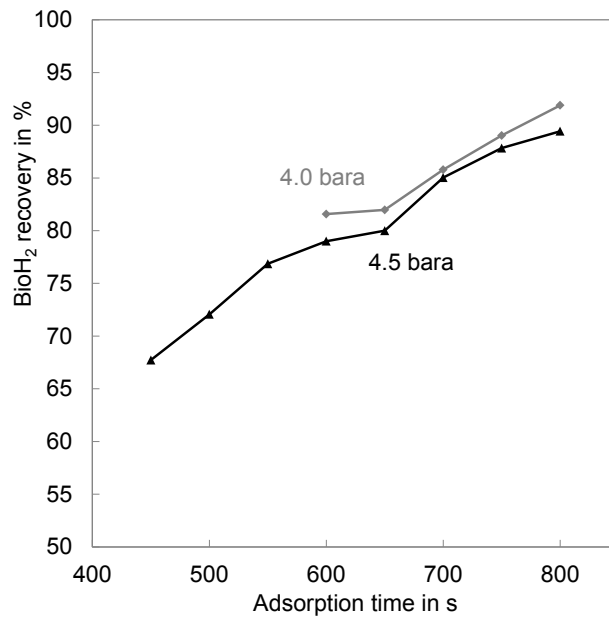


Figure 5: Results of PSA parameter study: BioH₂ recovery over adsorption time at an equalization pressure of 4.0 and 4.5 bara.

The influence of varying pressure equalization as well as adsorption time on the H₂ recovery is shown in Figure 5. As shown, the H₂ recovery was improved at lower equalization pressures of the PSA unit.

The aim of this study was to optimize the H₂ recovery provided that the components CO, CO₂ and CH₄ were reduced below the detection limit (BDL, 2 vol.ppm_{db}). As a result, the parameters in Table 3 (adsorption time of 650 s and equalization pressure of 4.5 bara) were chosen for the reported steady state operation during the 250 hours of continuous experimentation.

Under these fixed conditions, an H₂ purity of 99.97 vol.%_{db} as well as an H₂ recovery of 80.0 % were reached. These results are within the range of similar reported PSA systems obtaining H₂ purities up to 99.99 vol.%_{db} and H₂ recoveries between 70 % and 85 %²⁹⁻³³. The volumetric feed flow rate of 0.70 $\frac{\text{m}^3}{\text{h}}_{db}$ was split into an adsorbate fraction of 0.42 $\frac{\text{m}^3}{\text{h}}_{db}$ and a raffinate fraction (BioH₂) of 0.28 $\frac{\text{m}^3}{\text{h}}_{db}$. As shown in Table 6, the only detected impurities in the PSA raffinate were O₂ with 0.02 vol.%_{db} and N₂ with 0.01 vol.%_{db}.

Fuel Cell Unit

To demonstrate the high purity of the PSA raffinate, the generated BioH₂ was fed into a PEM fuel cell (MobixaneTM from AXANETM). The unit was operated flawlessly for over three hours. The comparison between its operation with the produced BioH₂ and Alphagaz 1TM H₂ is shown in Table 5.

Table 5: Comparison of the PEM fuel cell performance with BioH₂ and Alphagaz 1TM.

	BioH ₂	Alphagaz TM	Unit
Purity	≥ 99.97	≥ 99.999	vol.%
\dot{V}_{H_2}	0.28 ± 0.01	0.28 ± 0.01	$\frac{\text{m}^3}{\text{h}}$
p _{Feed}	1268 ± 27	1245 ± 24	mbara
T _{Fuel cell}	40.5 ± 1.5	36.8 ± 0.9	°C
η_{gross}	53.9 ± 1.0	54.2 ± 1.0	% _{LHVbase}

It could be demonstrated that there was no significant difference in the fuel cell perfor-

mance comparing the operation with BioH₂ and the operation with Alphagaz 1TM in the investigated period. It can be distinguished between the gross electrical efficiency and the net electrical efficiency of the fuel cell. In Table 5 the gross electrical efficiencies are presented. The inverter and the peripherals of the fuel cell cause a decrease of its electrical efficiency and account for the net electrical efficiency. A gross electrical efficiency of about 54 % was obtained which is in good accordance to²¹. The obtained value for the net electrical efficiency was not representative as the unit was operated below its nominal power range. The issue of electrical efficiencies and the setup of this fuel cell are described in detail in^{12,34}.

Chemical Analysis and Mass Balance

In this chapter the evolution of the dry gas composition along the process chain is presented. The results have to be regarded in combination with the corresponding sampling points (S.pt.) illustrated in Figure 2. All results are measured gas compositions, except for the mean adsorbate composition which was calculated via mass balance (the feed flow rate and the composition of the adsorbate vary strongly as a function of the cyclic PSA operation). Table 6 depicts the evolution of the main gas components on a dry base, detected with the TCD detector of the GC.

In Table 6, the given CO concentrations over the WGS unit represent a CO conversion rate of about 90.5 % at the outlet of the first reactor (GHSV_{wb} 510 h⁻¹) and a CO conversion rate of about 93.5 % at the outlet of the second reactor (GHSV_{wb} 255 h⁻¹). At the outlet of the last reactor (GHSV_{wb} 170 h⁻¹) an overall CO conversion rate of about 95 % was reached. The H₂ content was increased from 38 vol. %_{db} to about 50 vol.%_{db}. The simultaneous increase in the dry gas flow rate by 25 % led to a general dilution effect. C₂H₂ was totally hydrogenated to C₂H₄ and could not be detected at the outlet of the WGS unit. C₂H₄ was assumed to be partly hydrogenated to C₂H₆. The overall mass balance of the C₂H_y components was approaching 98 %. The slightly higher content of H₂ in the PSA feed (4) compared to the outlet of the WGS unit (2c) could be explained by the low solubility of

Table 6: Results of the analysis of the main gas components in vol.%_{db}; Sampling points (S.pt.) are illustrated in Figure 2; BDL = Below Detection Limit, DL = Detection Limit = 2 vol.ppm_{db}; the adsorbate composition (5) was calculated via mass balance.

S.pt.	CO ₂	C ₂ H ₄	C ₂ H ₆
1	22.7±0.8	2.3±0.3	0.17±0.03
2a	36.9±0.8	1.8±0.1	0.17±0.02
2b	37.0±0.8	1.8±0.1	0.17±0.03
2c	37.1±0.9	1.9±0.2	0.18±0.02
4	36.9±0.2	1.6±0.3	0.14±0.03
5	61.4	2.6	0.23
6	BDL	BDL	BDL
S.pt.	C ₂ H ₂	O ₂	N ₂
1	0.15±0.02	0.1±0.02	2.3±0.4
2a	0.001±0.001	0.06±0.01	1.8±0.1
2b	BDL	0.08±0.04	2±0.1
2c	BDL	0.07±0.06	1.9±0.3
4	BDL	0.03±0.01	1.5±0.1
5	BDL	0.03	2.6
6	BDL	0.02±0.0003	0.01±0.004
S.pt.	CH ₄	CO	H ₂
1	10.0±0.3	24±1	38.0±1.2
2a	8.2±0.1	1.9±0.3	49.2±0.9
2b	8.1±0.2	1.3±0.2	49.5±0.9
2c	8.2±0.2	1.0±0.1	49.6±0.9
4	8.0±0.2	0.98±0.04	50.9±0.4
5	13.3	1.63	18.2
6	BDL	BDL	99.97±0.004

hydrogen in water as well as by the removal of a series of gas components in the scrubber unit (e.g. benzene and ammonia). It is also seen that O₂ and N₂ were the only detectable impurities that were fed into the fuel cell. O₂ is reported to be tolerated up to 500 vol.ppm and N₂ has only dilution effects on the PEM fuel cell.²⁰

The evolution of the sulfur components along the process is provided in Table 7.

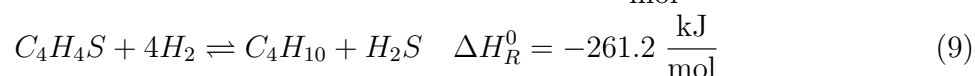
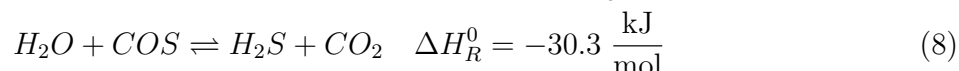
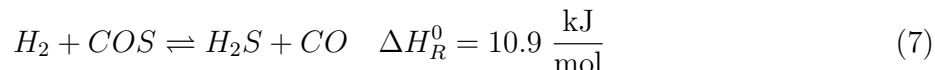
Table 7: Results of the analysis of the sulfur components (in vol.ppm_{db}); DL = 0.3 vol.ppm_{db}

S.pt.	H ₂ S	COS	C ₄ H ₄ S
1	59±10	1.0±0.1	7.2±3.1
2a	49±4	BDL	2.0±0.7
2b	50±3	BDL	1.0±0.5
2c	4±1	BDL	1.0±0.6
4	2.5±0.3	BDL	0.3±0.01
5	0.4±0.3	BDL	0.5±0.3
6	BDL	BDL	BDL

As proved by constant H₂S concentrations, the catalyst sulfidation was completed in the first two reactors, where the main CO conversion took place. However, only 4 vol.ppm_{db} of H₂S were measured after the third reactor, which shows an incomplete sulfidation of this stage during the presented study. Compared to the conditioning of the catalyst (carried out before the test run, 400 hours of operation at 350 °C) the last reactor was now operated at a lower temperature level which provided a favorable condition for an enhanced catalyst sulfidation³⁵. The WGS unit was basically designed for higher GHSV than applied during the operation of the process chain. In more recent experiments, the same conversion rate of 95 % could be achieved with the completely sulfided catalyst (same concentration of H₂S at the inlet and outlet) at GHSV_{wb.} of about 500 h⁻¹ and slightly higher operating temperatures.

COS was not detected at the outlet of the WGS unit, which could be explained by the reactions shown in Equations 7 and 8. The decrease in thiophene (C₄H₄S) along the WGS unit is suggested to be due to the reaction of thiophene hydrogenolysis in Equation 9.¹⁵ Less C₄H₄S and H₂S could be detected after gas scrubbing. The organic C₄H₄S was assumed to dissolve in the RME whereas the H₂S dissolved in the condensate. Table 7

also indicates that a fraction of the H_2S present in the feed was captured in the PSA unit. However, previous experiments at the PSA unit showed a complete desorption of H_2S from the activated charcoal at higher sulfur loads in the PSA feed.¹² The rather low sulfur load in the adsorbate was explained by adsorption effects of the used gas sampling bag.



Analyses of BTEX are shown in Table 8. In the WGS unit, no significant change in the content of benzene, toluene and xylene could be observed, apart from a dilution effect due to an increased volumetric gas flow rate. The hydrogenation of styrene (see Table 9) was assumed to be responsible for the formation of the ethylbenzene as a side reaction in the WGS unit. The scrubber unit removed the majority of the BTEX compounds. Only benzene and toluene could be detected at the inlet of the PSA unit. Analysis of the PSA raffinate and adsorbate suggests a complete adsorption and subsequent desorption of these compounds from the activated carbon.

Table 8: Results of the analysis of benzene, toluene, ethylbenzene, xylene (BTEX, in vol.ppm_{ab}); DL = 1 vol.ppm_{ab}

S.pt.	B	T	E	X
1	3296±36	201±5	1.3±0.6	1.1±0.6
2c	2850±54	176±6	33±12	2.2±0.9
4	536±5	17±2	BDL	1.2±0.6
5	641±13	21±1	BDL	BDL
6	BDL	BDL	BDL	BDL

The results of the tar analysis in Table 9 are based on three continuous long-term samples. Therefore, no standard deviations can be given. As a side reaction in the WGS unit, styrene and indene were probably hydrogenated to form ethylbenzene (see Table 8) and indane (not analyzed). Furthermore, a hydrogenation of phenylacetylene to ethylbenzene

as well as a hydrogenation of acenaphthylene to acenaphthene could be assumed. Besides the frequently observed dilution effect, naphthalene as the predominant tar component was probably not affected in the WGS unit. In the scrubbing unit all measured tar components except naphthalene could be removed to below the detection limit.

Table 9: Results of the analysis of tar components (one continuous sample) in $\frac{\text{mg}}{\text{m}_n^3 \text{ db}}$; DL = $1 \frac{\text{mg}}{\text{m}_n^3 \text{ db}}$.

Tar component	S.pt.		
	1	2c	3
Naphthalene	1139	824	2
Styrene	247	BDL	BDL
Indene	191	9	BDL
Phenylacetylene	25	BDL	BDL
Mesitylene	BDL	4	BDL
Benzofuran	2	BDL	BDL
1-Benzothiophene	2	BDL	BDL
2-Methylnaphthalene	5	4	BDL
1-Methylnaphthalene	3	2	BDL
Biphenyl	1	BDL	BDL
Acenaphthylene	13	BDL	BDL
Acenaphthene	2	7	BDL
Anthracene	2	4	BDL
Flouranthene	1	3	BDL
Pyrene	1	3	BDL

The results of the NH_3 analysis in Table 10 are also based on one continuous sample per sampling point. Therefore, no standard deviations can be given. Apart from the dilution effect in the WGS unit, no influence of the catalyst on the NH_3 was observed. In the scrubbing unit, the amount of NH_3 was reduced below the detection limit. Hence, there was no NH_3 present at the inlet of the PSA unit.

Table 10: Results of the analysis of NH_3 (one continuous sample) in vol.ppm_{db} ; $\text{DL} = 1 \text{ vol.ppm}_{db}$

S.pt.	NH_3
1	954
2c	740
3	1
4	BDL

Summing up, the aim of this polygeneration approach was to minimize its complexity at acceptable H_2 recoveries. The process used one single compression step and worked flawlessly for 250 hours. The obtained flow rates and water contents over the process chain are summarized in Table 11. The global mass balance of the established process is also illustrated by means of the Sankey diagram in Figure 6. The width of the arrows is shown proportionally to the molar flow of each component.

Table 11: Mass balance and H_2O content over the process chain, water considered as an ideal gas at standard conditions.

S.pt.	Description	Flow rate $\frac{\text{m}^3_{wb}}{\text{h}}$	H_2O content $\text{vol.}\%_{wb}$
1	Raw gas	0.60	5.21
2	WGS in	1.28	55.82
2c	WGS out	1.28	45.46
3	RME out	0.71	0.84
4	PSA in	0.70	0
5	Adsorbate	0.28	0
6	BioH_2	0.42	0

The diagram shows that more H_2 could be separated in the PSA unit than H_2 was present in the wood gas feed. The overall hydrogen recovery of 128 % was enabled by the production of additional H_2 in the WGS unit (recoveries of the single process steps: 160 % in the WGS unit, 100 % in the gas scrubber, and 80 % in PSA unit).

$0.56 \frac{\text{m}^3_{db}}{\text{h}}$ of dry wood gas was extracted after the scrubber of the CHP plant Oberwart. Catalysis of the WGS reaction caused an increase in the dry volumetric flow rate to $0.70 \frac{\text{m}^3_{db}}{\text{h}}$, decreasing the CO content from about 24 to 1 $\text{vol.}\%_{db}$. In the PSA unit the feed was split into $0.42 \frac{\text{m}^3_{db}}{\text{h}}$ of adsorbate and $0.28 \frac{\text{m}^3_{db}}{\text{h}}$ of raffinate, respectively BioH_2 . The only

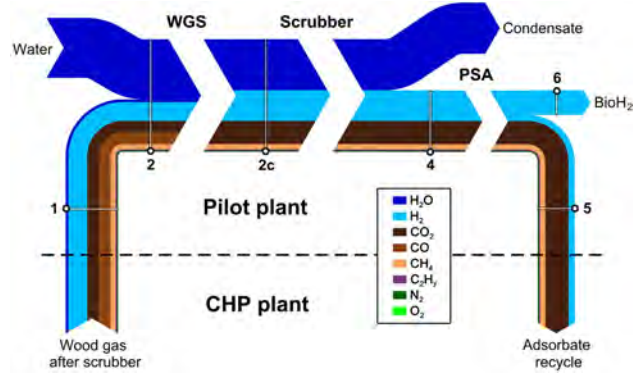


Figure 6: Sankey diagram of the process chain; the width of the arrows is shown proportionally to the molar flow of each component; including sampling points of chemical analysis.

detectable impurities in the PSA raffinate were O_2 (0.02 vol.%_{db}) and N_2 (0.01 vol.%_{db}). This gas composition enabled the operation of a PEM fuel cell.

Within this working group a master thesis was carried out to evaluate the presented process chain in terms of energy consumption³⁶. It was distinguished between the electricity demand for pumps and compressors, the heating demand and the cooling demand. A specific energy demand of $0.57 \frac{kWh_{el}}{m_n^3 BioH_2}$, $1.71 \frac{kWh_{cool}}{m_n^3 BioH_2}$, and $2.12 \frac{kWh_{heat}}{m_n^3 BioH_2}$ was calculated by means of the process simulation software IPSEproTM (LHV of H_2 : $3 \frac{kWh}{m_n^3}$). In order to reduce the heat demand for steam production, wood gas for $BioH_2$ production should be extracted upstream the scrubber of the CHP plant. A water content of already 35 mol.%_{wb} can be estimated at this point of the process.¹⁴ In that case, the catalyst of the WGS unit would have to face a considerably higher load of impurities. Future experimental work will cover the long-term stability of the catalyst in combination with this tar rich wood gas. Apart from this, an adsorption tube will be installed in the feed of the fuel cell in order to reduce the detection limit of impurities in the $BioH_2$.

A positive overall assessment will provide the basis for an upscale of the process to a capacity of about $50 \frac{m^3}{h} BioH_2$.

Acknowledgement

The authors would like to thank the project partners: Energie Burgenland, Air LiquideTM, Binder Industrieanlagenbau and cts. The company Clariant[©] is gratefully acknowledged for providing the WGS catalyst. Especially the CHP plant Oberwart should be thanked for providing a unique working environment and a stable supply of wood gas. The long-term conditioning of the WGS catalyst could only be achieved with the help of Matthias Binder. Christian Jordan is thanked for his commitment related to BTEX analysis. Nicolas Diaz received financial support from Conicyt-Becas Chile. Several research projects collaborated to realize the presented process chain: “Polygeneration 2” (Bioenergy2020+), “Green H₂” (FFG) and “Simple SNG” (FFG). Bioenergy2020+ is funded within the Austrian COMET program managed by the Austrian Research Promotion Agency (FFG). The financial support of the funding association FFG and the Austrian Climate and Energy Fund is gratefully acknowledged.

Supporting Information Available

The supporting information of this article provides pictures of the CHP plant Oberwart, the installed WGS unit, the PSA unit, and the PEM fuel cell. It also includes a matrix of the analyzed components and the available sampling points, as well as a flowchart of the sampling line for chemical analysis.

This material is available free of charge via the Internet at <http://pubs.acs.org/>.

References

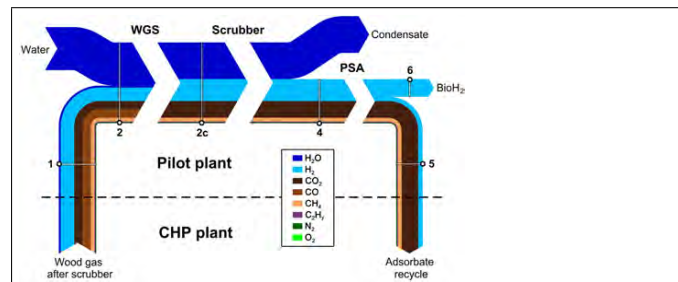
1. IEA, Hydrogen Production and Distribution, International Energy Agency - Energy Technology Essentials. 2007.
2. Liu, K.; Song, C.; Subramani, V. *Hydrogen and Syngas Production and Purification Technologies*; Wiley, 2010; pp 14–17, 313.
3. Dunn, S. Hydrogen futures: toward a sustainable energy system. *Int. J. Hydrogen Energy* **2002**, *27*, 235–264.
4. Hefner, R. A. The age of energy gases. *Int. J. Hydrogen Energy* **2002**, *27*, 1 – 9.
5. Chaubey, R.; Sahu, S.; James, O. O.; Maity, S. A review on development of industrial processes and emerging techniques for production of hydrogen from renewable and sustainable sources. *Renew. Sust. Energ. Rev.* **2013**, *23*, 443 – 462.
6. Gahleitner, G. Hydrogen from renewable electricity: An international review of power-to-gas pilot plants for stationary applications. *Int. J. Hydrogen Energy* **2013**, *38*, 2039 – 2061.
7. Abbasi, T.; Abbasi, S. Renewable hydrogen production: Prospects and challenges. *Renew. Sust. Energ. Rev.* **2011**, *15*, 3034 – 3040.
8. Tock, L.; Maréchal, F. Co-production of hydrogen and electricity from lignocellulosic biomass: Process design and thermo-economic optimization. *Energy* **2012**, *45*, 339 – 349.
9. Moreno, J.; Dufour, J. Life cycle assessment of hydrogen production from biomass gasification. Evaluation of different Spanish feedstocks. *Int. J. Hydrogen Energy* **2013**, *38*, 7616 – 7622.

10. Susmozas, A.; Iribarren, D.; Dufour, J. Life-cycle performance of indirect biomass gasification as a green alternative to steam methane reforming for hydrogen production. *Int. J. Hydrogen Energy* **2013**, *38*, 9961 – 9972.
11. Energie Burgenland - Booklet Biomassevergasungskraft Oberwart. 2014.
12. Diaz, N. Hydrogen Separation from Producer Gas Generated by Biomass Steam Gasification. Ph.D. thesis, Vienna University of Technology, 2013.
13. Hofbauer, H.; Rauch, R.; Bosch, K.; Koch., R.; Aicherning, C. In *Biomass CHP Plant Güssing, A Success Story*; Bridgwater, A., Ed.; CPL Press, 2003; pp 527–536.
14. Kotik, J. Über den Einsatz von Kraft-Wärme-Kopplungsanlagen auf Basis der Wirbelschicht-Dampfvergasung fester Biomasse am Beispiel des Biomassekraftwerks Oberwart. Ph.D. thesis, Technische Universität Wien, 2010.
15. Twigg, M. V. *Catalyst Handbook, 2nd Edition - Chapter 6: The Water-Gas Shift Reaction*; Manson Publishing, 1989; pp 200–201, 283–288, 302–306.
16. Pröll, T.; Siefert, I. G.; Friedl, A.; Hofbauer, H. Removal of NH₃ from Biomass Gasification Producer Gas by Water Condensing in an Organic Solvent Scrubber. *Ind. Eng. Chem. Res.* **2005**, *44*, 1576–1584.
17. Ruthven, D. M. *Pressure Swing Adsorption*; VCH, 1994; pp 235–238.
18. EG & G Technical Services, I. *Fuel Cell Handbook*; US Department of Energy, 2004.
19. Benesch, R.; Jacksier, T. Hydrogen and material quality issues for PEM fuel cells. Vehicle Power and Propulsion, 2005 IEEE Conference. 2005; pp 646–651.
20. Besancon, B. M.; Hasanov, V.; Imbault-Lastapis, R.; Benesch, R.; Barrio, M.; Milnikov, M. J. Hydrogen quality from decarbonized fossil fuels to fuel cells. *Int. J. Hydrogen Energy* **2009**, *34*, 2350–2360.

21. Kurzweil, P. In *Brennstoffzellentechnik*; Fister, M., Ed.; Springer Vieweg, 2013; pp 87, 98.
22. Blessing, I.; Gardner, C.; Ternan, M. Separation of hydrogen from a hydrogen / methane mixture using a PEM fuel cell. *Int. J. Hydrogen Energy* **2007**, *32*, 908–914.
23. Fail, S.; Diaz, N.; Konlechner, D.; Hackel, M.; Sanders, E.; Rauch, R.; Harasek, M.; Bosch, K.; Schwenninger, F.; Zapletal, P.; Schee, Z.; Hofbauer, H. An Experimental Approach for the Production of Pure Hydrogen Based on Wood Gasification, Proceedings of the International Conference for Polygeneration Strategies (ICPS). 2013.
24. Hla, S. S.; Morpeth, L.; Sun, Y.; Duffy, G.; Ilyushechkin, A.; Roberts, D.; Edwards, J. A CeO₂-La₂O₃-based Cu catalyst for the processing of coal-derived syngases via high-temperature water gas shift reaction. *Fuel* **2013**, *114*, 178 – 186.
25. Shiratori, Y.; Ijichi, T.; Oshima, T.; Sasaki, K. Internal reforming SOFC running on biogas. *Int. J. Hydrogen Energy* **2010**, *35*, 7905 – 7912.
26. Bartholomew, C. H. Mechanisms of catalyst deactivation. *Appl. Catal. A-Gen.* **2001**, *212*, 17 – 60, Catalyst Deactivation.
27. Moine, S. Mobixane operation manual. Axane Fuel Cell Systems, 2009.
28. Wolfesberger, U.; Aigner, I.; Hofbauer, H. Tar Content and Composition in Producer Gas of Fluidized Bed Gasification of Wood-Influence of Temperature and Pressure. *Environ. Prog. Sust. Energy* **2009**, *28*, 372–379.
29. Yang, J.; Hana, S.; Chob, C.; Lee, C.-H.; Lee, H. Bulk separation of hydrogen mixtures by a one-column PSA process. *Sep. Purif. Technol.* **1995**, *5*, 239–249.
30. Ribeiro, A. M.; Grande, C. A.; Lopes, F. V.; Loureiro, J. M.; Rodrigues, A. E. A parametric study of layered bed PSA for hydrogen purification. *Chem. Eng. Sci.* **2008**, *63*, 5258–5273.

31. Park, J.-H.; Kim, J.-N.; Cho, S.-H. Performance analysis of four-bed H₂ PSA process using layered beds. *AIChE J.* **2000**, *46*, 790–802.
32. Ahn, S.; You, Y.-W.; Lee, D.-G.; Kimb, K.-H.; Oh, M.; Lee, C.-H. Layered two- and four-bed PSA processes for H₂ recovery from coal gas. *Chem. Eng. Sci.* **2012**, *68*, 413–423.
33. Lopes, F. V.; Grande, C. A.; Rodrigues, A. E. Activated carbon for hydrogen purification by pressure swing adsorption: Multicomponent breakthrough curves and {PSA} performance. *Chem. Eng. Sci.* **2011**, *66*, 303 – 317.
34. Kraussler, M. PEM Fuel Cell Operation and Applications Using BioH₂. M.Sc. thesis, Vienna University of Technology, 2014.
35. Morpeth, L.; Sun, Y.; Hla, S. S.; French, D.; Duffy, G.; Edwards, J. Effect of H₂S on the performance of La_{0.7}Ce_{0.2}FeO₃ perovskite catalyst for high temperature water-gas shift reaction. *Int. J. Hydrogen Energy* **2012**, *37*, 1475 – 1481.
36. Hinteregger, J. Performance Evaluation of Process Chains for the production of BioH₂ from Wood Gas. M.Sc. thesis, Vienna University of Technology, 2014.

Graphical TOC Entry



Sankey diagram of the investigated process chain for BioH₂ production.

For Table of Contents Use Only

Manuscript title:

Wood Gas Processing to Generate Pure Hydrogen Suitable for PEM Fuel Cells.

Names of authors:

Silvester Fail, Nicolas Diaz, Florian Benedikt, Michael Kraussler, Julian Hinteregger, Klaus Bosch, Marius Hackel, Reinhard Rauch, Hermann Hofbauer.

Brief synopsis describing the graphic and explaining how the paper relates to sustainability:

The graphic illustrates the performance of the investigated process chain for biohydrogen (BioH₂) production. Nowadays the industrial hydrogen production is strongly based on fossil fuels. This work demonstrates the technical feasibility of a sustainable process based on thermochemical processing of biomass.

Supporting Information –

Wood Gas Processing to Generate Pure Hydrogen Suitable for PEM Fuel Cells

Silvester Fail,^{*} Nicolas Diaz, Florian Benedikt, Michael Kraussler, Julian Hinteregger, Klaus Bosch, Marius Hackel, Reinhard Rauch, and Hermann Hofbauer

E-mail: silvester.fail@tuwien.ac.at

The supporting information of this article has 4 pages excluding the cover sheet. It includes 4 figures and 1 table.

- Figure 1: S1 – Picture of the combined heat and power (CHP) plant Oberwart, Austria.
- Figure 2: S2 – Picture of the water gas shift (WGS) unit for hydrogen enrichment.
- Figure 3: S3 – Picture of the pressure swing adsorption (PSA) unit for hydrogen purification and the proton exchange membrane (PEM) fuel cell for the application of the generated biohydrogen (BioH₂).
- Figure 4: S4 – Flowchart of the sampling line for chemical analysis of the main gas components, sulfur, tar, and water.
- Table 1: S1 – Matrix of sampling points and the corresponding chemical analysis.

^{*}To whom correspondence should be addressed

Supporting Information Available



Figure 1: S1 – Picture of the CHP plant Oberwart, Austria.



Figure 2: S2 – Picture of the WGS unit employed for fixed bed catalysis of the WGS reaction.



Figure 3: S3 – Left: PEM fuel cell for the demonstration of the quality of the generated BioH₂; Right: PSA unit employed for H₂ separation of the preconditioned wood gas.

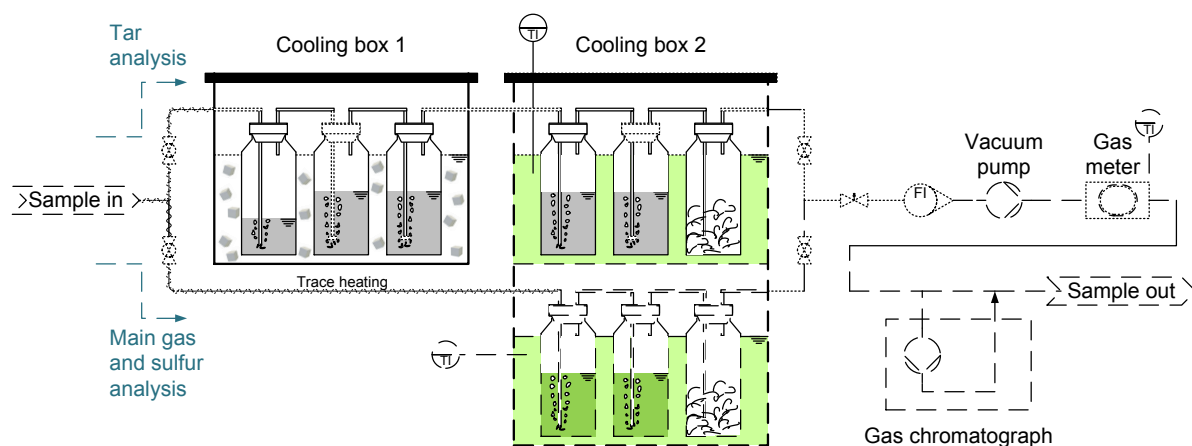


Figure 4: S4 – Sampling line of the experimental setup for chemical analysis of the main gas components, sulfur, tar, and water.

Table 1: S1 – Matrix of sampling points and the corresponding chemical analysis. The volumetric flow rates of the PSA feed, the raffinate, and the water addition were determined.

Analysis	Sampling point								
	1	2	2a	2b	2c	3	4	5	6
Main gas components	✓		✓	✓	✓		✓	✓	✓
Sulfur components	✓		✓	✓	✓		✓	✓	✓
Tar	✓				✓	✓			
Water	✓	✓	✓	✓	✓	✓	✓		
BTEX	✓				✓		✓	✓	✓
Ammonia	✓				✓	✓	✓		
Flow rate							✓		✓

This material is available free of charge via the Internet at <http://pubs.acs.org/>.

Chapter 8

Conclusions and outlook

Thermochemical processing can be carried out in order to produce hydrogen (biohydrogen, BioH₂) based on woody biomass. In this context, dual fluidized bed steam gasification of wood chips represents a promising technology. Wood gas with a low content of nitrogen and a high hydrogen content of about 40 vol.%_{db}. can be generated by means of this process.

The aim of this predominately experimental work was to investigate the applicability of the catalysis of the water gas shift reaction (WGSR) in wood gas. This technology provides an interesting sub-process with respect to the production of hydrogen based on thermal processing of woody biomass. By means of the catalyzed WGSR, contained carbon monoxide together with steam can be converted to additional hydrogen and carbon dioxide. Provided that carbon monoxide is converted almost completely, the hydrogen content in the wood gas mixture can be increased up to about 50 vol.%_{db}. Due to the production of additional hydrogen, a process aiming the production of biohydrogen can achieve significantly larger hydrogen yields per biomass input. Also, carbon dioxide can be separated more easily than carbon monoxide via the existing gas separation technologies (pressure swing adsorption or gas scrubbing).

Within this thesis two different commercially available catalysts were tested for the catalysis of the WGSR in wood gas. The first catalyst (Catalyst 1: Co/Mo-based) was developed for "sour shift" applications in gas mixtures containing hydrogen sulfide. The second catalyst (Catalyst 2: Fe/Cr-based) was developed for "sweet shift" processes downstream sulfur removal.

Both catalysts were investigated at two different experimental setups.

At the "Test rig for chemical kinetics" at the Vienna University of Technology, experiments were carried out on a laboratory scale using synthetic gas mixtures simulating wood gas composition. Based on these results, empirical power law rate models were established in order to describe the reaction kinetics for both catalysts. At higher temperatures, less sulfur was chemisorbed by both catalysts. The Co/Mo-based catalyst required sulfur to be present in the feed. Its activity increased strongly with increasing sulfur contents. In a reversible process, the activity of the Fe/Cr-based catalyst was reduced with increasing contents of hydrogen sulfide. The temperature response of Catalyst 2 was compared in a gas mixture

containing 100 vol.ppm_{db.} of hydrogen sulfide and a gas mixture without hydrogen sulfide. It was concluded that the performance of this catalyst was not affected by this sulfur content as long as the operating temperature is set higher than 320 °C. To sum it up, at the present sulfur load in the gas mixture, the activity of the Fe/Cr-based catalyst was higher than the activity of the Co/Mo-based catalyst. The poisoning effect of sulfur on Catalyst 2 got increasingly negligible at higher operating temperatures.

Based on preliminary experiments at the "Test rig for chemical kinetics", a pilot plant was designed to investigate the catalysis of the WGSR on a bigger scale using real wood gas derived from the combined heat and power plant in Oberwart, Austria. This commercial facility employs the dual fluidized bed steam gasification technology. Next to this facility, the designed pilot plant was assembled, commissioned and optimized within this thesis. This test rig was called "Pilot plant for catalytic wood gas processing" or WGS unit. About 2 $\frac{m^3}{h}$ of dry wood gas could be processed over three fixed bed reactors connected in series. At this pilot plant, both catalysts were exposed to real wood gas and successfully tested in the long term.

1500 hours of operation were achieved with the Co/Mo-based catalyst and about 800 hours of operation were achieved with the Fe/Cr-based catalyst. Also, at the "Pilot plant for catalytic wood gas processing" the performance of the Fe/Cr-based catalyst was significantly better than the performance of the Co/Mo-based catalyst. Once again, this was explained by the rather low sulfur load in the wood gas generated at the gasification power plant Oberwart (60–100 vol.ppm_{db.}).

Therefore, Catalyst 2 is recommended for future applications. Applying this Fe/Cr-based catalyst, a gas hourly space velocity on a wet base (GHSV_{wb.}) of about 400–500 h⁻¹, a steam to dry gas ratio at the inlet of at least 1, and inlet temperatures in the range of 350–400 °C should be adjusted in order to enable CO conversion rates of about 90 % (less than 2 vol.%_{db.} of CO in the raffinate). Using lower GHSV, higher steam to dry gas ratios at the inlet, and an approach of temperature optimization, CO conversion rates as high as 95 % (less than 1 vol.%_{db.} of CO in the raffinate) could be reached. The catalysis of the WGSR over a commercial Fe/Cr-based catalyst in real wood gas turned out to be a very stable process. During the first 800 hours of operation, no performance reduction of this catalyst could be observed. As a catalytic side effect, COS was converted to H₂S and some tar components were partly hydrogenated. Naphthalene as the most important tar component was not affected by the catalyst.

In cooperation with other research projects, this shifted gas mixture was further processed to produce pure hydrogen based on wood gas generated at the biomass steam gasification power plant in Oberwart. These results were summarized in [36] and [35]. The process chain 2 (described in Chapter 7.2) demonstrated the production of pure hydrogen by means of the catalyzed WGSR at the WGS unit, gas cleaning and drying by means of a gas scrubber, and hydrogen purification by means of pressure swing adsorption. As a demonstration of the high quality of the generated biohydrogen, a PEM fuel cell was operated in order to generate electricity and heat. This process chain should be preferred to process chain 1 (described in

Chapter 7.1) because of higher hydrogen yields and a lower specific electricity consumption.

Before considering an upscale of process chain 2 to a capacity of $50 \frac{\text{m}^3}{\text{h}}$ of hydrogen, a test run with tar-rich wood gas for about 1000–2000 hours is recommended to assure the long-term stability of the Fe/Cr-based catalyst.

As already discussed in the introduction of this work, most hydrogen is currently used for the synthesis of ammonia and methanol. Large hydrogen quantities are also required for the processing of crude oil in refineries.

Theoretically, also BioH₂ based on the thermochemical processing of woody biomass could be used for these applications. The production of BioH₂ based on wood gasification for refinery applications was already simulated in a PhD thesis [86]. The key result was that 30 MW_{th.} of hydrogen can be generated from 50 MW_{th.} of woody biomass by means of a process chain aiming the maximization of hydrogen production. In cooperation with OMV, this project was also submitted to the "NER300" funding program of the European Union.

However, large biomass-based facilities frequently suffer from low local availabilities of wood, high transport costs, rather low volumetric energy densities of biomass, and high prices of the raw material. These factors strongly limit the application and development of large scale biomass based plants; especially if the desired plant site is not available for transport by sea.

It is therefore questionable if large scale hydrogen production based on biomass provides an appropriate alternative to the established production methods based on fossil fuels. It was already discussed in the introduction, that these processes are not economically competitive. Decentral biomass-based facilities however, seem to represent a more promising future perspective.

Decentral biomass-based polygeneration plants can be regarded as a scenario for the future energy supply in rural areas. Within this work, the term polygeneration is defined as the simultaneous production of biofuels (here: BioH₂), electricity, and district heat. The advantage of these processes is, that analogous to combined heat and power plants, high overall efficiencies can be reached in polygeneration concepts. Also, the share of each product is not fixed and can be adjusted with respect to the current demand at the current season [56].

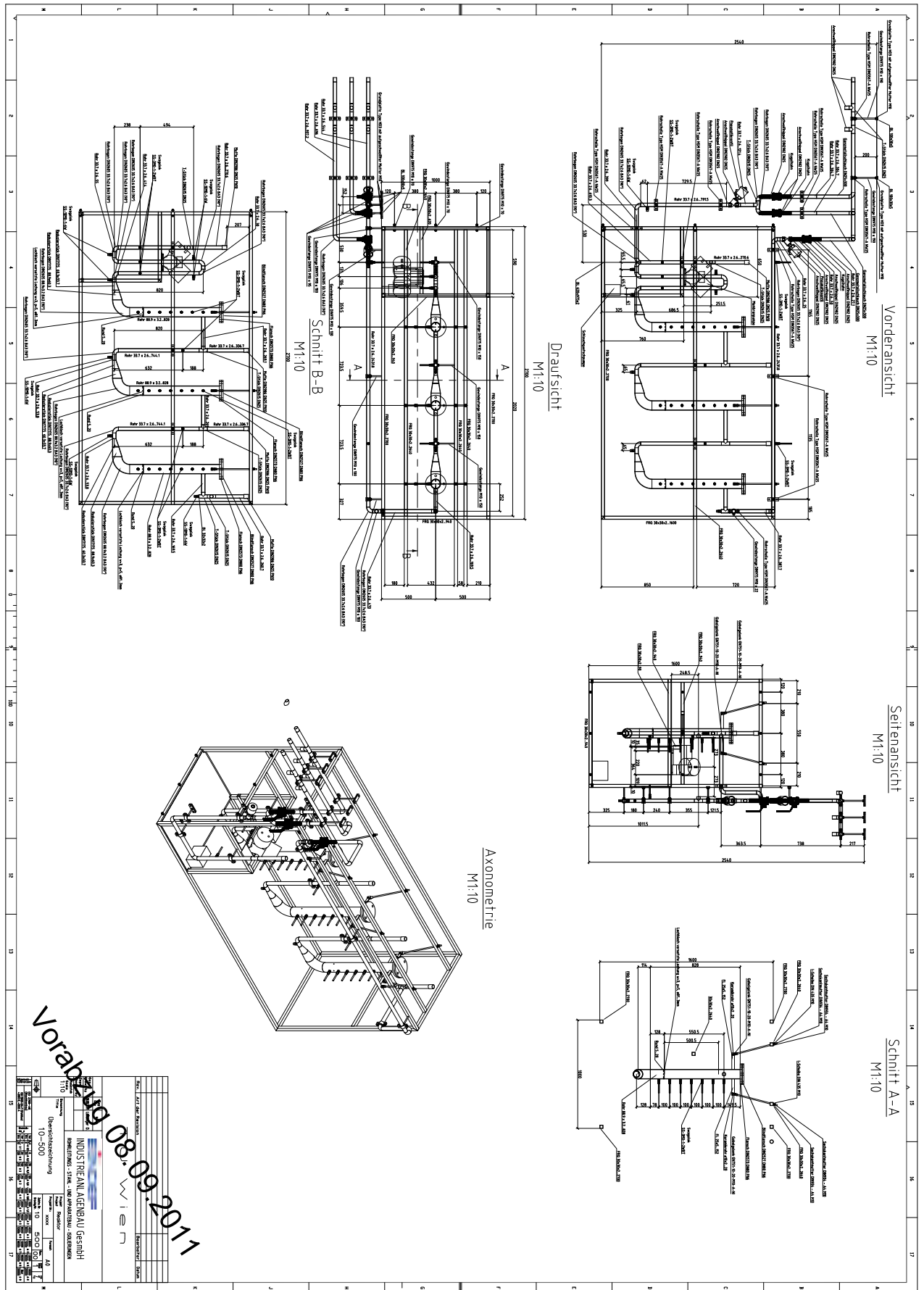
The possible applications of the generated BioH₂ were already discussed in a Master thesis that was carried out within this working group [71]. If the energetic usage of BioH₂ is desired, the first issue to be dealt with is the storage and the distribution of hydrogen. Hydrogen can be stored gaseous, in the liquid state, by physisorption, and as metal hydrid. Hydrogen fueling stations can be used to store the generated hydrogen and to enable the fueling of fuel cell vehicles or hydrogen based combustion engine cars. Depending on the storage technology of the fueling station, different material issues have to be faced. As an alternative, local hydrogen grids can be established for the distribution of the product. Perhaps the most simple and cheapest application of hydrogen produced by means of small decentral facilities, is the feeding into the natural gas grid. However strict statutory regulations have to be faced with respect to side gas components, and only a maximum H₂ content of 4 mol.% is tolerated in the Austrian natural gas grid [85]. If a cheap and clean source of carbon dioxide is available, also the methanation technology can be considered, enabling the unlimited feeding of the product into the national gas grid.

At any rate, the decentral hydrogen production based on biomass gasification seems to be

perfectly compatible with the increasing number of decentral power-to-gas installations [38]. The production of hydrogen based on renewable biomass and renewable electricity represents an interesting combination to satisfy the future needs for heat, electricity, and transportation fuel. A promising solution for the production of heat and electricity based on hydrogen, is the PEM fuel cell technology. Provided that future legislation tolerates higher hydrogen contents in the natural gas grid, PEM fuel cells represent also an interesting technology for the separation of hydrogen from a mixture of methane and hydrogen (or BioH₂ in natural gas) [16].

Chapter 9

Annex



List of Figures

2.1	Hydrogen production based on steam methane reforming (SMR).	11
2.2	Typical arrangement of an industrial WGS converter; based on [111].	15
2.3	Different reactor types of biomass gasifiers; reprint with permission from [97].	16
3.1	Thermal conversion of a wood particle; based on [61].	19
3.2	Thermogravimetric analysis (TGA) of maritime pine <i>Pinus Pinaster</i> in N ₂ atmosphere; heating rate 0.4 $\frac{^{\circ}\text{C}}{\text{s}}$; m(T) mass as a function of temperature; m ₀ initial mass of dry specimen; printed with permission from [81].	20
3.3	Tar conversion as a function of temperature, based on [33].	24
3.4	Recommended sampling line for tar sampling in [3]; 1. gas stream, 2. isokinetic sampling, 3. trace heated filter, 4. cooled impingers with solvent, 6. gas pump, 7. variable area flow meter, needle valve, and gas meter, 8. vent.	27
3.5	Schematic illustration of a sulfided Co/Mo-based hydrodesulfurization catalyst with MoS ₂ as an active species; from [110].	31
3.6	Reaction mechanism of the hydrogenolysis of thiophene on MoS ₂ ; from [114].	32
3.7	Variation of the equilibrium constant K_p of the WGSR at constant pressure with the temperature, based on [83].	33
3.8	Schematic illustration of the industrial catalysis of the WGSR over a two stage adiabatic bed system "sweet shift", equilibrium CO content (CO eq.) calculated based on the gas composition in Table 6.1, 50 mol.% H ₂ O in the wet gas mixture; based on [111].	35
3.9	Life cycles of a catalyst, based on [26].	40
3.10	Conceptual model of fouling; crystallite encapsulation and pore plugging of a supported metal catalyst due to coking or carbon deposition; from [13]. . . .	41
3.11	Ternary diagram of a gas mixture containing C, H, and O; C-H-O diagram; area of thermodynamically favored carbon formation; in atomic mol.%; atmospheric pressure; from [103, 102].	42
3.12	Conceptual model of poisoning by sulfur atoms (S) of a metal surface (M) during ethylene hydrogenation, from [13].	43
3.13	Variation of temperature profile with time for the poisoning of a LT WGS catalyst; the deactivation front progresses through the reactor, from [111]. . .	44

3.14	Basic setup of the two most common configurations for catalyst testing, Plug Flow Reactor (PFR) and Continuous Stirred Tank Reactor (CSTR) in the "Berty" configuration, based on [111].	48
4.1	Schematic diagram of the dual fluidized bed (DFB) steam gasification technology, based on [53].	52
4.2	Schematic diagram of the dual fluidized bed (DFB) gasification technology operated as a sorption enhanced reformer (SER), based on [95].	53
4.3	Picture of the DFB biomass steam gasification power plant Oberwart in 2014; from the left to the right: storage of wood chips, biomass feeding system, dryer, steel construction with gasification and gas cleaning, engine room, stack. . . .	54
4.4	Flowchart of the DFB biomass steam gasification power plant Oberwart, based on [28].	55
4.5	Sankey diagram of the energetic flows of the CHP plant Oberwart, based on [115].	57
4.6	Picture of research containers next to the DFB biomass steam gasification power plant Oberwart in 2014; in the container on bottom a series of analytical devices were placed; in the container on top a series of pilot plants for wood gas processing were realized.	58
5.1	Samples of the tested commercial WGS catalysts; raw catalysts: shape of pellets and disks according to Table 5.1, bulk density Catalyst 1: $0.78 \frac{g}{cm^3}$, Catalyst 2: $1.24 \frac{g}{cm^3}$; milled catalysts: particle range 500–800 μm , bulk density Catalyst 1: $0.73 \frac{g}{cm^3}$, Catalyst 2: $1.06 \frac{g}{cm^3}$	61
5.2	Picture of the setup of the "Test rig for chemical kinetics"; left: gas supply with gas cylinders; central: electrical cabinet with mass flow controllers and evaporator, visualization of the experiment, the glass reactor was placed at the backside of the electrical cabinet; right: gas analyzer.	63
5.3	Flowchart of the "Test rig for chemical kinetics" used for catalyst testing on a small scale.	64
5.4	Pictures of the "Test rig for chemical kinetics".	65
5.5	Screenshot of the operation surface of the test rig for chemical kinetics. . . .	65
5.6	Pictures of the realized "Pilot plant for catalytic wood gas processing" (WGS unit); top: picture prior to heat insulation 2012; bottom: picture of the final setup in 2013, including heat insulation, sampling for gas analysis, etc.	70
5.7	Connection of the "Pilot plant for catalytic wood gas processing" (WGS unit) to the CHP plant Oberwart.	71
5.8	Flowchart of the pilot plant for catalytic wood gas processing (WGS unit). . .	72
5.9	Three-dimensional engineering drawing of the pilot plant for catalytic wood gas processing (WGS unit).	73

5.10	Steam addition including the variable area flow meter, the peristaltic pump, the evaporator tube with the heating rod and the type J thermocouples. . . .	74
5.11	Fixed bed reactor of the pilot plant for catalytic wood gas processing (WGS unit).	76
5.12	Pictures of the electric control panel of the pilot plant for catalytic wood gas processing (WGS unit).	77
5.13	Screenshots of the graphical user interface of the pilot plant for catalytic wood gas processing (WGS unit).	80
5.14	Startup sequencer of the "Pilot plant for catalytic wood gas processing" (WGS unit).	81
5.15	Screenshot of the installed process visualization with LabVIEW during operation of the WGS unit; top left: peripheral thermocouples, top right: reactor A, bottom left: reactor B, bottom right: reactor C.	81
5.16	Hardware setup of one heating rod attached to the piping of the WGS unit, from [14].	82
5.17	Flowchart of the temperature control of one heating rod installed at the "Pilot plant for catalytic wood gas processing".	82
5.18	Screenshot of the LabVIEW™ visualization window of the most important delimiter thermocouples (T_{Del}) measuring the current surface temperature of the heating rods ($T_{4_{Beg}}$ preheating pipe before reactor A; $T_{5_{Beg}}$ heating before reactor B; $T_{6_{Beg}}$ heating before reactor C; $T_{9_{Beg}}$ heating of the evaporator).	83
5.19	Calibration of the gas pump (membrane pump) from KNF™ for wood gas feeding.	84
5.20	Calibration of the peristaltic pump for water addition and calibration of the variable area flow meter for the online control of water feeding.	85
5.21	Water saturation of wood gas extracted after the CHP scrubber depending on the temperature, values from [72].	86
5.22	Flowchart of the installed sampling line for chemical analysis of wood gas components; tar analyses were carried out over the sampling line on top, the temperature of cooling box 1 was 0 °C (ice bath); the temperature of regulated cooling box 2 was adjusted to -8 °C; standard gas analyses were carried out over the bottom path, during these analyses the temperature of the cooling box 2 was adjusted to -3 °C.	87
5.23	Molar balance of the WGS unit, and the most important formulas for the determination of the global mass balance.	90
5.24	Flow charts of the two different process chains which involved the operation of the "Pilot plant for catalytic wood gas processing".	91
6.1	Trend of wood gas composition September 2013.	93

6.2	Ternary diagram of a gas mixture containing C, H, and O; in atomic mol.%, from [103, 102]; wood gas composition from Table 6.1, 6 mol.% H ₂ O cleaned wood gas after scrubber, 35 mol.% H ₂ O raw wood gas after, 50–60 mol.% typical operation of the WGS unit.	98
6.3	Equilibrium composition of the wood gas mixture in Table 6.1 over the temperature, atmospheric pressure, hydrocarbons subsumed as N ₂ , 50 mol.% of H ₂ O in the wet gas.	99
6.4	Equilibrium composition of different two SER wood gas mixtures with the temperature, wet inlet gas composition plotted on the y-axis, all gas components not taking part at the WGSR are subsumed as "no WGS", 50 mol.% of H ₂ O in the wet gas.	100
6.5	Catalyst 1: Co/Mo-based; determination of apparent reaction orders; "Log-log" plot of the influence of the partial pressures of CO, CO ₂ , H ₂ and H ₂ O on the reaction rate; operating temperature 380 °C, ambient pressure, GHSV _{wb} . 16000 h ⁻¹	102
6.6	Catalyst 1: Co/Mo-based; Log-log plot of the effect of the H ₂ S partial pressure on the reaction rate, 380 °C, atmospheric pressure, GHSV _{wb} . 16000 h ⁻¹	103
6.7	Catalyst 1: Co/Mo-based; Arrhenius plot of the catalyzed WGSR, gas composition in Table 5.3, 320–470 °C, atmospheric pressure, GHSV _{wb} . 16000 h ⁻¹	104
6.8	Catalyst 1: Co/Mo-based, sulfidation procedure at the "Pilot plant for catalytic wood gas processing".	106
6.9	Temperature variation of Catalyst 1 at the "Pilot plant for catalytic wood gas processing"; cleaned wood gas; water content at the inlet 51 mol.% _{wb} ; GHSV _{wb} . 289 h ⁻¹	107
6.10	GHSV _{wb} . variation of Catalyst 1 at the "Pilot plant for catalytic wood gas processing"; cleaned wood gas; water content at the inlet 47–53 mol.% _{wb} ; T _{set} at the inlet of each reactor: 370 °C; average temperature over all reactors 377–389 °C.	108
6.11	Temperature variation of Catalyst 1 at the "Pilot plant for catalytic wood gas processing"; cleaned wood gas; water content at the inlet 60.4 mol.% _{wb} , average temperatures are plotted, gas sampling was carried out after each reactor (MV 6, MV 7, MV 8).	110
6.12	Temperature variation of Catalyst 1 at the "Pilot plant for catalytic wood gas processing"; cleaned wood gas after scrubber; water content at the inlet 52.1 mol.% _{wb} , overall GHSV _{wb} . 244 h ⁻¹ ; average temperatures over all concerned reactors are plotted.	112
6.13	Tar analysis at different operating temperatures, cleaned wood gas after scrubber, sampling during the operation in Figure 6.12.	113
6.14	Tar analysis at different operating temperatures, raw wood gas after filter. . .	113

6.15	Sulfur addition at the inlet of the "Pilot plant for catalytic wood gas processing"; operation according to Figure 6.12; setpoint temperatures of all 3 reactors 330 °C, gas sampling was carried out after each reactor (MV 6, MV 7, MV 8).	114
6.16	Catalyst 2: Fe/Cr-based; determination of power law rate model reaction orders; Log-log plot of the effect of CO, CO ₂ , H ₂ and H ₂ O partial pressure on the reaction rate; operating temperature: 300 °C, GHSV _{wb} . 16000 h ⁻¹	117
6.17	Catalyst 2: Fe/Cr-based; Log-log plot of the effect of the H ₂ S partial pressure on the reaction rate, 300 °C, atmospheric pressure.	118
6.18	Catalyst 2: Fe/Cr-based; Arrhenius plot of the catalyzed WGSR, E: gas composition in Table 5.3 without H ₂ S, E(H ₂ S): gas composition in Table 5.3 with a H ₂ S load of 100 vol.ppm _{db} , 220–305 °C, atmospheric pressure.	118
6.19	Temperature profile of reactor A and gas composition during activation of the Catalyst 2.	121
6.20	Induction period of the Fe/Cr-based catalyst, temperature and pressure trends over the WGS unit.	123
6.21	Induction period of the Fe/Cr-based catalyst, main gas composition over the operating time.	124
6.22	Induction period of the Fe/Cr-based catalyst, sulfur composition over the operating time.	125
6.23	Operation of process chain 2, temperature and pressure trends over the WGS unit, operation according to Table 6.14.	128
6.24	Operation of process chain 2, achieved composition and deviation from the equilibrium, optimum temperature to maximize the conversion rate with respect to the measured outlet composition.	129
6.25	Achieving full load of the pilot plant with cleaned wood gas after scrubber, temperature and pressure trends over the WGS unit, operation according to Table 6.17.	131
6.26	Achieving full load with cleaned wood gas after scrubber, average operating temperature over the height of the catalyst bed, achieved composition and deviation from the equilibrium, optimum temperature to maximize the conversion rate with respect to the measured outlet composition.	133
6.27	Achieving full load of the pilot plant with raw wood gas after filter, temperature and pressure trends over the WGS unit, operation according to Table 6.21.	135
6.28	"Concept of optimal operating line"; (a): motivation from the literature [23] ; (b): result from this thesis, this plot was basically used for the estimation of the optimum reaction temperature in Figure 6.24 and Figure 6.26.	139

List of Tables

3.1	Catalyst cooling in industrial fixed bed reactors.	30
3.2	Overview of the main reaction conditions during industrial catalysis of the WGSR over a LT and a HT stage, collected from [78, 111].	35
3.3	Mechansims of catalyst deactivation, reviewed in [13].	40
3.4	Power law rate model of the WGSR: List of symbols, explanation and units.	47
3.5	Differential rector: List of symbols, explanation and units.	50
4.1	Typical wood gas composition range in a DFB steam gasification process operated conventionally (olivine as bed material) and according to the SER concept (limestone as bed material); experimental data obtained from the 100 kW_{th} pilot plant at Vienna University of Technology; from [107].	53
4.2	Comparison of the key data of the performance of the CHP plant Oberwart during calender week 47, 2013, based on [115]; and the design data of the plant, based on [70].	56
4.3	Design gas compositions of the CHP plant Oberwart; Wood gas: given values of dust load and tar load at sampling point before wood gas filter; Flue gas: composition for combined flue gas derived from the combustion zone of the gasifier and the gas engines, dust load given for the combustion zone at the sampling point before flue gas filter; from [70].	57
5.1	Investigated commercial catalysts for the catalysis of the WGSR.	61
5.2	Power law rate model with respect to sulfur: List of symbols, explanation and units.	67
5.3	Adjusted gas composition to obtain Arrhenius plots for both catalysts (Catalyst 1: Co/Mo-based; Catalyst 2:Fe/Cr-based).	67
5.4	Process conditions at the interfaces of the WGS unit and the CHP plant Oberwart, temperatures and pressures from CHP plant operation calendar week 29 (2013), water content after gas filter from [70], water content after scrubber calculated based on the saturation with steam at the corresponding outlet temperature of the scrubber, NH_3 after filter from [96], NH_3 after scrubber measured in calendar week 2 (2014), Tar contents from [70].	71

5.5	List of pneumatic valves integrated into the "Pilot plant for catalytic wood gas processing" (WGS unit), the pneumatic valves were controlled by means of magnetic valves (MV) and are labeled according to these valves, MV 3 and MV 9 were designed normally open.	76
5.6	Overview of signals integrated into the process control system (PCS) of the "Pilot plant for catalytic wood gas processing" (WGS unit); DI (digital input), DO (digital output), AI (analogous input), AO (analogous output), TI (thermocouple input).	78
6.1	Averaged wood gas composition and standard deviation of cleaned wood gas on a dry base measured in September 2013, methanethiol (MeSH), ethanethiol (EtSH), thiophene (C ₄ H ₄ S), below detection limit (BDL).	94
6.2	Results of the analysis of ammonia and benzene, toluene, ethylbenzene, xylene (BTEX); cleaned gas after filter; detection limit 1 vol.ppm _{db.}); n.a. (not analyzed); from [28, 36, 35].	94
6.3	Results of the tar analysis of cleaned wood gas after scrubber from the CHP plant Oberwart; detection limit 1 $\frac{\text{mg}}{\text{Nm}_3^{\text{db.}}}$; including results from [36, 35].	95
6.4	Results of the tar analysis of raw wood gas after filter from the CHP plant Oberwart; detection limit 1 $\frac{\text{mg}}{\text{Nm}_3^{\text{db.}}}$; results from tar analysis Apr 2014 published with permission from DI Robert Bardolf.	96
6.5	Catalyst 1: Co/Mo-based; variation of partial pressures at the inlet of the reactor to obtain the reaction orders of each reacting agent; applied temperature for catalyst testing: 380 °C, GHSV _{wb.} 16000 h ⁻¹ , CO conversion rate (X _{CO}), reaction rate (r).	101
6.6	Catalyst 1: Co/Mo-based; obtained apparent reaction orders of each reacting agent; applied temperature for catalyst testing: 380 °C, GHSV _{wb.} 16000 h ⁻¹	102
6.7	Basic operating conditions and results of the WGS unit during operation of process chain 1.	109
6.8	Measured gas composition, temperatures, and key figures of the operation at an inlet temperature of 420 °C.	111
6.9	Catalyst 2: Fe/Cr-based; variation of partial pressures to obtain the reaction orders of each reaction partner; applied temperature for catalyst testing: 300 °C, GHSV _{wb.} 16000 h ⁻¹	116
6.10	Catalyst 2: Fe/Cr-based; obtained apparent reaction orders of each reacting agent; applied temperature for catalyst testing: 300 °C, GHSV _{wb.} 16000 h ⁻¹	116
6.11	Induction period of the Fe/Cr-based catalyst, basic operating conditions.	122
6.12	Induction period of the Fe/Cr-based catalyst, averaged gas composition of Figure 6.21 at the inlet and at the outlet of each reactor of the WGS unit, measured in September 2013.	122
6.13	Induction period of the Fe/Cr-based catalyst, key results, operation according to Table 6.11.	123

6.14	Operation of process chain 2, basic operating conditions of the WGS unit. . .	127
6.15	Operation of process chain 2, averaged gas composition at the inlet and at the outlet of each reactor of the WGS unit.	127
6.16	Operation of process chain 2, key results, operation according to Table 6.14. .	127
6.17	Catalyst 2: Fe/Cr-based; basic operating conditions for achieving full load with cleaned wood gas after scrubber.	130
6.18	Achieving full load of the pilot plant with cleaned wood gas after scrubber, averaged main gas and sulfur composition at the inlet and after each WGS reactor, Catalyst 2 : Fe/Cr-based, February 2014.	132
6.19	Achieving full load of the pilot plant with cleaned wood gas after scrubber, tar analysis at the inlet and at the outlet of the WGS unit, detection limit $1 \frac{\text{mg}}{\text{Nm}^3_{db}}$	132
6.20	Achieving full load with cleaned wood gas after scrubber, key results, operation according to Table 6.17.	133
6.21	Catalyst 2: Fe/Cr-based; basic operating conditions for achieving full load with raw wood gas after filter.	134
6.22	Achieving full load of the pilot plant with raw wood gas after filter, averaged main gas and sulfur composition at the inlet and after each WGS reactor, Catalyst 2 : Fe/Cr-based, February 2014.	136
6.23	Achieving full load of the pilot plant with raw wood gas after filter, tar analysis at the inlet and at the outlet of the WGS unit, detection limit $1 \frac{\text{mg}}{\text{Nm}^3_{db}}$	136
6.24	Achieving full load with raw wood gas after filter, key results, operation according to Table 6.21.	137

Nomenclature

Abbreviations & Acronyms

Ac	Activated carbon
AI	Analogous input
AO	Analogous output
ATR	Autothermal reforming
BDL	Below detection limit
BioH ₂	Biohydrogen, hydrogen generated by biomass or out of biomass
BTEX	Benzene, toluene, ethylbenzene, and xylene
BTX	Benzene, toluene, and xylene
CEM	Controlled evaporator mixer
C-H-O	Carbon-hydrogen-oxygen
CHP	Combined heat and power
CPU	Central processing unit
CSTR	Continuous stirred tank reactor
DFB	Dual fluidized bed
DI	Digital input
DME	Dimethyl ether, CH ₃ OCH ₃
DN	Diameter nominal according to standard: DIN 2440
DO	Digital output
EtSH	Ethanethiol, CH ₃ CH ₂ SH
FI	Flow indicator

FPD	Flame photometric detector
GC	Gas chromatograph
GC/MS	Gas chromatography coupled with mass spectrometry
GHSV	Gas hourly space velocity
HDS	Hydrodesulfurization
HHV	Higher heating value
HT	High temperature
ID	Inner diameter
IEA	International Energy Agency
IGCC	Integrated gasification combined cycle
LHV	Lower heating value
ln	Natural logarithm
LT	Low temperature
MeSH	Methanethiol, CH ₃ SH
MFC	Mass flow controller
MV	Magnetic valve
n.a.	Not analyzed
PAH	Polycyclic aromatic hydrocarbons
PCS	Process control system
PEM	Proton exchange membrane
PFR	Plug flow reactor
PI	Pressure indicator
POX	Partial oxidation
ppm	Parts per million
PTFE	Polytetrafluoroethylene
RME	Rapeseed oil methyl ester
SER	Sorption enhanced reforming

SMR	Steam methane reforming
SNG	Synthetic natural gas
TCD	Thermal conductivity detector
TGA	Thermogravimetric analysis
TI	Temperature indicator
TI	Thermocouple input
TOF	Turnover frequency, converted molecules of reactant per active site of the catalyst
WGSR	Water gas shift reaction
WGS	Water gas shift

Indices

0	Initial, at time 0
<i>a</i>	Actual, at the present operating temperature and pressure
<i>cat</i>	Catalyst
<i>d.a.f.</i>	Dry ash free base
<i>db.</i>	Dry base
<i>Del</i>	Delimiter of heating rod
<i>el</i>	Electric
<i>eq.</i>	Equilibrium
<i>meas.</i>	Measured
<i>i</i>	Specific gas component, for example CO ₂ , CO, H ₂ , or H ₂ O
<i>in</i>	Inlet
<i>n</i>	At standard conditions: 0 °C and 101.325 kPa
<i>op.</i>	Operation, present operating condition
<i>opt</i>	Optimum
<i>out</i>	Outlet
<i>rec</i>	Recovery
<i>Set</i>	Setpoint

th Thermal

Tol Tolerated

wb. Wet base

vol. Volumetric base

wt. Weight base

Symbols

A Pre-exponential factor in $\frac{mol}{g_{cat} \cdot s} kPa^{-(a+b+c+d)}$

a, b, c, d Apparent reaction order with respect to component i, dimensionless

c Concentration in $\frac{mol}{L}$

d Day

ΔT Temperature control, temperature difference in °C

ΔH_R^0 Enthalpy of reaction at standard conditions (0 °C and 101.325 kPa) in $\frac{kJ}{mol}$

d_p Particle diameter in *mm*

e Sulfur modeling, apparent reaction order with respect to H₂S, dimensionless

E_A Apparent activation energy in $\frac{kJ}{mol}$

η_G Cold gas efficiency of the gasifier, dimensionless

\dot{F} Volumetric feed flow rate in $\frac{L}{h}$

\dot{G} Molar flow rate of wood gas before steam addition in $\frac{mol}{h}$

R Universal gas constant, $8.314 \cdot 10^{-3} \frac{kJ}{mol \cdot K}$

GHSV Gas hourly space velocity in h^{-1}

HHV Higher heating value in $\frac{kJ}{m_n^3}$

Hys. Temperature control, hysteresis in °C

k Reaction rate constant in $\frac{mol}{g_{cat} \cdot s} kPa^{-(a+b+c+d)}$

K_p Equilibrium constant at constant pressure, dimensionless

LHV Lower heating value in $\frac{kJ}{m_n^3}$

\dot{M} Molar flow rate of wood gas after steam addition in $\frac{mol}{h}$

\dot{m} Mass flow rate in $\frac{kg}{h}$

y_i	Molar fraction of component i , dimensionless
m	Mass in kg
\dot{n}	Molar flow rate in $\frac{mol}{h}$
P	Power in W
p	Partial pressure in kPa
\dot{R}	Molar flow rate of raffinate after the catalysis of the WGSR in $\frac{mol}{h}$
$r_{wt.}$	Reaction rate on a weight base in $\frac{mol}{g_{cat} \cdot s}$
$r_{vol.}$	Reaction rate on a volumetric base in $\frac{mol}{L_{cat} \cdot h}$
S	Sulfur modeling, factor representing the catalyst and the experimental conditions in $\frac{mol}{g_{cat} \cdot s} \cdot kPa^{-e}$
*	Active site of the catalyst, dimensionless
T	Temperature in °C
\dot{V}	Volumetric flow rate in $\frac{m^3}{h}$
V	Volume in L
\dot{W}	Molar water flow rate in $\frac{mol}{h}$
X_{CO}	CO conversion rate, dimensionless
X_i	Conversion rate of component i , dimensionless
Y_i	Molar fraction of component i , dimensionless

Bibliography

- [1] *Operating Manual of the Co/Mo-based catalyst.*
- [2] *Operating manual of the Fe/Cr-based catalyst.*
- [3] Vornorm: Biomassevergasung–Teer und Staub in Produktgasen– Probenahme und analytische Bestimmung; Deutsche Fassung CEN/TS 15439:2006.
- [4] N. Abatzoglou, N. Barker, P. Hasler, and H. Knoef. The development of a draft protocol for the sampling and analysis of particulate and organic contaminants in the gas from small biomass gasifiers. *Biomass and Bioenergy*, 18:5 – 17, 2000.
- [5] Energie Burgenland AG. Biomassekraftwerk Oberwart: Strom-, Wärme- und Gasproduktion aus Holz, <http://www.energieburgenland.at/oekoenergie/biomasse/biomassekraftwerke/>. Webpage, Zugriff August 2014.
- [6] J. Ahrenfeldt, T. P. Thomsen, U. Henriksen, and L. R. Clausen. Biomass gasification cogeneration - A review of state of the art technology and near future perspectives. *Applied Thermal Engineering*, 50:1407 – 1417, 2013.
- [7] S. Anis and Z.A. Zainal. Tar reduction in biomass producer gas via mechanical, catalytic and thermal methods: A review. *Renewable and Sustainable Energy Reviews*, 15:2355 – 2377, 2011.
- [8] M. Appl. *Ullmann's Encyclopedia of Industrial Chemistry*, chapter "Ammonia", page 121. Wiley-VCH Verlag GmbH & Co. KG, 2000.
- [9] Sozialministerium Arbeitsinspektion. Grenzwerteverordnung 2011: Verordnung des Bundesministers für Arbeit, Soziales und Konsumentenschutz über Grenzwerte für Arbeitsstoffe sowie über krebserzeugende und über fortpflanzungsgefährdende Arbeitsstoffe, 2011.
- [10] M. B.-Nordenkamp, R. Rauch, K. Bosch, C. Aicherning, and H. Hofbauer. Biomass CHP plant Güssing – Using gasification for power generation. In *International Conference for Biomass Utilization*, pages 567–572, 2003.
- [11] T. Bak, J. Nowotny, M. Rekas, and C.C. Sorrell. Photo-electrochemical hydrogen generation from water using solar energy. Materials-related aspects. *International Journal of Hydrogen Energy*, 27:991 – 1022, 2002.

- [12] C. H. Bartholomew. Carbon deposition in steam reforming and methanation. *Catal.Rev.–Sci.Eng.*, 24:67–112, 1982.
- [13] C. H. Bartholomew. Mechanisms of catalyst deactivation. *Applied Catalysis*, 212:17 – 60, 2001.
- [14] Florian Benedikt. Experimental evaluation of a process chain to produce hydrogen from wood gas. Master’s thesis, Vienna University of Technology, 2014.
- [15] S. N. Bizzari and M. Blagoev. Chemical industries newsletter CEH marketing research report abstract- Hydrogen. Technical report, SRI Consulting, 2007.
- [16] I. Blessing, C. Gardner, and M. Ternan. Separation of hydrogen from a hydrogen / methane mixture using a PEM fuel cell. *International Journal of Hydrogen Energy*, 32:908–914, 2007.
- [17] H. Boerrigter, S.V.B. van Paasen, P.C.A. Bergman, J.W. Könemann, R. Emmen, and A. Wijnands. ”OLGA“ tar removal technology – Proof-of-Concept (PoC) for application in integrated biomass gasification combined heat and power (CHP) systems. Technical report, ECN (Energy research Centre of the Netherlands) and Dahlman Industrial Group, 2005.
- [18] Markus Brune. *Verfahren zur Entschwefelung von flüssigen handelsüblichen Brennstoffen*. PhD thesis, Karlsruher Institut für Technologie, 2009.
- [19] C. Callaghan, I. Fishtik, R. Datta, M. Carpenter, M. Chmielewski, and A. Lugo. An improved microkinetic model for the water gas shift reaction on copper. *Surface Science*, 541:21 – 30, 2003.
- [20] R. Chaubey, S. Sahu, O. O. James, and S. Maity. A review on development of industrial processes and emerging techniques for production of hydrogen from renewable and sustainable sources. *Renewable and Sustainable Energy Reviews*, 23:443 – 462, 2013.
- [21] G. Chen, J. Andries, and H. Spliethoff. Catalytic pyrolysis of biomass for hydrogen rich fuel gas production. *Energy Conversion and Management*, 44:2289 – 2296, 2003.
- [22] T. Chen, H. Liu, P. Shi, D. Chen, L. Song, H. He, and R. L. Frost. CO₂ reforming of toluene as model compound of biomass tar on Ni/Palygorskite. *Fuel*, 107:699 – 705, 2013.
- [23] I. Chorkendorff and J.W. Niemantsverdriet. *Concepts of Modern Catalysis and Kinetics*. Wiley-VCH, 2013.
- [24] M. Conte and M. Ronchetti. Hydrogen economy. In *Reference Module in Chemistry, Molecular Sciences and Chemical Engineering*. Elsevier, 2013.

- [25] José Corella, Maria P. Aznar, Miguel A. Caballero, Gregorio Molina, and José M. Toledo. 140g H₂ per kg biomass_(d.a.f.) by a CO-shift reactor downstream from a FB biomass gasifier and a catalytic steam reformer. *International Journal of Hydrogen Energy*, 33:1820 – 1826, 2008.
- [26] S. M. Csicsery. Catalyst testing: How and how not to test catalysts. Catalyst Consultants Publishing, 1991.
- [27] Ayhan Demirbas. Gaseous products from biomass by pyrolysis and gasification: Effects of catalyst on hydrogen yield. *Energy Conversion and Management*, 43(7):897 – 909, 2002.
- [28] Nicolas Diaz. *Hydrogen Separation from Producer Gas Generated by Biomass Steam Gasification*. PhD thesis, Vienna University of Technology, 2013.
- [29] R. Diem, S. Müller, M. Fuchs, J. Schmid, and H. Hofbauer. Experimental investigation of sorption enhanced reforming with limestone from iron production. In *Proceedings of the ICPS 2013*, 2013.
- [30] Axel Düker. Hydrogen Production and Application in Industry. In *Presentation Süd - Chemie*, 2011.
- [31] S. Dunn. Hydrogen futures: Toward a sustainable energy system. *International Journal of Hydrogen Energy*, 27:235–264, 2002.
- [32] R. Ehrig and M. Wörgetter. Biomasseverfügbarkeit zur Versorgung einer Biowasserstoffanlage am Standort Wien. Projektbericht, BioH₂ -4refineries, 2011.
- [33] D.C. Elliott. Relation of reaction time and temperature to chemical composition of pyrolysis oils. In *ACS Symposium Series 376, Pyrolysis Oils from Biomass*, 1988.
- [34] R.J. Evans and T.A. Milne. Molecular characterization of the pyrolysis of biomass. *Energy and Fuels*, 1:123–138, 1987.
- [35] S. Fail, N. Diaz, F. Benedikt, M. Kraussler, J. Hinteregger, K. Bosch, M. Hackel, R. Rauch, and H. Hofbauer. Wood gas processing to generate pure hydrogen suitable for PEM fuel cells. *American Chemical Society, Sustainable Chemistry and Engineering*, accepted 13th of October 2014, unknown:unknown, 2014.
- [36] S. Fail, N. Diaz, D. Konlechner, M. Hackel, E. Sanders, R. Rauch, M. Harasek, K. Bosch, F. Schwenninger, P. Zapletal, Z. Schee, and H. Hofbauer. An experimental approach for the production of pure hydrogen based on wood gasification. In *Proceedings of the ICPS 2013*, pages 109–126, 2013.
- [37] S. Fail, G. Thomas, and R. Rauch. Schwefelresistente Katalyse der Wassergasshift-Reaktion zur Wasserstoffherstellung aus dem Produktgas einer Holzvergasung. In *9. Minisymposium Verfahrenstechnik Montanuniversitt Leoben 2013*, 2013.

- [38] G. Gahleitner. Hydrogen from renewable electricity: An international review of power-to-gas pilot plants for stationary applications. *International Journal of Hydrogen Energy*, 38:2039 – 2061, 2013.
- [39] Union Instruments GmbH. *Manual of the Biogas Analyser InCa Bio04*, 2012.
- [40] A. Gomez-Barea, P. Ollero, and B. Leckner. Optimization of char and tar conversion in fluidized bed biomass gasifiers. *Fuel*, 103:42–52, 2013.
- [41] D.C. Grenoble, M.M. Estadt, and D.F. Ollis. The chemistry and catalysis of the water gas shift reaction: 1. The kinetics over supported metal catalysts. *Journal of Catalysis*, 67(1):90 – 102, 1981.
- [42] R. Hakkarainen, T. Salmi, and R.L. Keiski. Comparison of the dynamics of the high-temperature water-gas shift reaction on oxide catalysts. *Catalysis Today*, 20:395, 1994.
- [43] R. Hakkarainen and T.Salmi. Water-gas shift reaction on a cobalt-molybdenum oxide catalyst. *Applied Catalysis. A, General*, 99:195, 1993.
- [44] Robert A. Hefner. The age of energy gases. *International Journal of Hydrogen Energy*, 27(1):1 – 9, 2002.
- [45] H. Hellsmark and S. Jacobsson. Opportunities for and limits to academics as system builders, The case of realizing the potential of gasified biomass in Austria. *Energy Policy*, 37:5597–5611, 2009.
- [46] J. J. Hernandez, G. Aranda-Almansa, and A. Bula. Gasification of biomass wastes in an entrained flow gasifier- Effect of the particle size and the residence time. *Fuel Processing Technology*, 91:681 – 692, 2010.
- [47] K. Hertwig and L. Martens. *Chemische Verfahrenstechnik*, volume 2. Oldenburg Verlag, 2012.
- [48] Julian Hinteregger. Performance evaluation of process chains for biohydrogen production from wood gas. Master’s thesis, Vienna University of Technology, 2014.
- [49] S. S. Hla, G.J. Duffy, L.D. Morpeth, A. Cousins, D.G. Roberts, and J.H. Edwards. Investigation of the effect of total pressure on performance of the catalytic water gas shift reaction using simulated coal-derived syngases. *Catalysis Communications*, 11:272 – 275, 2009.
- [50] S. S. Hla, G.J. Duffy, L.D. Morpeth, A. Cousins, D.G. Roberts, and J.H. Edwards. Investigation into the performance of a Co/Mo based sour shift catalyst using simulated coal-derived syngases. *International Journal of Hydrogen Energy*, 36:6638 – 6645, 2011.
- [51] S. S. Hla, L.D. Morpeth, Y. Sun, G.J. Duffy, A.Y. Ilyushechkin, D.G. Roberts, and J.H. Edwards. A CeO₂-La₂O₃-based Cu catalyst for the processing of coal-derived syngases via high-temperature water gas shift reaction. *Fuel*, 114:178 – 186, 2013.

- [52] S. S. Hla, D. Park, G.J. Duffy, J.H. Edwards, D.G. Roberts, A. Ilyushechkin, L.D. Morpeth, and T. Nguyen. Kinetics of high-temperature water-gas shift reaction over two iron-based commercial catalysts using simulated coal-derived syngases. *Chemical Engineering Journal*, 146:148 – 154, 2009.
- [53] H. Hofbauer, G. Veronik, T. Fleck, R. Rauch, H. Mackinger, and E. Fercher. The FICFB - gasification process. *Developments in Thermochemical Biomass Conversion*, 1:1016–1025, 1997.
- [54] H. Hofbauer, R. Rauch, K. Bosch, R. Koch., and C. Aichering. *Biomass CHP Plant Güssing A Success Story*. CPL Press, 2003.
- [55] H. Hofbauer, R. Rauch, and G. Löffler. Six years of experience with the FICFB-gasification process. In *12th European Conference on Biomass and Bioenergy*, 2002.
- [56] Hermann Hofbauer. *Brennstoff- und Energietechnologie. Vorlesungsunterlagen*, Technische Universität Wien, 2013.
- [57] Gerhard Hofer. “Langfristig setzt die OMV auf Wasserstoff”. Tageszeitung : “Die Presse”, 6.Mai 2014. Interview.
- [58] Jitka Hrbek. International Energy Agency (IEA) Bioenergy, Thermal Gasification of Biomass, Task 33, [http : //www.ieatask33.org/content/thermal_gasification_facilities](http://www.ieatask33.org/content/thermal_gasification_facilities), 2014.
- [59] G.H. Huisman, G.L.M.A. Van Rens, H. De Lathouder, and R.L. Cornelissen. Cost estimation of biomass-to-fuel plants producing methanol, dimethylether or hydrogen. *Biomass and Bioenergy*, 35:155 – 166, 2011.
- [60] J. Jung, Y. S. Jeong, Y. Lim, C. S. Lee, and C. Han. Advanced CO₂ capture process using MEA scrubbing, configuration of a split flow and phase separation heat exchanger. *Energy Procedia*, 37:1778 – 1784, 2013.
- [61] M. Kaltschmitt, H. Hartmann, and H. Hofbauer. *Energie aus Biomasse*. Springer Verlag, 2. edition, 2009.
- [62] Jürgen Karl. *Dezentrale Energiesysteme- Neue Technologien im liberalisierten Energiemarkt*. Oldenburg Wissenschaftsverlag, 2012.
- [63] Riitta L. Keiski, Tapio Salmi, Pekka Niemistö, Jorma Ainassaari, and Veikko J. Pohjola. Stationary and transient kinetics of the high temperature water-gas shift reaction. *Applied Catalysis A: General*, 137(2):349 – 370, 1996.
- [64] S. Kern, C. Pfeifer, and H. Hofbauer. Dual fluidized bed steam gasification of coal and biomass: Influence of the state of pyrolysis on the process performance. In *Clean Coal Conference*, 2013.

- [65] F. Kirnbauer and H. Hofbauer. The mechanism of bed material coating in dual fluidized bed biomass steam gasification plants and its impact on plant optimization. *Powder Technology*, 245:94 – 104, 2013.
- [66] F. Kirnbauer, J. Kotik, and H. Hofbauer. Investigations on inorganic matter in DFB biomass steam-gasification plants in Güssing/Austria and Oberwart/Austria. In *19th European Biomass Conference and Exhibition*, page 6, 2011.
- [67] KIT. Karlsruhe Institute of Technology, bioliq [®], <http://www.bioliq.de/index.php>. website, Zugriff August 2014.
- [68] S. Koppatz, C. Pfeifer, R. Rauch, H. Hofbauer, T. M.-M., and M. Specht. H₂ rich product gas by steam gasification of biomass with in situ CO₂ absorption in a dual fluidized bed system of 8MW fuel input. *Fuel Processing Technology*, 90:914–921, 2009.
- [69] J. Kotik, U. Wolfesberger, and H. Hofbauer. Analysen und Messungen am Biomassekraftwerk Oberwart. Projektbericht Bioenergy 2020+, Projekt "C-II-1-2 Steam gasification plant Oberwart", 2009.
- [70] Jan Kotik. *Über den Einsatz von Kraft-Wärme-Kopplungsanlagen auf Basis der Wirbelschicht-Dampfvergasung fester Biomasse am Beispiel des Biomassekraftwerks Oberwart*. PhD thesis, Technische Universität Wien, 2010.
- [71] Michael Kraussler. PEM fuel cell operation and applications using BioH₂. Master's thesis, Vienna University of Technology, 2014.
- [72] Horst Kuchling. *Taschenbuch Physik*. Carl Hanser Verlag München, 2011.
- [73] E. Kurkela and M. Kurkela. Advanced biomass gasification for high-efficiency power, Publishable final activity report of BiG Power Project. Technical report, VTT, TUV, Kokemäen Kaasutin, Carbona, RPT, MEL, Nortta, GEJ, MTU, BKG, CERTH, TKK, Clear Edge, 2009.
- [74] D. H. Lee and L. H. Chiu. Development of a biohydrogen economy in the United States, China, Japan, and India: With discussion of a chicken-and-egg debate. *International Journal of Hydrogen Energy*, 37:15736 – 15745, 2012.
- [75] W. Y. Lee, J. Hanne, and A. F. Ghoniema. Improvements to predictions of carbon deposition on the nickel anode of a SOFC under open-circuit conditions. Department of Mechanical Engineering, Massachusetts Institute of Technology, USA, 2012.
- [76] Octave Levenspiel. *Chemical Reaction Engineering Third Edition*. John Wiley and Sons, 1999.
- [77] Q. Li, Y. Xu, C. Liu, and J. Kim. Catalytic synthesis of thiophene from the reaction of furan and hydrogen sulfide. *Catal Lett*, 122:354358, 2008.

- [78] K. Liu, C. Song, and S. Velu. *Hydrogen and Syngas Production and Purification Technologies*. Wiley, 2010.
- [79] Y.J. Lu, L.J. Guo, C.M. Ji, X.M. Zhang, X.H. Hao, and Q.H. Yan. Hydrogen production by biomass gasification in supercritical water, A parametric study. *International Journal of Hydrogen Energy*, 31:822 – 831, 2006.
- [80] K Maniatis and A.A.C.M Beenackers. Tar protocols. IEA Bioenergy Gasification Task. *Biomass and Bioenergy*, 18:1 – 4, 2000.
- [81] Mathieu Milhé. Comparaison des profils ATG: Influence des différentes atmosphères de pyrolyse (N₂ ou CO₂ à 100% et H₂O à 50% dans N₂) : étude de l'étape de pyrolyse à 500 °C. CIRAD, Montpellier, France, 2010.
- [82] T.A. Milne and R.J. Evans. *Biomass Gasifier Tars, Their Nature, Formation, and Conversion*. National Renewable Energy Laboratory, 1998.
- [83] J. M. Moe. Design of water-gas shift reactors. *Chemical Engineering Progress*, 58:33–36, 1962.
- [84] L.D. Morpeth, Y. Sun, San Shwe Hla, D. French, G.J. Duffy, and J.H. Edwards. Effect of H₂S on the performance of La_{0.7}Ce_{0.2}FeO₃ perovskite catalyst for high temperature water-gas shift reaction. *International Journal of Hydrogen Energy*, 37:1475 – 1481, 2012.
- [85] G. Müller. Erarbeitung von Basisinformationen zur Positionierung des Energieträgers Erdgas im zukünftigen Energiemix in Österreich, Technical report, Österreichische Vereinigung für das Gas und Wasserfach, 2012.
- [86] Stefan Müller. *Hydrogen from Biomass for Industry, Industrial Application of Hydrogen Production Based on Dual Fluid Gasification*. PhD thesis, Vienna University of Technology, 2013.
- [87] M. Ni, D. Y. C. Leung, M. K. H. Leung, and K. Sumathy. An overview of hydrogen production from biomass. *Fuel Processing Technology*, 87:461 – 472, 2006.
- [88] T. Nordgreen, T. Liliedahl, and K. Sjöström. Metallic iron as a tar breakdown catalyst related to atmospheric, fluidised bed gasification of biomass. *Fuel*, 85:689 – 694, 2006.
- [89] C. Odabasi, M. E. Gunay, and R. Yildirim. Knowledge extraction for water gas shift reaction over noble metal catalysts from publications in the literature between 2002 and 2012. *International Journal of Hydrogen Energy*, 39:5733 – 5746, 2014.
- [90] C.E.G Padró and V. Putsche. Techreport: Survey of the economics of hydrogen technologies. Technical report, National Renewable Energy Laboratory, 1999.

- [91] A. Paethanom, S. Nakahara, M. Kobayashi, P. Prawisudha, and K. Yoshikawa. Performance of tar removal by absorption and adsorption for biomass gasification. *Fuel Processing Technology*, 104:144 – 154, 2012.
- [92] C. Pfeifer, B. Puchner, and H. Hofbauer. In-situ CO₂ absorption in a dual fluidized bed biomass steam gasifier to produce a hydrogen rich syngas. *International Journal of Chemical Reactor Engineering*, 5:1542–6580, 2007.
- [93] C. Pfeifer, B. Puchner, and H. Hofbauer. Comparison of dual fluidized bed steam gasification of biomass with and without selective transport of CO₂. *Chemical Engineering Science*, 64:5073 – 5083, 2009.
- [94] W. F. Podolski and Y. G. Kim. Modeling the water-gas shift reaction. *Ind. Eng. Chem. Process Des. Dev.*, 13:415–421, 1974.
- [95] T. Pröll and H. Hofbauer. H₂ rich syngas by selective CO₂ removal from biomass gasification in a dual fluidized bed system, Process modelling approach. *Fuel Processing Technology*, 89:1207 – 1217, 2008.
- [96] T. Pröll, I. Siefert, A. Friedl, and H. Hofbauer. Removal of NH₃ from biomass gasification producer gas by water condensing in an organic solvent scrubber. *Industrial & Engineering Chemistry Research*, 44:1576–1584, 2005.
- [97] R. Rauch, J. Hrbek, and H. Hofbauer. Biomass gasification for synthesis gas production and applications of the syngas. *Wiley Interdisciplinary Reviews: Energy and Environment*, 1:1–20, 2013.
- [98] Reinhard Rauch. FICFB - Fast Internally Circulating Fluidized Bed Technology, www.ficfb.at, Zugriff Mai 2011.
- [99] C. Rhodes, B. P. Williams, F. King, and G. J. Hutchings. Promotion of Fe₃O₄/Cr₂O₃ high temperature water gas shift catalyst. *Catalysis Communications*, 3:381 – 384, 2002.
- [100] E. Rodriguez-Castellon, A. Jimenez-Lopez, and D. Eliche-Quesada. Nickel and cobalt promoted tungsten and molybdenum sulfide mesoporous catalysts for hydrodesulfurization. *Fuel*, 87:1195 – 1206, 2008.
- [101] Rosemount. *Instruction Manual - Model NGA 2000 Platform*. Emerson, Ohio USA, 2001.
- [102] Andreas Schweiger. Entwicklungsstand der HT-Entschwefelung und der trockenen Reformierung. In *Institut für Wärmetechnik - TU Graz*, 2007.
- [103] Y. Shiratori, T. Ijichi, T. Oshima, and K. Sasaki. Internal reforming SOFC running on biogas. *International Journal of Hydrogen Energy*, 35:7905 – 7912, 2010.

- [104] P. Simell, P. Stahlberg, E. Kurkela, J. Albrecht, S. Deutsch, and K. Sjöström. Provisional protocol for the sampling and analysis of tar and particulates in the gas from large-scale biomass gasifiers. Version 1998. *Biomass and Bioenergy*, 18:19 – 38, 2000.
- [105] S. Sircar, T.C. Golden, and M.B. Rao. Activated carbon for gas separation and storage. *Carbon*, 34:1–12, 1996.
- [106] B. Smith, M. Loganathany, and M. S. Shanthaz. A review of the water gas shift reaction kinetics. *International Journal of Chemical Reactor Engineering*, 8:1–32, 2010. .
- [107] G. Soukup, C. Pfeifer, A. Kreuzeder, and H. Hofbauer. In situ CO₂ capture in a dual fluidized bed biomass steam gasifier, Bed material and fuel variation. *Chem. Eng. Technol.*, 3:348–354, 2009.
- [108] K. Stahl, L.Waldheim, M.Morris, U.Johnsson, and L. Gardmark. Biomass IGCC at Värnamo, Sweden – Past and future, 2004.
- [109] Gerald Thomas. Schwefelresistente Katalyse der Wassergas-Shift-Reaktion zur Wasserstoffherstellung aus dem Produktgas einer Holzvergasung. Bachelor Thesis, October 2012.
- [110] H. Topsoe and B. Clausen. Importance of Co-Mo-S Type Structures in Hydrodesulfurization. *Catalysis Reviews in Science and Engineering*, 26:395–420, 1984.
- [111] Martyn V. Twigg. *Catalyst Handbook*, 2nd edition. Manson Publishing, pages: 200-201, 283-339, 1989.
- [112] S.V.B. van Paasen, L.P.L.M. Rabou, and R. Bär. Tar removal with a wet electrostatic precipitator; a parametric study. In *The 2nd World Conference and Technology Exhibition on Biomass for Energy, Industry and Climate Protection*, 2004.
- [113] A. Villot, Y. Gonthier, E. Gonze, A. Bernis, S. Ravel, M. Grateau, and J. Guillaudeau. Separation of particles from syngas at high-temperatures with an electrostatic precipitator. *Separation and Purification Technology*, 92:181 – 190, 2012.
- [114] Wikipedia. Hydrodesulfurization - Hydrodesulfurization cycle for thiophene (simplified diagram) – Wikipedia, the free encyclopedia. *http : //en.wikipedia.org/wiki/Hydrodesulfurization*, Access July 2014.
- [115] Veronika Wilk. Biomass CHP Oberwart: Status and future potentials. In *Proceedings of the International Symposium on Gasification and its Applications (iSGA-4)*, 2014.
- [116] U. Wolfesberger, I. Aigner, and H. Hofbauer. Tar content and composition in producer gas of fluidized bed gasification of wood-influence of temperature and pressure. *Environmental Progress & Sustainable Energy*, 28:372–379, 2009.

- [117] Y. M. Wong, T. Y. Wu, and J. C. Juan. A review of sustainable hydrogen production using seed sludge via dark fermentation. *Renewable and Sustainable Energy Reviews*, 34:471 – 482, 2014.
- [118] B. Zhao, X. Zhang, L. Chen, R. Qu, G. Meng, X. Yi, and L. Sun. Steam reforming of toluene as model compound of biomass pyrolysis tar for hydrogen. *Biomass and Bioenergy*, 34:140 – 144, 2010.